

DTIC FILE COPY

4

GL-TR-90-0032(II)
ENVIRONMENTAL RESEARCH PAPERS, NO. 1052

Proceedings of the Second Symposium on
GPS Applications in Space

EDITOR:

CHRISTOPHER JEKELI

AD-A219 979



13 February 1990



Approved for public release; distribution unlimited.

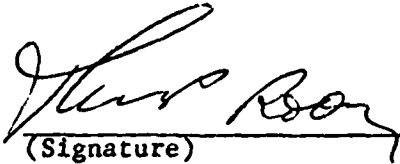


DTIC
ELECTE
APR 3 1990
S B D
CO

EARTH SCIENCES DIVISION
PROJECT 2309
GEOPHYSICS LABORATORY
HANSCOM AFB, MA 01731-5000

90 04 03 071

"This technical report has been reviewed and is approved for publication"



(Signature)
THOMAS P. ROONEY, Chief
Geodesy and Gravity Branch



(Signature)
DONALD H. ECKHARDT, Director
Earth Sciences Division

This report has been reviewed by the ESD Public Affairs Office (PA) and is releasable to the National Technical Information Service (NTIS).

Qualified requestors may obtain additional copies from the Defense Technical Information Center. All others should apply to the National Technical Information Service.

If your address has changed, or if you wish to be removed from the mailing list, or if the addressee is no longer employed by your organization, please notify GL/IMA, Hanscom AFB, MA 01731. This will assist us in maintaining a current mailing list.

UNCLASSIFIED

SECURITY CLASSIFICATION OF THIS PAGE

| REPORT DOCUMENTATION PAGE | | | | Form Approved OMB No. 0704-0188 | |
|---|-------|--|--|--|---|
| 1a. REPORT SECURITY CLASSIFICATION UNCLASSIFIED | | | 1b. RESTRICTIVE MARKINGS | | |
| 2a. SECURITY CLASSIFICATION AUTHORITY | | | 3. DISTRIBUTION / AVAILABILITY OF REPORT APPROVED FOR PUBLIC RELEASE: DISTRIBUTION UNLIMITED | | |
| 2b. DECLASSIFICATION / DOWNGRADING SCHEDULE | | | | | |
| 4. PERFORMING ORGANIZATION REPORT NUMBER(S) GL-TR-90-0032(II) ERP, No. 1052 | | | 5. MONITORING ORGANIZATION REPORT NUMBER(S) | | |
| 6a. NAME OF PERFORMING ORGANIZATION GEOPHYSICS LABORATORY (AFSC) | | 6b. OFFICE SYMBOL (If applicable) LWG | 7a. NAME OF MONITORING ORGANIZATION | | |
| 6c. ADDRESS (City, State, and ZIP Code) Hanscom Air Force Base Bedford, MA 01731-5000 | | | 7b. ADDRESS (City, State, and ZIP Code) | | |
| 8a. NAME OF FUNDING / SPONSORING ORGANIZATION | | 8b. OFFICE SYMBOL (If applicable) | 9. PROCUREMENT INSTRUMENT IDENTIFICATION NUMBER | | |
| 8c. ADDRESS (City, State, and ZIP Code) | | | 10. SOURCE OF FUNDING NUMBERS | | |
| | | | PROGRAM ELEMENT NO. 61102F | PROJECT NO. 2309 | TASK NO. 2309G1 |
| | | | | | WORK UNIT ACCESSION NO. 2309G112 |
| 11. TITLE (Include Security Classification) Proceedings of the Second Symposium on GPS Applications in Space, Volume I (pp.1-244) and Volume II (pp.245-458) | | | | | |
| 12. PERSONAL AUTHOR(S) Christopher Jekeli (editor) | | | | | |
| 13a. TYPE OF REPORT Scientific | | 13b. TIME COVERED FROM _____ TO _____ | | 14. DATE OF REPORT (Year, Month, Day) 1990 February 13 | |
| 15. PAGE COUNT 216 | | | | | |
| 16. SUPPLEMENTARY NOTATION | | | | | |
| 17. COSATI CODES | | | 18. SUBJECT TERMS (Continue on reverse if necessary and identify by block number) | | |
| FIELD | GROUP | SUB-GROUP | Global Positioning System, Orbit Determination, Space Navigation, Attitude Determination, ATTITUDE | | |
| | | | | | |
| | | | | | |
| 19. ABSTRACT (Continue on reverse if necessary and identify by block number) SCORPOL SYSTEM, Symposium | | | | | |
| <p>This collection of abstracts, papers, and presentation material constitutes the Proceedings of the Second Symposium on GPS Applications in Space, which was held at the Geophysics Laboratory (Air Force Systems Command), Hanscom Air Force Base, Massachusetts, on 10-11 October, 1989. The Symposium was divided into four sessions covering "Space Missions with GPS", "Orbit Determination with GPS", "Attitude Determination with GPS", and "Other Applications and Topics." Both the application of GPS to a variety of NASA and DOD space missions, as well as corresponding GPS receiver development were discussed at this symposium. Specific applications included orbit determination of the GPS satellites and low Earth orbiters, space navigation, and, in particular, attitude determination of space vehicles.</p> | | | | | |
| 20. DISTRIBUTION / AVAILABILITY OF ABSTRACT <input checked="" type="checkbox"/> UNCLASSIFIED/UNLIMITED <input type="checkbox"/> SAME AS RPT. <input type="checkbox"/> DTIC USERS | | | 21. ABSTRACT SECURITY CLASSIFICATION Unclassified | | |
| 22a. NAME OF RESPONSIBLE INDIVIDUAL Christopher Jekeli | | | 22b. TELEPHONE (Include Area Code) 617-377-5255 | | 22c. OFFICE SYMBOL GI (AFSC)/LWG |

TABLE OF CONTENTS - VOLUME I

| | |
|---|-----|
| Foreword | iii |
| Conference Agenda | vi |
| Geoscience From GPS Tracking By Earth Satellites, William G. Melbourne | 1 |
| The GPS Precise Orbit Demonstration (POD) Experiment, E.S. (Ab) Davis | 25 |
| NRL Activities On Spaceborne GPS Receivers, Ronald L. Beard | 43 |
| GL's Proposed Satellite-to-Satellite Tracking Mission Using GPS: STAGE (STS-GPS Tracking for Anomalous Gravitation Estimation), Christopher Jekeli | 57 |
| GPS Attitude Determination Activities At The Naval Surface Warefare Center, Alan G. Evans | 65 |
| GPS Application To NASA Upper Stages, A. Wayne Deaton | 79 |
| Space Station Freedom GPS Implementation Plans - An Overview, Penny E. Saunders | 95 |
| Recent Results In High-Precision GPS Orbit Determination, Stephen Lichten, Susan Kornreich Wolf, Willy I. Bertiger, Ulf J. Lindqwister, and Geoff Blewitt | 107 |
| Closed Loop Orbit Trim Using GPS, Penina Axelrad and Bradford W. Parkinson | 135 |
| Global Gravity Field Mapping With GPS Tracking Of The Space Shuttle, George J. Priovolos, Triveni N. Upadhyay, and Christopher Jekeli | 161 |
| Techniques Of GPS-Based Precision Orbit Determination For Low Earth Satellites, Sien C. Wu | 179 |
| Ambiguity Bootstrapping To Determine GPS Orbits And Baselines, Charles C. Counselman | 193 |
| Status Of DARPA Guidance And Control Program, Larry Stotts and Joseph M. Aein | 205 |
| "The Multipath Simulator", A Tool Toward Controlling Multipath, George A. Hajj | 229 |



| | |
|----------|-------------------------------------|
| or | <input checked="" type="checkbox"/> |
| | <input type="checkbox"/> |
| | <input type="checkbox"/> |
| on | |
| / | |
| by Codes | |
| and/or | |
| special | |

TABLE OF CONTENTS - VOLUME II

| | |
|---|-----|
| Autonomous Integrated GPS/INS Navigation Filter For Advanced Spacecraft Applications, Triveni N. Upadhyay, George J. Priovolos, Harley Rhodehamel . . . | 245 |
| An Experiment In Attitude, Position And Velocity Determination With Rogue GPS Receivers, Tom K. Meehan . . . | 271 |
| Preliminary GPS Pointing Data Results, Phil Ward . . . | 281 |
| Algorithms For Spacecraft Attitude Determination With GPS, Duncan B. Cox, Haywood S. Satz, Ronald L. Beard, and G. Paul Landis . . . | 303 |
| Preliminary Experimental Performance Of The TOPEX Global Positioning System Demonstration Receiver (GPSDR), Lance Carson . . . | 323 |
| Design and Performance For The GPS Receiver Unit (GPSRU) For The NASA Orbital Maneuvering Vehicle, Roger M. Weninger and Richard Sfeir . . . | 333 |
| Applications Of GPS To Space-Based Tethered Array Radar, Horst Salzwedel, Ken Kessler, and Fred Karkalik . . . | 343 |
| Special Purpose Inexpensive Satellite (SPINSAT) GPS Receiver, Roger M. Weninger, Richard Sfeir, and Ronald L. Beard . . . | 363 |
| The Defense Mapping Agency's Operational GPS Orbit Processing System, James A. Slater . . . | 371 |
| A Shuttle Experiment To Demonstrate 6-Degree-Of-Freedom Navigation With GPS, Duncan B. Cox, Steven Gardner, and Neal Carlson . . . | 415 |
| Large Space Structure Displacement Sensing Using Advanced GPS Technology, Gaylord K. Huth . . . | 437 |
| Alternatives to Becoming an "Authorized User", Thomas Yunck . . . | 445 |
| List of Attendees and Addresses . . . | 453 |

AUTONOMOUS INTEGRATED GPS/INS NAVIGATION FILTER FOR ADVANCED SPACECRAFT APPLICATIONS

Triveni N. Upadhyay, George J. Priovolos, Harley Rhodehamel
MAYFLOWER COMMUNICATIONS CO., Reading, MA

and

A. Wayne Deaton
NASA MARSHALL SPACE FLIGHT CENTER

The paper summarizes the results of a recently completed feasibility study on GPS-based techniques for navigation and attitude update. The motivation for autonomous navigation, and some results for both low-earth and high altitude users are provided. The need for autonomy will grow in the future as missions require faster decision making, continuous coverage and increased survivability. The GPS/INS integrated navigation system offers one solution with increased accuracy and mission flexibility compared to conventional systems.

Three GPS-based attitude determination techniques were analyzed for providing improved total navigation solution. The autonomous integrated navigation filter will use a combination of these techniques, depending on the spacecraft mission phase, to provide the best solution and flexibility in mission planning. The reconfigurability of the integrated navigation filter, in real-time, to adapt to the spacecraft mission phases is also discussed. A knowledge-based navigation filter manager (i.e., expert system) is discussed which will be designed to automatically select the navigation filter states and filter modes depending on the mission phase and available resources, e.g., thrust versus coast phase, one GPS antenna versus multiple GPS antennae, translation versus rotational dynamics, gyro failure versus accelerometer failure.

The integrated navigation filter results presented in this paper correspond to a 17-state Kalman filter which was implemented in its U-D factor formulation for improved numerical stability. Two spacecraft applications: (1) low-earth orbit users (e.g., OMV, Space Station, Shuttle-C) and (2) high altitude users (e.g., NASA GEO platform, Lunar-return and Mars-return transfer vehicles) are analyzed and numerical simulation results are presented for these cases. The LEO user simulated for performance evaluation consisted of an OMV high-thrust trajectory burn of approximately 300

two antennas and to IMUs. We looked at two cases, one where GPS was available prior to a burn phase (good initial conditions) and one where GPS was not available (poor initial conditions). Details are presented for the second case.

The simulation results indicate the excellent performance of the filter even for the case of poor initial conditions. This test case assumed that the OMV did not use GPS during the coast phase and a large position and velocity error had accumulated prior to the start of the burn. The application of the integrated GPS/INS navigation filter allowed the large initial condition errors to be reduced in a short-time and resulted in excellent position, velocity and attitude estimation solution accuracy.

The application of the integrated navigation filter for a high altitude user consisted of a spacecraft at GEO altitude. Since the GPS availability is limited at altitudes higher than 10,000 nmi (the GPS satellite antennae are pointed towards the earth), the availability of a high gain antenna and a rubidium clock onboard the spacecraft was assumed for this analysis. The simulation results for a GEO STV user, with the above assumptions, were obtained. These results further support the utility of GPS for high altitude spacecraft missions. It is believed that for these missions GPS may be the sole provider of the required navigation accuracies.

The application of autonomous integrated GPS/INS system technology is shown in this paper to provide excellent total navigation performance, flexibility in contingency mission planning, and may help eliminate attitude update sensors which will reduce the cost and size, power and weight for a wide class of spacecraft missions.

A successful application of GPS tracking of advanced spacecraft will alleviate the requirement for ground tracking (or TDRSS tracking), and the real-time onboard reconfigurability feature of the integrated navigation filter will reduce the cost of mission planning and will support the NASA requirement of developing advanced fault-tolerant spacecraft missions.

AUTONOMOUS INTEGRATED GPS/INS NAVIGATION FILTER

- GPS-based navigation and attitude update techniques
- Navigation filter reconfigurability
 - Autonomy
- Application
 - low earth orbit users (OMV, Space Station, Shuttle-C)
 - high altitude users (GEO platform, Lunar-return transfer vehicles LTV, Mars-return transfer vehicles)

AUTONOMOUS INTEGRATED GPS/INS NAVIGATION FILTER

Onboard Autonomous Capability

- Need for autonomous systems will continue in the future
 - Faster decisions
 - Continuous coverage
 - Increased survivability
- Current spacecraft tracking systems, such as Ground Spacecraft Tracking Data Network (GSTDN) and TDRSS have limited coverage and accuracy
- Requirement for improved navigation accuracy and autonomy has resulted in heavy reliance on GPS. Previous efforts have not fully explored the synergism between GPS and INS
- The GPS/INS navigation system tightly integrates the two systems resulting in:
 - Improved accuracy
 - Flexibility in mission planning

AUTONOMOUS INTEGRATED GPS/INS NAVIGATION FILTER

Navigation Accuracy and Coverage

TABLE I: Shuttle - Onorbit Navigation Accuracies

| Tracing System | Position (Km) | | | Velocity (m/s) | | |
|---------------------------|---------------|-------------|-------------|----------------|-------------|-------------|
| | Radial | Along Track | Cross Track | Radial | Along Track | Cross Track |
| GSTDN | 1.5 | 10.5 | 1.5 | 11.7 | 1.8 | 3.0 |
| TDRSS | 1.1 | 5.6 | 1.2 | 6.7 | 1.0 | 1.2 |
| GPS (18-SV Constellation) | 0.03 | 0.03 | 0.03 | 0.1 | 0.1 | 0.1 |

TABLE II: Shuttle Tracking Coverage

| Tracking System | Percent Coverage |
|-----------------|------------------|
| GSTDN | 15% |
| TDRSS | 85% |
| GPS (1992) | 100% |

AUTONOMOUS INTEGRATED GPS/INS NAVIGATION FILTER

GPS-Based Attitude Techniques

- The three GPS-based attitude determination techniques employed here are:
 1. Velocity vector matching technique employing one GPS antenna during spacecraft orbit maneuvers
 2. Interferometric GPS carrier phase processing technique using two or more antennae during spacecraft coast and maneuver phases
 3. Attitude vector matching technique employing one GPS antenna during spacecraft rotation maneuvers
- The autonomous integrated GPS/INS navigation experiment will use a combination of these techniques for providing improved total navigation solution

AUTONOMOUS INTEGRATED GPS/INS NAVIGATION FILTER

- The navigation filter is implemented in the Mayflower GPS Inertial Navigation System Simulator (GINSS) Software
 - 17 - state Kalman filter in its U-D factor formulation
 - Reconfigurable at run-time (novel feature)
 - Navigation Filter Designer (Automatic Selection and inclusion of relevant filter modes and error states depending on mission phase)
 - Switch between absolute/relative navigation and attitude determination
 - Identify and include error states of interest
 - Will be developed in Ada (Portability to NASA and DoD missions)

AUTONOMOUS INTEGRATED GPS/INS NAVIGATION PROCESSING FOR THE OMV (Proof-Of-Concept Demonstration)

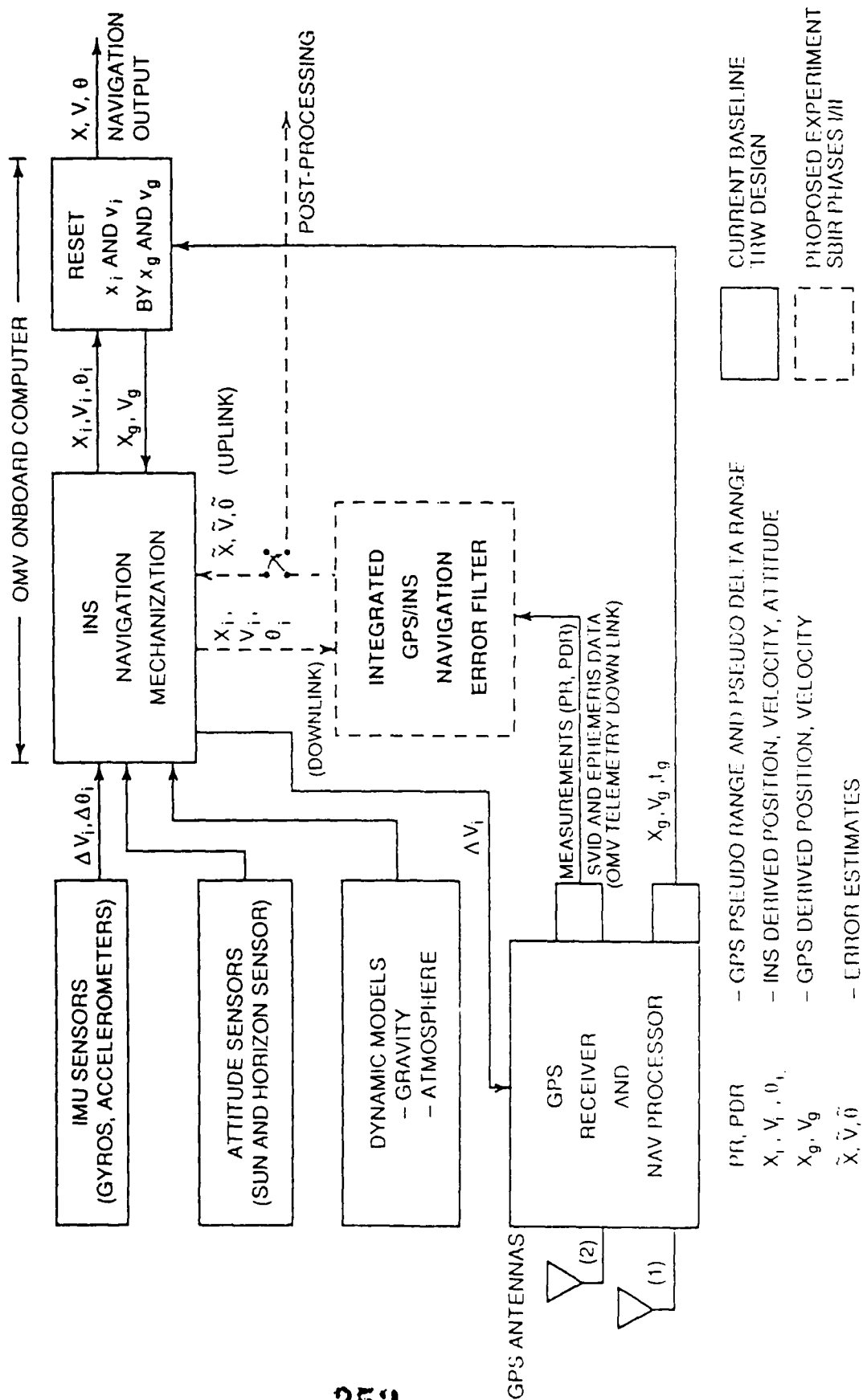


FIGURE 2

AUTONOMOUS INTEGRATED GPS/INS NAVIGATION FILTER

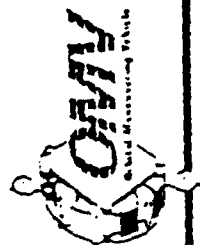
GINSS (GPS-Inertial Navigation System Simulator) Overview

- Developed by Mayflower as a general tool
 - Navigation system simulation and performance analysis
- Covariance analysis and Monte Carlo capability
- Previous applications
 - NASA/MSFC: GPS-attitude determination (velocity vector matching)
 - DARPA/Raytheon: Integrated GPS-INS system
 - AFGL: Study of inertial transfer alignment
- Targeted on DEC VAX and 80386-based PC
- Written in FORTRAN
 - Approximately 75 modules and 12,000 lines of code

AUTONOMOUS INTEGRATED GPS/INS NAVIGATION FILTER

I. LOW-ORBIT USER: OMV APPLICATION

- GPS Receiver
 - 2 channel sequential unit developed by Rockwell International
 - Data rate 1 per second
 - Error model
 - Pseudo-range measurement noise = 1.8 m (1- σ)
 - Delta-range measurement noise = 2.5 cm (1- σ)
 - Clock frequency drift noise = 10^{-8} sec/sec (1- σ)
- Inertial Measuring Unit
 - 2 Mod II E/S gyroflex gyros
 - 3 Mod VII accelerometers
 - Error Model
 - Gyro bias drift = 0.022 deg/hr (3- σ)
 - Gyro input axis alignment = 7 arcsec (3- σ)
 - Gyro scale factor stability = 93 ppm (3- σ)
 - Accelerometer bias stability = 27 micro-g (3- σ)



LOW GAIN ANTENNA ASSEMBLY (REVISED PLUME IMPINGEMENT CONFIGURATION)

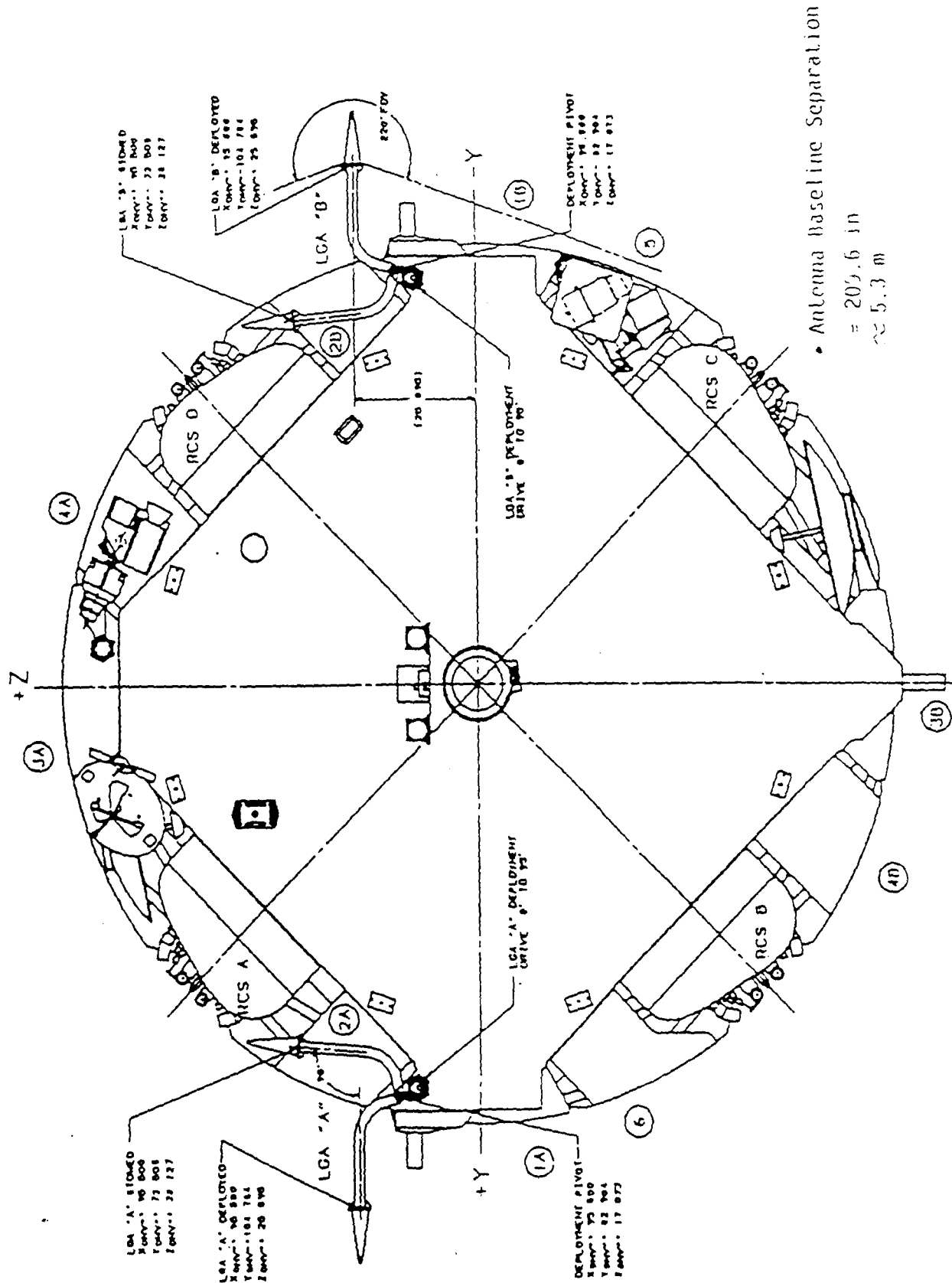
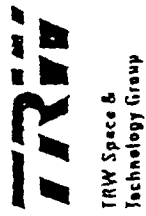


Figure 3: Location of the GPS Antennae on the OMV

AUTONOMOUS INTEGRATED GPS/INS NAVIGATION FILTER

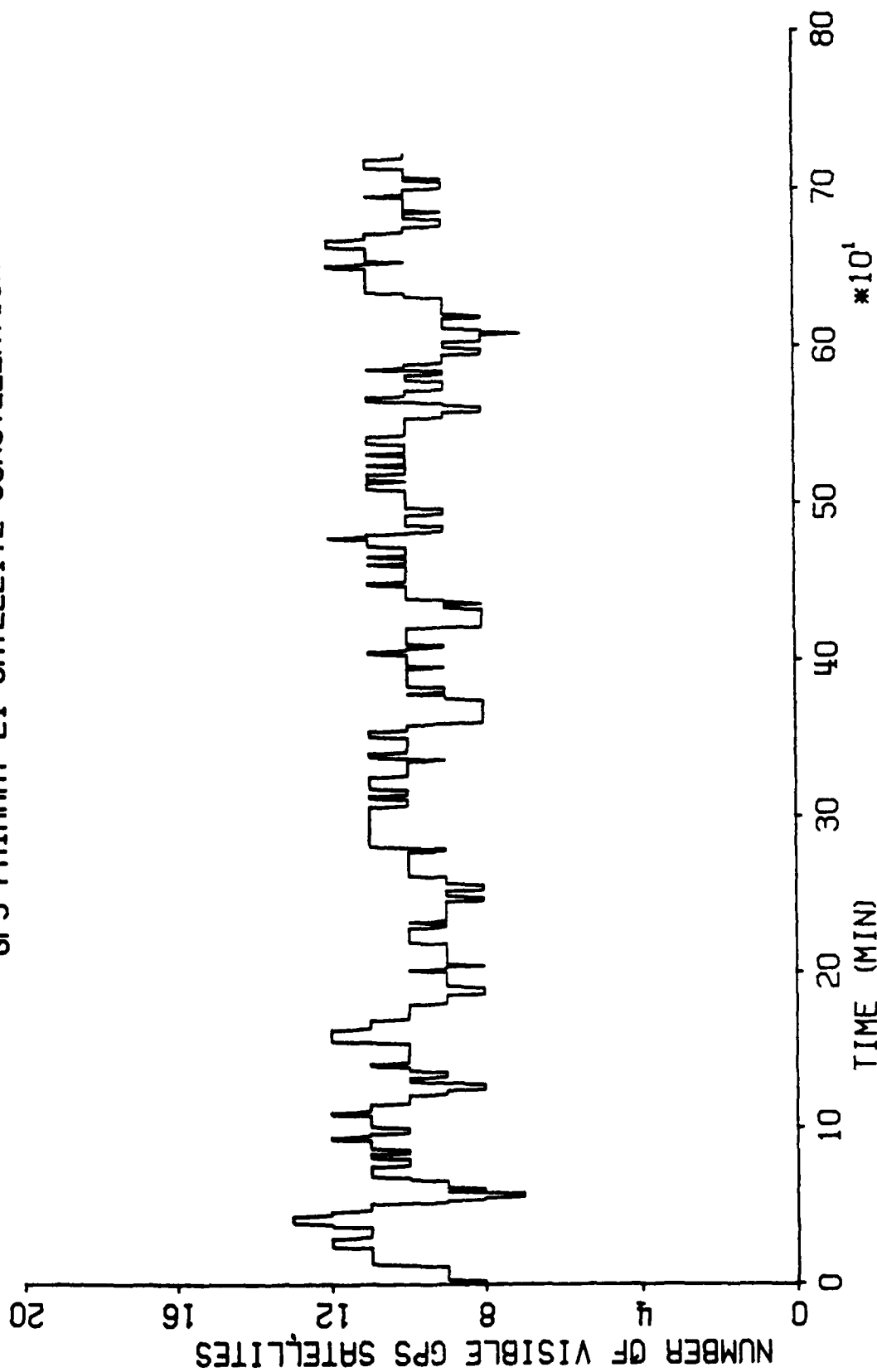
- High thrust trajectory - 5.5 minutes
- Two Cases
 - Good initial conditions (correspond to GPS update prior to burn stage), 1-sigma
 - Position 15 m
 - Velocity 0.1 m/sec
 - Tilt 1 degree
 - Clock bias 1 μ sec
 - Poor initial conditions (correspond to GPS outage prior to burn stage)
 - Position 50 km
 - Velocity 70 m/sec
 - Tilt 5 degrees
 - Clock bias 1 sec
- Excellent performance of filter under both conditions

OMV Simulation Results

Test Case II : Poor Initial Conditions

AUTONOMOUS INTEGRATED GPS/INS NAVIGATION FILTER

VISIBILITY TEST WITH ONE ANTENNA
GPS PRIMARY 21 SATELLITE CONSTELLATION

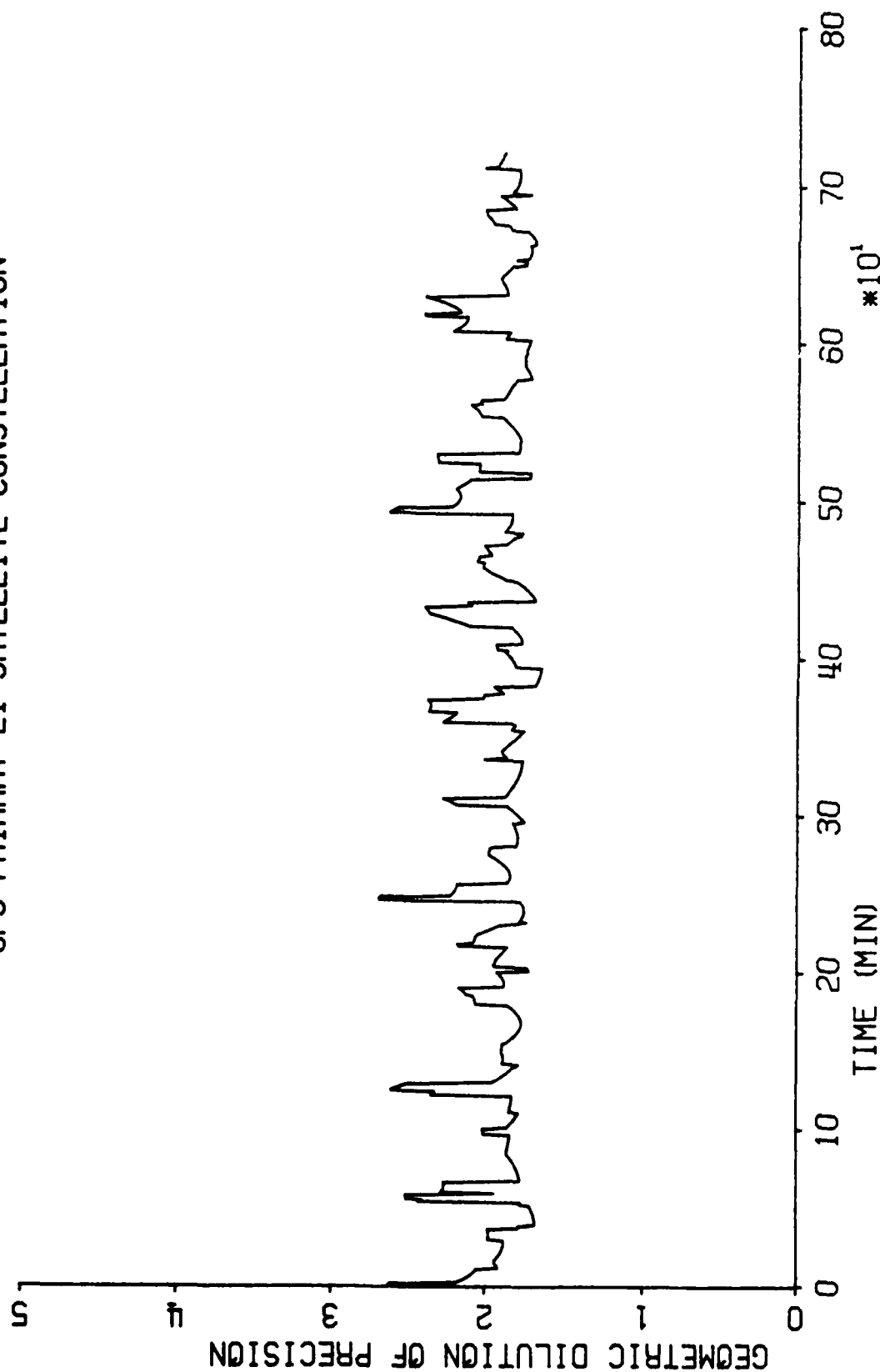


EVALUATION FOR A 12 HOUR PERIOD - ZENITH ANGLE = 110 DEG

INCLINATION=55 DEG, ALTITUDE=1000 N.MI.

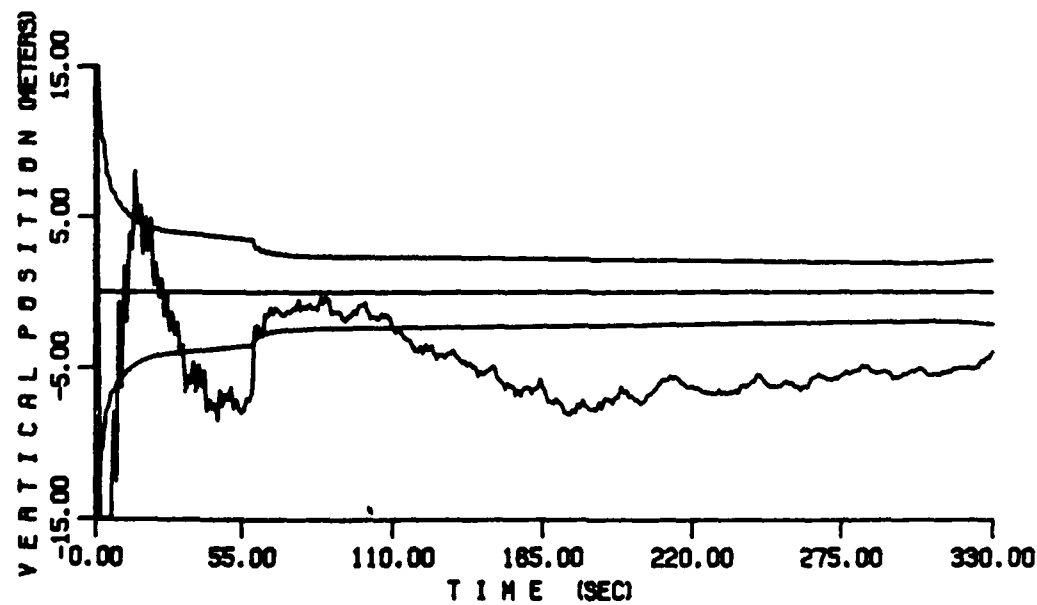
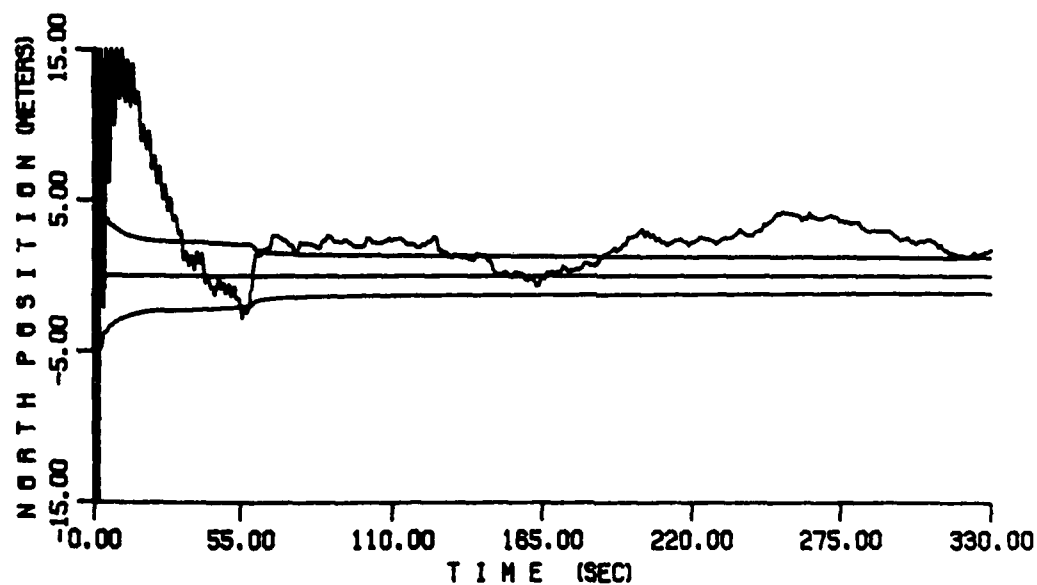
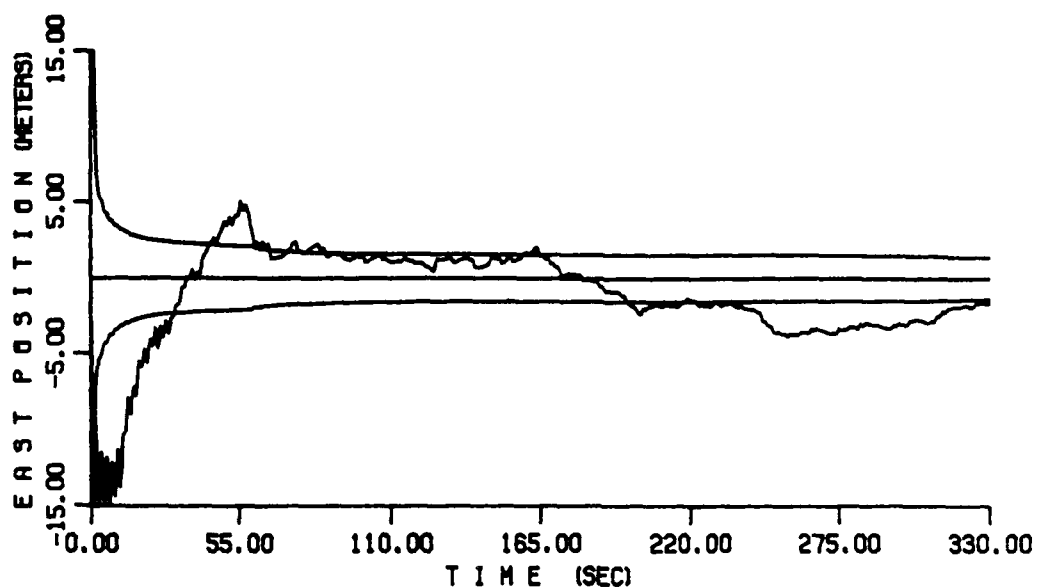
AUTONOMOUS INTEGRATED GPS/INS NAVIGATION FILTER

VISIBILITY TEST WITH ONE ANTENNA
GPS PRIMARY 21 SATELLITE CONSTELLATION

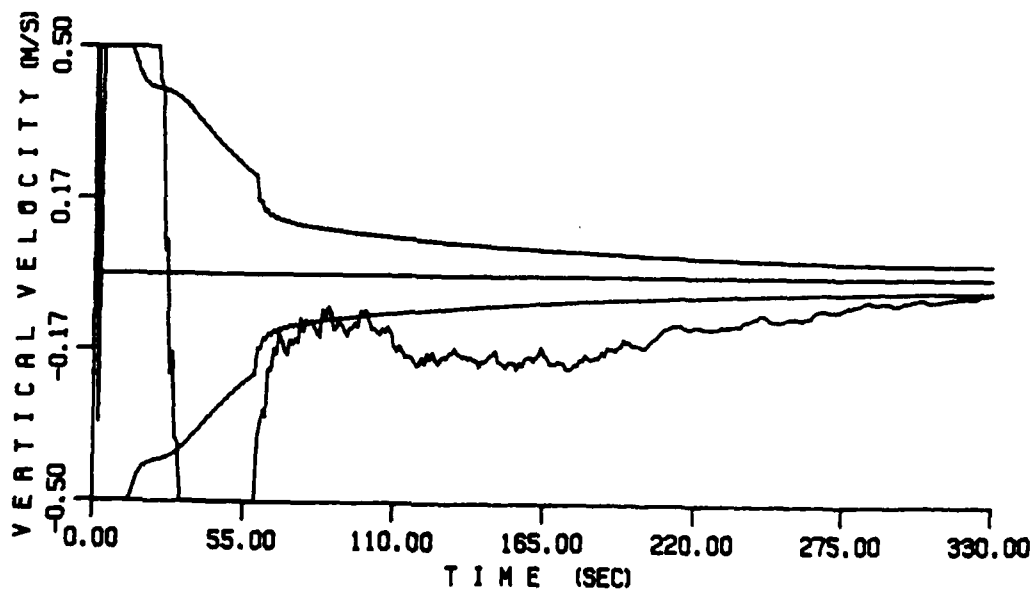
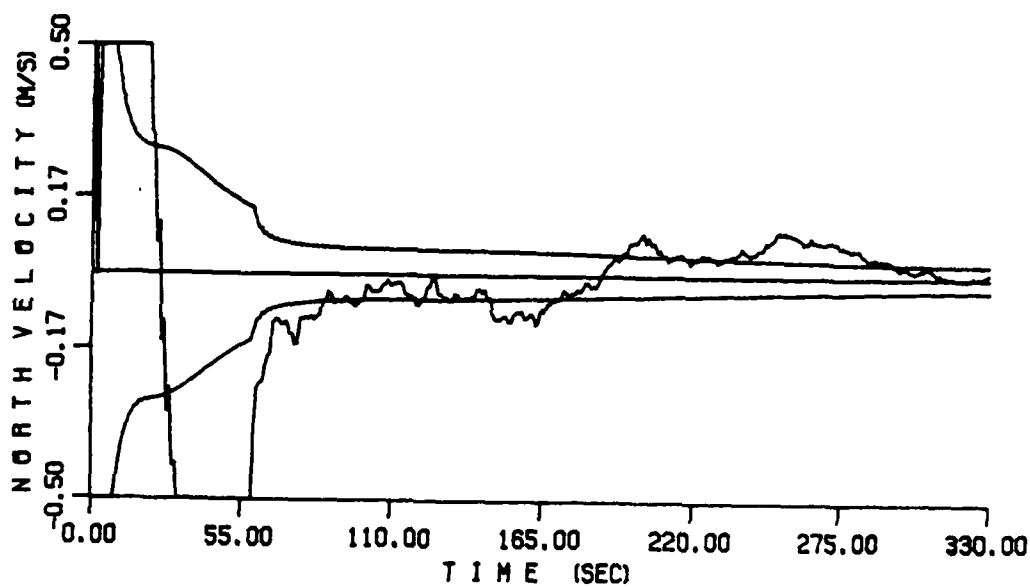
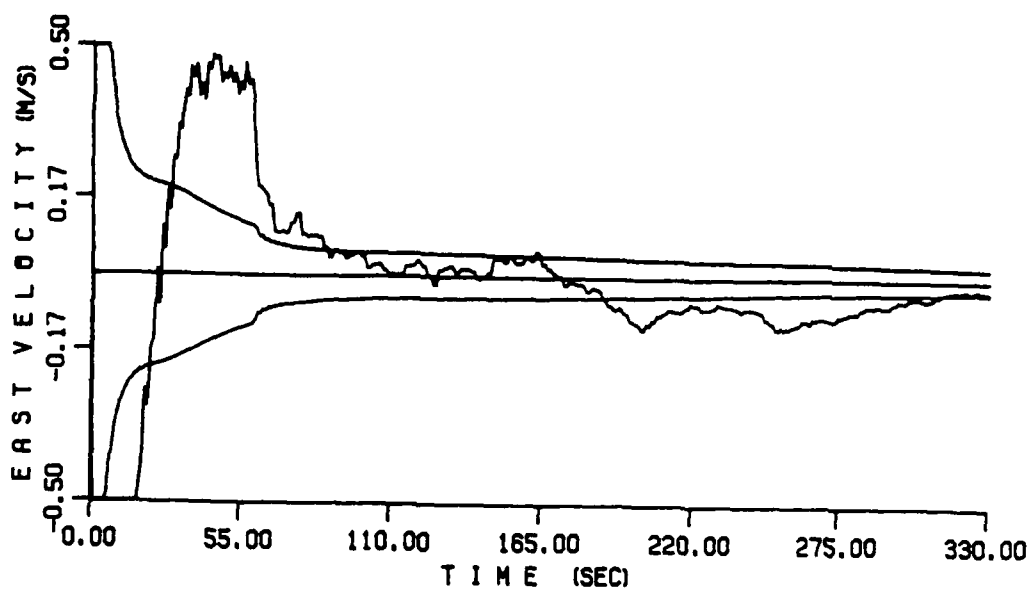


EVALUATION FOR A 12 HOUR PERIOD - ZENITH ANGLE = 110 DEG
INCLINATION=55 DEG, ALTITUDE=1000 N.MI.

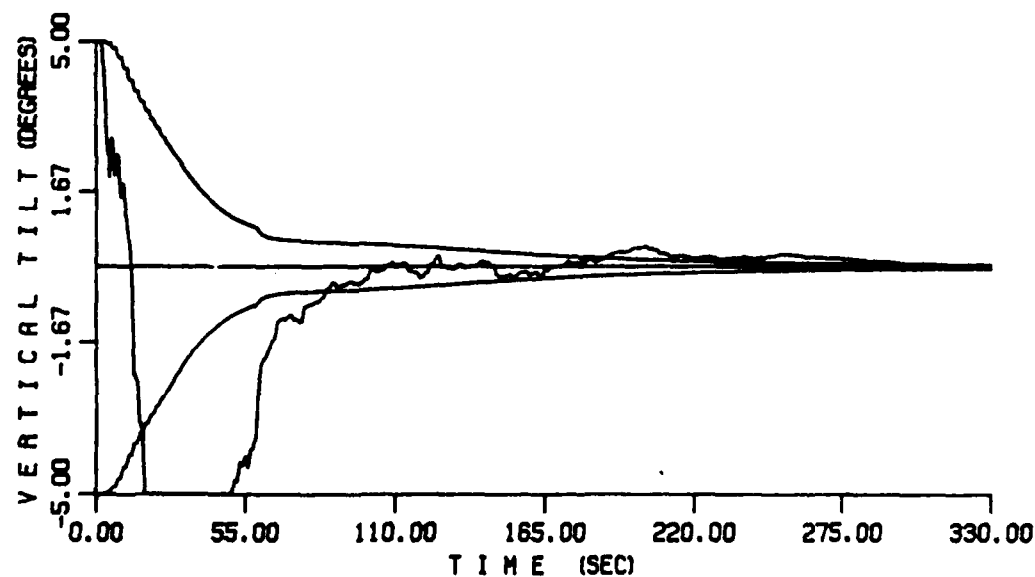
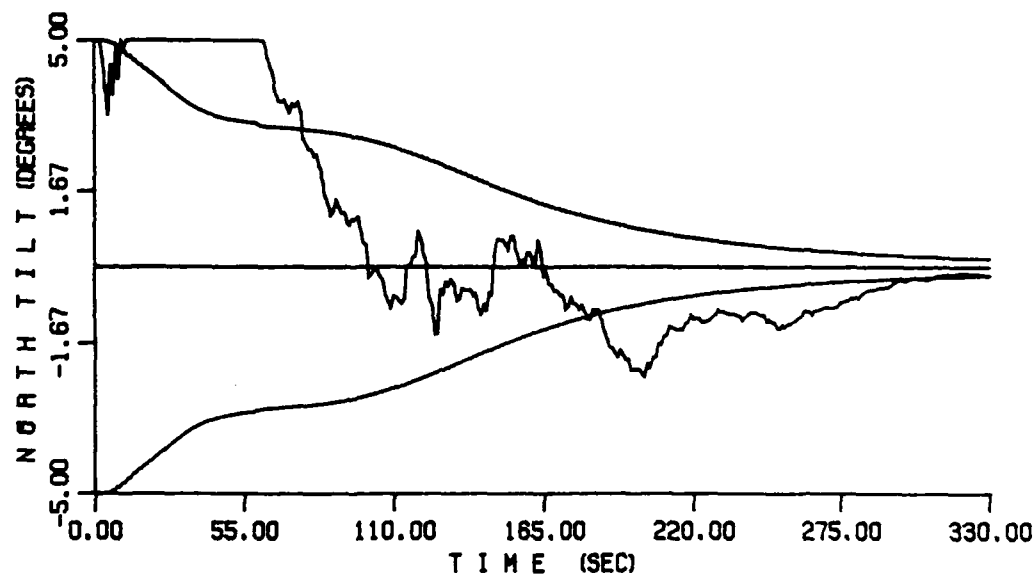
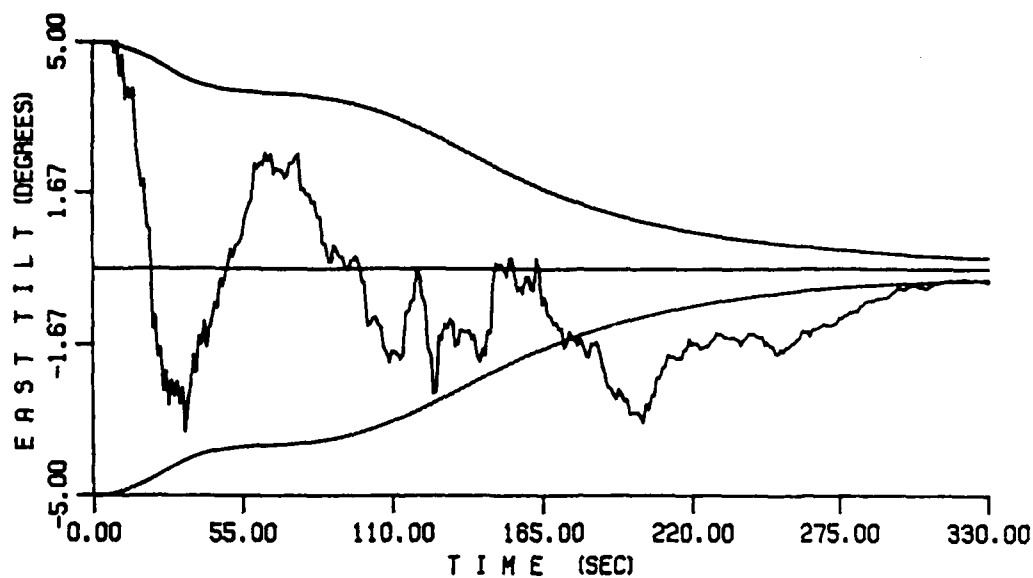
AUTONOMOUS INTEGRATED GPS/INS NAVIGATION FILTER



AUTONOMOUS INTEGRATED GPS/INS NAVIGATION FILTER



AUTONOMOUS INTEGRATED GPS/INS NAVIGATION FILTER

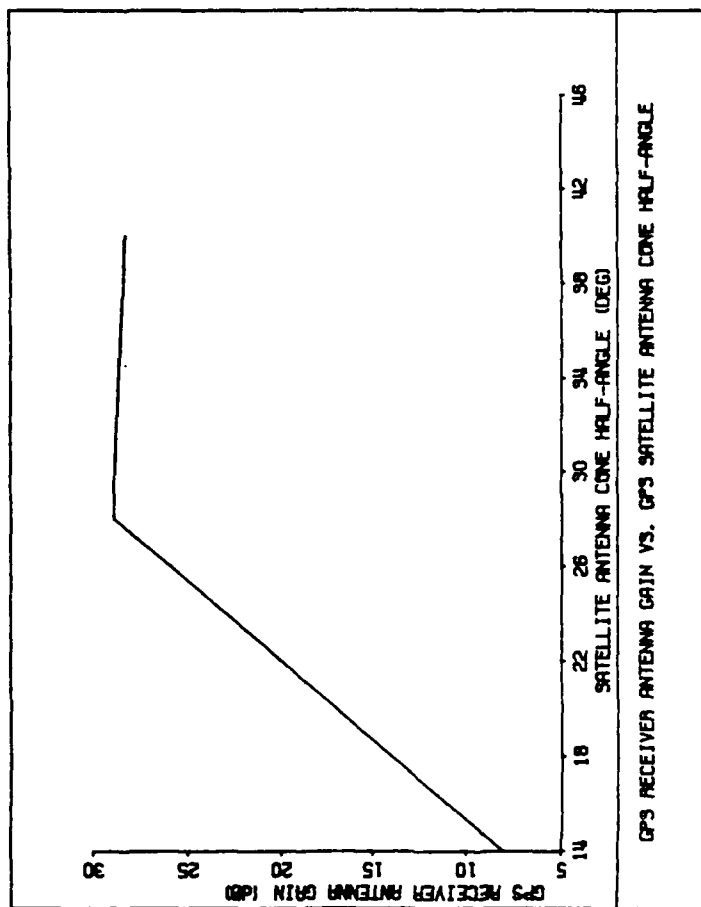
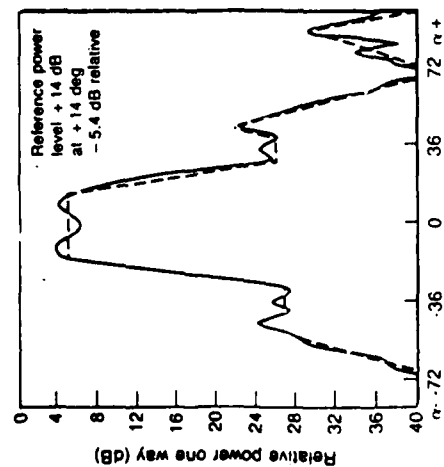


AUTONOMOUS INTEGRATED GPS/INS NAVIGATION FILTER

II. HIGH ALTITUDE USER: STV APPLICATION

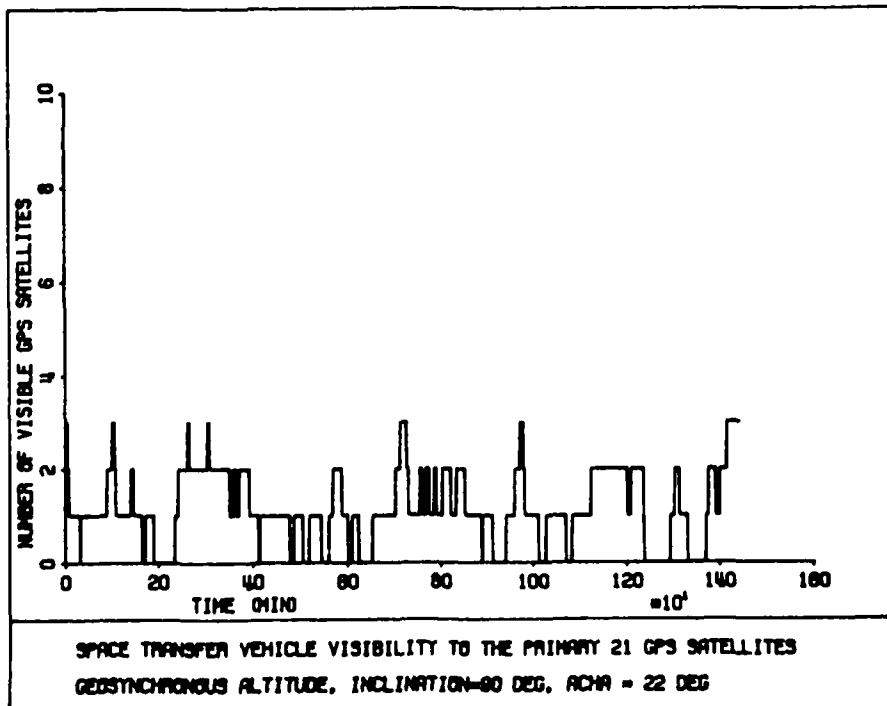
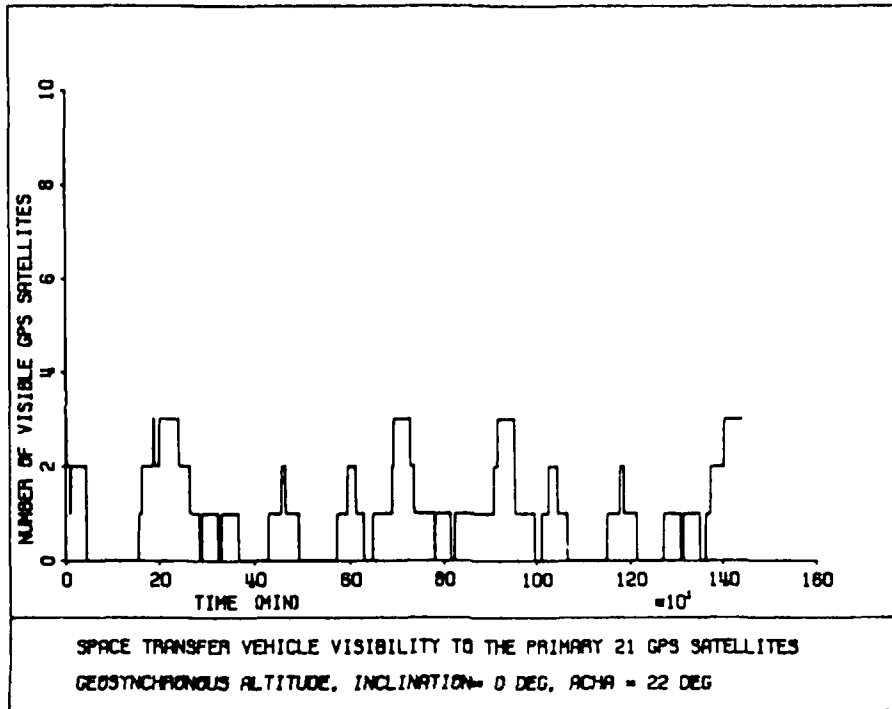
- For GPS code and carrier tracking a signal-to-noise power threshold of 30 dB Hz is assumed
- Need about 20 dB gain for a 22 degree GPS satellite antenna cone half-angle
- Visibility
 - There are periods of GPS outages
 - Average number of visible GPS satellites = 1
- Navigation filter performance
 - Coast phase - 24 hours
 - OMV GPS receiver and IMU models were used
 - Poor Initial conditions
 - Rubidium clock (Drift = 10^{-12} sec/sec)

AUTONOMOUS INTEGRATED GPS/INS NAVIGATION FILTER

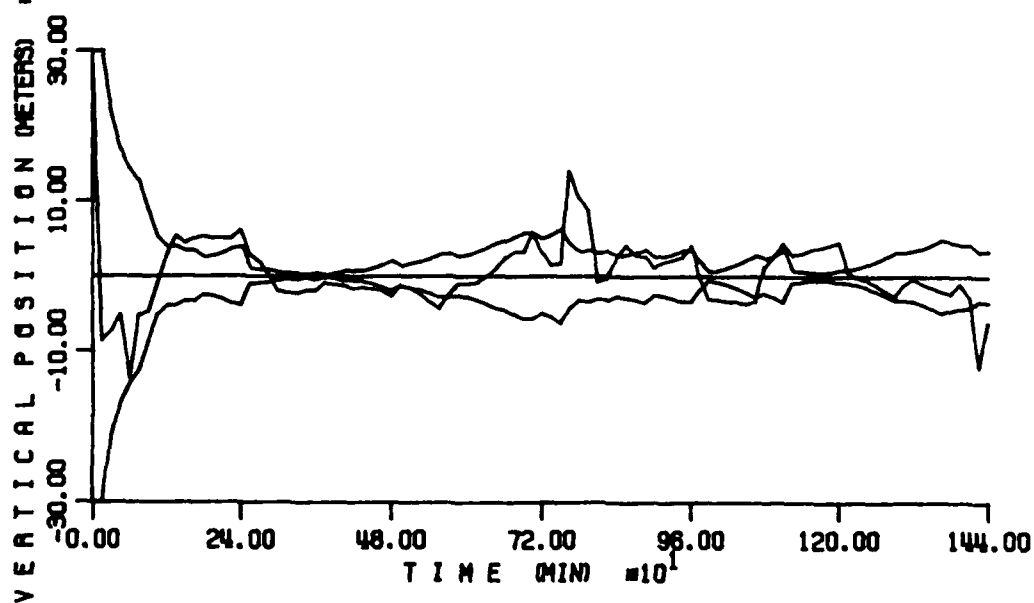
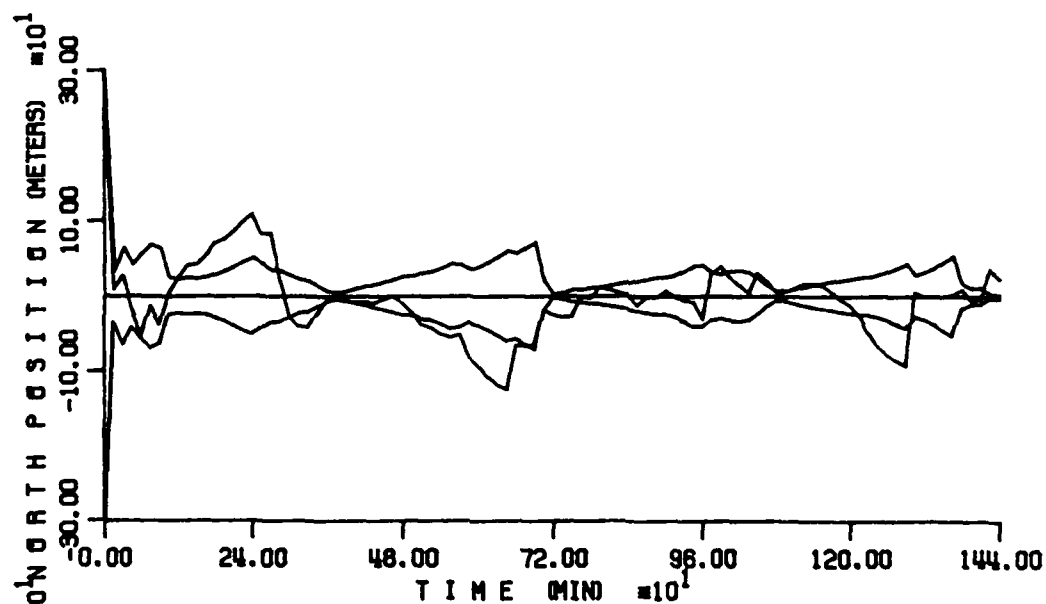
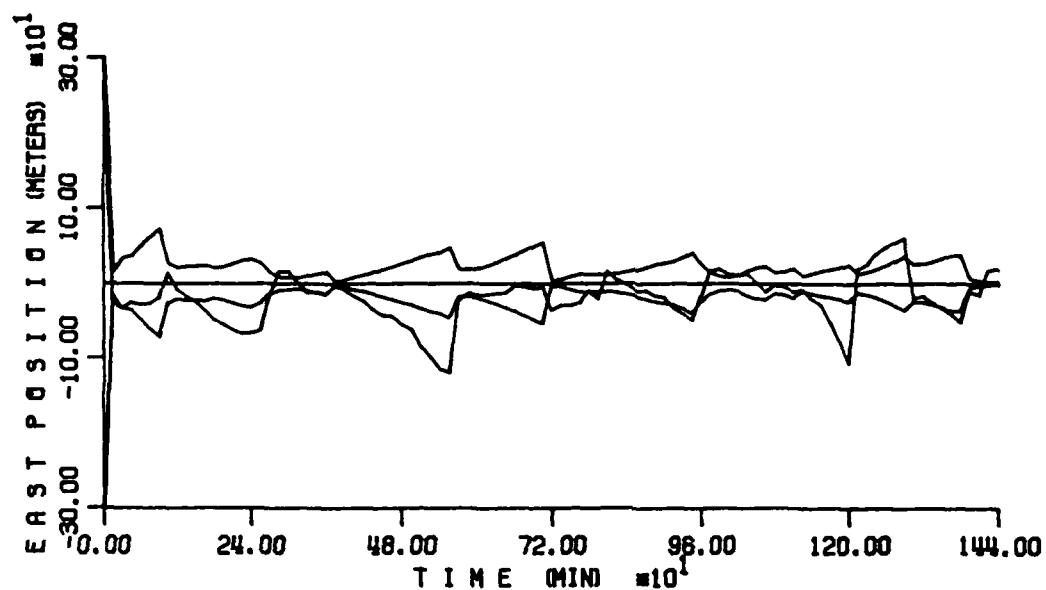


AUTONOMOUS INTEGRATED GPS/INS NAVIGATION FILTER

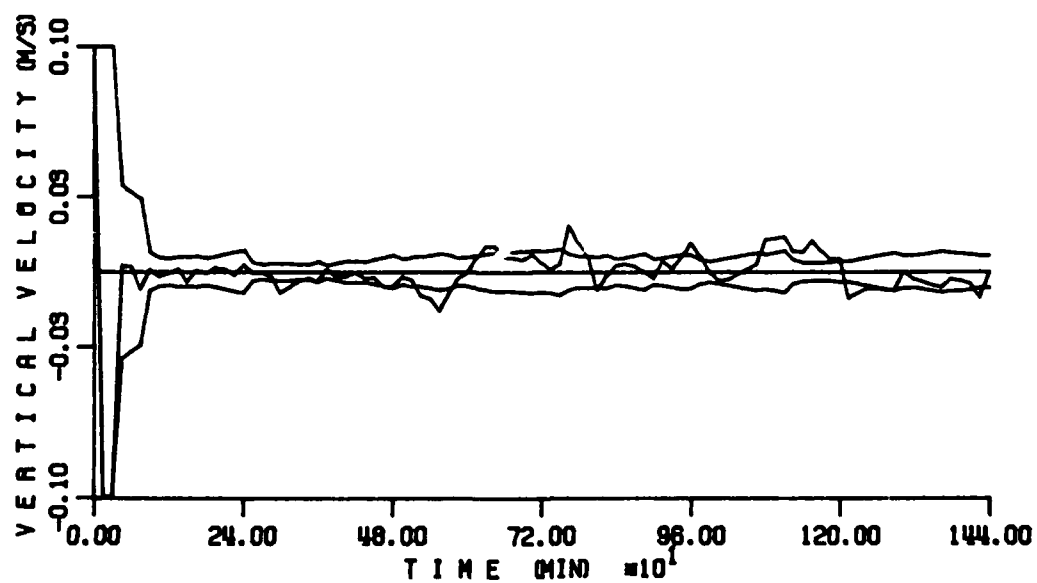
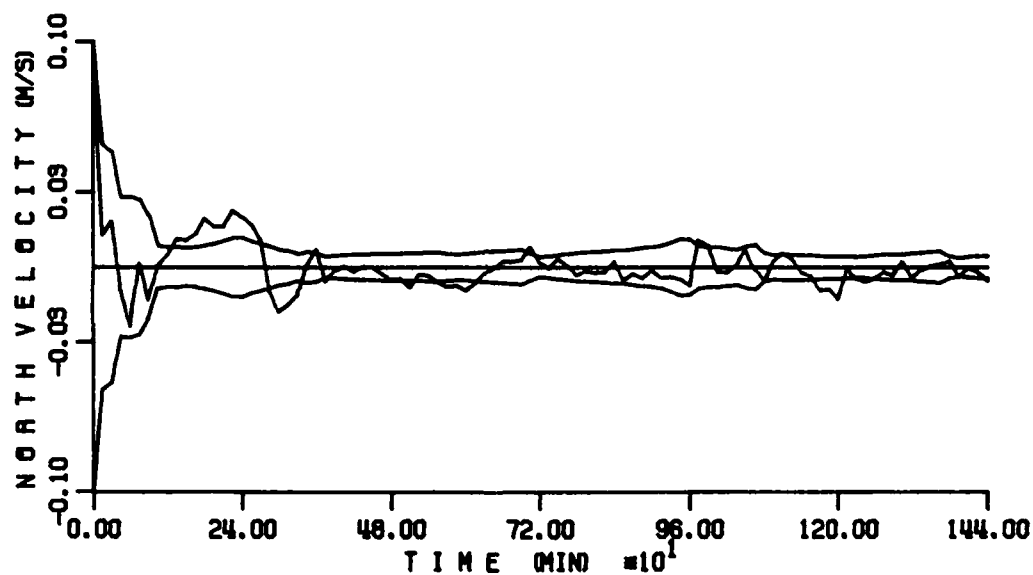
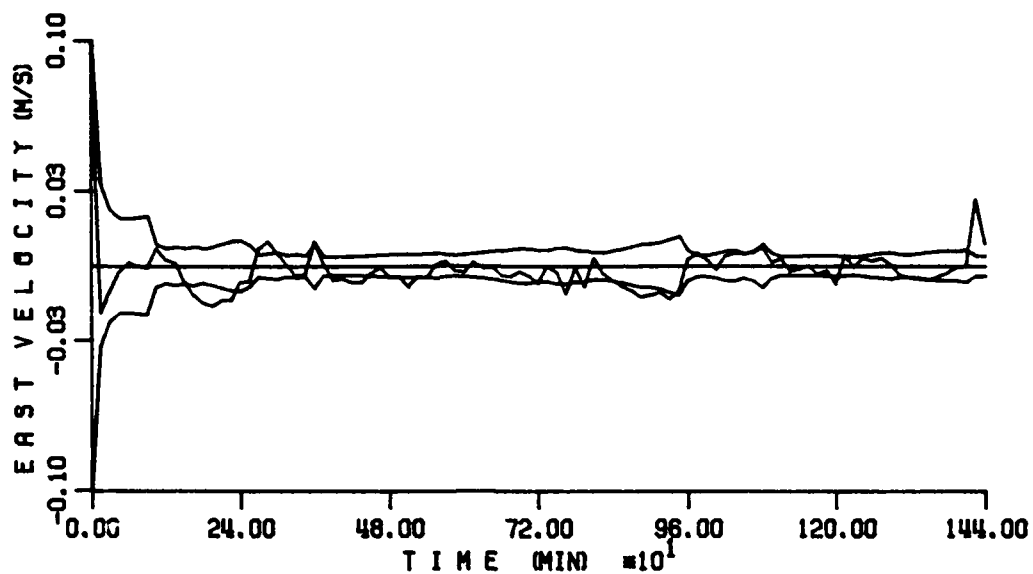
GPS Satellite Visibility for the STV



AUTONOMOUS INTEGRATED GPS/INS NAVIGATION FILTER



AUTONOMOUS INTEGRATED GPS/INS NAVIGATION FILTER



AUTONOMOUS INTEGRATED GPS/INS NAVIGATION FILTER

SUMMARY

- Integrated GPS/Inertial system technology augments the current navigation and attitude update capability of advanced spacecraft missions
- low earth users (LEO), such as OMV, Space Station, Shuttle-C will receive maximum benefit via improved performance
 - excellent GPS availability
 - OMV (low Earth user with very good GPS satellite visibility)
 - RSS Position Error: 1.6 m (1- σ)
 - RSS Velocity Error: 0.03 m/sec (1- σ)
 - RSS Tilt Error: 0.18 degrees (1- σ)
- high altitude users, such as GEO Platform, Lunar-return and Mars-return missions can potentially use this technology to obtain critical navigation data to complete their mission
 - limited GPS availability
 - STV (geosynchronous user with almost poor GPS satellite visibility)
 - RSS Position error: 47 m (1- σ)
 - RSS Velocity error: 0.013 m/sec (1- σ)

AUTONOMOUS INTEGRATED GPS/INS NAVIGATION FILTER

SUMMARY (continued)

- Application of Integrated GPS/Inertial system technology provides improved total navigation performance and flexibility in contingency mission planning
 - may eliminate attitude update sensors
- An onboard real-time Integrated GPS/Inertial system can be designed without seriously constraining the onboard computing resources (within 10-20%).

AN EXPERIMENT IN ATTITUDE, POSITION AND VELOCITY DETERMINATION WITH ROGUE GPS RECEIVERS

Tom K. Meehan
JET PROPULSION LABORATORY

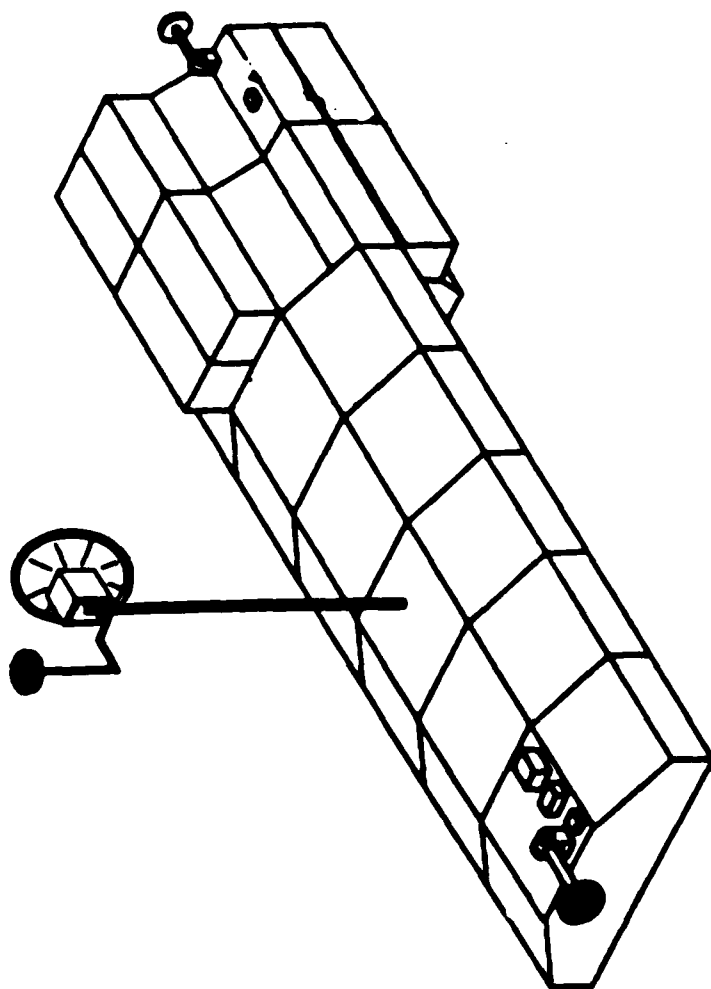
An experiment was performed on an aircraft to investigate the attitude determination capability of GPS. This was done in anticipation of an application on EOS, to be launched in 1996, which will have three antennas as shown and a GPS receiver similar to the JPL Rogue receiver with 1 cm accuracy for pseudorange and submillimeter for carrier phase. The goal with EOS is to get real-time attitude determination of about 0.1 mrad, real-time position error of about 1 m, and post-processing errors of 0.03 mrad and a few centimeters, respectively.

Another objective of the aircraft experiment was to prove the concept of using Rogue GPS receivers to calibrate SAR (Synthetic Aperture Radar) measurements to obtain ocean current velocities. Two SAR antennas on the bottom of the aircraft fuselage are side looking (45°), one transmits, both receive. From the interferometric recombination of the two received signals one can determine the ocean wave propagation (i.e., current velocity). One significant error source is yaw and pitch in the aircraft; e.g., an error of 0.01° in yaw yields an error of 4 cm/s in current velocity versus a requirement of about 0.6 cm/s.

GPS was used to demonstrate the potential for controlling these errors - the initial goal was to achieve an accuracy of 0.1° in pitch and yaw. Two antennas were mounted on a DC-8 and two Rogue GPS receivers were used (8 satellites, L1, L2 carrier phases, P1, P2 codes, 1 s data rate). A twenty-minute segment in which 4 satellites were simultaneously visible by both antennas was extracted from the test flight. The first graph shows the heading of the aircraft as determined from the velocity which was obtained by differencing GPS position information. The second graph shows the difference between heading and azimuth and reveals the 3° bias due to the second GPS antenna not being on the center line of the aircraft and a drift due to change in wind velocity (pilot had to introduce yaw). Most of the detailed features of this plot are real (not noise) and due to aircraft maneuvers.

The results were better than our goals for pitch and yaw. The largest error source precluding the achievement of SAR requirements is multipath. A repositioning of the rear antenna would improve this as would the availability of more GPS satellites.

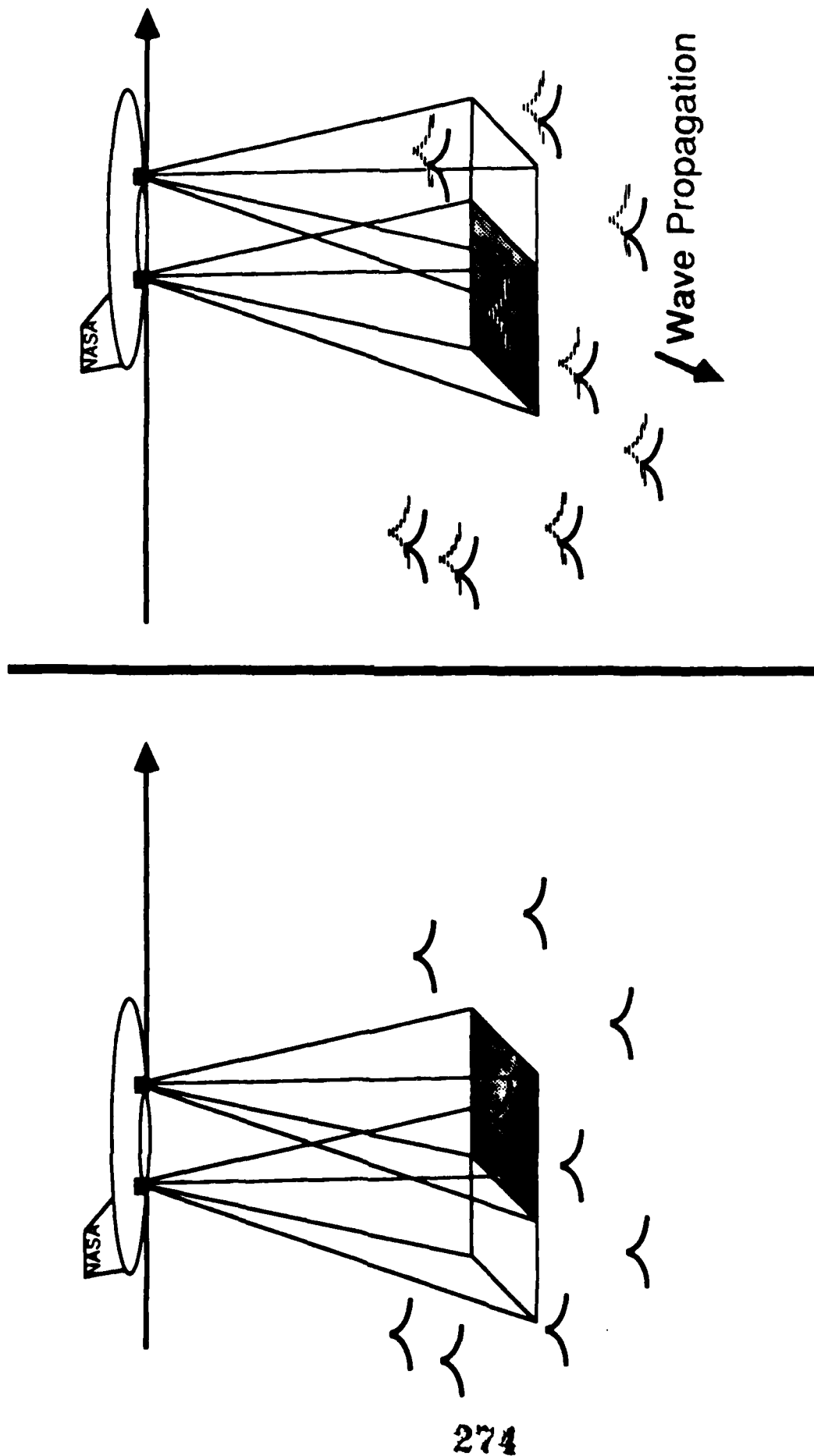
GPS Antenna Placement for Eos-A Platform



Purpose of SAR Experiment:

Demonstrate GPS capability for precise attitude determination

Demonstrate ability of Rogue GPS receivers for calibrating SAR measurements of ocean currents



**Calibration Requirements for Mid-ocean mapping
and Demonstration Goals:**

| | Mapping Requirement | Demo Goal |
|----------|---------------------|-----------|
| Position | 10 m | 0.1 m |
| Velocity | 0.6 cm/s | 0.1 cm/s |
| Yaw | 0.002 deg. | 0.1 deg. |
| Pitch | 0.002 deg. | 0.1 deg. |

**FLIGHT PATH
05-23-88**

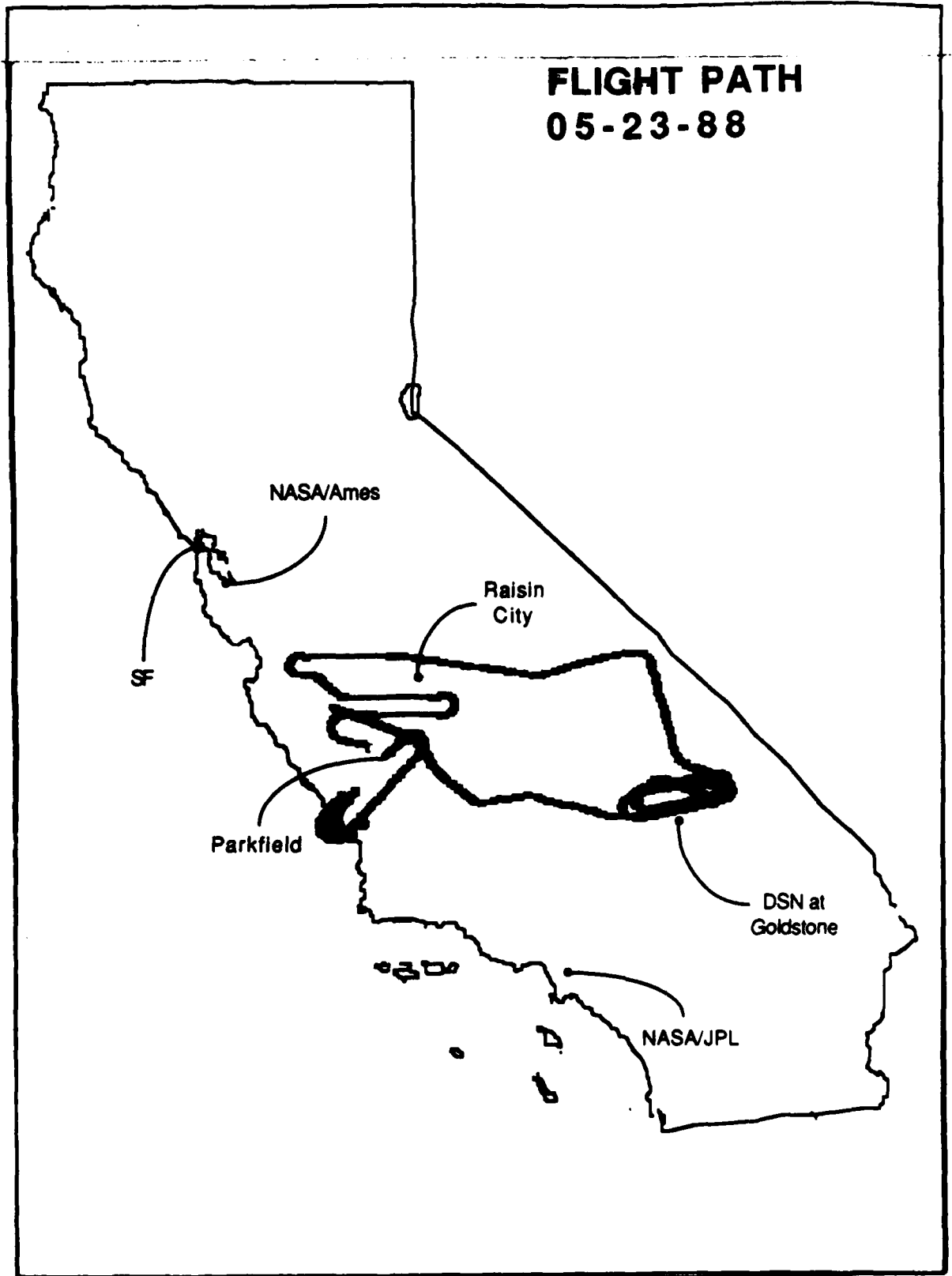


FIGURE 1

AZIMUTH OF AIRCRAFT VELOCITY

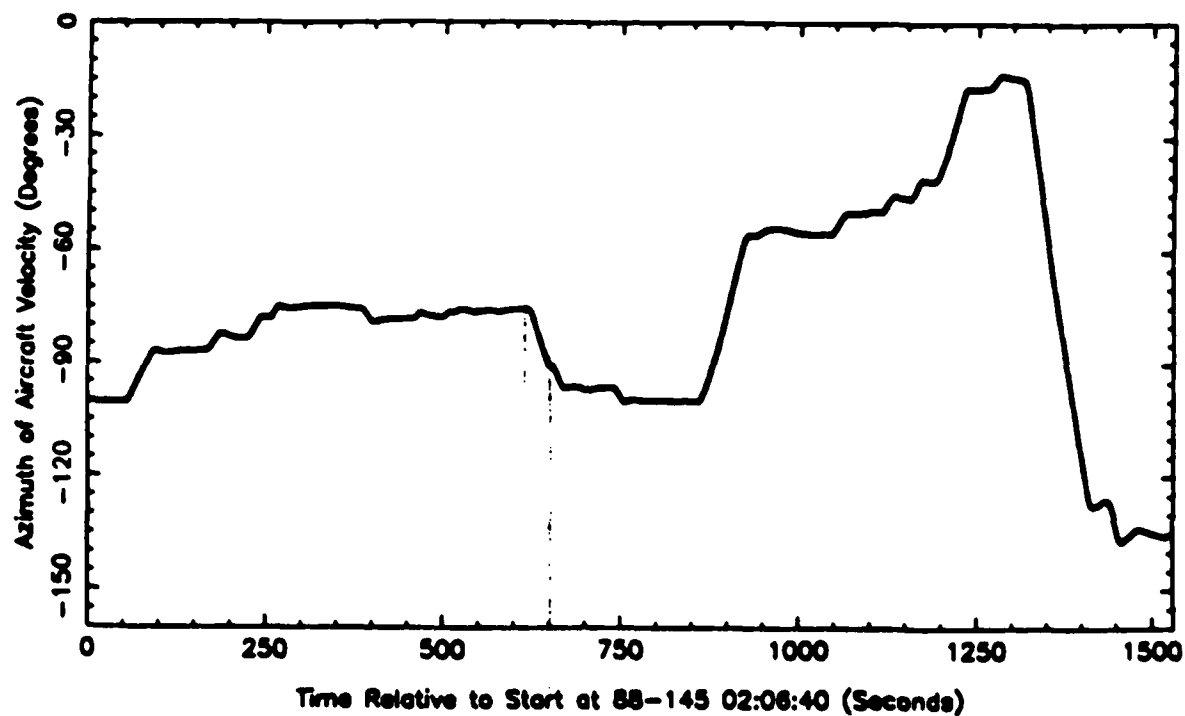
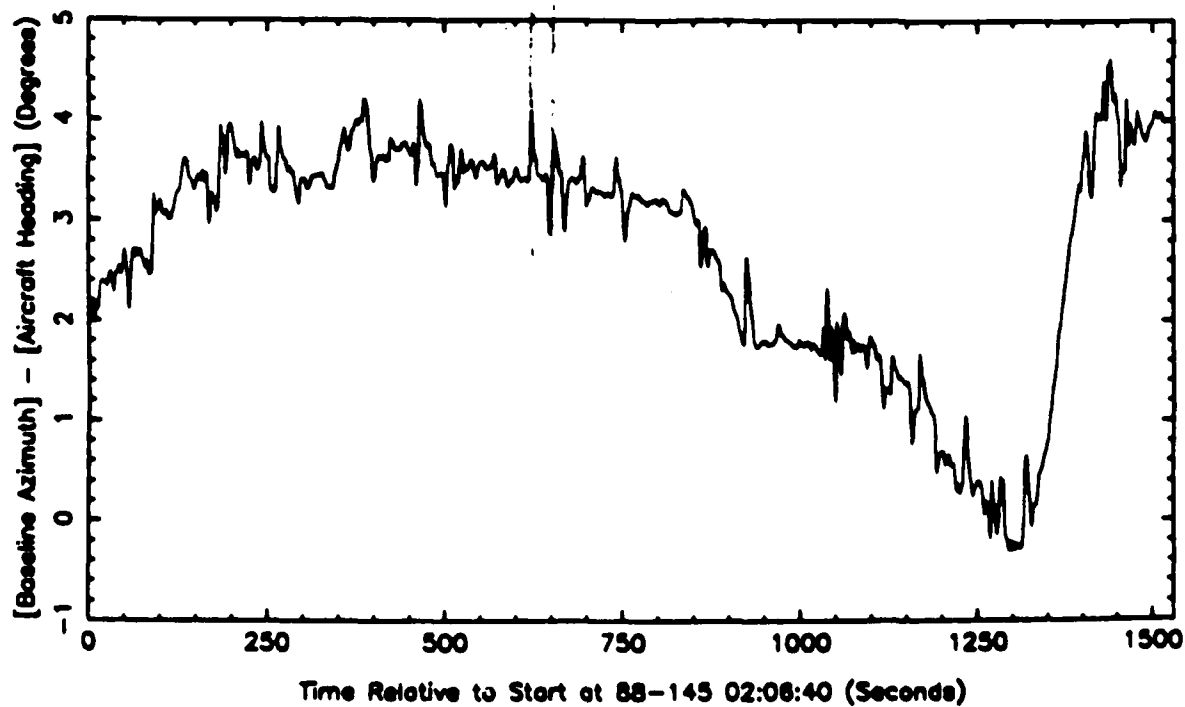


FIGURE 2

OFFSET OF BASELINE AZIMUTH FROM AIRCRAFT HEADING, L1



Error Budget for Demo Results

| Error Source | Azimuth (deg.) | Pitch (deg.) |
|--------------|-------------------|-----------------|
| Orbit | <0.0001 | <0.0001 |
| Multipath | 0.012 | 0.038 |
| System Noise | 0.0012 | 0.0030 |
| Ionosphere | <0.0001 | <0.0001 |
| Troposphere | <0.0001 | <0.0001 |
| Total (RSS) | 0.0121 | 0.0381 |
| Demo Goal | 0.1 | 0.1 |
| Eos Goal | 0.008 | 0.008 |

JPL

Future Developments

Lower Multipath Errors

More Satellites Simultaneously Tracked

PRELIMINARY GPS POINTING DATA RESULTS

BY

PHIL WARD

SENIOR MEMBER TECHNICAL STAFF
TEXAS INSTRUMENTS INCORPORATED
6600 CHASE OAKS BOULEVARD
P.O. BOX 869305 MS 8449
PLANO, TEXAS 75086
(214) 575-3824

PRELIMINARY GPS POINTING DATA RESULTS ABSTRACT

GPS attitude measurement promises to become a cost effective source of precise alignment and calibration for inertial systems on space platforms whose orbits are within GPS coverage such as low earth orbit satellites, the Space Shuttle and the Space Station. GPS has already proven itself to be effective for determining an ultra precise vector between two GPS antennas for first order geodetic surveying using carrier doppler phase interferometry techniques. The same principles can be applied to obtain two orthogonal pointing vectors to provide attitude determination. Two advantages of GPS pointing over geodetic surveying are that the antenna phase center separation (the absolute value of the unknown vector) is known a priori and the antennas are one to ten meters apart rather than thousands of meters. The known antenna separation can be used to speed up the solution of the phase ambiguity problem while the close proximity of the antennas ensures negligible differential atmospheric delay error, permits the differential multipath error to be smaller and a single dual port GPS receiver can be used to obtain both sets of observables.

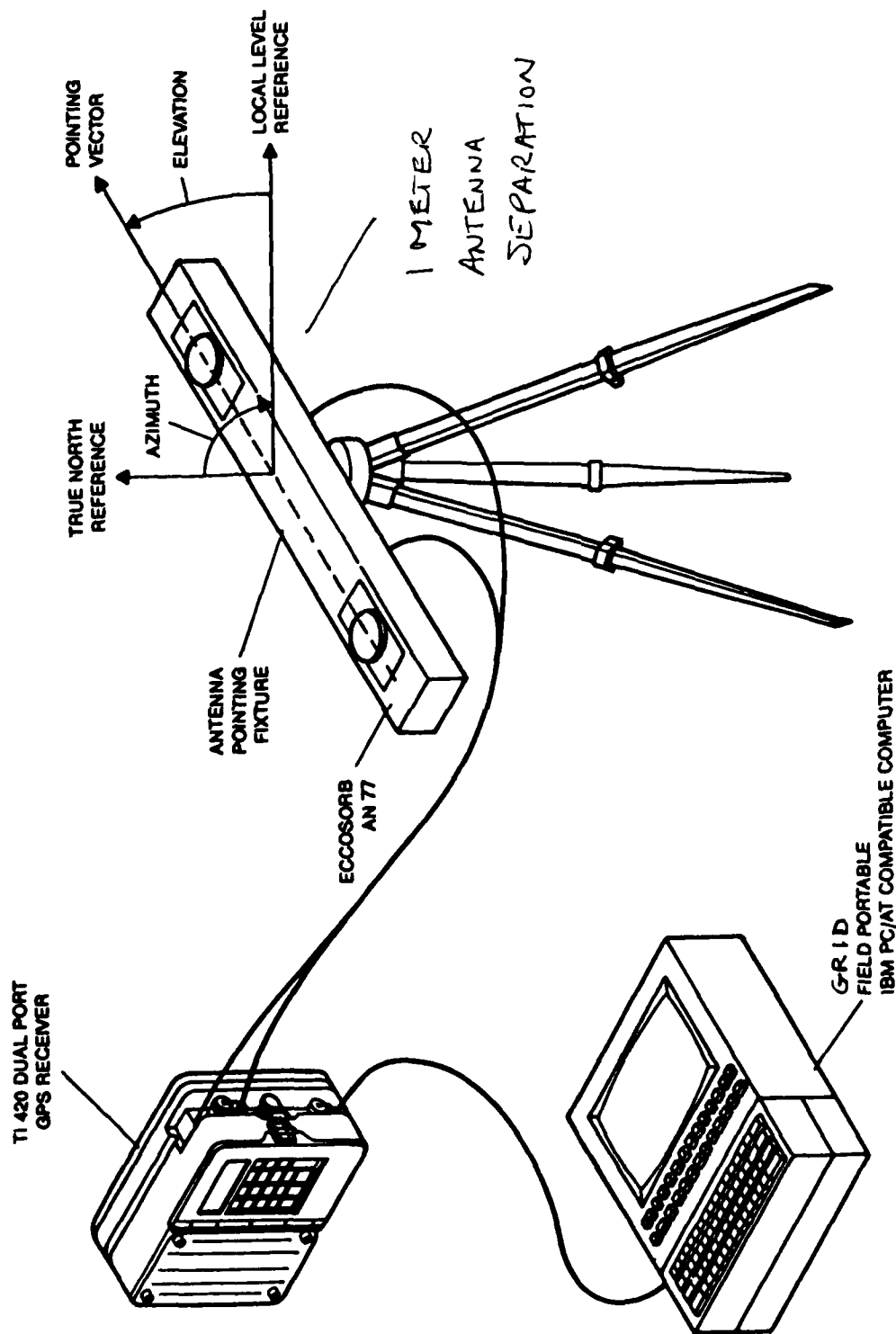
This paper describes some preliminary field test pointing data taken with a Texas Instruments Incorporated (TI) GPS Receiver which has been slightly modified for this experiment. The receiver is the new AN/PSN-9 5-Channel, C/A-Code, 10 pound, portable manpack/vehicular (MP/V) receiver now under production contract to the U.S. Air Force Joint Program Office. At the heart of the AN/PSN-9 is a receiver channel-on-a-chip design which embodies a TI invention specifically designed to obtain pointing observables from two GPS antennas, but requiring only one GPS receiver: a 5-Channel, two port per channel design. A tripod mounted beam with one meter antenna separation was used to obtain pointing data from real GPS satellites while continuing to navigate in the normal manner with respect to the reference antenna. TI has also invented a technique which resolves the phase ambiguity problem without external aiding within a few seconds under dynamic conditions rather than the half hour or more typically required for stationary geodetic observations. A rapid convergence example is presented. Single difference and double difference raw data from real GPS satellites are illustrated as well as the pointing results determined from these observations (azimuth and elevation) which verify that the invention actually works. The initial field data taken with 1 meter antenna separation indicate that an azimuth accuracy of 0.5 milliradian will be obtained with 1 meter antenna separation with no special antenna phase matching, calibration or smoothing of the raw data. Owing to the nature of the TI invention, the noise contribution within the receiver is essentially thermal noise. The major sources of pointing error are expected to be differential multipath and differential antenna phase center migration, but further experimentation will be required to characterize all sources of error and to determine what is the limit to which these sources of error can be reduced. A "truth" pointing reference is currently under construction and phase matched antennas will be used in future tests. These results will be reported in a second paper at the IEEE PLANS '90 in Las Vegas, Nevada, March 20 to 23, 1990.

• • •

PRELIMINARY GPS POINTING DATA RESULTS

OUTLINE

- HARDWARE DESCRIPTION OF TI 420 GPS POINTING UNIT (GPU)
- PRELIMINARY GPS POINTING DATA
- FUTURE PLANS
- SUMMARY

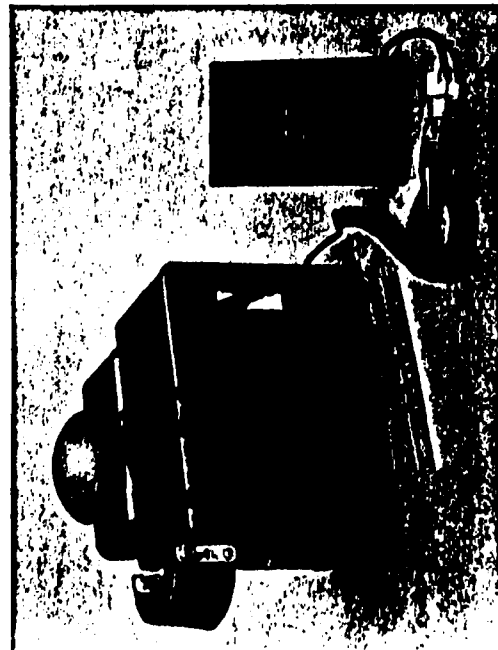


T96002001

Artist's concept of TI 420 GPU



TI 420 POSITION/NAVIGATION SYSTEMS



FEATURES:

- 5-CHANNEL CONTINUOUS L₁ C/A RECEIVER
- FULL-FUNCTION NAVIGATOR
- MILITARIZED CONSTRUCTION
- BUILT-IN TEST
- HAVE QUICK INTERFACE
- KYK-13 INTERFACE
- 1-PPS TIME MARK
- SATELLITE VEHICLE SELECT/OVERRIDE
- VEHICLE MOUNTING ADAPTER
- STORAGE FOR 100 WAYPOINTS
- STORAGE FOR 4 DIFFERENT MISSIONS (EACH WITH UP TO 10 WAYPOINTS)
- COORDINATE SYSTEMS INCLUDE: LAT/LONG, UTM/UPS, MGRS
- 42 OPERATOR SELECTABLE DATUMS (INCLUDES WGS-72 & 84)
- ADDITIONAL RS-422 INSTRUMENTATION PORT

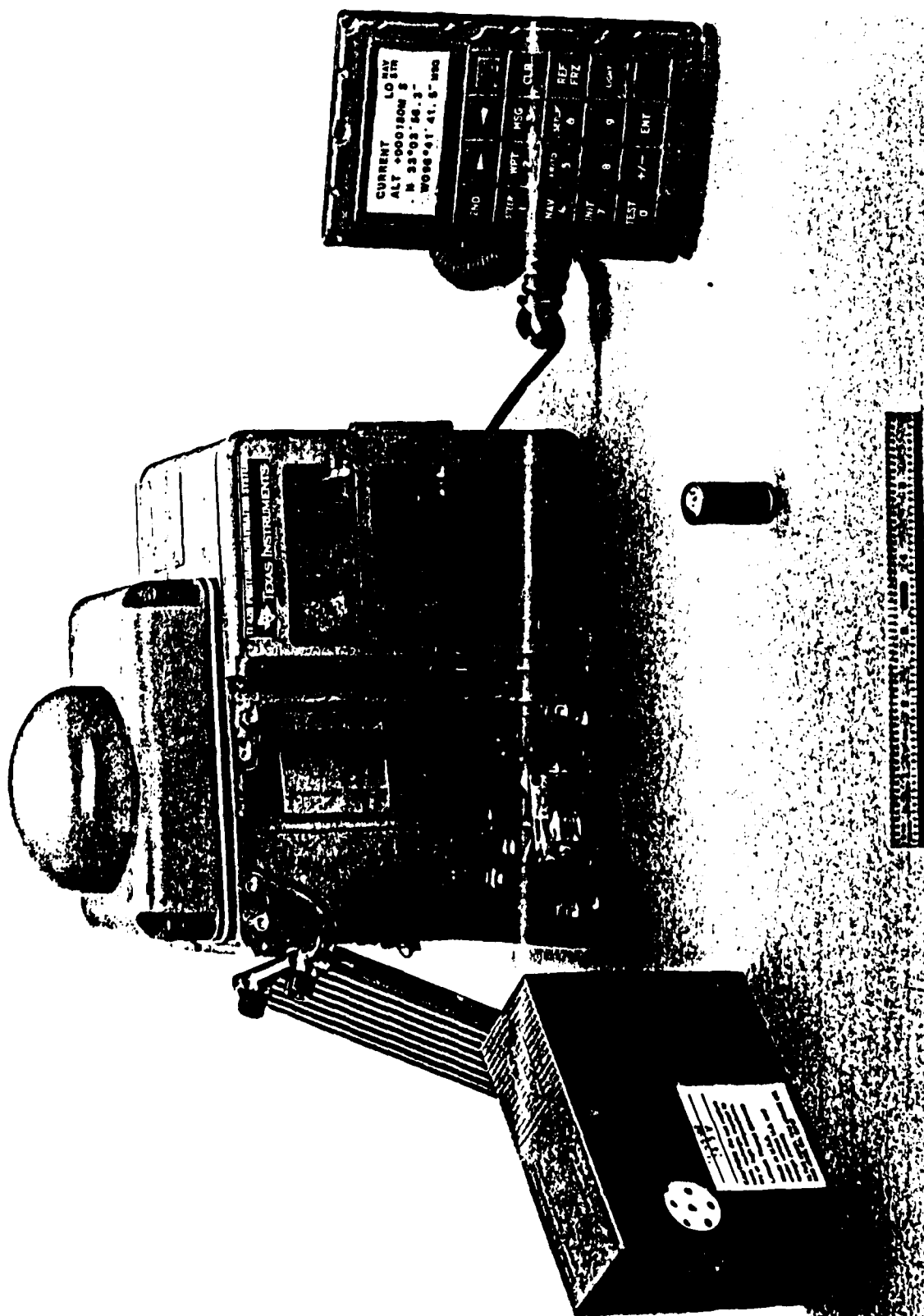
SPECIFICATIONS:

| SIZE | |
|---|--|
| • 299 IN ³ (4900 CM ³) | |
| • < 10 LBS (4.5 KG) | |
| POWER REQUIREMENTS | |
| • < 10 WATTS | |
| • BATTERY LIFE (BA-6598) - UP TO 22 HOURS CONTINUOUS (+20°C) OR > 160 HOURS AT 4 SOLUTIONS PER HOUR | |
| MTBF | |
| • > 3700 HOURS AT 50°C | |

PERFORMANCE:

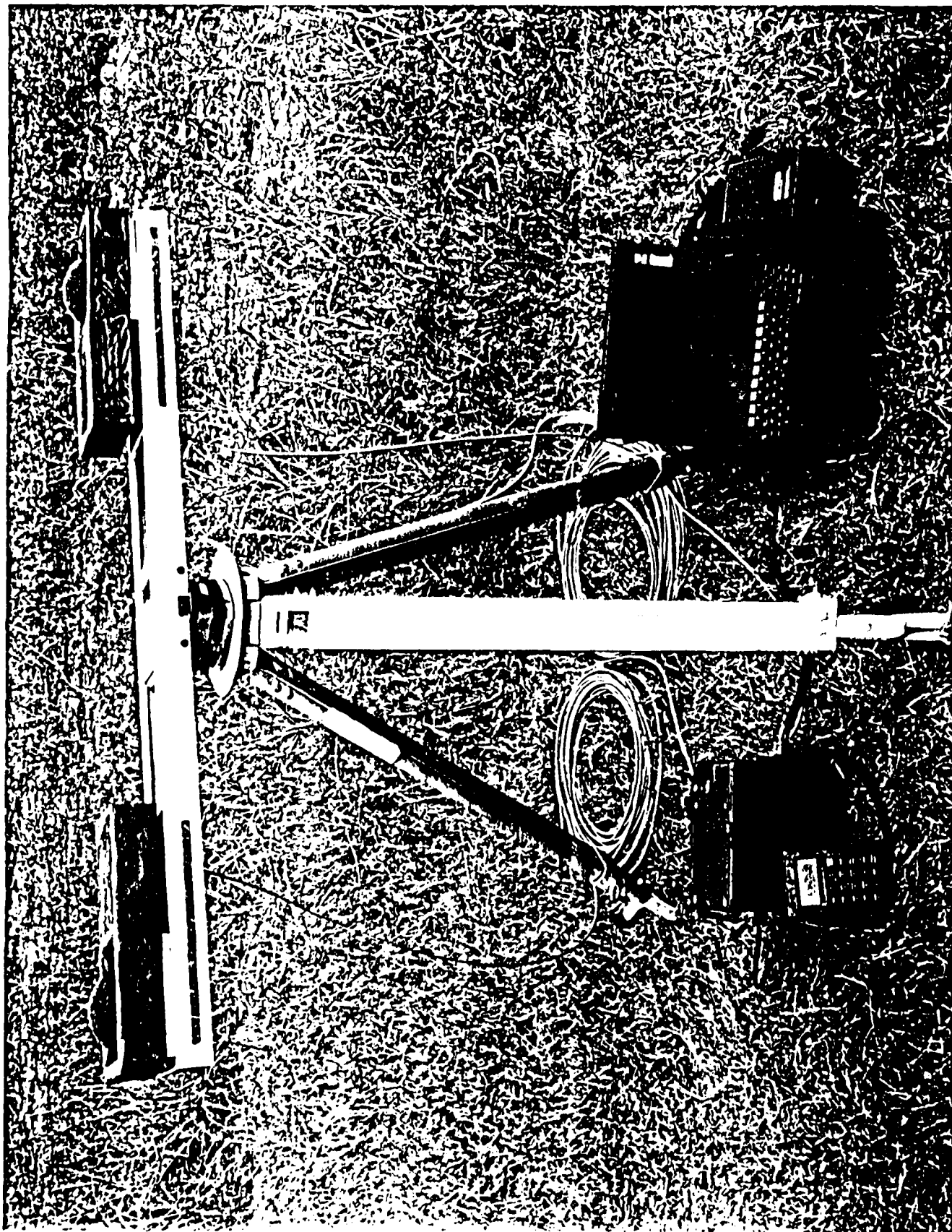
| POSITION ACCURACY: | |
|-------------------------------|--|
| HORIZONTAL (CEP) | 5 TO 12M |
| VERTICAL (LEP) | 8 TO 20M |
| | (DEPENDENT UPON IONOSPHERIC ACTIVITY AND SATELLITE GEOMETRY) |
| MAXIMUM DYNAMICS | 0 TO 4 + G |
| J/S THRESHOLD (NOISE) | 37 dB |
| TIME TO FIRST POSITION (TTFP) | 1.5 MIN (TYPICAL) |

Defense Systems & Electronics Group



TEXAS INSTRUMENTS 1260-770
INCORPORATED





WHAT IS UNIQUE ABOUT THE TI POINTING INVENTION?

- ONLY ONE RECEIVER REQUIRED TO ACCEPT MULTIPLE ANTENNA INPUTS
 - ONE ANTENNA IS SELECTED AS THE REFERENCE
 - REMAINING ANTENNAS DESIGNATED AS SLAVES
 - TI 420 GPU CAN ACCOMMODATE TWO ANTENNAS
- LOCAL OSCILLATOR COMMON TO ALL RECEIVER CHANNELS
 - SAMPLING TIMES OF IN-PHASE AND QUADRATURE DATA IS PERFECT
 - DOUBLE DIFFERENCING WITH PERFECT SAMPLE TIME IS OPTIMUM
- MAXIMUM COMMON MODE NOISE REJECTION BETWEEN GPS SIGNALS FROM MULTIPLE ANTENNAS
 - COMMON MODE NOISE CANCELS WITH SINGLE DIFFERENCE
 - RECEIVER MEASUREMENT NOISE IS EFFECTIVELY THERMAL NOISE
- OPERATES AT FULL DYNAMICS OF REFERENCE ANTENNA AND INSENSITIVE TO CYCLE SLIPS
- GEODETIC QUALITY RECEIVER/OSCILLATOR NOT REQUIRED

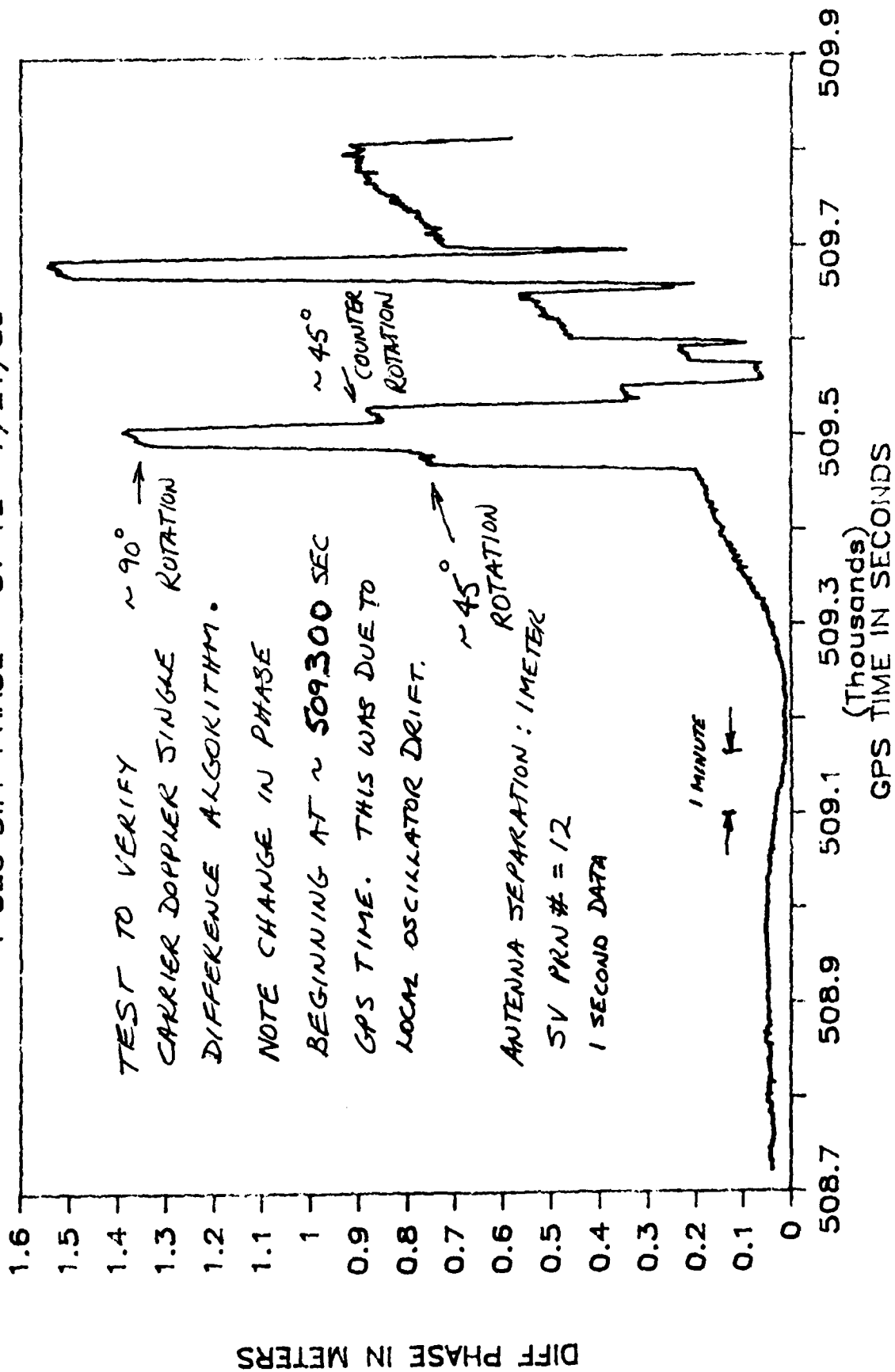
PRELIMINARY GPS POINTING DATA

- INITIAL TESTS PERFORMED TO VERIFY THAT THE INVENTION AND RAW DATA POINTING ALGORITHMS WORKED (SV PRN # 6,9,11,12,13)
 - LEFT POINTING FIXTURE STATIONARY FOR ABOUT 12 MINUTES TO OBTAIN FIXED AZIMUTH/ELEVATION CARRIER DOPPLER PHASE DATA
 - THEN ROTATED ANTENNA 45 DEGREES AND 90 DEGREES TO VERIFY AMBIGUITY RESOLUTION CONVERGENCE ALGORITHM
 - VERIFIED CARRIER DOPPLER SINGLE DIFFERENCE ALGORITHM
 - PERFORMED DOUBLE DIFFERENCE TO VERIFY COMMON MODE ERROR CANCELLATION
 - VERIFIED CODE SINGLE DIFFERENCE ALGORITHM (30 METER MOVEMENT)
 - VERIFIED THAT CODE NOISE TOO EXCESSIVE FOR AIDING AMBIGUITY RESOLUTION

- PERFORMED DATA REDUCTION ON PRELIMINARY DATA TO PREDICT EXPECTED ACCURACY PERFORMANCE

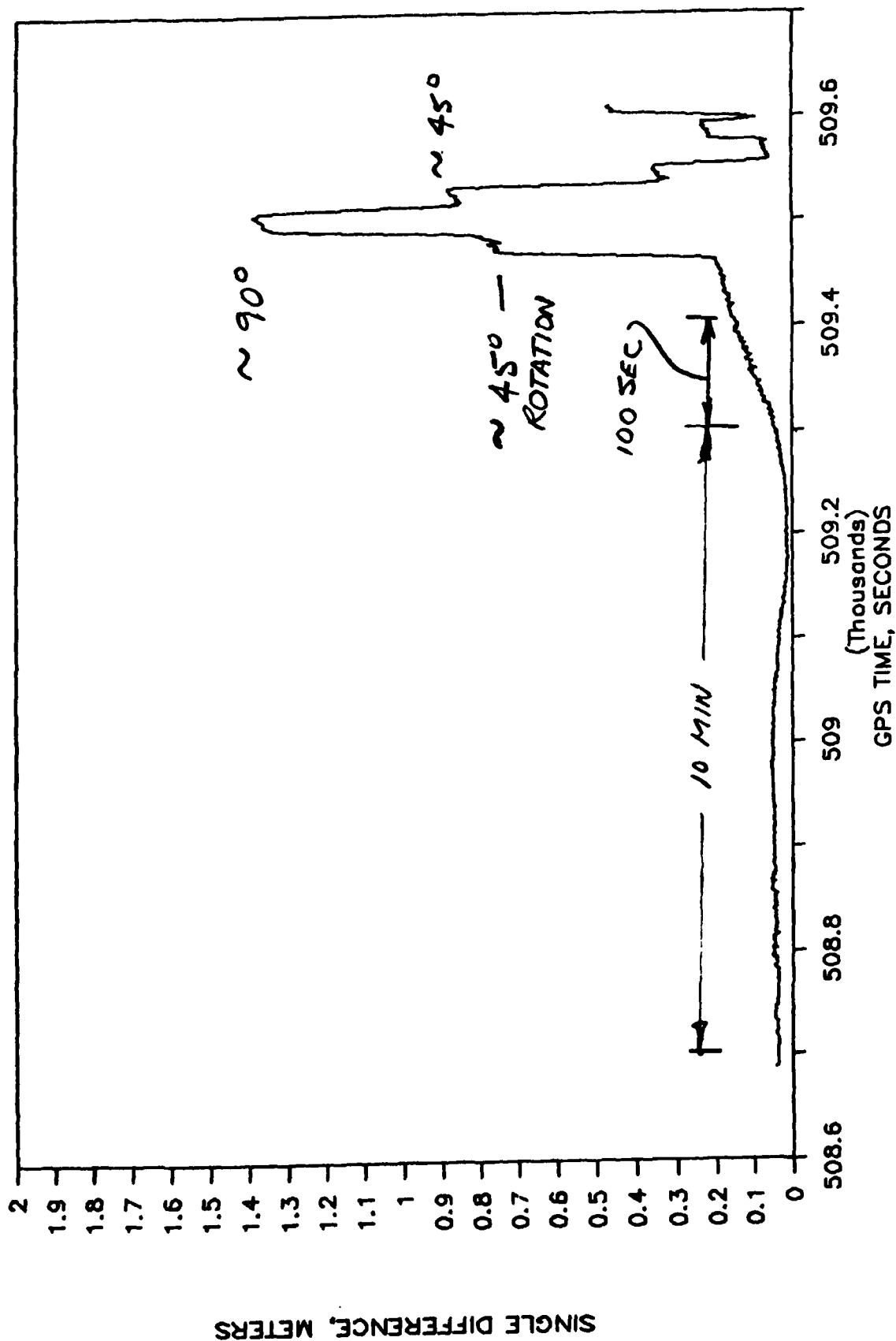
TI420 GPU - PARKING LOT

1 SEC DIFF PHASE - SV 12- 7/21/89



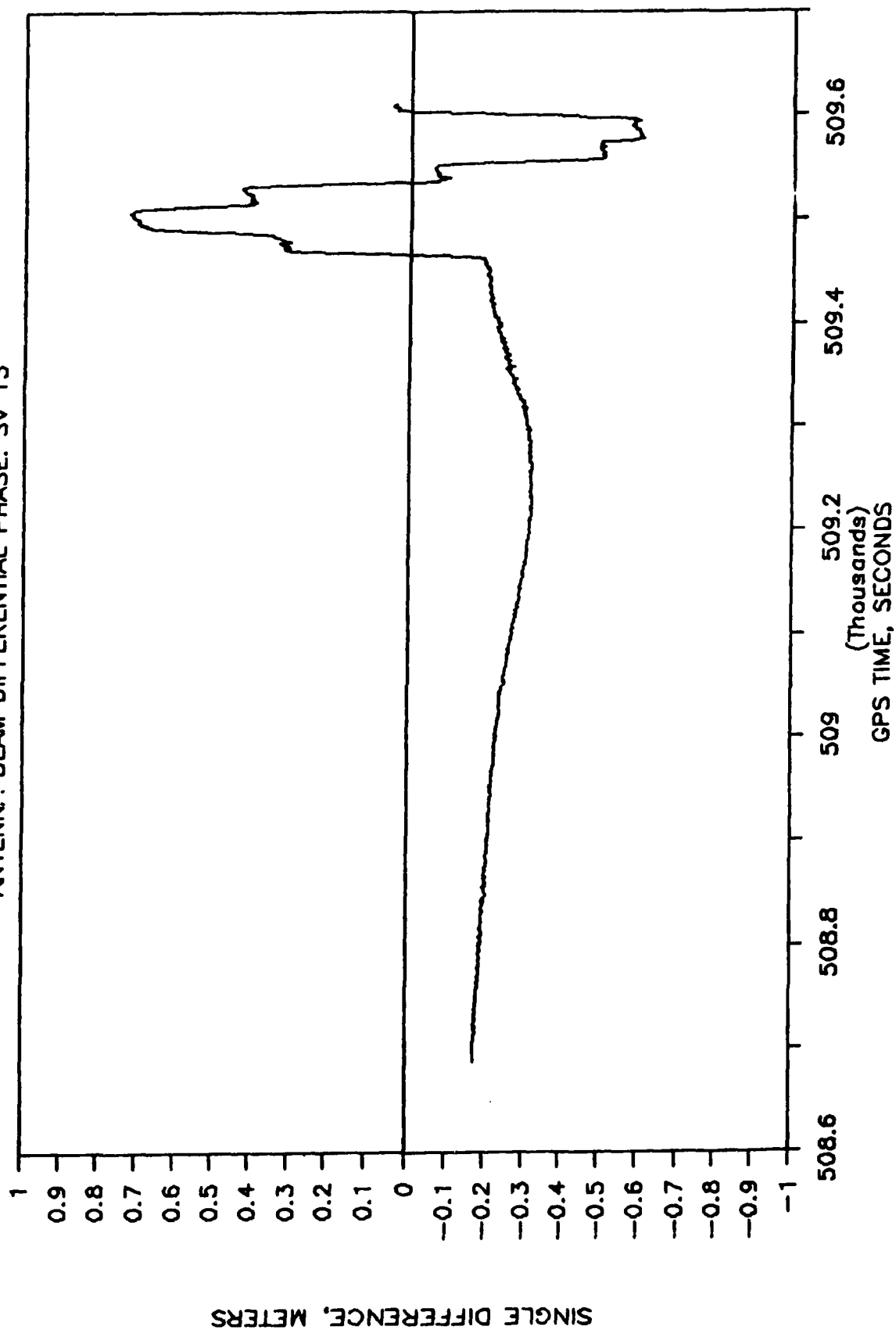
AN/PSN-9 RECEIVER 21 JULY 1989

ANTENNA BEAM DIFFERENTIAL PHASE: SV 12

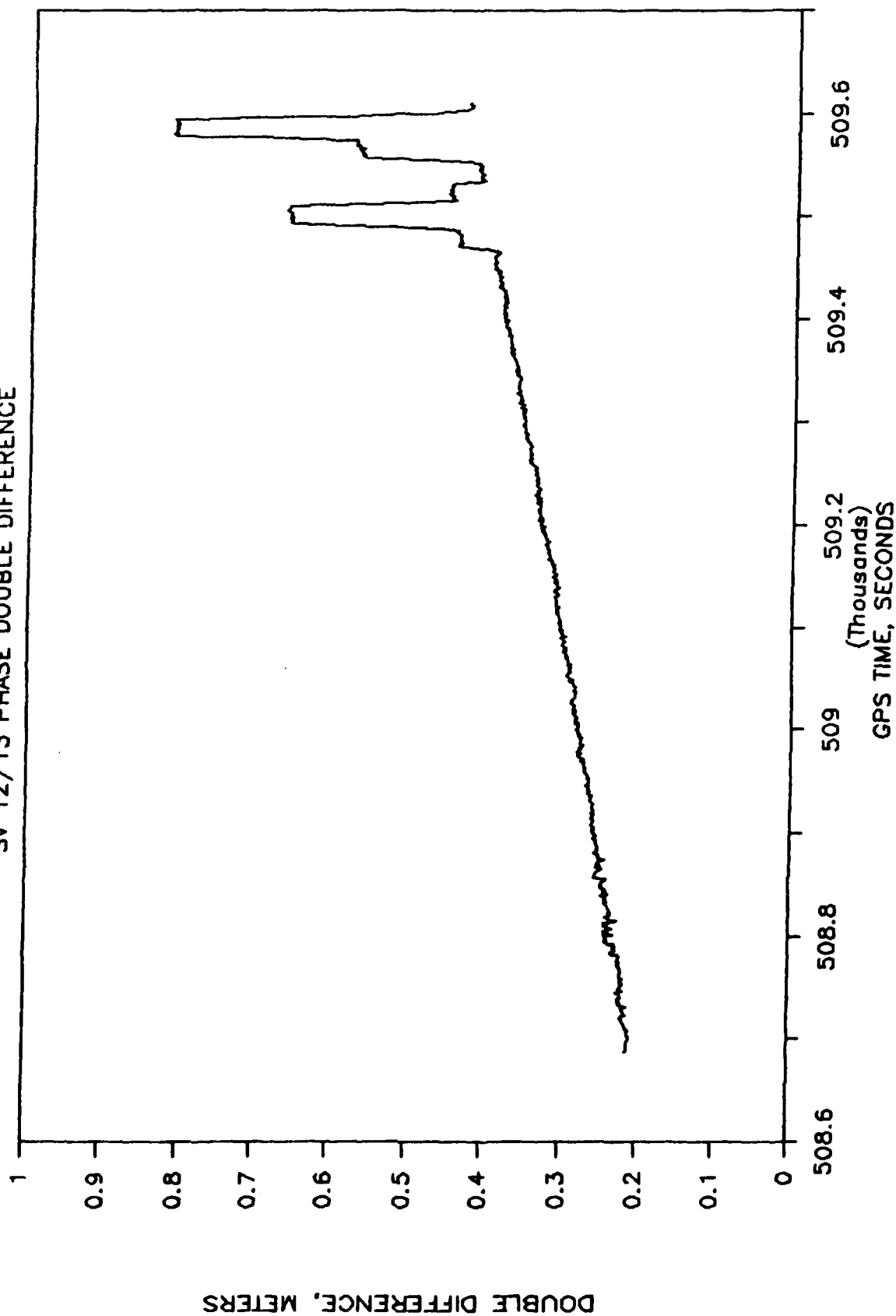


AN/PSN-9 RECEIVER 21 JULY 1989

ANTENNA BEAM DIFFERENTIAL PHASE: SV 13

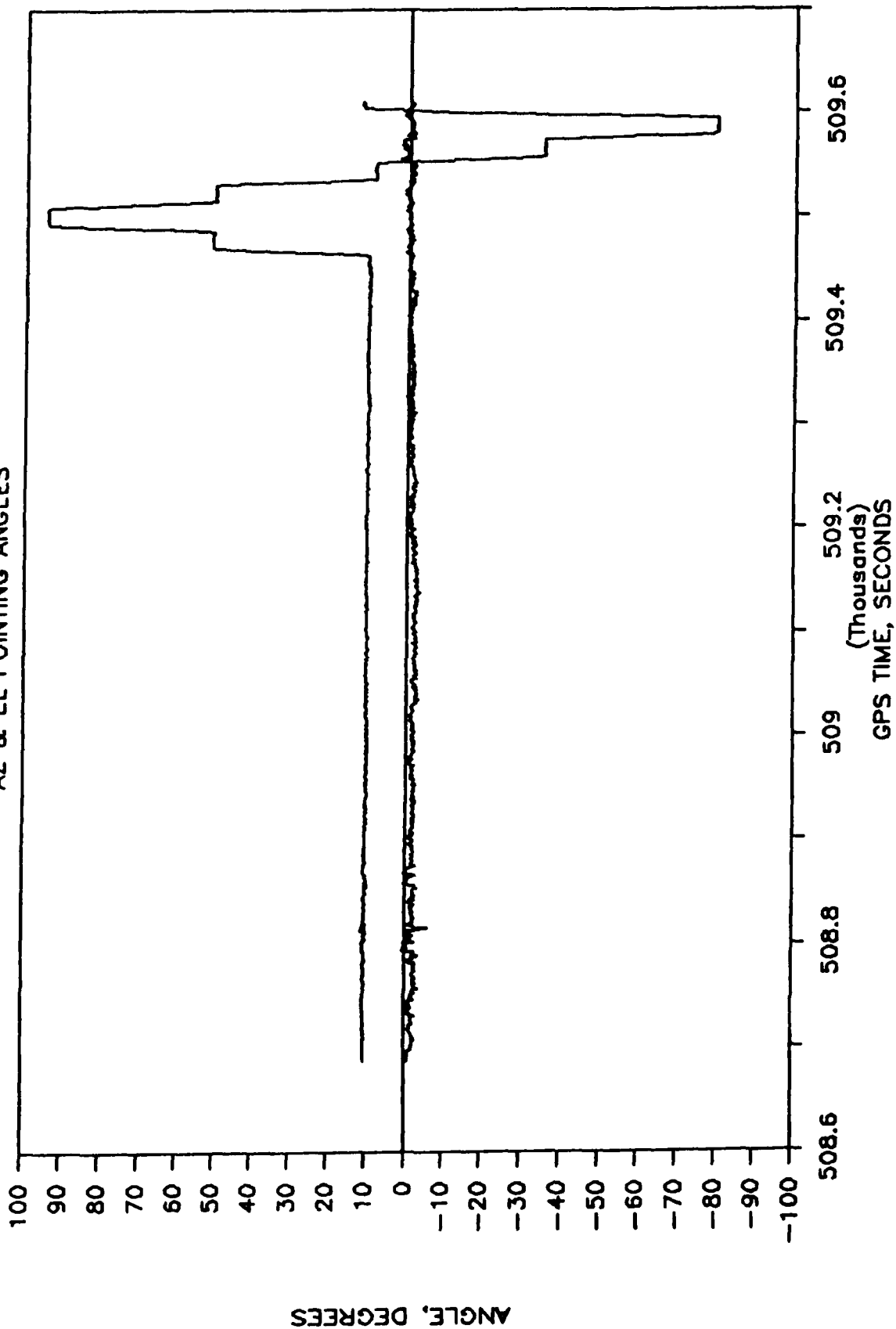


AN/PSN-9 RECEIVER 21 JULY 1989
SV 12/13 PHASE DOUBLE DIFFERENCE



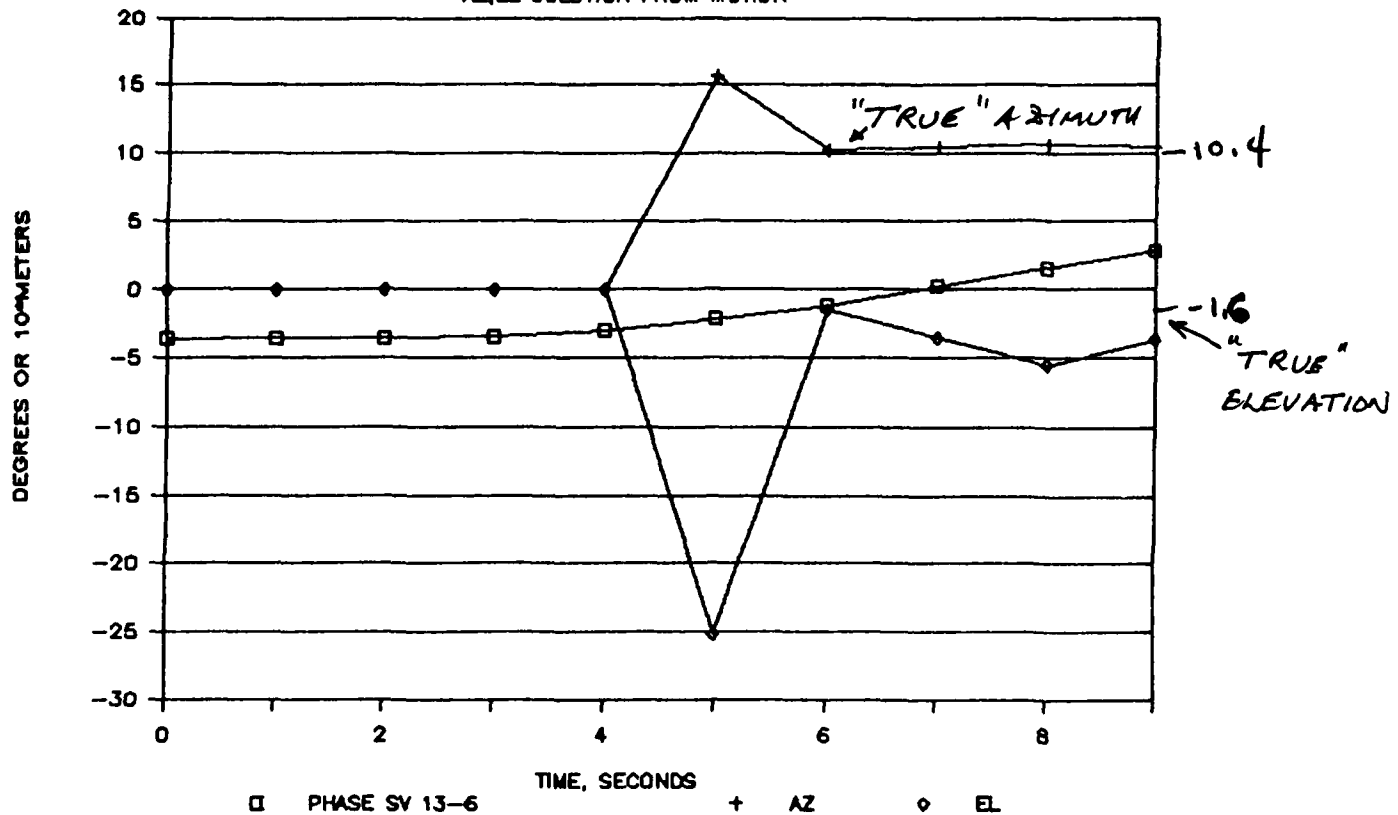
AN/PSN-9 RECEIVER 21 JULY 1989

AZ & EL POINTING ANGLES



TI420 GPU - PARKING LOT 7/21/89

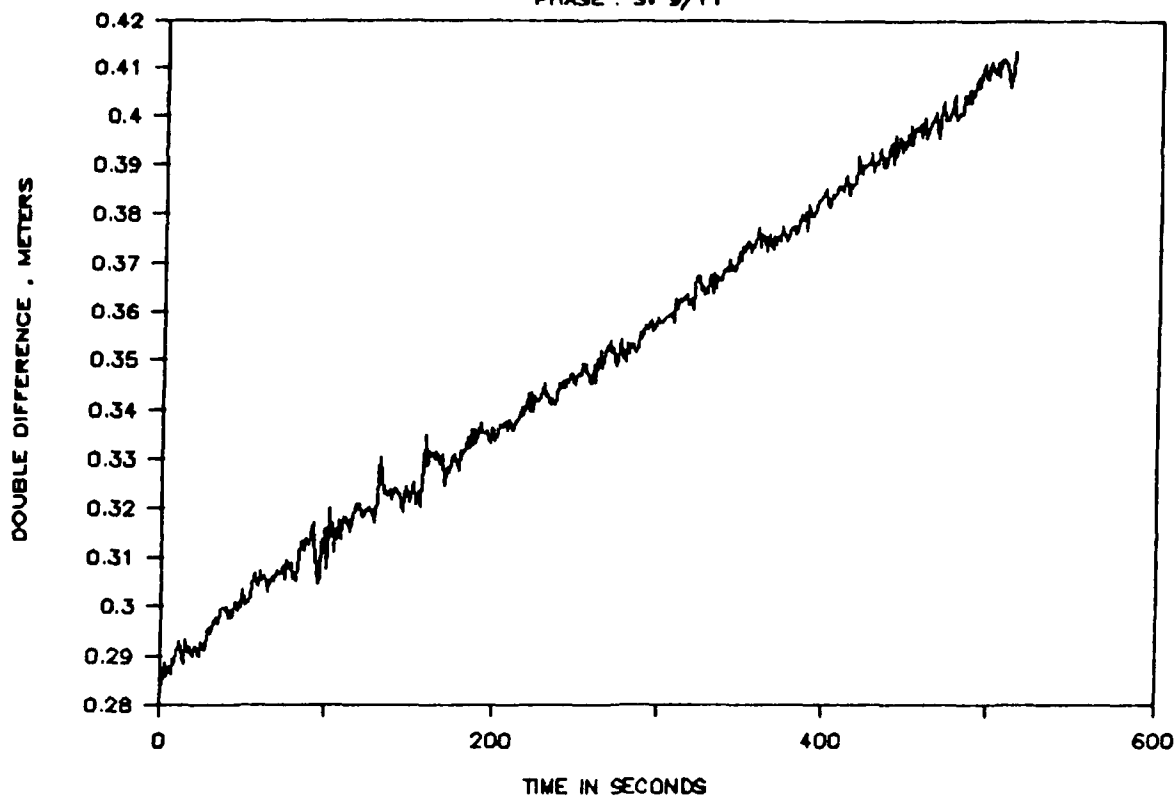
AZ, EL SOLUTION FROM MOTION



CONVERGENCE TIME USING ANTENNA
MOTION TO RESOLVE AMBIGUITY. POINTING
ANGLE AND AMOUNT OF ROTATION UNKNOWN
INITIALLY. (~ 25 AZIMUTH & ~ 55
ELEVATION, AFTER ROTATION STARTS @ 4 S).

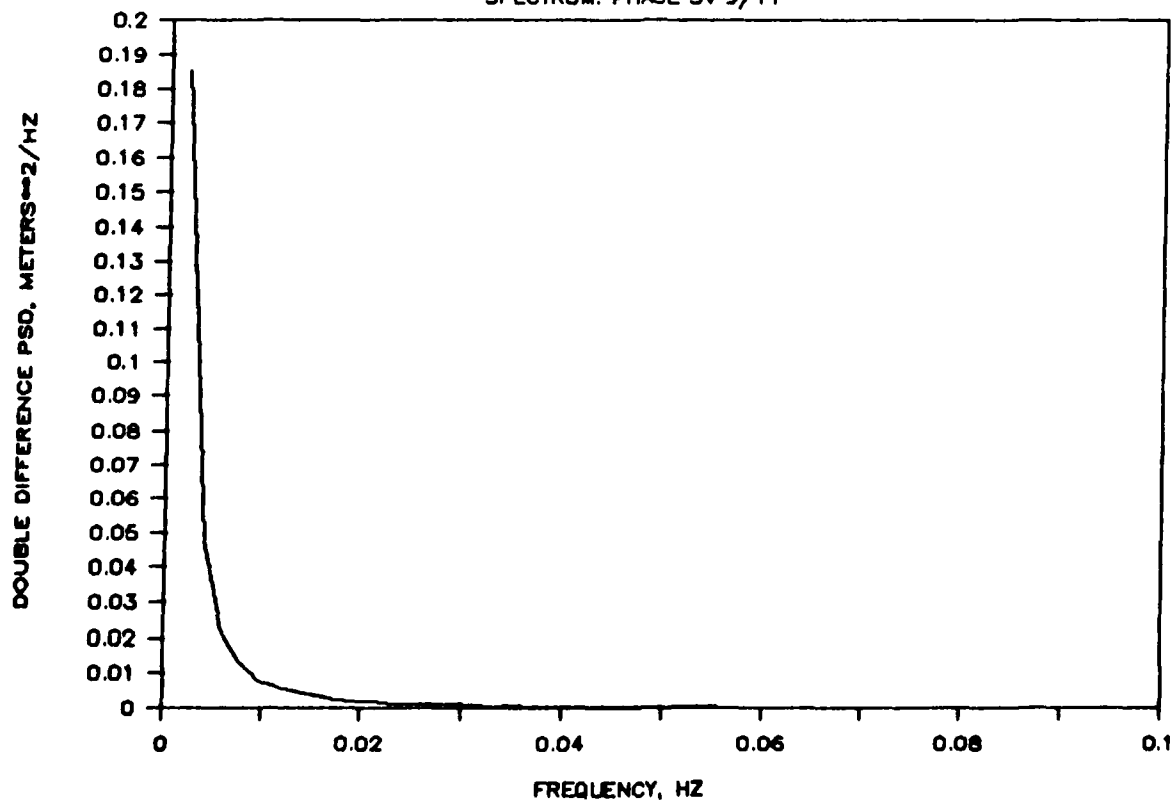
TI420 GPU — PARKING LOT 7/21/89

PHASE : SV 9/11



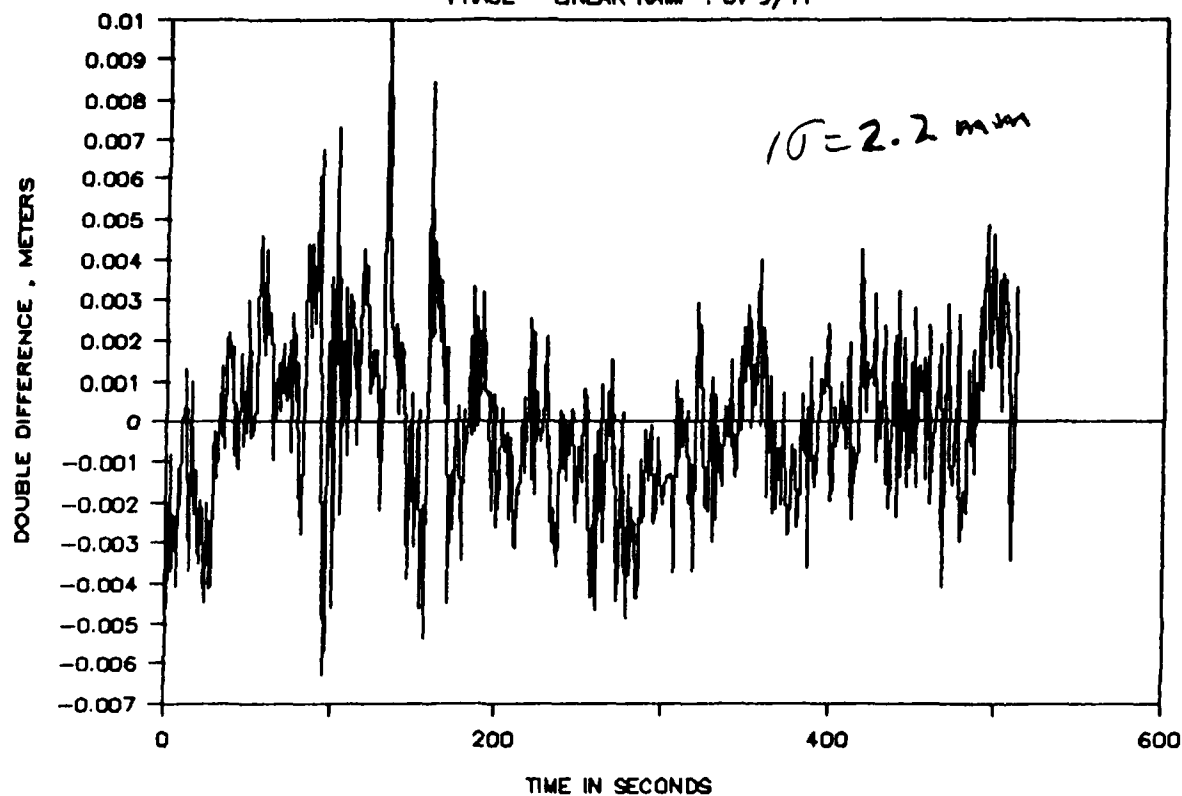
TI420 GPU — PARKING LOT 7/21/89

SPECTRUM: PHASE SV 9/11



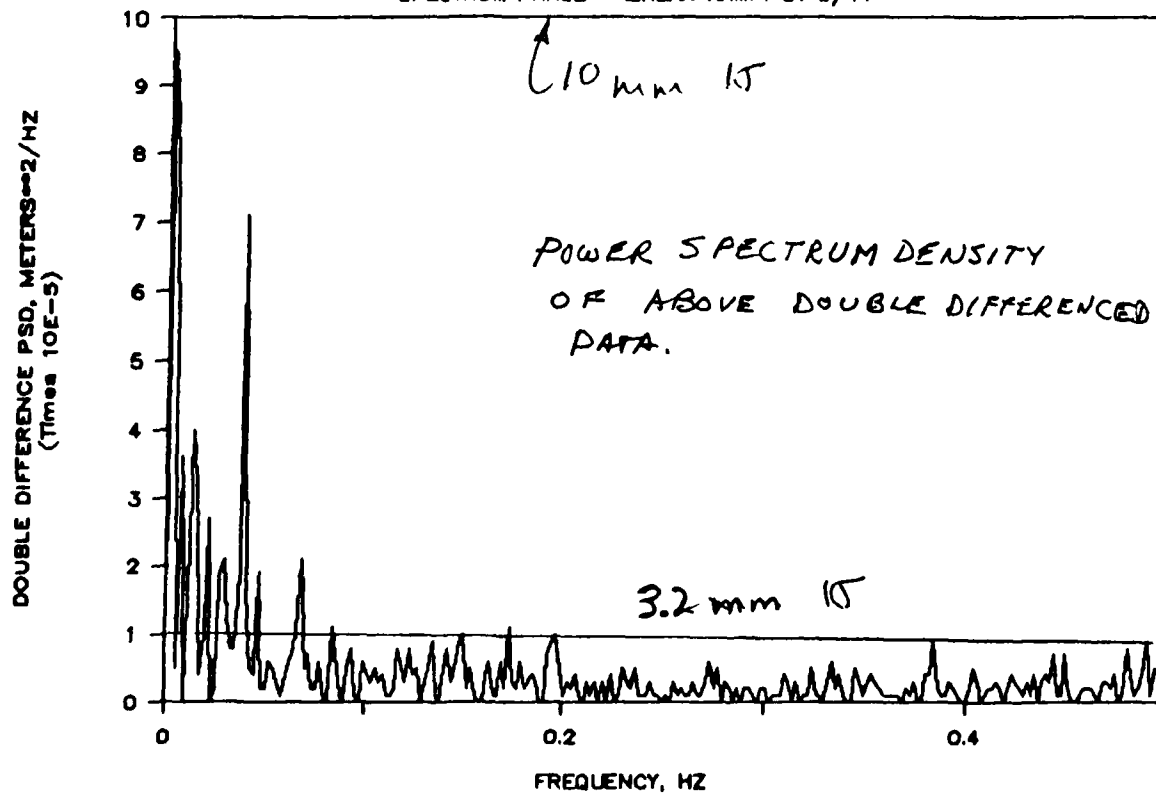
TI420 GPU - PARKING LOT 7/21/89

PHASE - LINEAR RAMP : SV 9/11

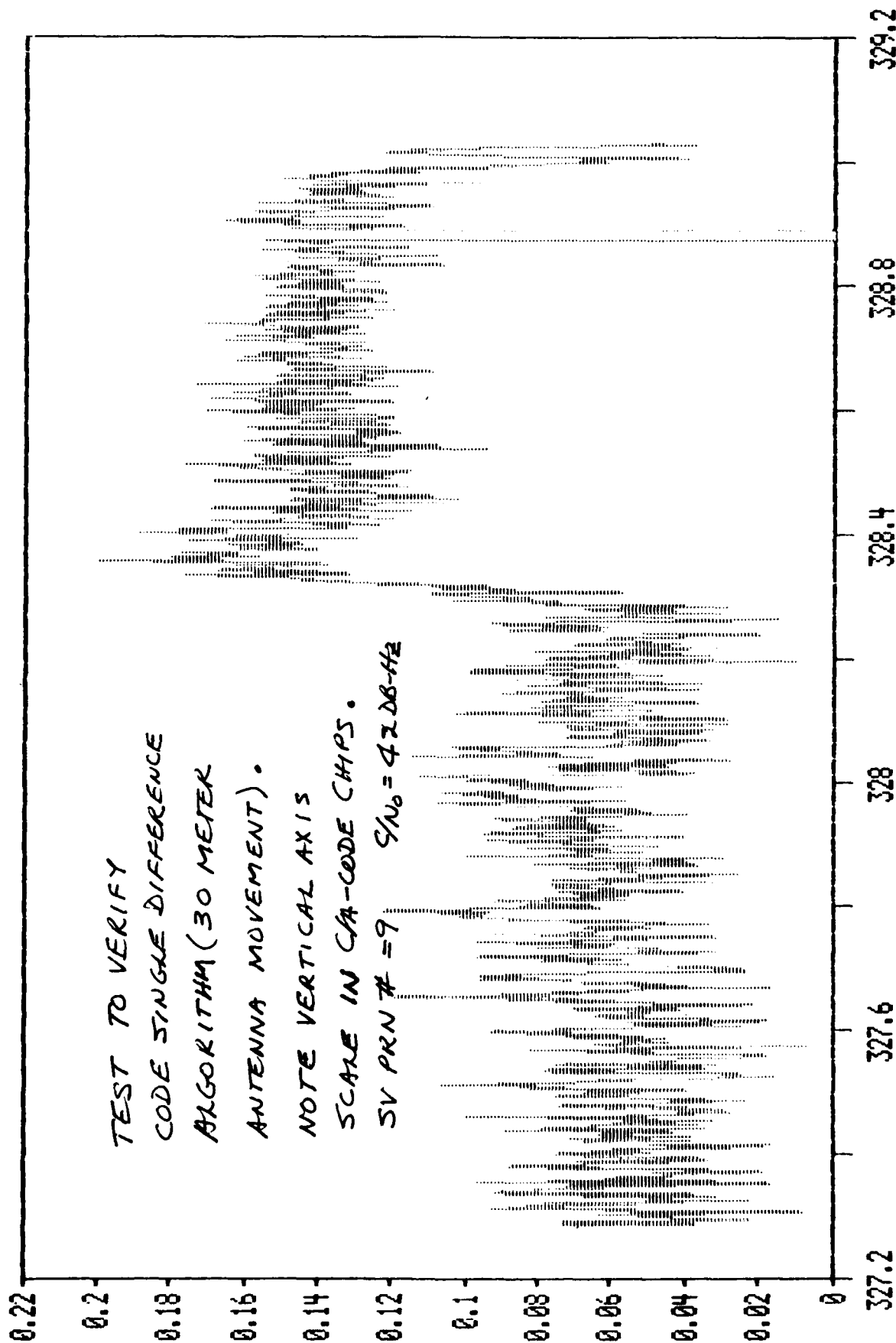


TI420 GPU - PARKING LOT 7/21/89

SPECTRUM PHASE - LINEAR RAMP: SV 9/11



TI420 GPU - PK LOT DATA
 30 M. ANTEN SEPAR. - SV 9 7/26/89

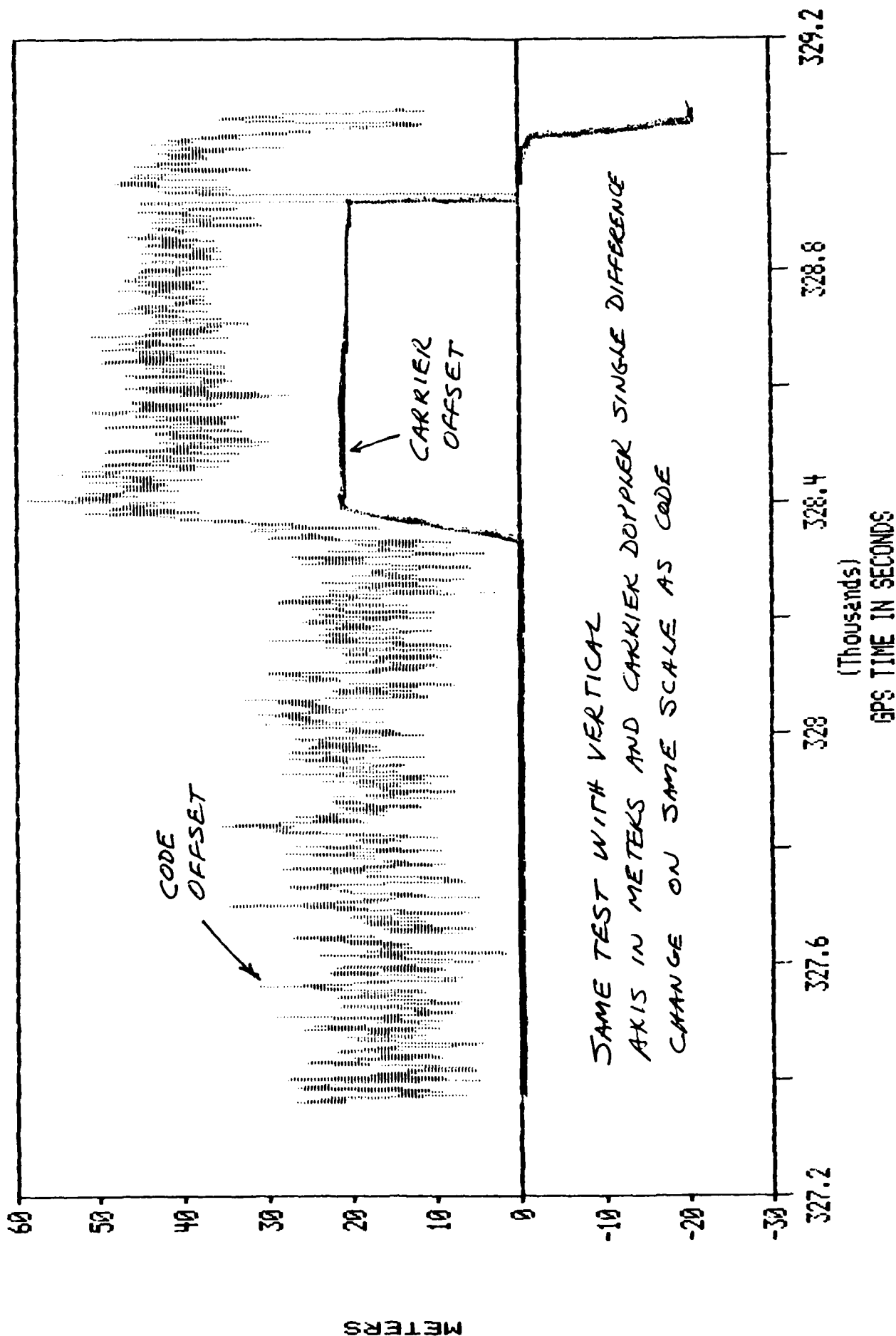


TEST TO VERIFY
 CODE SINGLE DIFFERENCE
 ALGORITHM (30 METER
 ANTENNA MOVEMENT).
 NOTE VERTICAL AXIS
 SCALE IN C/A-CODE CHIPS.
 SV PRN # = 9 $C/N_0 = 47.08 \text{ dB-Hz}$

(Thousands)
 GPS TIME IN SECONDS

CODE OFFSET IN CHIPS

TI420 GPU - PK LOT DATA
30 M. ANTEN SEPAR. -SU 9 7/26/89



FUTURE PLANS

- SUPPORT ADROIT SYSTEMS, INC. WITH SPACE RELATED GPS POINTING EXPERIMENTS FOR THE STRATEGIC DEFENSE INITIATIVE OFFICE
- PERFORM GPS POINTING EXPERIMENTS WITH TRUTH DATA
 - UNDER CONTRACT WITH ARMY ENGINEERING TOPOGRAPHIC LAB TO DEMONSTRATE 3.0 MIL (0.168 DEGREES) ACCURACY WITH 0.5 MIL (0.028 DEGREES) ACCURACY PREFERRED
 - EXPECT TO ACHIEVE 0.5 MIL ACCURACY WITH 1 METER ANTENNA SEPARATION WITH OFF-THE-SHELF ANTENNAS
 - IMPLEMENT POINTING AMBIGUITY RESOLUTION AND VECTOR COMPUTATIONS IN REAL TIME IN TI 420 GPU
- ISOLATE SOURCES OF POINTING ERROR IN GPS OBSERVABLES
 - EXPECT THAT TI 420 GPU WILL PROVIDE IDEAL POINTING DATA FOR NUMEROUS SPACE RELATED EXPERIMENTS
 - EXPECT SOURCES OF BIAS ERROR TO BE DIFFERENTIAL ANTENNA PHASE CENTER MIGRATION AND DIFFERENTIAL MULTIPATH
- PERFORM POINTING EXPERIMENTS WITH MINIMUM BIAS ERROR
 - USE PHASE MATCHED GPS ANTENNAS
 - MINIMIZE DIFFERENTIAL MULTIPATH
 - ALIGN AN INERTIAL ATTITUDE PLATFORM

SUMMARY

- TI GPS POINTING INVENTION WORKS AS PREDICTED
- PLAN TO CONDUCT TRUTH DATA EXPERIMENTS
- UNDER CONTRACT TO DEMONSTRATE 3.0 MIL POINTING ACCURACY AND EXPECT TO DEMONSTRATE 0.5 MIL AZIMUTH ACCURACY WITH 1 METER ANTENNA SEPARATION
- WILL REPORT RESULTS AT IEEE PLANS '90 IN LAS VEGAS IN MARCH
- HAVE DELIVERED ONE TI 420 GPU TO ADROIT SYSTEMS, INC. WHO IS CONDUCTING GPS POINTING EXPERIMENTS FOR THE STRATEGIC DEFENSE INITIATIVE OFFICE

ALGORITHMS FOR SPACECRAFT ATTITUDE DETERMINATION WITH GPS

Duncan B. Cox and Haywood S. Satz
MAYFLOWER COMMUNICATIONS COMPANY, INC.

and

Ronald L. Beard and G. Paul Landis
NAVAL RESEARCH LABORATORY

A filter is under development that utilizes GPS data and accelerometer and gyro data, if available, and/or spacecraft models to estimate position, velocity, and attitude, among other variables. The emphasis here is on using GPS data, in particular, the accumulated carrier phase, not only for attitude determination but also for navigation. The difference between the accumulated phase data and the delta phase measurements is that in many conventional filters that treat delta phase, the time intervals spanning the delta phase do not cover the entire time history and data are lost. The filter design has an additional goal of fault detection and isolation.

The integrated navigation filter, designed for autonomy (real-time solutions), is based on the Kalman filter which processes accumulated phase, pseudorange, delta phase, delta attitude, and delta velocity. In the accumulated phase model, the initial unknown constant is treated as a state in the filter (this yields many states representing measurements of different satellites at different antennas).

The simulation results are based on observations to four GPS satellites using three antennas (12 simultaneous measurements) with a 6 s data rate. Only accumulated phase measurements are used and initial position and clock errors are assumed to be 15 m; while initial velocity is assumed to be known to 1 m/s and orientation error is 0.1 rad. In this case the vehicle is not rotated and ambiguities (individual and differential) are not known. Note, however, that even position is being estimated since information is coming from the changing gravity gradient as the satellite orbits in space. Velocity is determined after two samples because the constants are assumed to be really constant and the accumulated phase at two points yields the velocity directly. Attitude is not determined at all because there is no rotation. Rotation of the spacecraft supplies information on the ambiguity constants and attitude can be determined. Knowledge of the ambiguity constants now provides consistency checks of the data (detection of cycle slips).

In conclusion, the general concept for an integrated navigation filter has been developed with the unique additional feature of accommodating accumulated phase measurements. Using the accumulated phase to determine attitude and perform navigation is believed to be superior to using delta phase. However, more study and simulation analyses are required.

GPS-INERTIAL
SIX-DEGREE-OF-FREEDOM NAVIGATION ALGORITHMS
FEATURES

- Integrated system, allows variety of measurements to be utilized autonomously
 - GPS data from one or more antennas
 - Code delay
 - Accumulated carrier phase
 - Delta phase
 - Accelerometer delta velocity
 - Gyro delta attitude
- Estimates position, velocity, attitude and other states
- Aimed at high performance in estimation and fault detection
 - Without excessive memory and throughput

Mayflower Communications

89093007.CHT

SIX-DEGREE-OF-FREEDOM NAVIGATION ALGORITHMS

GPS-INERTIAL

FEATURES

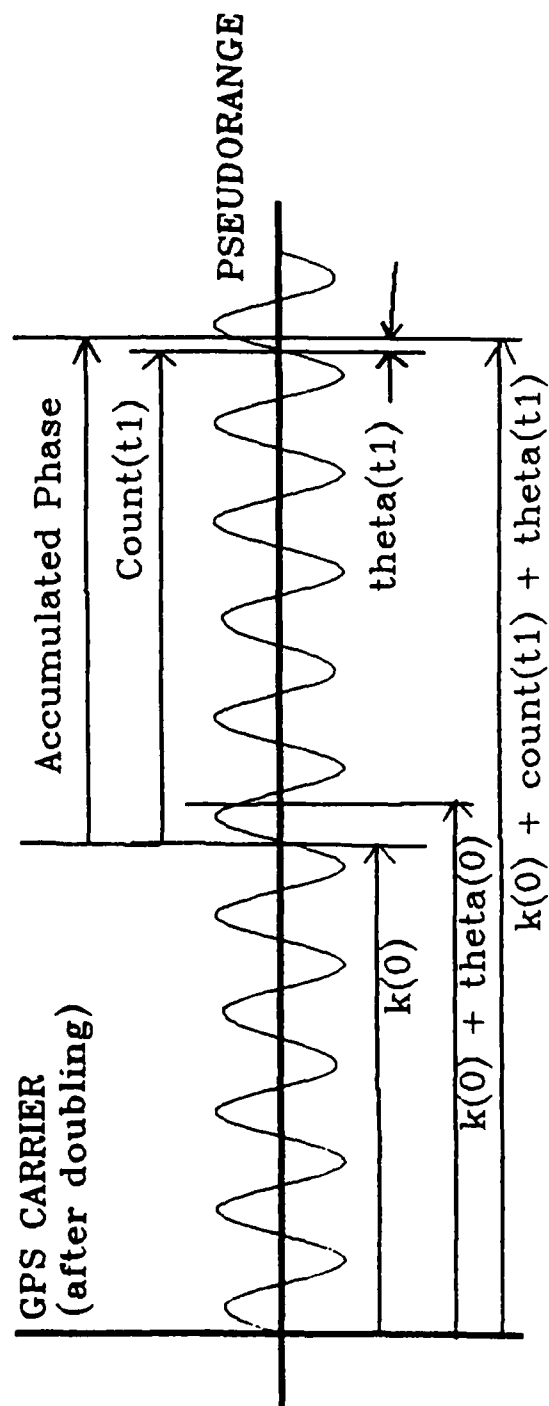
- Takes advantage of GPS accumulated-phase data.
Processes GPS front-end noise optimally.
Allows unusual accuracy in estimation
of ionospheric error.
Estimates ambiguity constants.
Checks for differential cycle slips
- Provides three integrated approaches to
attitude estimation:
Interferometry with known cycle counts
Information from spacecraft rotations
Vector matching against accelerometer data

Mayflower Communications

89093008.cht

ACCUMULATED-PHASE MEASUREMENT MODEL

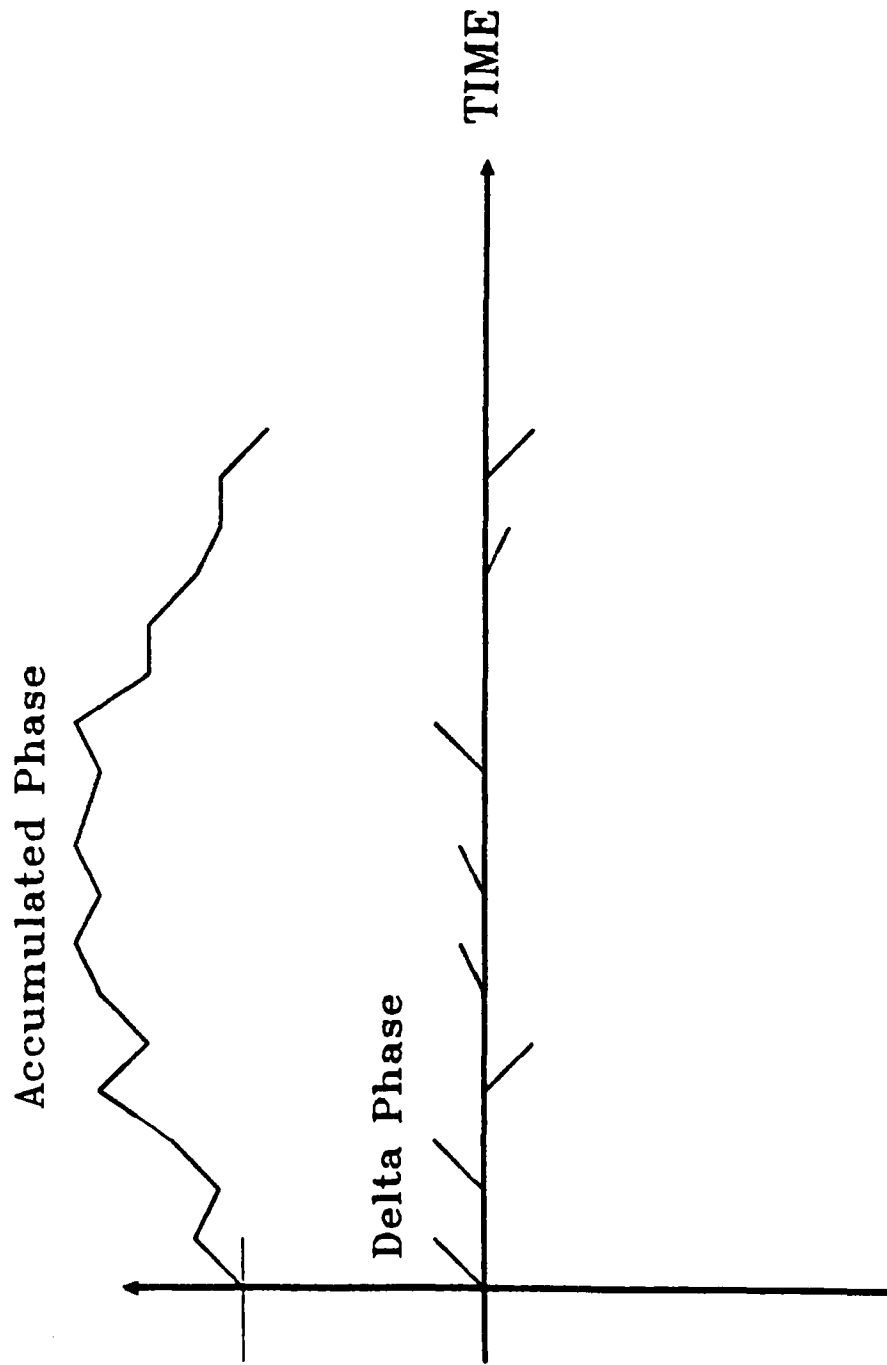
Represent $k(0)$ as a constant state.



Mayflower Communications

89093005.cht

FEATURES OF ACCUMULATED PHASE MODEL

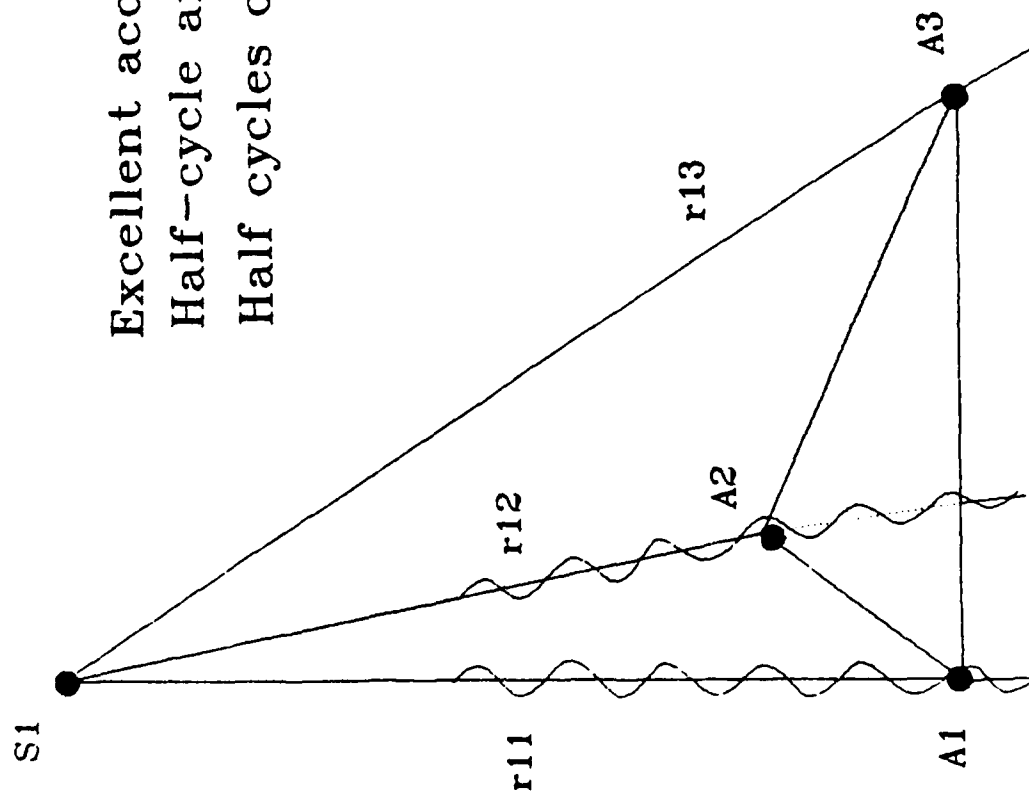


Mayflower Communications

89093016.cht

DIFFERENTIAL PHASE MEASUREMENTS

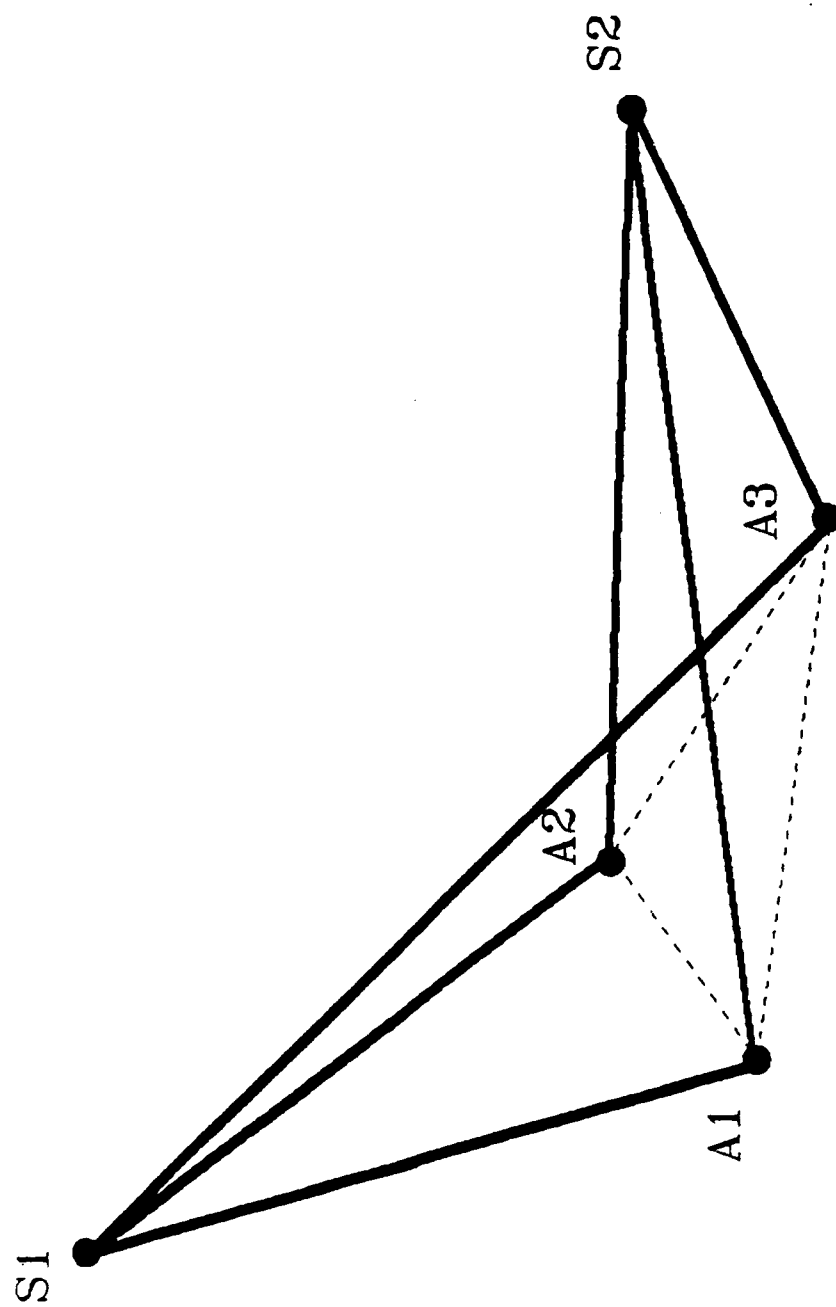
Excellent accuracy & resolution
Half-cycle ambiguities
Half cycles can be accumulated



Mayflower Communications
89093004.cht

GEOMETRY

FOR ATTITUDE DETERMINATION WITH GPS



Mayflower Communications

89093003

GINSS OVERVIEW

GPS-Inertial System Simulation

- Developed by Mayflower as a general tool
Nav system sim and perf analysis
- Previous applications
 - NASA/GSFC: GPS-accelerometer vector matching
 - DARPA/Raytheon: integrated GPS-INS system
 - AFGL: study of inertial transfer alignment
- Written in VAX FORTRAN
 - Approx 75 modules and 12,000 lines of code
- GIA (GPS-Inertial Attitude) algorithms being developed and added to GINSS
 - Under sponsorship of NRL

Mayflower Communications

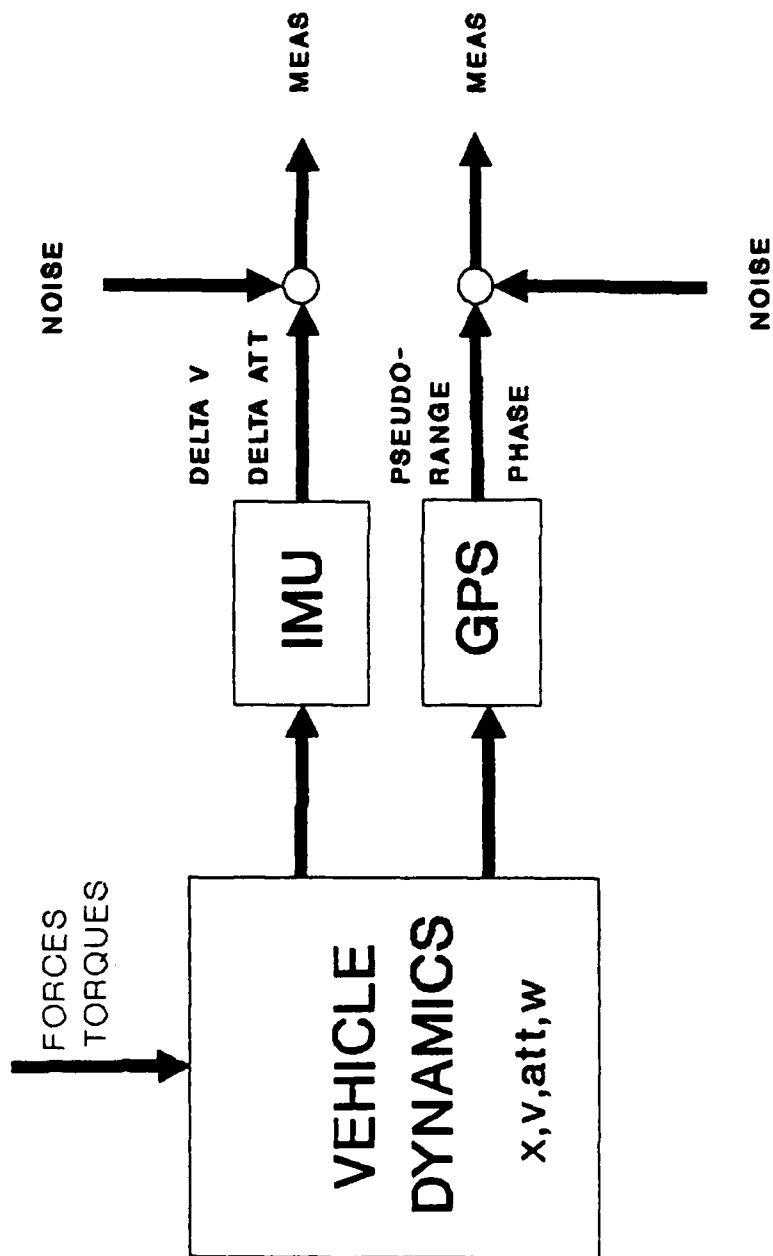
89093009.cht

GINSS FEATURES

- Covariance time history
 - 18-state navigation filter
 - 45-state environment model
- Filter error time history
- Vehicle and satellite trajectories
 - Off-line data files
- Modular structure
 - Facilitates definitions of new systems

Mayflower Communications

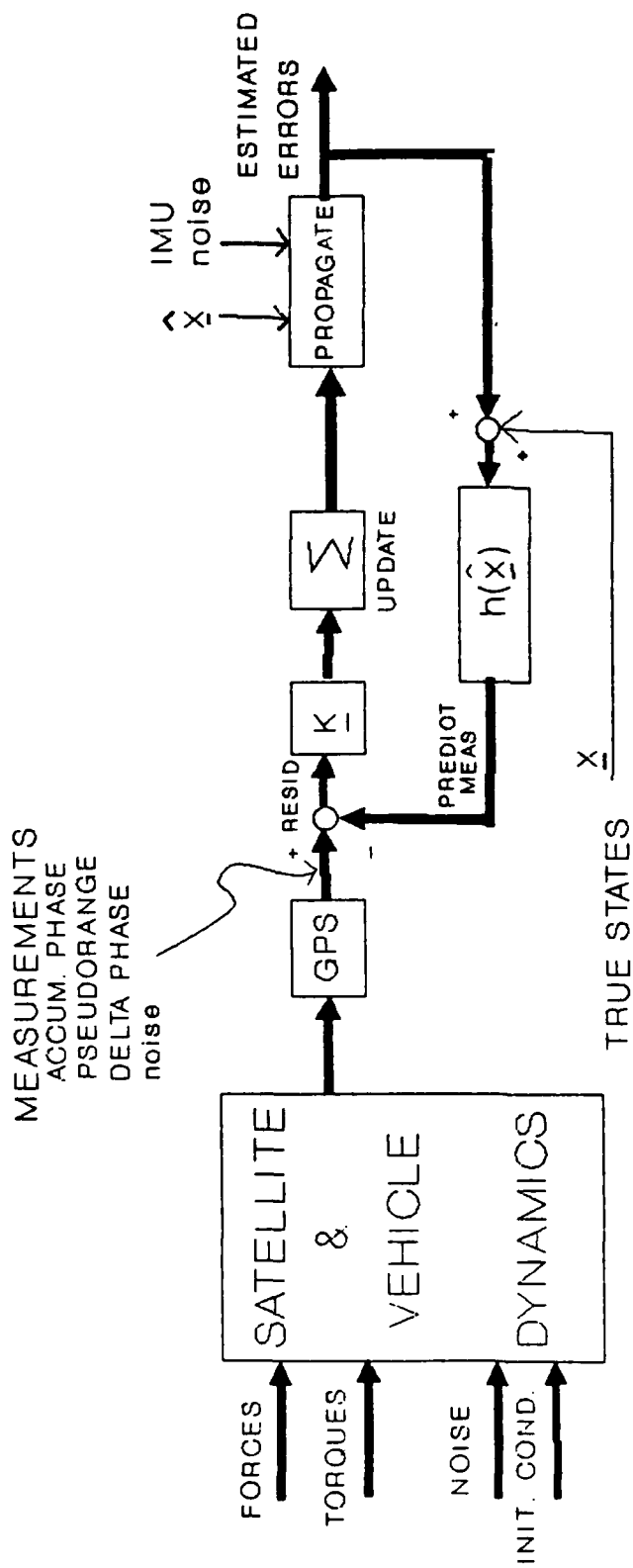
89093017.cht



SYSTEM AND SENSORS

Mayflower Communications

88093001



GINSS/GIA MODEL

Mayflower Communications

89093002.cht

GINSS-GIA SIMULATION RESULTS

(Following charts)

- Preliminary filter covariance and error time histories
 - 1- When ambiguity states unknown
 - 2- When differential ambiguity states known
- Interesting features
 - Confirmation of ambiguity state model
 - Attitude observability due to rotations
 - Attitude observability when differential half cycle counts are known
 - Observability of cycle slips
 - Numerical issues
 - Large and small eigenvalues
 - Large and small numbers in predicted accumulated phase

Mayflower Communications

89093010

PRELIMINARY RESULTS FOR NON-ROTATING VEHICLE
WITH FREE AMBIGUITY STATES

- Conditions

Four satellites, three antennas

Twelve simultaneous measurements every 6 sec

Accumulated-phase measurements only

Initial errors: 15 m, 1 m/s, 0.1 rad

- Results

Position observable from gravity gradient effect

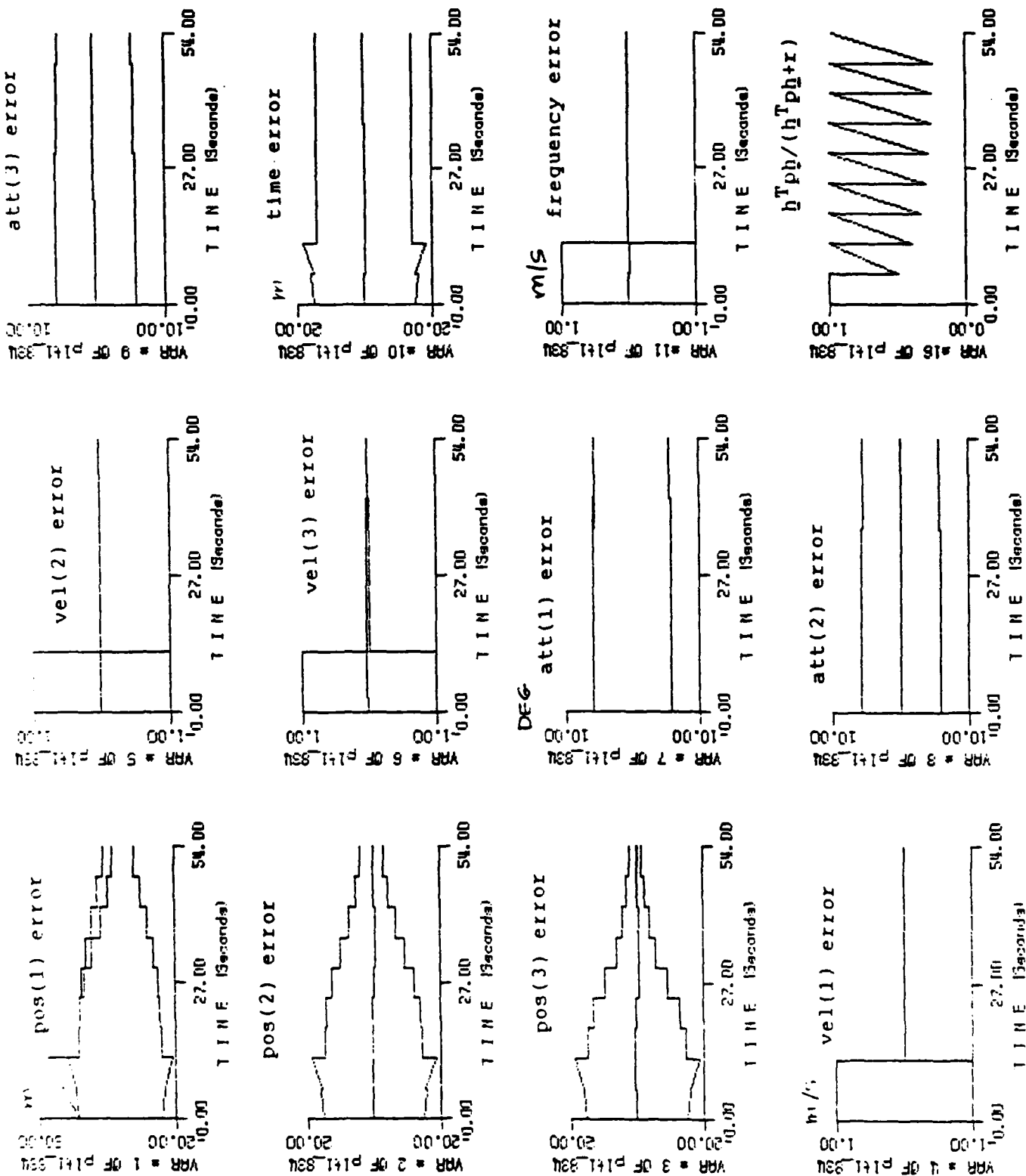
Vel & freq observable after 2nd set of measurements

Attitude not observable

Mayflower Communications

89093011.cht

NON-ROTATING SPACECRAFT, UNCONSTRAINED AMBIGUITIES



MAYFLOWER COMMUNICATIONS COMPANY, INC.

PRELIMINARY RESULTS FOR ROTATING VEHICLE
WITH FREE AMBIGUITY STATES

- Conditions

Four satellites, three antennas

Rotation rate: $(1.0 \text{ rad})/(6 \text{ s})$

Twelve simultaneous measurements every 6 sec

Accumulated-phase measurements only

Initial errors: 15 m, 1 m/s, 0.1 rad

- Results

Position observable from gravity gradient effect

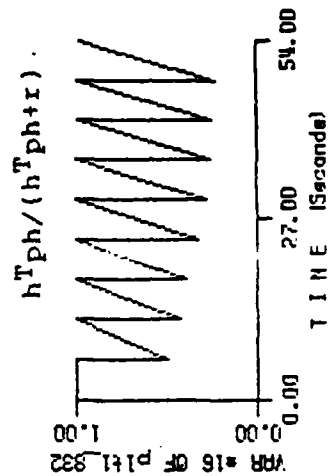
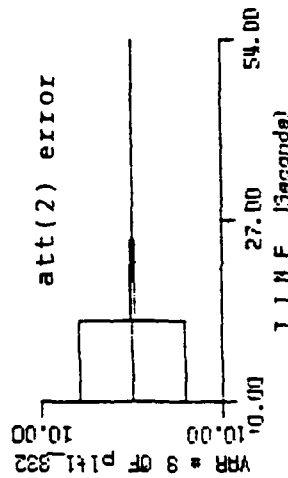
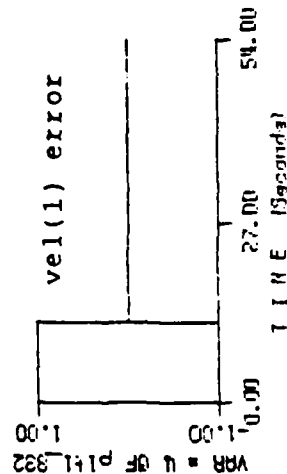
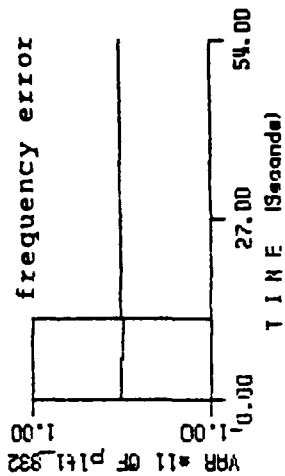
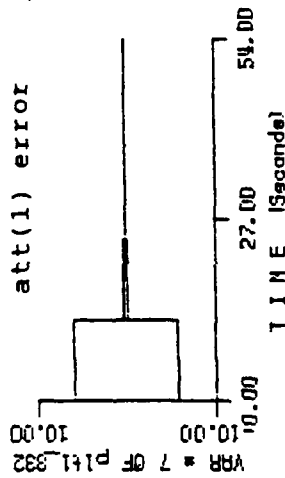
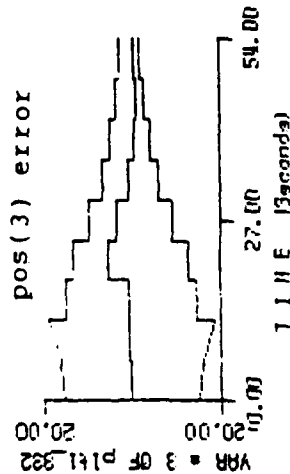
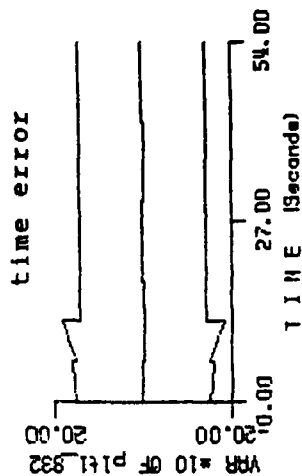
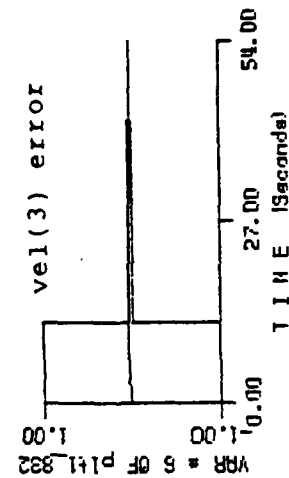
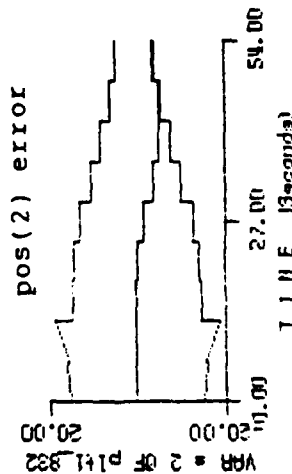
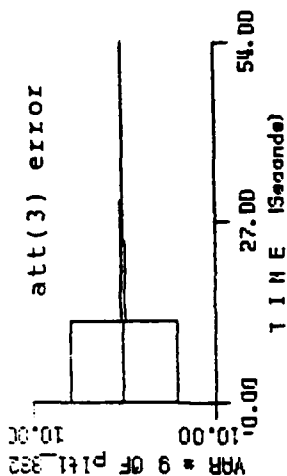
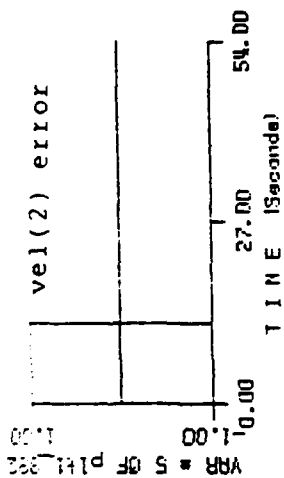
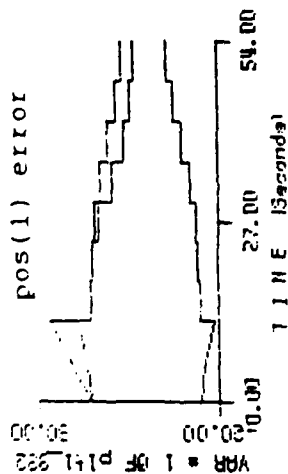
Vel & freq observable after 2nd set of measurements

Attitude observable after 2nd set of measurements

Mayflower Communications

89093012.cht

ROTATING SPACECRAFT, UNCONSTRAINED AMBIGUITIES



MAYFLOWER COMMUNICATIONS COMPANY, INC.

PRELIMINARY RESULTS FOR NON-ROTATING VEHICLE
WITH CONSTRAINED AMBIGUITY STATES

- Conditions

Four satellites, three antennas

Twelve simultaneous measurements every 6 sec

Accumulated-phase measurements only

Initial errors: 15 m, 1 m/s, 0.1 rad

Constraints set after 6 seconds

- Results

Position observable from gravity gradient effect

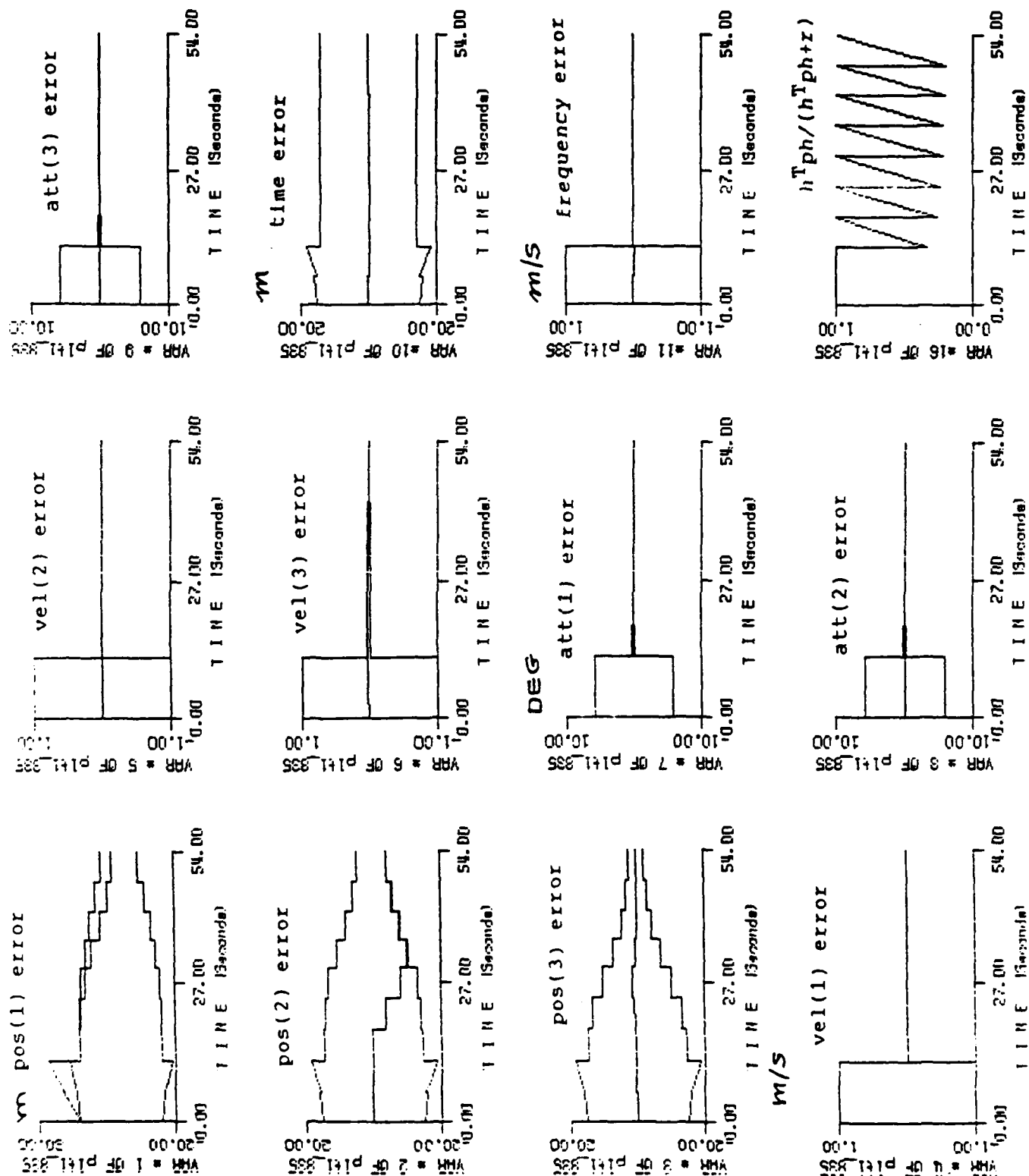
Vel & freq observable after 2nd set of measurements

Attitude observable after constraints set

Mayflower Communications

89093013.cht

NONROTATING SPACECRAFT, CONSTRAINED AMBIGUITIES



MAYFLOWER COMMUNICATIONS COMPANY, INC.

ALGORITHMS FOR SPACECRAFT ATTITUDE DETERMINATION WITH GPS *CONCLUSIONS*

- An integrated GPS-INS navigation system structure has been defined
 - Includes information from multiple GPS antennas
 - Processes accumulated phase, delta phase, code data
 - Processes accelerometer and gyro data, if available
- Preliminary algorithms have been written, coded, and integrated with GINSS
- Expected observabilities have been demonstrated
- Work is continuing on
 - Model refinements
 - Detailed accuracy studies
 - Acquisition and FDI
 - Code optimization

Mayflower Communications

89093018.cht

Preliminary Experimental Performance of the TOPEX Global Positioning
System Demonstration Receiver (GPSDR)

Lance Carson
MOTOROLA GOVERNMENT ELECTRONICS GROUP

This paper summarizes the basic requirements of the TOPEX Demonstration Receiver, overviews its architecture, reviews the measurement techniques, and offers some preliminary results. The TOPEX receiver is a fully space-qualified receiver designed and built from the ground up. The key requirements imposed by JPL for the TOPEX receiver include continuity in measurements of L1 and L2 carrier phase simultaneously on 6 channels; autonomous selection of GPS satellites that are optimum for TOPEX; high accuracy in time, carrier phase, and pseudorange, and low interchannel bias; and the ability to use an existing external frequency reference. The architecture of the receiver implements a double conversion for L1 and L2 with the local oscillator as common reference both for maximum symmetry and delay tracking, and samples are digitized at 40 MHz rate. Channel-on-a-chip technology is used (6 chips for each frequency) - one difference in the TOPEX chip architecture is that measurements are integrated to the 20 msec level allowing the processor to accommodate many other functions, such as navigation and interface software.

The program status shows that hardware and software design are completed and that the engineering model hardware has been built. Hardware/software integration is in progress and the two flight receivers for TOPEX are ready to be assembled.

The technique used to measure the random error of carrier phase and pseudorange is based on the difference of two channels that are tracking two different satellites having the same dynamics (this can be done with a simulator), thus eliminating drift and oscillator errors. The performance of the advanced development model receiver is close to the predicted value of about 1 mm for the carrier phase and about 14.7 cm (versus 8 cm predicted) for the pseudorange. The latter disparity may be due to some residual contribution from the simulator entering even after the differencing technique is applied. By tracking just one satellite with all channels yields the interchannel biases which turn out to be less than the noise of the measurements.

Discussion:

Question: Are there any data on the reliability (i.e., MTBF) of the TOPEX receiver?

Answer: We have some rough numbers based on correlations with similar equipment (on the order of 100000 hours).

Question: Are the interchannel biases constants?

Answer: They seem to be more random in this particular case; but ideally with the digital architecture of the receiver they should be zero. We are still investigating the mechanism for these biases.

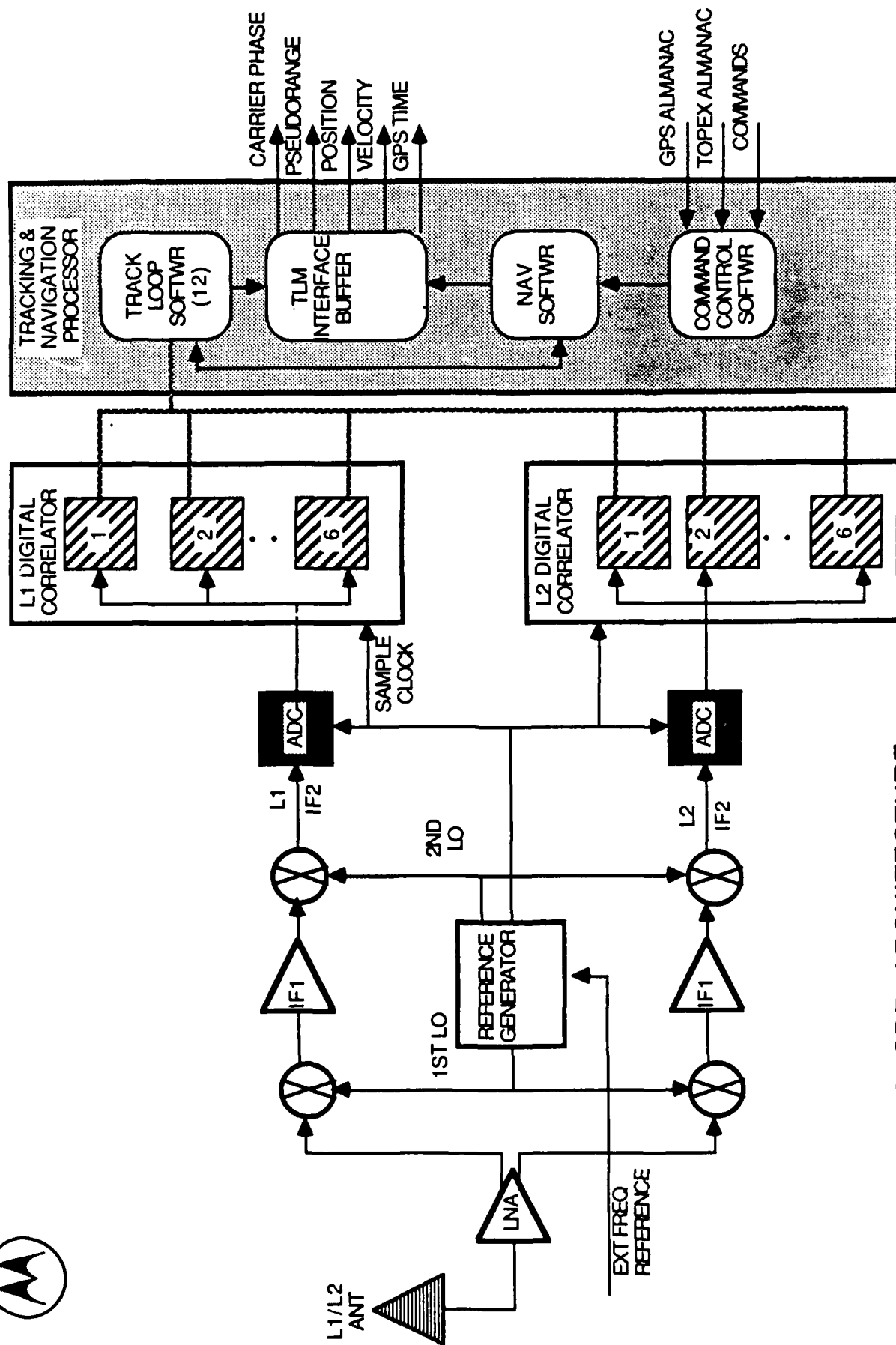
Question: Are the chips dedicated to process either L1 or L2, or both?

Answer: They are identical but their physical location constrains them to process either L1 or L2.



TOPEX GPSDR KEY REQUIREMENTS SUMMARY

- O CONTINUOUS MEASUREMENT OF BOTH L1 AND L2 CARRIER PHASE AND PSEUDO-RANGE FOR UP TO 6 GPS SATELLITES WHICH ARE TIME TAGGED AND SENT TO THE GROUND VIA THE TELEMETRY LINK.
- O AUTONOMOUS SELECTION OF SATELLITES TO BE TRACKED
- O RE-PROGRAMMABILITY OF PROCESSOR MEMORY VIA COMMAND LINK
- O ON-BOARD NAVIGATION SOLUTION ACCURACY TO ACHIEVE TIME TAG ACCURACY OF 500 NS
- O RANDOM ERROR PERFORMANCE (1 SEC, 1 SIGMA) OF 1 CM FOR CARRIER PHASE AND 60 CM FOR PSEUDO-RANGE
- O INTERCHANNEL BIAS ERRORS LESS THAN 0.5 CM AND 10 CM FOR CARRIER PHASE AND PR RESPECTIVELY
- O OPERATE FROM EXTERNAL SPACECRAFT FREQUENCY REFERENCE

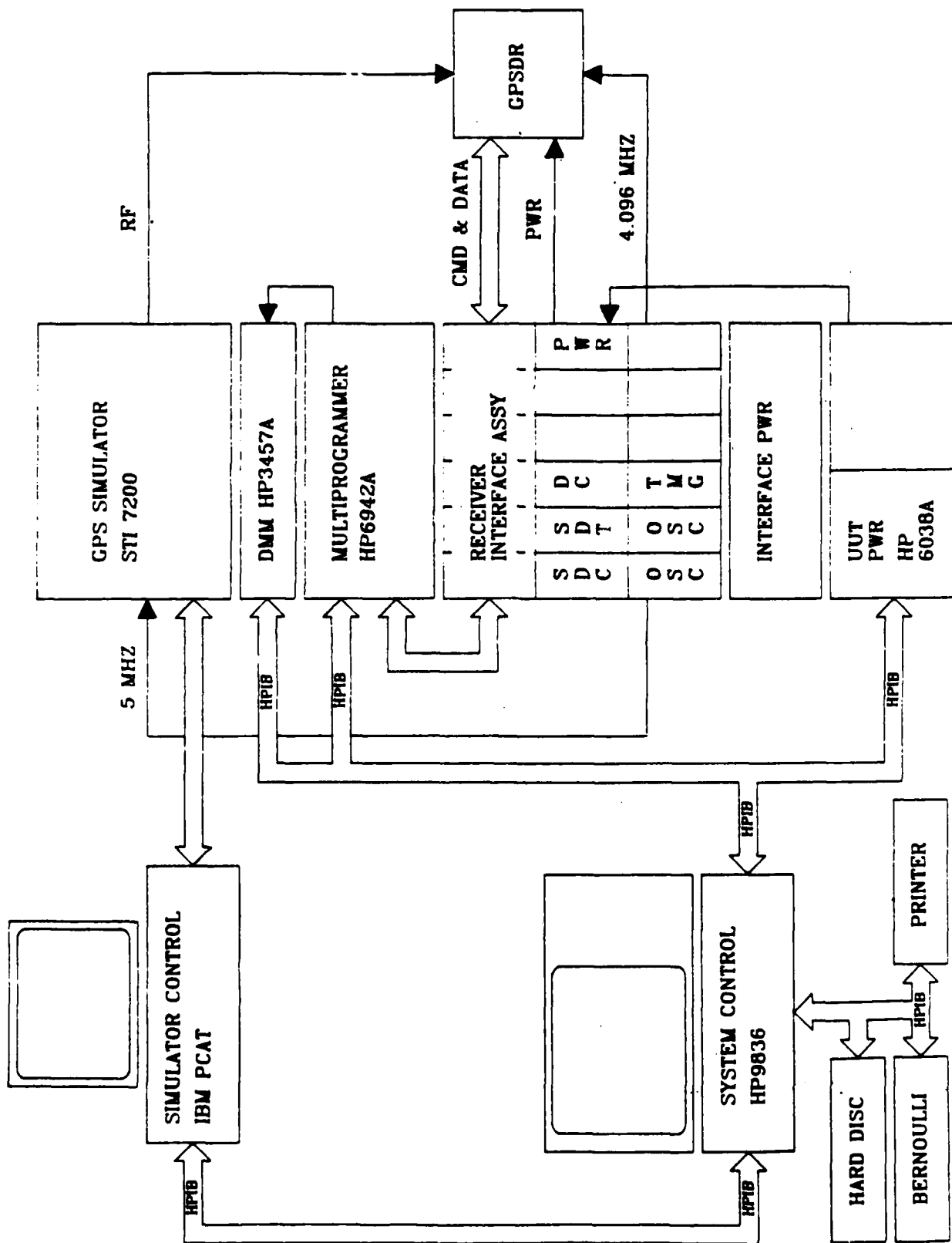


GPSDR ARCHITECTURE



GPSDR DEVELOPMENT STATUS

- O HARDWARE AND SOFTWARE DESIGN COMPLETE
- O CODER/CORRELATOR ASIC SUCCESSFUL ON FIRST PASS AND PROTOTYPES HAVE BEEN INSTALLED IN ADVANCED DEVELOPMENT MODEL (ADM)
- O ADM HARDWARE ASSEMBLY COMPLETE
- O HARDWARE/SOFTWARE INTEGRATION CURRENTLY IN PROCESS
 - TRACKING LOOP FUNCTIONS 90% VERIFIED
 - COMMAND AND TLM SOFTWARE 50% VERIFIED
 - NAVIGATION SOFTWARE 5% VERIFIED
- O FLIGHT HARDWARE ASSEMBLY READY TO COMMENCE



GPSDR SUPPORT EQUIPMENT



RANDOM ERROR MEASUREMENT TECHNIQUE

- O COLLECTING STATISTICS ON THE ABSOLUTE CARRIER PHASE OR PSEUDO-RANGE RESULTS IN NON-RANDOM CONTRIBUTIONS DUE TO DRIFTS AND OSCILLATOR SPURIOUS IN THE TEST EQUIPMENT.
- O A BETTER MEASURE OF RANDOM ERROR IS OBTAINED BY COMPUTING STATISTICS ON THE DIFFERENCES BETWEEN TWO CHANNELS TRACKING DIFFERENT GPS SV's WITH EXACTLY THE SAME DYNAMICS.
- O THIS TECHNIQUE PROVED TO ELIMINATE CARRIER PHASE DRIFTS AND OSCILLATOR CONTRIBUTIONS TO PHASE MEASUREMENT. HOWEVER, SOME CODE CLOCK SPURIOUS WAS IDENTIFIED IN THE SIMULATOR WHICH WAS NOT HIGHLY CORRELATED BETWEEN CHANNELS.



RANDOM ERROR PERFORMANCE SUMMARY

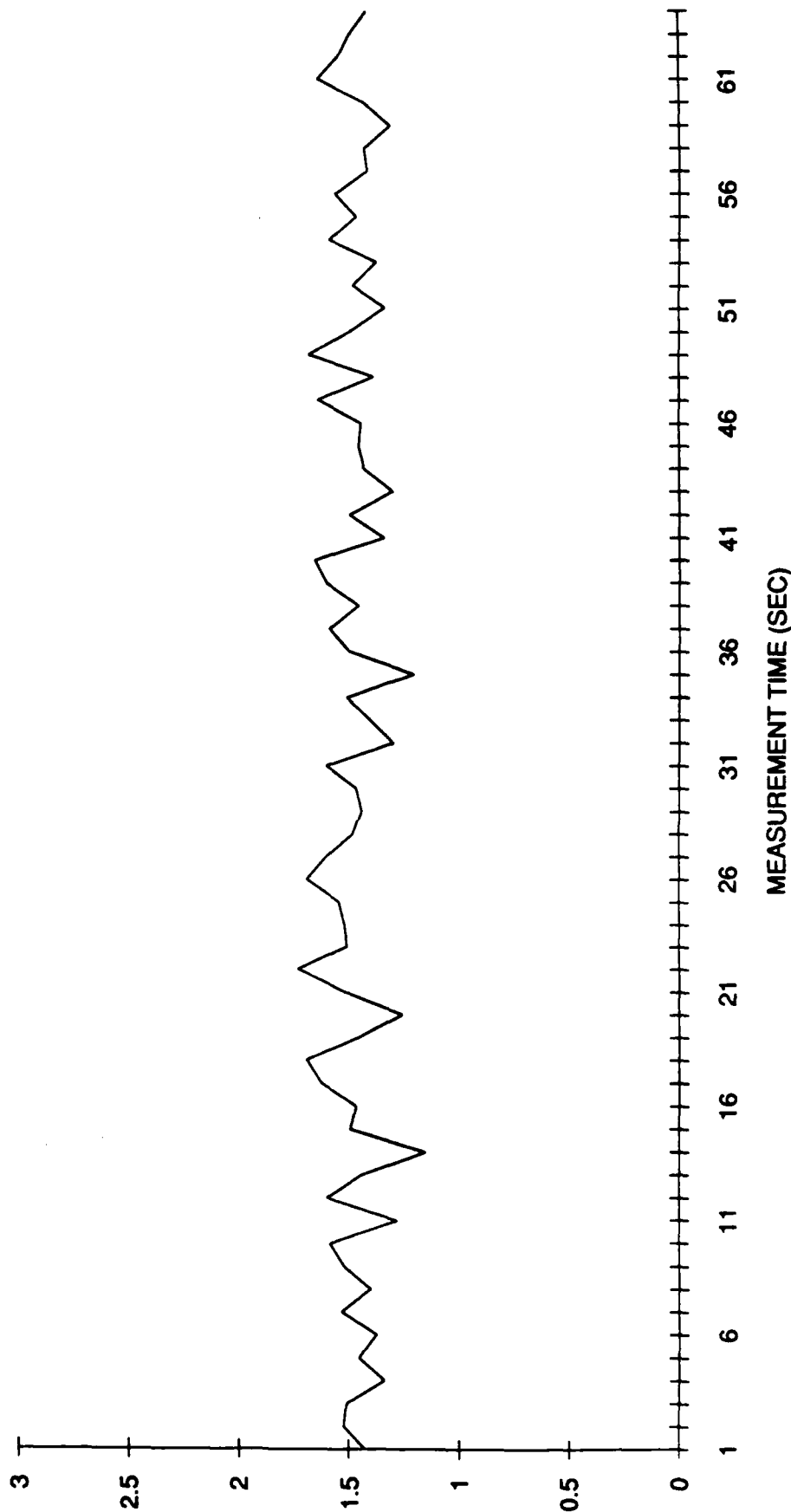
| <u>PARAMETER</u> | <u>C/N₀</u> | <u>LOOP BW</u> | <u>PREDICTED ERROR</u> | <u>MEASURED ABSOLUTE ERROR</u> | <u>MEASURED RANDOM ERROR</u> |
|-------------------------|------------------------|--------------------|----------------------------|--|--------------------------------------|
| P CODE CARRIER PHASE | 40 dB-Hz | 11 Hz | 0.11 CM | 0.34 CM | 0.134 CM |
| P CODE PSEUDO RANGE | 40 dB-Hz | 0.1 Hz | 8 CM | 37 CM | 14.7 CM |



CARRIER PHASE RANDOM ERROR

CARRIER PHASE - CENTIMETERS

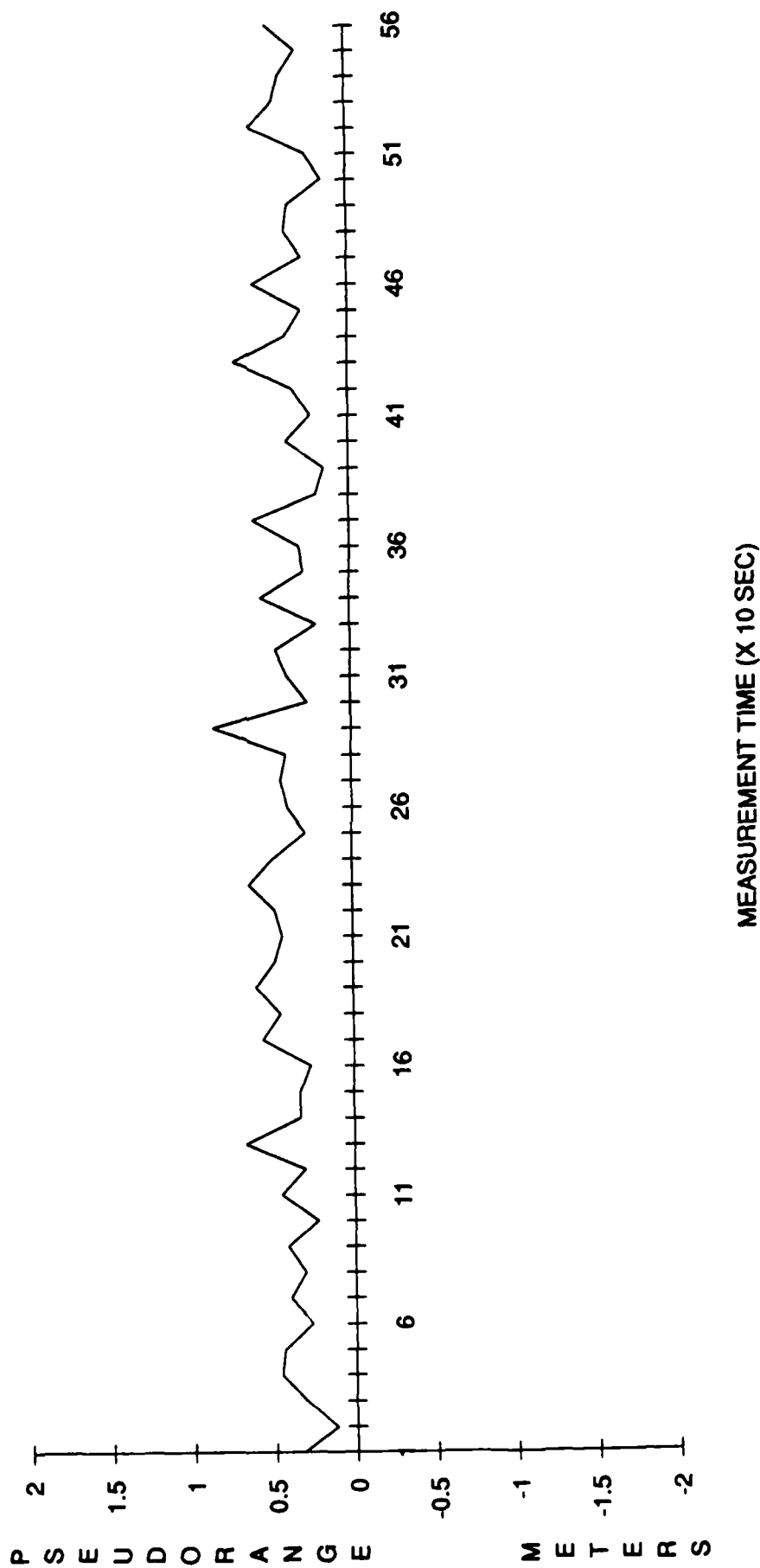
PH1-PH2 = 0.134 CM, ONE SIGMA; C/No = 40





PSEUDORANGE RANDOM ERROR

PR1 - PR2 = 0.147 METERS, ONE SIGMA; C/N0 = 40





INTERCHANNEL BIAS MEASUREMENT SUMMARY

- O MEASUREMENT TECHNIQUE - ALL CHANNELS TRACKING ONE GPS SV SIGNAL (L1-P)
- O CARRIER PHASE BIAS = PAIRWISE DIFFERENCES BETWEEN CHANNELS
 $|PH_i - PH_j| < 0.019 \text{ CM (1 LSB OF PHASE WORD)}$
- O PSEUDO-RANGE BIAS = PAIRWISE DIFFERENCES BETWEEN CHANNELS
 $|PR_i - PR_j| \leq 0.1 \text{ CM } (\pm 2 \text{ LSB OF PR WORD})$

DESIGN AND PERFORMANCE OF THE
GPS RECEIVER UNIT (GPSRU) FOR THE
NASA ORBITAL MANEUVERING VEHICLE

Roger M. Weninger
Richard Sfeir

Satellite & Space Electronics Division
Rockwell International
Anaheim, California

ABSTRACT

This paper provides a description of the spaceborne GPS Receiver Unit (GPSRU) planned for installation on NASA's Orbital Maneuvering Vehicle (OMV). The receiver's hardware and software implementation, and its interfaces with the OMV, will be presented. Simulation results demonstrating the receiver's performance will also be reported. A breadboard unit has been operating at Rockwell since May 1989. The qualification test is planned for August 1991, and the flight units are scheduled for delivery in March 1992.

INTRODUCTION

In August 1988 a contract was awarded to the Satellite and Space Electronics Division of Rockwell International to provide GPS receivers for the Orbital Maneuvering Vehicle (OMV). This receiver is based on a Miniature GPS Receiver (MGR) chipset developed by Rockwell under contract to DARPA (1). This chip set is shown in Figure 1 and their physical parameters are summarized in Table 1. It consists of a GaAs MMIC RF/IF Translator, a Silicon Frequency Synthesizer, a CMOS Signal Processor, a CMOS Multi-Function Interface and an

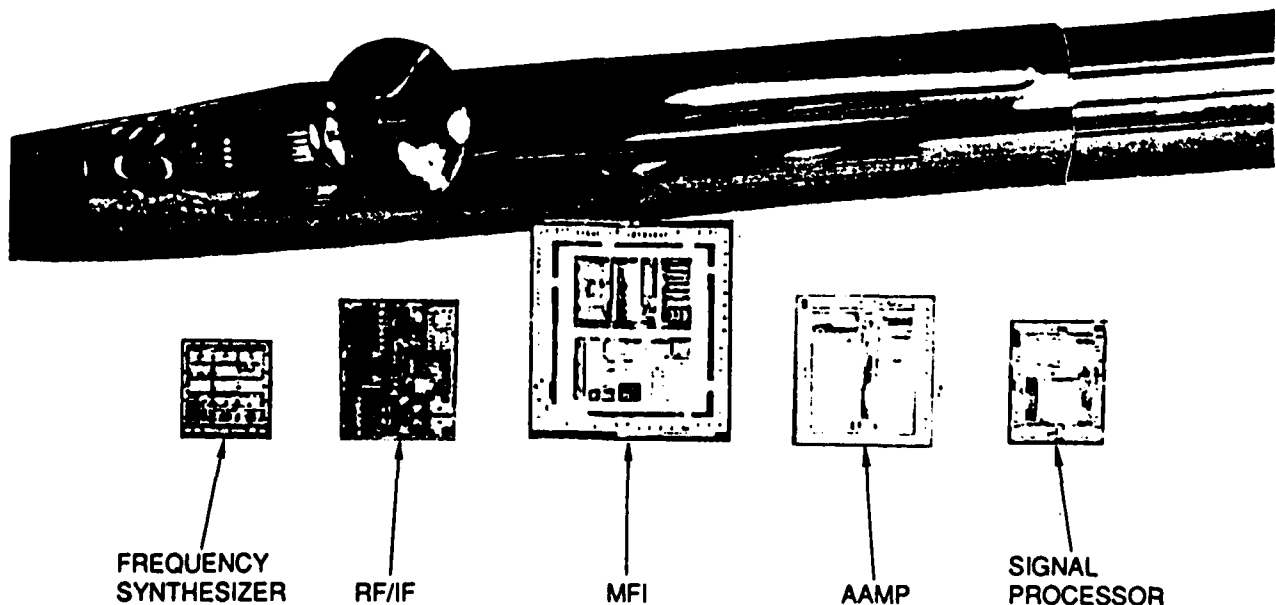


Figure 1. Miniature GPS Receiver (MGR) Chip Set

Table 1. MGR Chip Set Summary

| CHIP TYPE | DEVICE COUNT | DIMENSIONS (inches) | IMPLEMENTATION TECHNOLOGY | POWER (mW) |
|---|--------------|---------------------|---------------------------|------------|
| RF/IF Translator | 420 | 0.340 x 0.350 | Gallium Arsenide | 1500 |
| Signal Processor | 19,800 | 0.185 x 0.220 | 1.25 Micron Bulk CMOS | 90 |
| Multifunction Interface (MFI) | 29,000 | 0.370 x 0.370 | 1.6 Micron Bulk CMOS | 20 |
| Advanced Architecture Microprocessor (AAMP) | 74,000 | 0.250 x 0.261 | 2 Micron Bulk CMOS | 90 |
| Frequency Synthesizer | 350 | 0.165 x 0.165 | Bipolar Silicon | 500 |

Advanced Architecture Micro-Processor. This chip set is configured with memory, a frequency standard, a power supply, and user interface circuitry to make up the OMV GPSRU described herein. The receiver will have two channels capable of tracking either C/A or P code, and will determine position, velocity and time for the OMV. Two receivers will be installed on the spacecraft, each operates independently of the other.

The OMV prime contractor is TRW and the responsible NASA agency is the Marshall Space Flight Center.

SPECIFICATION REQUIREMENTS/ PREDICTED PERFORMANCE

The following performance parameters were extracted from the OMV GPSRU specification document (2). Actual receiver performance is expected to be better than these values. As an example the simulated navigation position and velocity errors summarized in Table 3 are better than the specified performance defined in h) and i).

a) Minimum carrier to noise ratio of 33.2 dB-Hz for the C/A signal and 30.2 dB-Hz for the P-code signal.

b) Use the L1 signal of 1.57542 GHz only.

c) Input signal power of the L1 C/A signal within the range of -138 dBm to -104 dBm.

d) Achieve navigation accuracy within 10 minutes (90% probability) after an initialization accuracy of:

time ± 1 second
position ± 80 nmi
velocity ± 600 ft/sec

e) Pseudo range error not to exceed 28 feet for C/A-code and 6 feet for P-code (1 sigma).

f) Pseudo range-rate error not to exceed 0.08 feet/second (1 sigma).

g) Absolute GMT time error of 1 micro-second (1 sigma).

h) Navigation position error per axis not to exceed 397 feet (3 sigma) when GDOP = 4.6.

i) Navigation velocity error per axis not to exceed 1.19 feet/second (3 sigma) when GDOP = 4.6.

- j) The receiver shall be capable of correcting the corrupted data resulting from Selective Availability (SA).

The specified (2) system errors for the evaluation of navigation performance are shown in Table 2. Using these errors in a computer simulation to predict GPSRU navigation performance produced the results shown in Table 3. These results show a predicted one-sigma, spherical position error with P-code of 11.7, 11.9 and 12.6 feet for OMV altitudes of 125, 200 and 1000 nautical miles, respectively.

FUNCTIONAL DESCRIPTION

The two channel GPSRU sequentially tracks a selected group of GPS satellites. The channels function independently so that data from two satellites can be processed in parallel. During normal tracking, the two channels are

allocated a one-second processing interval for each satellite, i.e., within one second all of the real-time functions associated with acquisition, tracking and navigation are accomplished. At the end of the one second, the two channels reacquire and track the next two satellites in their respective satellite assignments.

The receiver can operate on either or both the Clear Access (C/A) code, or on Precision Code (P-code) depending upon performance requirements. As a general rule when estimated position is not well known C/A code is used for acquisition and then handover occurs to the P-code; however, if the estimated position and time error is within ± 300 P-code chips (± 30000 feet), a satellite can be acquired with P-code.

A functional configuration of the GPSRU is shown in the flow diagram of Figure 2 which is designed to show the signal/data flow from the antenna input to the

Table 2. GPS System Error Assignment

| ERROR SOURCE | PSEUDO RANGE ERROR 1-SIGMA (ft) | |
|---|------------------------------------|----------|
| | P-CODE | C/A CODE |
| Space Segment: | | |
| Clock and Navigation Sub-system Stability | 9.8 | 9.8 |
| Prediction of Satellite Perturbation | 3.3 | 3.3 |
| Other | 1.6 | 1.6 |
| Control Segment: | | |
| Ephemeris Prediction Model Implementation | 13.8 | 13.8 |
| Other | 3.0 | 3.0 |
| Tropospheric Delay Compensation | 0 | 0 |
| Multipath | 3.9 | 3.9 |
| Other | 1.6 | 1.6 |
| Receiver Noise and Resolution | 6.0 | 28.0 |
| Ionospheric Delay Compensation | 17.0 | 17.0 |
| RSS | 25.5 | 37.4 |

Table 3. Predicted Navigation Performance

| ALT. OF OMV (nmi) | NO. OF GPS SATS | CODE TYPE | 1σ POSITION ERROR (ft) | | | 1σ VELOCITY ERROR (ft/sec) | | | PROBABILITY ERROR EXCEEDS 3σ LIMITS | | | | | | 1σ CLOCK ERROR (ns) |
|----------------------------|--------------------------|--------------|---------------------------|-----|-----|-------------------------------|-------|-------|--|---|---|----------|---|---|------------------------------|
| | | | | | | | | | POSTIION | | | VELOCITY | | | |
| | | | X | Y | Z | X | Y | Z | X | Y | Z | X | Y | Z | |
| 125 | 21 | P | 6.5 | 7.0 | 6.8 | 0.040 | 0.046 | 0.045 | 0 | 0 | 0 | 0 | 0 | 0 | 5.0 |
| 125 | 21 | C/A | 7.9 | 8.6 | 9.1 | 0.039 | 0.043 | 0.042 | 0 | 0 | 0 | 0 | 0 | 0 | 5.8 |
| 200 | 21 | P | 6.3 | 7.9 | 6.3 | 0.039 | 0.044 | 0.042 | 0 | 0 | 0 | 0 | 0 | 0 | 4.9 |
| 200 | 21 | C/A | 7.1 | 8.9 | 7.5 | 0.039 | 0.046 | 0.043 | 0 | 0 | 0 | 0 | 0 | 0 | 5.6 |
| 1000 | 21 | P | 7.1 | 7.5 | 6.7 | 0.039 | 0.045 | 0.048 | 0 | 0 | 0 | 0 | 0 | 0 | 5.2 |
| 1000 | 21 | C/A | 8.5 | 9.0 | 9.1 | 0.044 | 0.052 | 0.045 | 0 | 0 | 0 | 0 | 0 | 0 | 5.5 |

data output to the host vehicle. The flow diagram also shows the functional partitioning of receiver elements among RF and digital hardware, and software processing.

RF PROCESSING

The incoming L_1 signal is routed through an overload protection limiter with broadband low signal linearity and a low noise amplifier which is followed by a band limiting filter. The signal is then down-converted to an IF of 173.91 MHz by the injection of 1401.51 MHz signal to the first mixer. The down converted signal is further filtered and amplified through an IF bandpass filter and an IF amplifier. The IF signal is then fed to an inphase and a quadrature mixer to generate the I and Q signals. The I and Q mixer local oscillator frequency is obtained by dividing the 1401.51 MHz signal by 8, yielding a frequency of 175.18875 MHz. The resultant I and Q mixer outputs are video signals at a frequency of 1.27875 MHz. Each of the I and Q signals are followed by a low pass filter and a wideband video amplifier. The video

amplifier is gain controlled over a range of 30 dB. These stages are used for Automatic Gain Control (AGC).

The 1.27875 MHz I&Q AGC output signals are converted to digital signals in A/D converters. The A/D conversion process is accomplished using a null zone limiter which provides a +1, 0, or -1 output as a function of input signal amplitude. The null zone limiter was chosen over a binary hard limiter since it maintains the signal processing simplicity while providing superior performance. It should be noted that the finite quantization of the A to D converter will be reflected in a processing loss rather than a measurement error or bias. The I and Q quantized signals are fed to a pair of CMOS drivers to drive the signal processing functions.

SIGNAL PROCESSING

The major functions performed by signal processing are carrier demodulation and C/A or P-code removal. As illustrated in Figure 2, each of the two receiver channels has its own signal processor

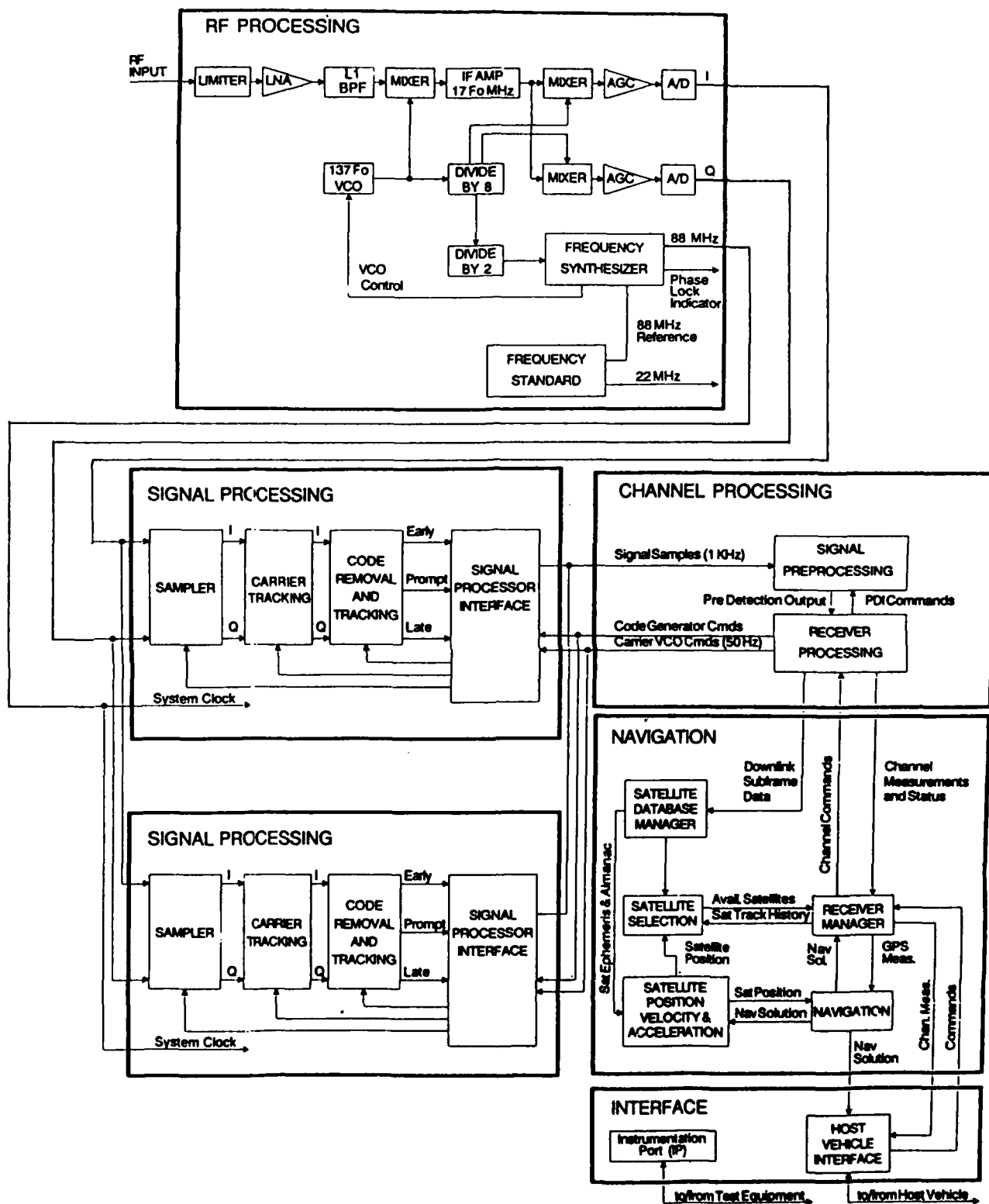


Figure 2. GPSRU Functional Flow Diagram

chip. Each signal processor synchronous samples the incoming I and Q signals at twice the P-code rate (20.46 MHz) and inputs them to the carrier and code tracking function.

The sampled I and Q signal is a 1.27875 MHz carrier shifted by any doppler frequency and quadrature phase modulated by the 1.023 MHz C/A code modulo-two summed with the 50 Hz navigation data, and in-phase modulated by the 10.23 MHz P-code also modulo-two summed with the 50 Hz data. The I and Q samples are input to a digital phase rotator driven by the carrier VCO output. The phase rotator, acting as a single sideband mixer, translates the signal to baseband by removing the carrier and its doppler frequency leaving the sampled C/A code, P-code, and data.

The signal is then passed to code removal logic which correlates the selected code (C/A or P-code) from the Code Generator to the incoming code. The Code Generator output is essentially moved back and forth in time until it exactly matches the incoming code, at which point the code signals cancel and only the data plus any tracking errors remain. The amount of time shift required to make the codes match is directly proportional to pseudorange. An Integrator then sums the sampled data signal into 1.0 millisecond samples coherent with the assumed C/A epochs for software processing.

CHANNEL PROCESSING

Channel processing functions derive carrier phase, code delay, and signal amplitude estimates from the raw (1 ms) signal samples. The processed signals are further summed and directed to the code and carrier loop filters, which are integrated at a 50 Hz (20 ms) rate and provide control outputs to the hardware VCOs. Although primarily concerned with signal tracking, channel processing provides signal search, acquisition, reacquisition and subframe

data demodulation as well. Internally the channel processing function accepts signal samples at a 1 kHz rate from the signal processor and provides back commands at a 50 Hz rate. The channel processing function also provides the pseudo-range measurement from the code loop, the delta pseudo-range measurement from the carrier loop, and the carrier power to noise spectral density ratio (C/N_0) estimate. It interfaces to the navigation and interface processing functions at a 1 Hz rate, providing channel measurements and status, downlink subframe data (when required), and accepting channel command data.

NAVIGATION

The navigation function accepts pseudo-range and delta pseudorange measurements, combines them with the corresponding GPS satellite position, velocity, and acceleration in Earth-Centered-Inertial (ECI) coordinates, and calculates optimal estimates of the host vehicle position, velocity and time. Linearized measurement data and measurement error variances are input to an 8-state, extended Kalman filter which estimates corrections to the nominal navigation solution. The filter also maintains estimated error statistics in the form of an error covariance matrix.

In addition to providing navigation outputs, the navigation solution provides estimates of pseudorange, pseudorange rate and pseudorange acceleration to the code correlator to aid the receiver during acquisition to position the Code Generator for sequential tracking operation.

INTERFACE

The GPSRU has an Instrumentation Port (IP) that provides a standard bidirectional serial data interface, accepts data capture commands and generates a precise time mark at a 1 Hz rate. The IP is used for testing and is suitable

as a host vehicle interface. The data format is compatible with ICD-GPS-204 data format for an Instrumentation Port. This is compatible with an RS232C serial interface port operating at 9600 baud.

The GPSRU also has an OMV specified interface consisting of discretes and of four buffers with unidirectional serial interfaces. There are three output buffers and one input buffer to provide for the following data transfer and receiver control:

Input Buffer:

Mode control (Off, Standby 1, Standby 2, Built-In-Test and Navigate)

Initialization data (position, velocity and time) in ECI

GPS constellation almanac data

Thrust vector (when available) in ECI

Update output data buffer requests

Output Buffer 1:

X, Y and Z position in ECI coordinates

X, Y and Z velocity in ECI coordinates

Time tag (GMT) for navigation data

Pseudorange and range rate (integrated carrier VCO commands) to satellites currently being tracked

Navigation data error variances from the Kalman filter

C/N₀ for all satellites being tracked

Indication of which satellites are being tracked at any specified time

Receiver health/mode status

GDOP of primary constellation

Output Buffer 2:

GPS satellite almanac data (when requested)

Output Buffer 3:

GMT at a 1 Hz (nominal) time mark

HARDWARE DESCRIPTION

The GPSRU consists of four modules:

- RF Module
- Digital Module
- Interface Module
- Power Supply Module

A block diagram of the GPSRU is shown in Figure 3. The RF module includes the RF/IF translator, the frequency synthesizer and the frequency standard. The digital module contains the signal processors, AAMP, MFI and memory. The interface module contains an AAMP, MFI, memory and user interface circuitry.

The overall dimensions of the receiver shown in Figure 4 are 7.70 in. wide x 8.28 in. long x 4.75 in. high, including flanges. The unit weight is 8.8 lbs. and the total power dissipation is 11.6 watts. The size, weight and power are summarized in Table 4.

The modules plug directly into a Master Interconnect Board (MIB) for their electrical interface and are secured to the chassis with wedgelocks. Each module is uniquely keyed to prevent cross-plugging. A chassis assembly showing the plug-in modules is provided in Figure 5. The Host Vehicle interface connectors are mounted on one side of the receiver chassis, as shown in Figure 4. The OMV interface consists of one 9 pin input power connector, one SMA type coaxial RF input connector, and one 50 pin interface connector. In addition, there is one SMA type coaxial Test Connector.

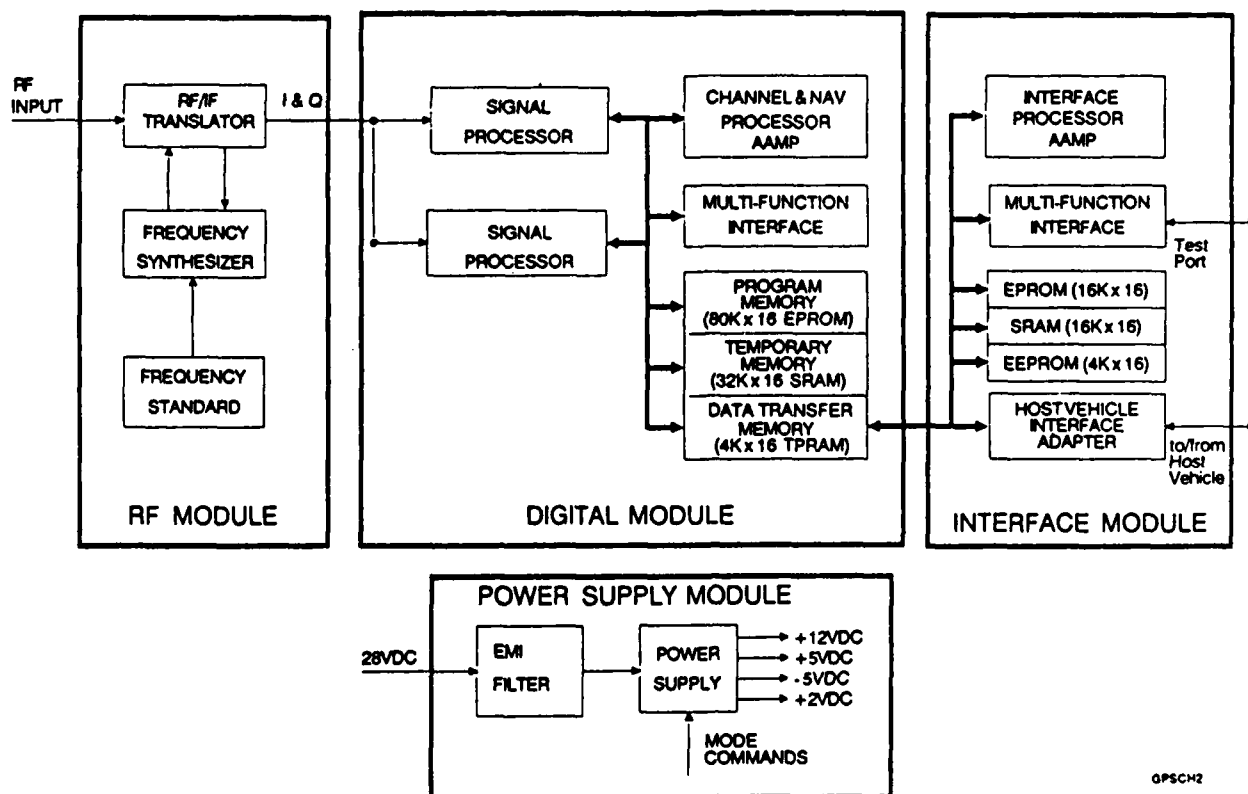


Figure 3. GPSRU Block Diagram

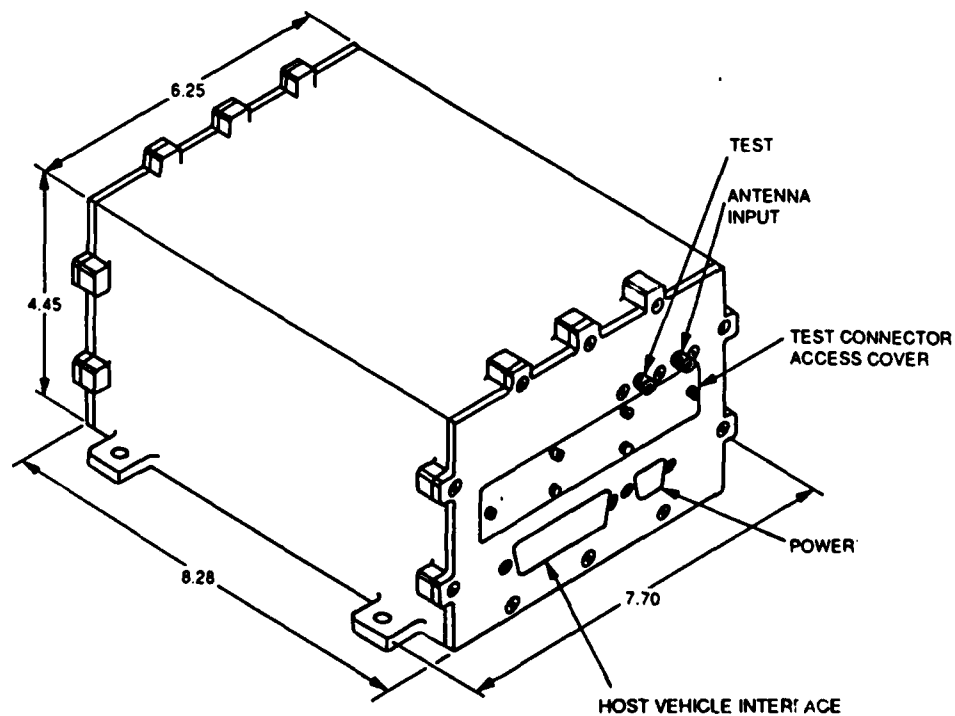


Figure 4. GPSRU Assembly

Table 4. GPSRU Size, Weight and Power Summary

| COMPONENT | SIZE (in.) L x W x H | WEIGHT (lbs) | POWER DISSIPATION (w) |
|-------------------------------------|-------------------------|-----------------|-----------------------------|
| RF Module | 7.00 x 5.75 x 1.25 | 1.10 | 2.6 |
| Digital Module | 7.00 x 5.75 x 0.6 | 0.54 | 2.6 |
| Interface Module | 7.00 x 5.75 x 0.6 | 0.54 | 3.5 |
| Power Supply Module | 7.00 x 5.75 x 1.15 | 1.25 | 2.9 |
| MIB | 5.75 x 3.50 x 0.125 | 0.34 | N/A |
| RCVR Chassis (Includes Hardware) | 8.28 x 7.70 x 4.75 | 5.04 | N/A |
| TOTAL | 8.28 x 7.70 x 4.75 | 8.8 | 11.6 |
| SPECIFICATION | 10.25 x 8.0 x 8.5 | 10.0 | 18.0 |

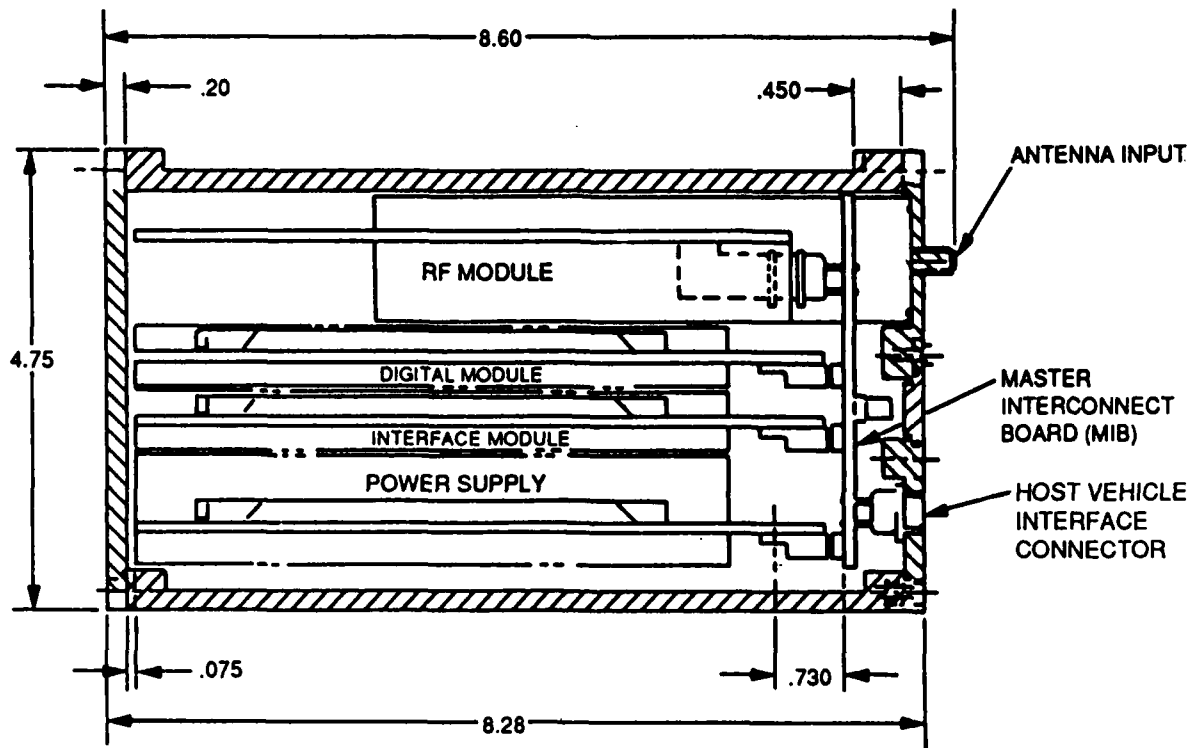


Figure 5. GPSRU Cross Section Side View

SUMMARY

A spaceborne GPS receiver unit (GPSRU) utilizing an advanced technology chipset has been described. This receiver weighs 8.8 pounds, occupies less than 0.2 cubic foot and requires 11.6 watts. It will provide GMT and spacecraft position and velocity. The navigation position and velocity accuracy of the GPSRU is expected to be approximately 16 feet (1 sigma) per axis and 0.05 feet/second (1 sigma) per axis, respectively.

ACKNOWLEDGEMENTS

The work described in this paper was performed under subcontract DA7917NZ8H from TRW for prime contract NAS8-36800 issued by NASA Marshall Space Flight Center for the Orbital Maneuvering Vehicle (OMV).

The chipset used in the receiver was developed for DARPA under contract F29601-85-C-0022.

The authors also acknowledge the support received from Juergen Bruckner of Rockwell International's Collins Government Avionics Division.

REFERENCES

1. N.B. Hemesath, J.M.H. Bruckner, "DARPA's Advanced Technology GPS Chipset," Rockwell International Corporation, Collins Government Avionics Division, 1988.
2. Equipment Specification Orbital Maneuvering Vehicle Global Positioning System Receiver Unit, EQ4-3734 Rev. E, TRW Space & Technology Group, 16 August 1988.

Application of GPS to Space-Based Tethered Array Radar

Horst Salzwedel, Kenneth M. Kessler and Fred Karkalik

Systems Control Technology, Inc.

2300 Geng Road

Palo Alto, California 94303

Abstract

This paper investigates the use of GPS as an aid in establishing and maintaining coherence of a highly distributed Space-based Tethered Array Radar (STAR) system. The STAR concept is a network of distributed small satellite subarrays each of which is a linear array of elements or "string". Each subarray is made up of many dipole elements, each with its own receive module. In order to achieve beamforming and the radar performance desired, the relative position and orientation of each dipole element must be estimated within a fraction of a wavelength of the radar frequency.

A subset of the general problem is considered here. A single tether, subjected to environmental disturbances, is modeled by a lumped mass dynamic model of the motion. Candidate GPS receiver elements with code and phase measurements are located at the end-satellites and along the tether. Based on this configuration a linear Kalman filter was developed using a model of the longitudinal and lateral motions of the tether. Torsional effects were neglected for this analysis.

The errors caused by solar pressure, atmospheric drag, and earth-shadow transitions were investigated for an altitude of 1000 kilometers. The estimation error in the filter was determined by covariance analysis, linear filtering and nonlinear simulations using the interactive CAE software Ctrl-C[®]/Model-CTM.

1. Introduction

Consider two satellites separated vertically by a string several kilometers long. This is a very long antenna that could be used for long-wavelength communications. Or, one could attach many receivers along this string and have multiple strings next to each other forming a phased array radar. Such a space-based radar can be made very light-weight. The launch and maintenance costs are therefore low even for higher altitude orbits. For a surveillance radar application it is necessary that signals received along the tether and between tethers are combined coherently to form a radar image. It is therefore necessary to know the relative position and orientation of the receive elements to a fraction of the radar wave length and the absolute position to observation accuracy requirements. This paper investigates the use of GPS as an aid in establishing and maintaining coherence of such a highly distributed space based radar system subject to environmental disturbances of solar pressure and atmospheric drag.

Second Symposium on GPS Applications in Space, Hanscom AFB, Lexington, MA, October 1989.

The Space-Based Tethered Array Radar (STAR) concept under consideration evolved from the DOD need for an affordable, improved surveillance system [1]. The STAR concept is a network of distributed small satellite subarrays each of which is a linear array of elements or "string" (Figure 1). In order to achieve the radar performance desired, the relative position and orientation of each dipole element must be estimated within a fraction of a wavelength of the radar frequency. The tether concept, in addition of being lightweight, appears to provide a basis for achieving the power aperture product needed to detect the small targets of interest. However, the concept presents a challenge in terms of dynamic stability, pointing, and control. One aspect of the problem requiring a solution is the development of an adequate integrated estimator/sensor system to accurately predict tether motion.

The approach taken in this paper is to consider a subset of the problem and to analyze the dynamic behavior of a single tether due to high altitude disturbances. After development of a lumped mass dynamic model of the motion of a tether in space, a candidate GPS receiver configuration that makes use of available GPS code and phase measurement data is discussed. Based on this configuration and dynamic model, a linear Kalman filter was developed using a model of the longitudinal and lateral motions of the tether. Torsional effects were neglected for this analysis.

Section 2 describes the basic tether dynamics, section 3 describes candidate GPS sensor configurations, section 4 shows the simulation, and section 5 evaluates GPS based filters.

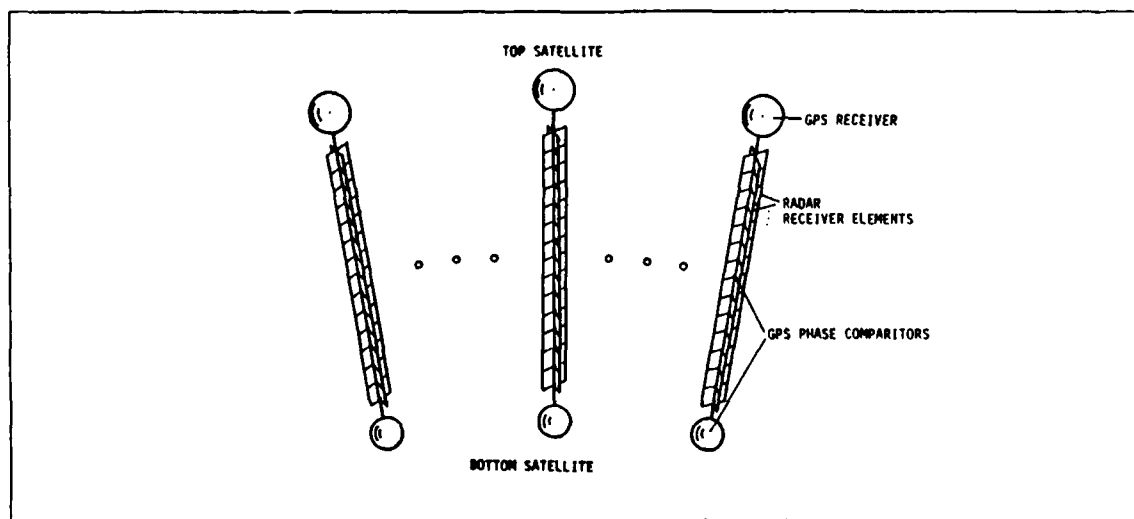


Figure 1: Space-Based Tethered Array Radar.

2. Tether Dynamics

The dynamics of a tether in orbit around the earth may be conveniently analyzed in terms of its steady state and its transient behavior. The steady state behavior is the

nominal motion of the tether in the average gravity field of the earth. The gravity gradient forces of this uniform gravity field hold the tether nominally in a vertical position relative to the Earth's surface. The transient behavior is the flexible motion and perturbation of the tether due to non-uniformity of the earth's gravity potential, solar pressure, and interaction with the earth's magnetic field. In addition, thermal heating due to solar, earthen and lunar radiation, magnified by the rapid transition into and out of the Earth shadow will deform the string and introduce further dynamic perturbations.

The dynamics of the tether may be modeled as a continuum or as interconnected point masses or rigid bodies. The continuum model is well suited to determine the steady state characteristics of the string as well as the basic eigen-frequencies. However, a super-computer would be needed to integrate the resulting partial differential equation derived from a force balance equation written for the earth's orbit perturbation environment. For this analysis we shall therefore use discretized models.

Three types of discretizations are being used in modeling the dynamics of aerospace systems. They are finite element, finite difference and lumped mass models. Finite element models are primarily used for detailed analysis of nearly linear dynamics. Finite difference methods are dominant in fluid and thermodynamics. Lumped mass models are the easiest to implement and are used for modeling the overall characteristics of complete aerospace systems. In this analysis we shall model libration and bowing - stretching characteristics by lumped mass models, generally referred to as *bead* models in the literature on tether dynamics.

Consider a string of point masses connected by spring/damper combinations, that are described in coordinate frames (Orlov frames) that rotate at the nominal circular orbits of these masses about the earth (Figure 2). The D'Alembert force of a point mass is equal to the forces acting on the point mass.

$$m_i \overset{II}{\vec{r}} = \vec{F}_{g_i} + \sum_j \vec{F}_{SP_{ij}} + \vec{F}_{S_i} + \vec{F}_{D_i} + \vec{F}_{E_i} \quad (1)$$

where $()^I$ denotes the derivative in inertial coordinates, \vec{F}_{g_i} is the gravity force, $\vec{F}_{SP_{ij}}$ is the spring force between the i -th and j -th mass, \vec{F}_{S_i} denotes the solar force, \vec{F}_{D_i} denotes the drag force and \vec{F}_{E_i} is the electrodynamic force.

The acceleration may also be described by

$$\overset{II}{\vec{r}}_i = \overset{BB}{\vec{\rho}}_i + 2\vec{\omega} \times \overset{B}{\vec{\rho}}_i + \vec{\omega} \times (\vec{\omega} \times (\vec{R}_i + \vec{\rho}_i)), \quad (2)$$

where $\vec{\rho}_i$ is the vector from the i -th Orlov frame to the i -th point mass, $()^B$ is the derivative relative to the Orlov frame, $\vec{\omega}$ is the angular velocity vector from the center of the earth to the i -th Orlov frame, and \vec{R}_i is the vector from the center of the earth to the i -th Orlov frame, where

$$\vec{R}_1 = -R_1 \hat{k}_1, \quad \vec{R}_2 = -(R_1 + l_1) \hat{k}_2, \dots \quad \text{and} \quad \overset{B}{\vec{R}}_i = 0 \quad (3)$$

Coordinizing the vectors in the Orlov frames gives,

$$\rho_i = \begin{bmatrix} x_i \\ y_i \\ z_i \end{bmatrix}, \quad \omega = \begin{bmatrix} 0 \\ -\omega \\ 0 \end{bmatrix}, \quad (4)$$

and

$$\frac{\Pi}{\vec{r}_i}|_i = \begin{bmatrix} \dot{\tilde{x}}_i \\ \dot{\tilde{y}}_i \\ \dot{\tilde{z}}_i \end{bmatrix} + 2\omega \begin{bmatrix} -\dot{z}_i \\ 0 \\ \dot{x}_i \end{bmatrix} - \omega^2 \begin{bmatrix} x_i \\ 0 \\ z_i - R_i \end{bmatrix} \quad (5)$$

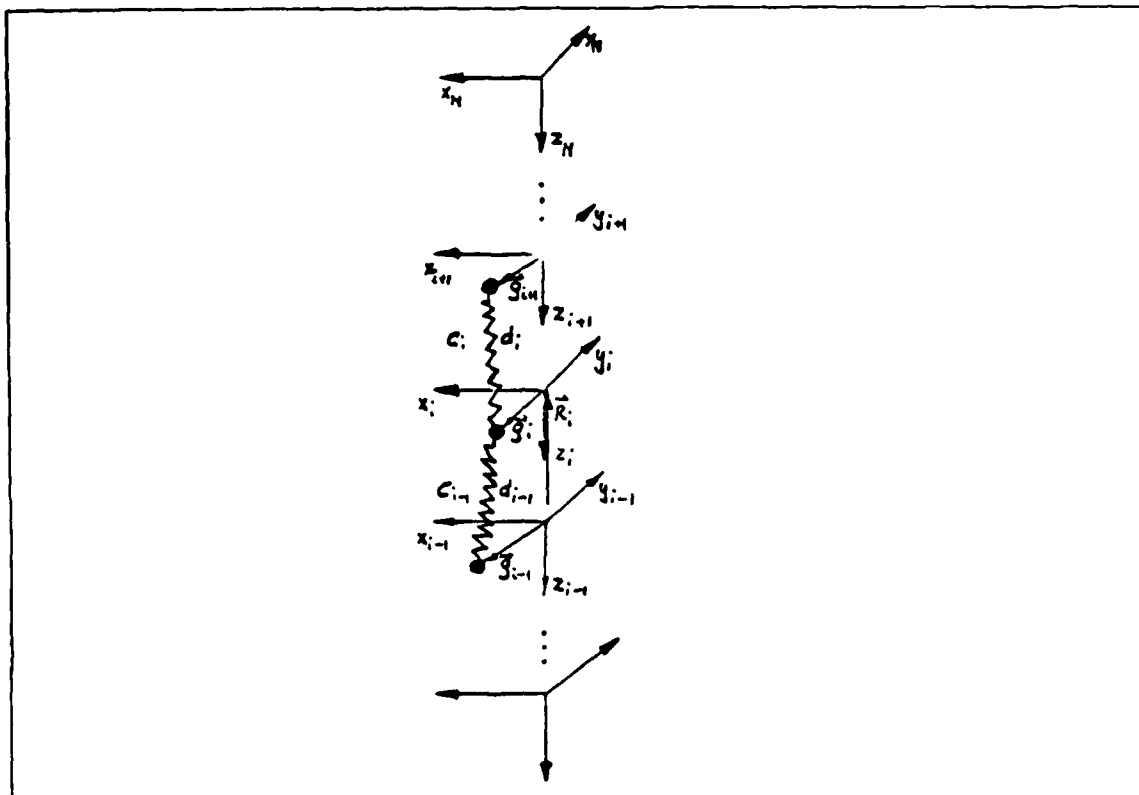


Figure 2: Bead Model of Tethered Satellite in Orlov Frames.

The gravity force is,

$$\vec{F}_{g_i} = -\frac{\mu m_i}{r_i^2} \hat{r}_i, \quad (6)$$

where $r_i^2 = x_i^2 + y_i^2 + (z - R_i)^2$ and \hat{r}_i is the unit vector along \vec{r}_i ,

$$\hat{r}_i = \frac{\vec{r}_i}{|\vec{r}_i|}, \quad (7)$$

giving

$$\vec{F}_{g_i}|_i = -\frac{\mu m_i}{r_i^3} \begin{bmatrix} x_i \\ y_i \\ z_i - R_i \end{bmatrix} \quad (8)$$

The spring damper force of a tether element between mass i and j is,

$$\vec{F}_{SP,ij} = C_{ij}(r_{ij} - l_{0,ij})\hat{r}_{ij} + D_{ij}((\vec{v}_j - \vec{v}_i) \cdot \hat{r}_{ij})\hat{r}_{ij} \quad (9)$$

for stretching and small compressions, and is approximately constant for buckling, where C_{ij} is the spring constant, D_{ij} is the damping constant, \vec{r}_{ij} is the vector from mass i to mass j , \vec{v}_i is the velocity of mass i relative to the i -th frame, \vec{v}_j is the velocity of mass j relative to the j -th frame and $l_{0,ij}$ is the zero-force length of the tether element between mass i and mass j . The zero-force length is a function of its temperature and changes with the periodicity of the solar incident angle and during Earth shadow transitions.

Solar Radiation Forces

An exposed surface is subjected to radiation pressure equal to the difference between incident and reflected momentum flux. The main sources of electromagnetic radiation pressure in an Earth's orbit are,

- Solar illumination ($F_S \simeq 1360 \text{ W/m}^2$)
- Solar radiation reflected by the Earth and its atmosphere ($100 - 300 \text{ W/m}^2$)
- Radiation emitted by Earth and its atmosphere
- Solar radiation reflected by the Moon

The momentum flux, p , acting on a surface element normal to the direction of the radiation is

$$p = \frac{F}{c} \quad (10)$$

where F is the radiation energy flux and c is the speed of light.

The radiation forces acting on a surface element may be divided into forces due to absorbed radiation, forces due to reflected radiation, and forces due to diffused reflected radiation. With the absorption coefficient, C_a , the reflection coefficient, C_r , the diffusion coefficient, C_d , and $C_a + C_r + C_d = 1$, the total radiation force for one radiation source may be expressed by,

$$\vec{F} = -p \int_A (1 - C_r) \cos \theta \hat{S} + 2(C_r \cos^2 \theta + \frac{C_d}{3} \cos \theta) \hat{N} dA, \quad (11)$$

where θ is the angle between the unit surface normal, \hat{N} , and the unit vector, \hat{S} , towards the light source.

The body surface is assumed to be comprised of spherical end-satellites, and flat surface elements and cylinders along the tether. Integrating over different surface types we get, for a flat surface:

$$\vec{F} = -pA \left[(1 - C_r) \hat{S} + 2(C_r \cos \theta + \frac{C_d}{3}) \hat{N} \right] \cos \theta, \quad (12)$$

for a sphere of radius r :

$$\vec{F} = -p4\pi r^2 \left[\frac{1}{4} + \frac{1}{9}C_d \right] \hat{S}, \quad (13)$$

and for a cylinder of height h :

$$\vec{F} = -p2rh \left[\left(\sin \psi \left(1 + \frac{1}{3}C_r \right) + \frac{\pi}{6}C_d \right) \hat{S} - \left(\frac{4}{3}C_r \sin \psi + \frac{\pi}{6}C_d \right) \cos \psi \hat{Z} \right], \quad (14)$$

where \hat{Z} is along the cylinder axis and ψ is the angle between the cylinder axis and the solar direction, $\psi = \arccos(\hat{Z} \cdot \hat{S})$. NOTE: In the simulation additional shadowing effects were considered.

The total solar torque may be computed by integrating the torques caused by the solar forces acting on the spacecraft. Figure 3 shows the analytically computed torque due to solar pressure on a 2000m tether configuration and the sun in the orbital plane. The total torque oscillates between $\pm 1.4Nm$ (Units are in Newton-meter). The resulting steady state angle oscillates between $\pm 0.04^\circ$, which corresponds to $\pm 1.4m$ in orbit offset of the lower satellite relative to the upper satellite.

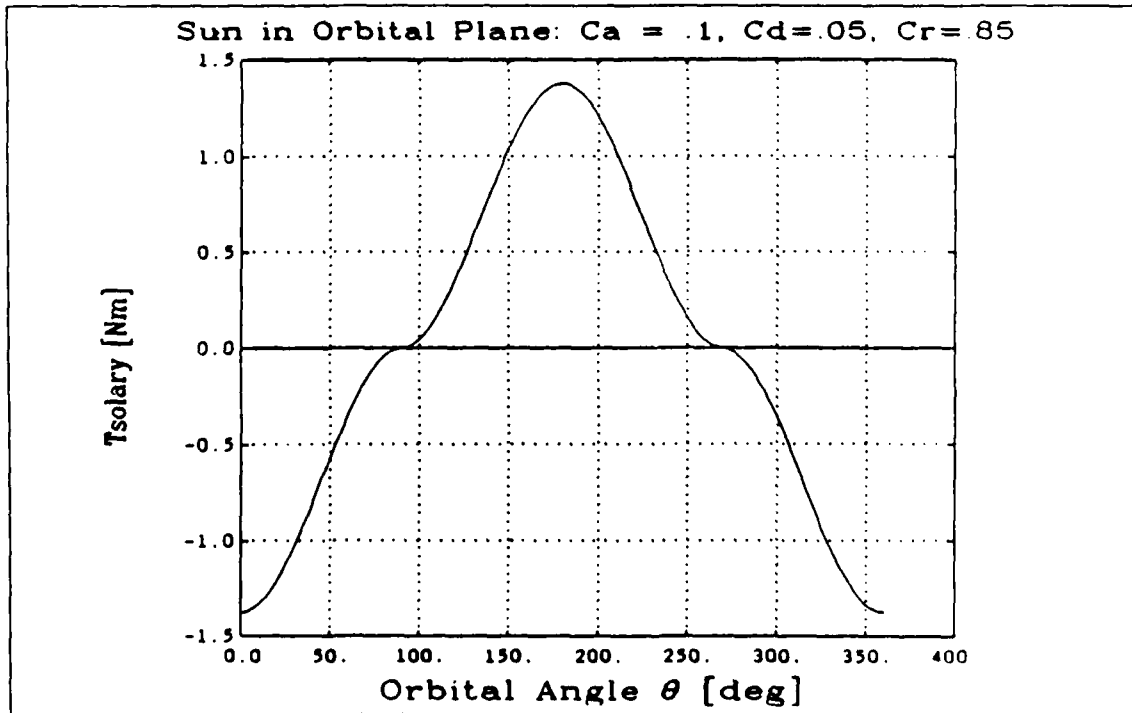


Figure 3: Solar Pressure Torque on Sample Configuration.

Atmospheric Forces and Torques

Even though the solar pressure forces are more than 30 times larger than the forces due to atmospheric drag, the drag forces are significant since they are opposite the orbital velocity and slowly de-orbit the spacecraft. For the example configuration at an altitude of 1000km this drag results in a de-orbit rate of 20 m/day. For this investigation, the 1977 Jacchia density model [5] was used, which accounts for different atmospheric temperatures due to changes in solar activities.

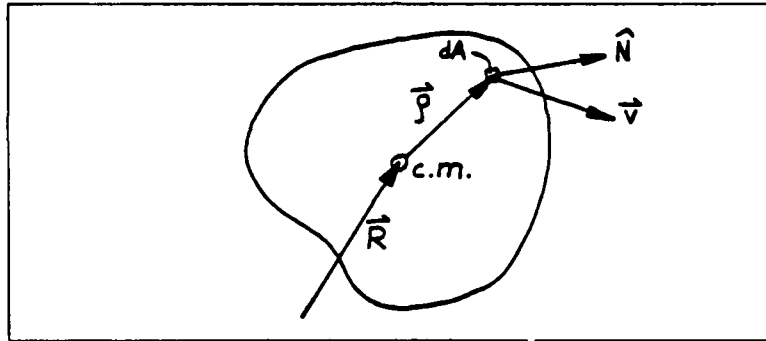
The force due to the impact of atmospheric molecules on the spacecraft surface can be modeled as an elastic impact without reflection [3]. The differential force, $d\vec{f}_{AERO}$, on a surface element dA , with outward normal \hat{N} , is given by,

$$d\vec{f}_{AERO} = -C_D \frac{\rho}{2} v^2 (\hat{N} \cdot \hat{v}) \hat{v} dA \quad (15)$$

where $\hat{v} = \vec{v}/v$ is the unit vector in the direction of \vec{v} , ρ is the atmospheric density and $C_D \leq 2$ is the drag coefficient. The aerodynamic drag for a surface perpendicular to \vec{v} is then

$$\vec{F}_D = -C_D \frac{\rho}{2} A \vec{v} |\vec{v}| \quad (16)$$

The aerodynamic torque on a spacecraft about its center of mass is



$$T_{AERO} = \int \vec{\rho} \times d\vec{f}_{AERO} = - \int \vec{\rho} \times (C_D \frac{\rho D}{2} (\hat{N} \cdot \vec{v}) \vec{v} dA), \quad (17)$$

where the integral is over the surface of the tethered spacecraft for which $\hat{N} \cdot \hat{v} > 0$, and $\vec{v} = \vec{v}_{cm} + \vec{\omega} \times \vec{\rho}$,

$$T_{AERO} = \int C_D \frac{\rho D}{2} (\hat{N} \cdot (\vec{v}_{cm} + \vec{\omega} \times \vec{\rho})) (\vec{v}_{cm} + \vec{\omega} \times \vec{\rho}) \times \vec{\rho} dA \quad (18)$$

$$\begin{aligned} T_{AERO} = & \int C_D \frac{\rho D}{2} (\hat{N} \cdot \vec{v}_{cm}) (\vec{v}_{cm} \times \vec{\rho}) dA \\ & + \int C_D \frac{\rho D}{2} (\hat{N} \cdot (\vec{\omega} \times \vec{\rho})) (\vec{v}_{cm} \times \vec{\rho}) dA \\ & + \int C_D \frac{\rho D}{2} (\hat{N} \cdot \vec{v}_{cm}) (\vec{\omega} \times \vec{\rho}) \times \vec{\rho} dA \\ & + \int C_D \frac{\rho D}{2} (\hat{N} \cdot (\vec{\omega} \times \vec{\rho})) (\vec{\omega} \times \vec{\rho}) \times \vec{\rho} dA \end{aligned} \quad (19)$$

Integrating over the length of the tether, the torque on the tether about the center of mass pitch axis becomes

$$T_{AERO_s} = \frac{A}{l} C_D \frac{\rho_D}{2} \left[\frac{\dot{\theta}^2}{4} (l_2^4 - l_1^4) - \frac{2}{3} v_c \cos \theta \dot{\theta} (l_2^3 + l_1^3) + \frac{v_c^2}{2} \cos^2 \theta (l_2^2 - l_1^2) \right], \quad (20)$$

where l_1 is the distance from the center of mass to the lower S/C, l_2 is the distance from the center of mass to the string to the upper S/C, and θ is the pitch angle. Additional perturbations due to atmosphere dynamics were not considered in this analysis.

3. Candidate Sensor Configurations

A sensor system is required to meet the absolute and relative positioning requirements of the radar antenna elements. Knowledge of the relative positions of the radar receive antenna elements to an accuracy on the order of a fraction of the radar wavelength is required to support the phase coherency requirements of the space based radar. This translates to approximately 2cm for L-Band and 10cm for the low end of the UHF Band. The absolute positioning requirement of the entire array, with respect to the earth, is on the order of 10 to 100m. A number of sensor systems were considered, including:

- Laser Ranging
- NAVSTAR Global Positioning System (GPS)
- Radar's own signals
- Laser Diode/CCD Array
- Combinations of the above.

In this analysis the NAVSTAR GPS was investigated, since:

1. It appears that GPS can serve as the attitude determination sensor in addition to meeting both the absolute and relative positioning requirements [8]
2. The GPS satellites will be in place along with complete ground support by the time needed for space based radar. Thus, only receivers for the space based arrays need to be considered. The GPS solution is entirely passive.
3. The GPS is highly robust. At the altitudes of interest, 10 to 15 satellites are in view. Based on a solution using the best 5 satellites, the Positional Dilution of Precision (PDOP) is less than 1.7. A 5 satellite solution was selected as a trade-off between solution redundancy and receiver complexity, however, there are receivers available today that process up to 12 satellites per solution.
4. The DARPA GaAs GPS chip set has made available miniature space qualified hardware suitable for space based radar applications. By the time such components will be needed for SBR applications, it is expected that multiple sources will be available.
5. At least three programs are already underway developing GPS receivers for precise motion and attitude sensing in space applications [8, 9, 10, 11].

6. The GPS satellites can be augmented with "pseudolites" on the earth, if necessary, to provide a more robust mode of absolute position calibration.

Consider now a configuration with a 5 channel GPS receiver at the top spacecraft and multiple differential phase comparators mounted along the tether, aided by the top receiver for carrier tracking. The carrier phase of each satellite can be tracked to a few degrees of the GPS L-Band carrier which places the phase tracking measurement error at 1cm , one standard deviation. However, the carrier phase position solution will be implemented in a relative mode requiring measurements from two satellites, thus the error of the measurement will be on the order of 1.4cm , one standard deviation.

For this analysis, satellites depressed lower than 9 degrees below the local horizon were excluded in order to eliminate those signals grazing the earth that would have large IONO and TROPO propagation delay variations. Based on a unity gain antenna over this elevation range and omnidirectional in azimuth, the received C/A Code signal strength, in terms of carrier-to-noise ratio (C/N_0) available for tracking, ranges from 32 to 55dB Hz , which is more than adequate to maintain track through the benign dynamics of the tether elements. For comparison, the C/N_0 observed by GPS receivers in airborne and terrestrial applications is in the range of 25 to 30dB Hz .

In airborne and terrestrial applications the tracking loop bandwidths must be wide enough to accommodate the dynamics which are more severe than for the space based radar. A typical airborne GPS receiver might use tracking loop bandwidths of 2 to 5Hz for the code loops and 20 to 30Hz for the carrier loop. Because of the higher C/N_0 and lower dynamics environment of the space based radar, it should be possible to reduce the bandwidths to 1Hz or less for the code loop, and to less than 5Hz for the carrier loop. The longer integration times should result in sufficient measurement accuracy to support the space based radar position, velocity, and attitude estimation requirements.

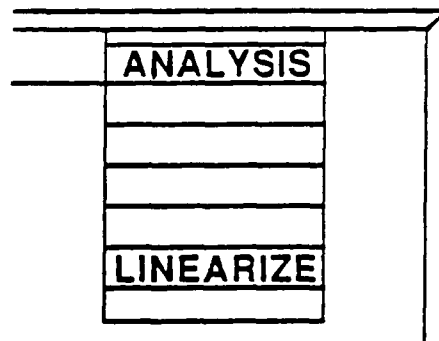
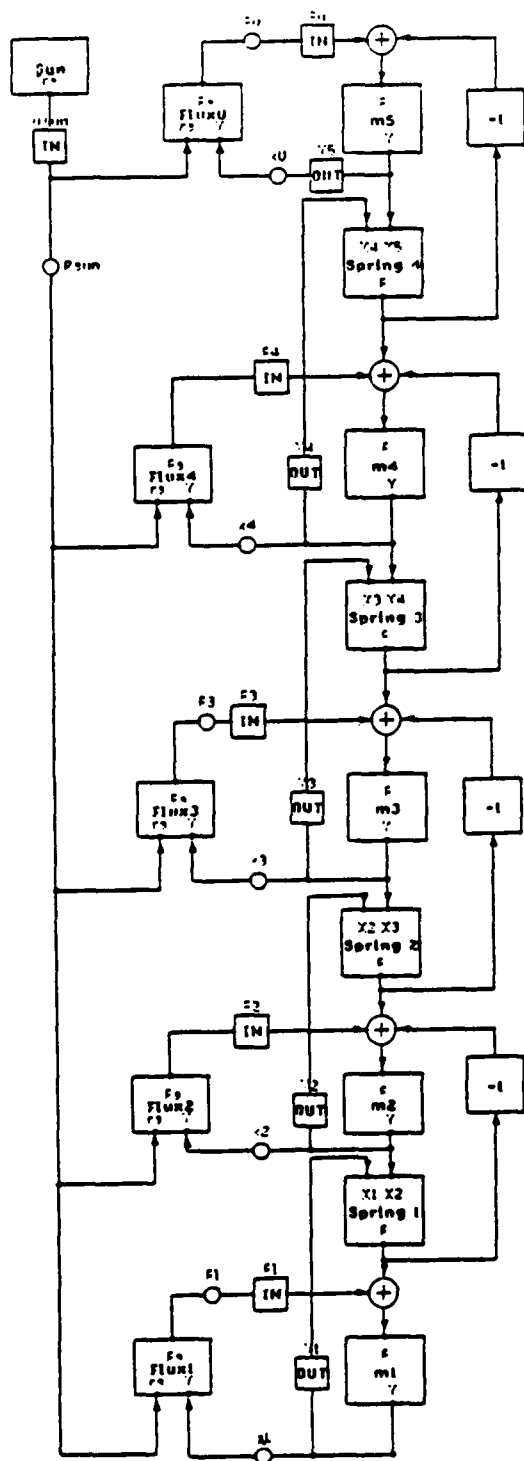
4. Simulation Development

The control and/or estimation problem requires a linearized model upon which to base the design. For this reason, the interactive CAE program *Ctrl-C[®]/Model-CTM* [6,7], was used for further analysis. *Ctrl-C[®]/Model-CTM* is a graphical interactive simulation program. The components of the non-linear simulation, masses, springs, and disturbance forces, are configured into the desired model with a mouse on the computer screen. Based on this graphical description, *Model-CTM* generates the simulation code in FORTRAN or C computer languages. *Model-CTM*'s greatest benefit for this analysis is the capability to generate a linearized model of a simulation at a push of a button on the screen. The linear model is automatically placed into the workspace of the program to be available for further analysis including control and estimation designs.

The nonlinear model, developed within the *Model-CTM* framework, is shown in Figure 4. Masses are connected by spring/dampers and are forced by solar pressures that consider earth shadow transitions. The sun-vector and solar pressure computations are performed in the "sun block", shown in the upper left of the figure.

NON-LINEAR MODEL

MODEL-C



LINEARIZED MODEL

- $\dot{X} = Fx + Gu + \Gamma w$
- X = STATE (POS/VEL AT DISCRETE TETHER LOCATIONS)
- u = "KNOWN" DISTURBANCES
- w = DISTURBANCE NOISE

Figure 4: Simulation Model.

Note that it is very easy to modify and manipulate the simulation. Blocks and regions may be copied and/or moved around in the screen. Parameters may be changed by clicking on the block and changing a few numbers in the opening menu. Outputs may be obtained by placing probes at the desired points in the block diagram. Linear models may be obtained by placing input-output markers and selecting *LINEARIZE* in the analysis capabilities menu.

Figure 5 shows the probe outputs of the simulation for solar pressure forces on the upper S/C, F_{u_solar} , the center *bead*, F_{3_solar} , and the lower S/C, F_{l_solar} for a STAR string with solar panel above the upper S/C and receiver elements along the tether. In order to analyze the effects of solar pressure transients, the simulation was initialized prior to the tether coming out of the earth shadow. Figure 6 shows the time delay between the sun illuminating the upper and lower S/C.

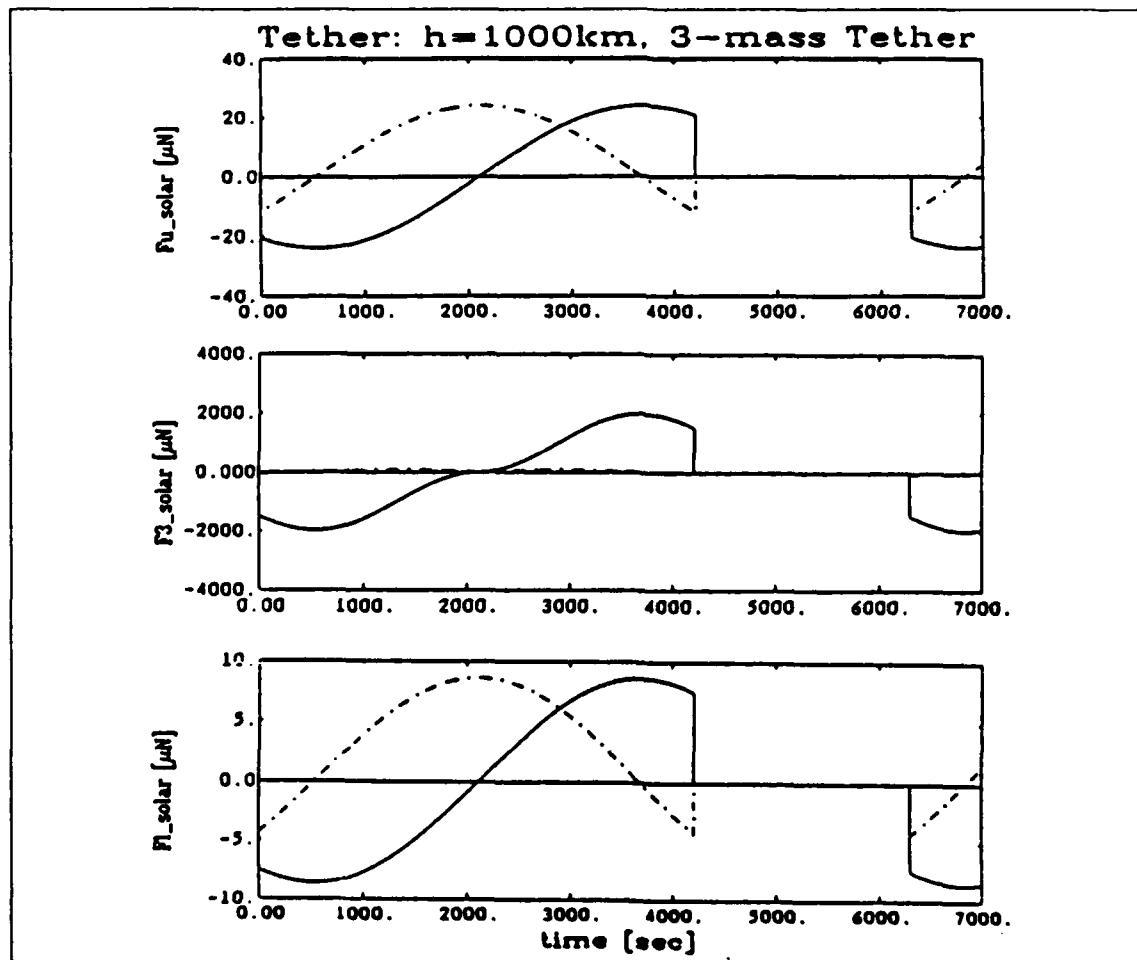


Figure 5: Solar Pressure Forces on the Upper S/C, Center Bead and Lower S/C.

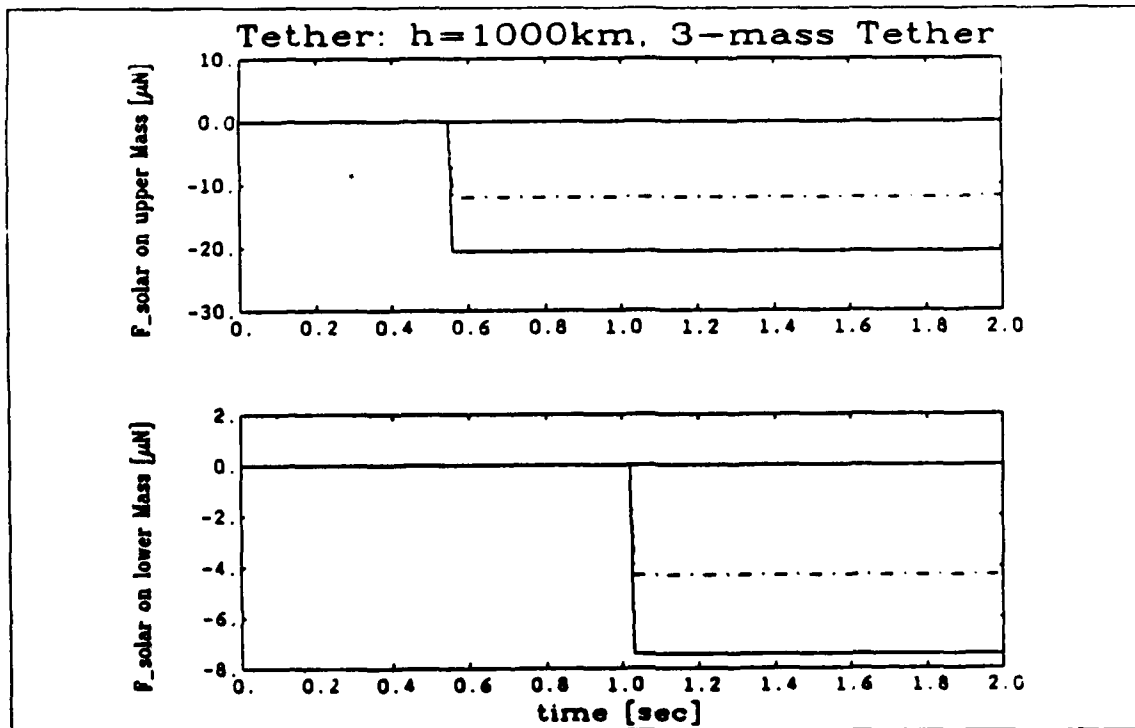


Figure 6: Solar Pressure Forces on Upper and Lower S/C.

Figure 7 compares simulations describing the tether by three and five *beads*. The positions of the center of the tether relative to the upper satellite in the in-orbit direction, $X_{t2} - X_u$, and in the vertical direction, $Z_{t2} - Z_u$, do not change significantly between the two simulations indicating that a 3-mass *bead* model may be used for basic analysis of estimator and controller analysis. However, higher order models need to be used for the analysis of the high-frequency bobbing motion.

Two locations along the orbit were used to obtain linear perturbation models. Specifically, shadow and sun-lit trim points were used. *Model-CTM* numerically perturbs dynamic states and inputs to generate linear models of the form,

$$\begin{aligned}\dot{x}(t) &= Fx(t) + Gu(t) \\ y(t) &= Hx(t) + Ju(t)\end{aligned}\tag{21}$$

where x is the linear state space, u is the input at the location of the input markers (see Figure 4), and y is the linearized output at the location of the output markers.

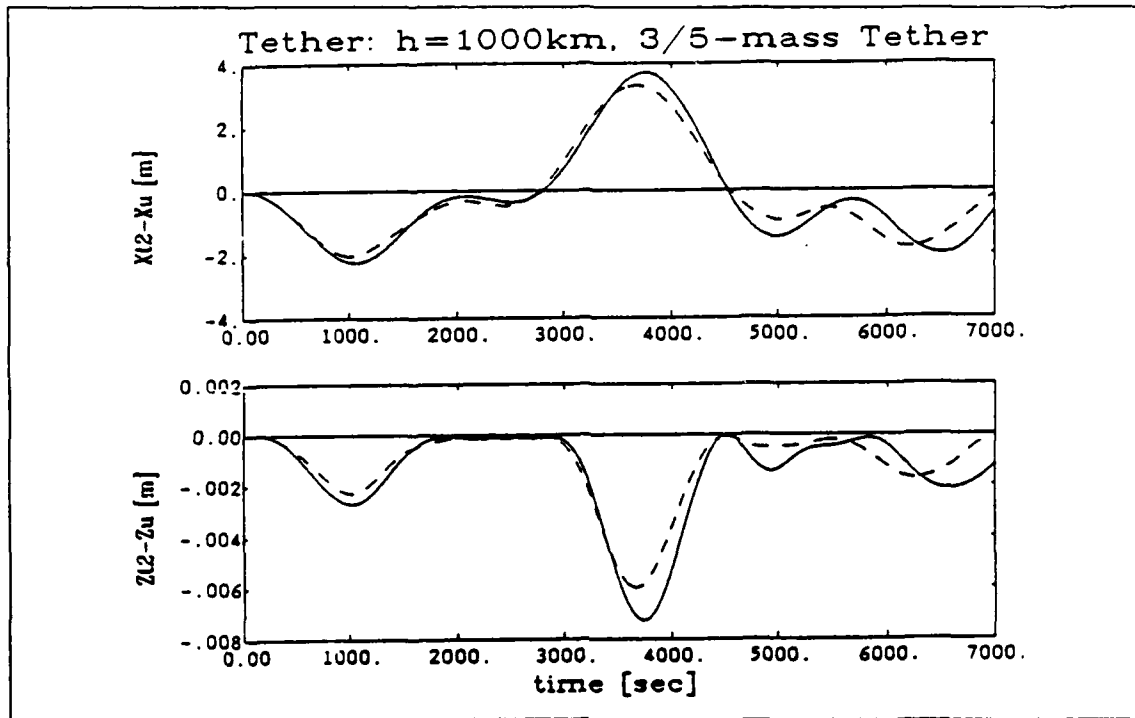


Figure 7: Comparison of the Relative Tether Position for 3 and 5 Mass Simulations.

5. Filter Analysis

From the separation theorem for linear systems, the design of the estimator is independent of the design of the controller. Though the bowing and stretching of the tether includes non-linear coupling, the separation of control and estimation will be assumed in order to get an upper estimate of the performance of the estimator.

This analysis investigates the capability and performance of a Kalman filter to reconstruct the absolute and relative position and velocity of receiver elements from GPS measurements. This analysis consists of two parts. These are:

- (1) A covariance analysis is performed to investigate the achievable estimation accuracies for different GPS accuracies.
- (2) A linear filter and its performance in reconstructing receiver positions and velocities from non-linear simulation data, corrupted by receiver noise, is investigated.

Covariance Analysis

The filter was designed using a linearized model of a *Model-CTM* based non-linear simulation of a string,

$$\begin{aligned} \dot{x}(t) &= Fx(t) + G_1w(t) \\ y(t) &= Hx(t) + v(t) \end{aligned} \tag{22}$$

where $w(t)$ was chosen to be a random noise of ten percent of the solar pressure force plus a small contribution stemming from unmodeled dynamics, and $v(t)$ was selected to be a random GPS receiver position and velocity measurement error,

$$E(ww'^T) = Q\delta(t - t'),$$

$$E(vv'^T) = R\delta(t - t'),$$

$$E(wv'^T) = 0.$$

The GPS configuration model included a GPS receiver at the top satellite providing absolute position and velocity based on code and phase measurements. In addition, phase comparator receivers, located at the center and bottom of the tether, were included to provide very accurate position and velocity data (relative to the topmost satellite).

For the design of the filter, the linear model, obtained by linearizing about the trim point, was converted to a discrete model at the sample rate of the GPS measurement, giving,

$$\begin{aligned} x_{i+1} &= Ax_i + B_1 \bar{w}_i, & E(\bar{w}\bar{w}_i^T) &= Q\Delta t \\ y_i &= Cx_i + v_i, \end{aligned} \quad (23)$$

where Δt is the sample rate. The sample rate chosen for this analysis was a conservative $\Delta t = 2 \text{ sec.}$ if x^- is the state estimate before a measurement is made and x^+ is the state estimate after the measurement, we may define,

$$M \stackrel{\text{def}}{=} E(x - x^-)(x - x^-)^T, \quad (24)$$

and denote the covariance of the estimation error after the measurement update by,

$$P \stackrel{\text{def}}{=} E(x - x^+)(x - x^+)^T. \quad (25)$$

The measurement update equations for the Kalman filter are then [12],

$$\begin{aligned} x_i^+ &= x_i^- + L_i(y_i - Hx_i^-), \\ L_i &= M_i C^T (CM_i C^T + R)^{-1}, \\ P_i &= M_i - L_i CM_i \end{aligned} \quad (26)$$

and the prediction equations are

$$\begin{aligned} x_{i+1}^- &= Ax_i^+ + B_1 u_i, \\ M_{i+1} &= AP_i A^T + B_1 Q B_1^T, \end{aligned} \quad (27)$$

After some transient period, the covariance equations will converge towards steady state values, resulting in the steady state optimal filter equations, with

$$\bar{L} = \bar{M}G^T(C\bar{M}C^T + R)^{-1}, \quad (28)$$

and \bar{M} being the steady state prediction error covariance. It is \bar{M} that is a measure of the filter performance. The estimated values of the state estimation errors are then the square root of the diagonal elements of \bar{M} , and the estimated output estimation errors are the square roots of the diagonal elements of the output prediction covariance matrix $C\bar{M}C^T$.

In order to evaluate the sensor requirements the achievable accuracies were evaluated for different absolute and relative GPS sensor accuracies. Figure 9 shows the position and velocity estimation errors for fixed sigmas of the GPS relative measurement error of 1cm and $.01\text{cm/s}$, absolute measurement errors ranging from 0.2m to 10m and a 2sec sampling time. The resulting position estimation errors are $.05 - 0.55\text{m}$ in the in-orbit direction, and $.02 - .55\text{m}$ in the vertical directions. The velocity estimation errors range from $.0001\text{m/s}$ to $.035\text{m/s}$. These values are well within those required for the STAR system. The depicted lines are for different points along the tether. The lower values are for the upper end-satellite and the upper line is for the lower end satellite. Figure 10 shows the relative position and velocity estimation errors for fixed sigmas of the GPS measurements in the upper S/C of 2m and $.02\text{m/s}$ and relative measurement errors of the GPS phase comparison ranging from $.1\text{cm}$ to 5cm . The maximum error of 5cm for relative position and $.038\text{cm/s}$ for relative velocity are less than those permissible for STAR.

Reference [13] shows that the estimation errors may be further reduced by using a higher order models with an associated reduced model uncertainty. Additional improvements may be achieved by using a faster GPS sample rate.

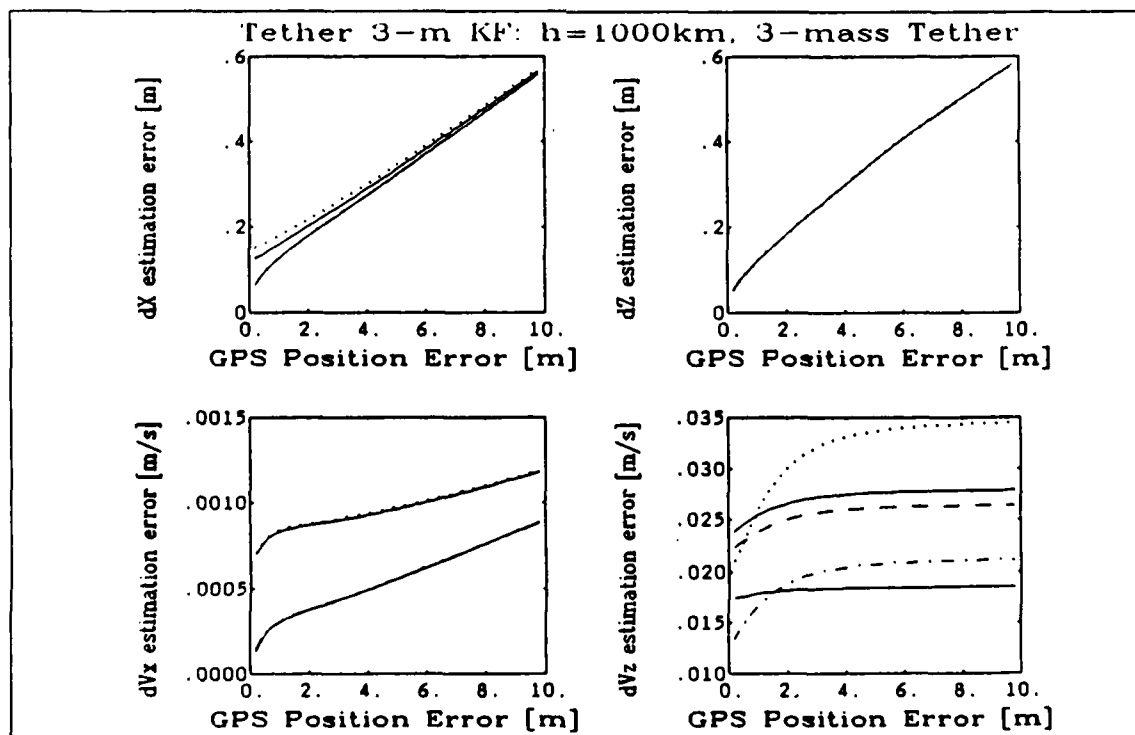


Figure 9: Achievable Estimation Accuracy.

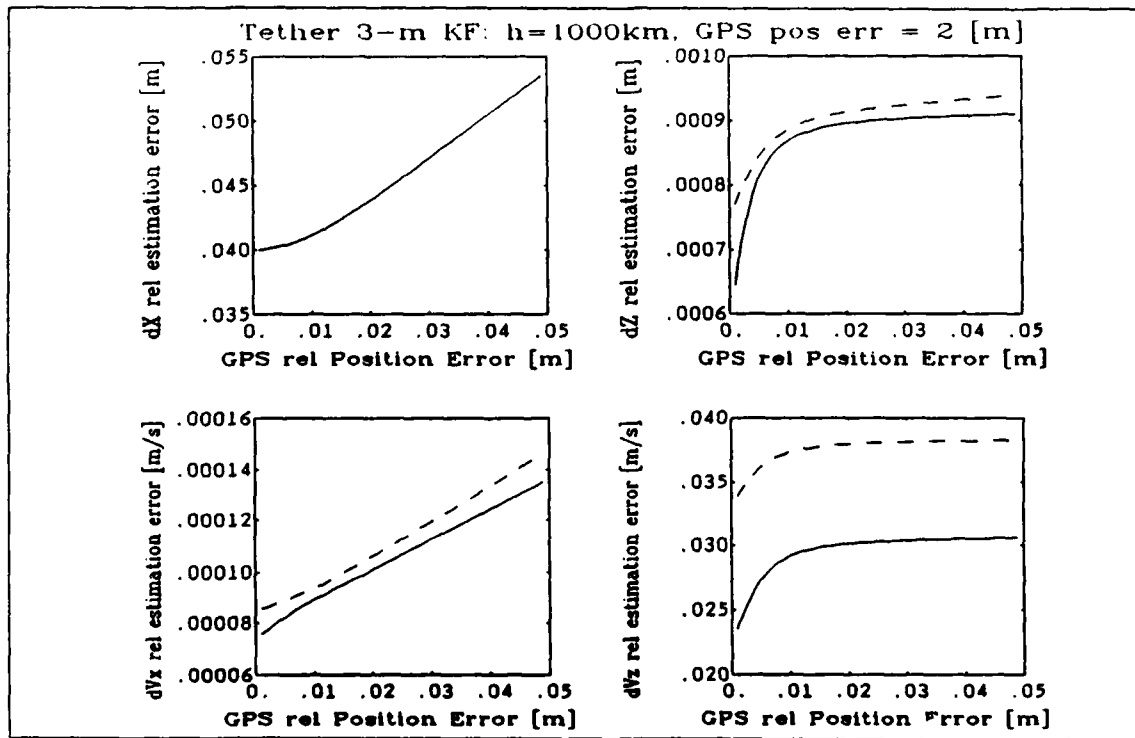


Figure 10: Achievable Relative Estimation Accuracy.

Linear Filtering of Non-Linear Tether Simulation Data

The CAE package combination, *Ctrl-C^R* and *Model-CTM*, provided a convenient and efficient environment in which to simulate the non-linear string dynamics and GPS receiver element position and velocities with a Kalman filter and compare the estimated outputs with truth data. The GPS sensor data were simulated by adding uncorrelated, Gaussian measurement noise to the outputs of the non-linear simulation. The simulation was initialized in a trim condition in the Earth shadow just before solar forces begin impinging on various elements of the string. The outputs at the probe locations (see Figure 4) were stored as "truth" data and corrupted by assumed white, Gaussian measurement noise. To reduce the computation time, the filter equations may be put into the form

$$\begin{aligned} \bar{x}_{i+1} &= A_F \bar{x}_i + B_F y_{F_i}, \\ \hat{y}_i &= C \bar{x}_i, \end{aligned} \quad (29)$$

where

$$\begin{aligned} A_F &= A - ALC, \\ B_F &= C \bar{x}_i^-, \\ y_{F_i} &= \begin{bmatrix} y_i \\ u_i \end{bmatrix}. \end{aligned}$$

The combined propagation and update filter equations are now in the form of a discrete simulation and may be propagated by a discrete simulator, i.e., in *Ctrl-C*[®]. Figures 11 - 12 show overlays of the non-linear simulated "truth" data and estimated values as well as differences between "truth" and estimated outputs. In the Figures $()u$ denotes the upper end-satellite, $()L$ denotes the lower end-satellite, $()i...$ denote locations along the tether, $()h$ denotes estimated values, and $\delta()$ denote differences between "truth" and estimated values.

Figure 11 compares absolute position and velocity estimates for the upper S/C. The absolute position estimation errors are less than 25cm.

Figure 12 compares relative position and velocity estimates for the center of the tether. The relative position estimation errors are less than 3cm at locations with GPS phase comparisons and twice to three times that value for locations without a relative GPS measurement. These results are similar to those of the covariance analysis and indicate that the non-linear effects do not overly burden the linear filter.

6. Conclusions

For the radar architectures and tether dynamics considered, it is shown that GPS positioning sensors have sufficient accuracy to maintain radar signal coherence for the antenna elements mounted along a single tether. The analysis considered a tether of length 2000m at an altitude of 1000km subject to solar pressure and atmospheric disturbances, including earth shadow transitions. A covariance and Kalman filter analysis was performed to estimate the achievable relative and absolute position of the radar receiver elements. The results show that a 2m absolute GPS sensor accuracy, a 1cm relative accuracy of GPS phase comparitors and a 2sec sample rate suffice to combine signals along the tether with a Kalman filter to an accuracy of 2cm and achieve a 25cm absolute positioning accuracy of the string. The wave length of radar frequencies of interest range from 20cm (L-band) to 70cm (UHF). Thus this estimator, given the GPS error assumptions and the considered disturbance environment, can meet the position estimation requirements for coherence, even for a L-band radar.

Further analysis is necessary to investigate the solar heating effects, higher order gravity harmonics and unmodeled dynamics, particular torsional effects. Non-linear filter designs, that include the bowing coupling, may be required to get better estimates for receiver elements between sensor locations. Additional analysis is necessary for coherently combining signals of different strings.

Absolute position accuracy requirements are a function of mission requirements, radar performance and geometry. The shown achievable absolute positioning accuracy of 25cm seems to be sufficient for most applications. However, a more detailed total system analysis must be performed to investigate the subsystem error budget required to support coherence among several tethers in space.

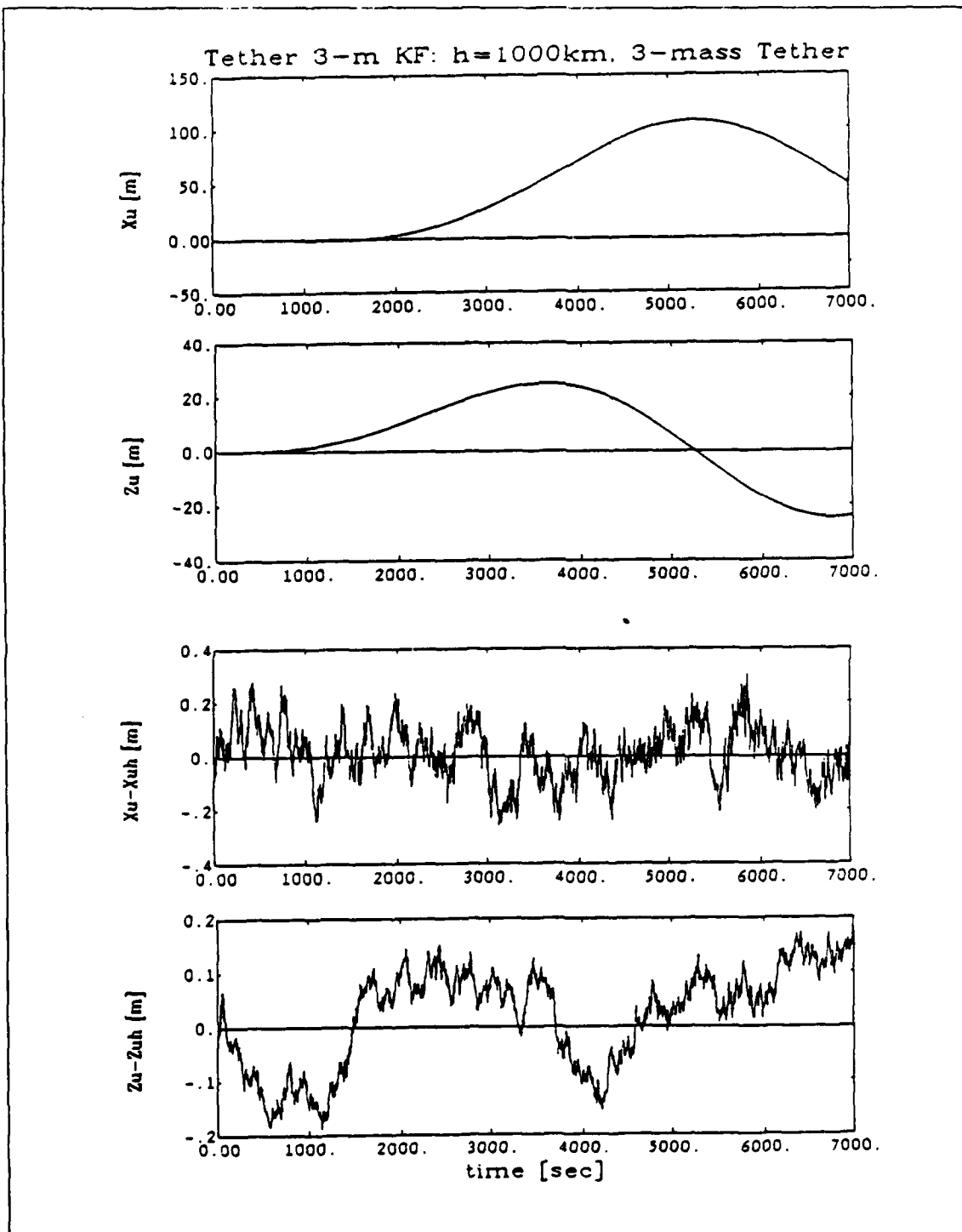


Figure 11: Absolute Estimates for Top Spacecraft.

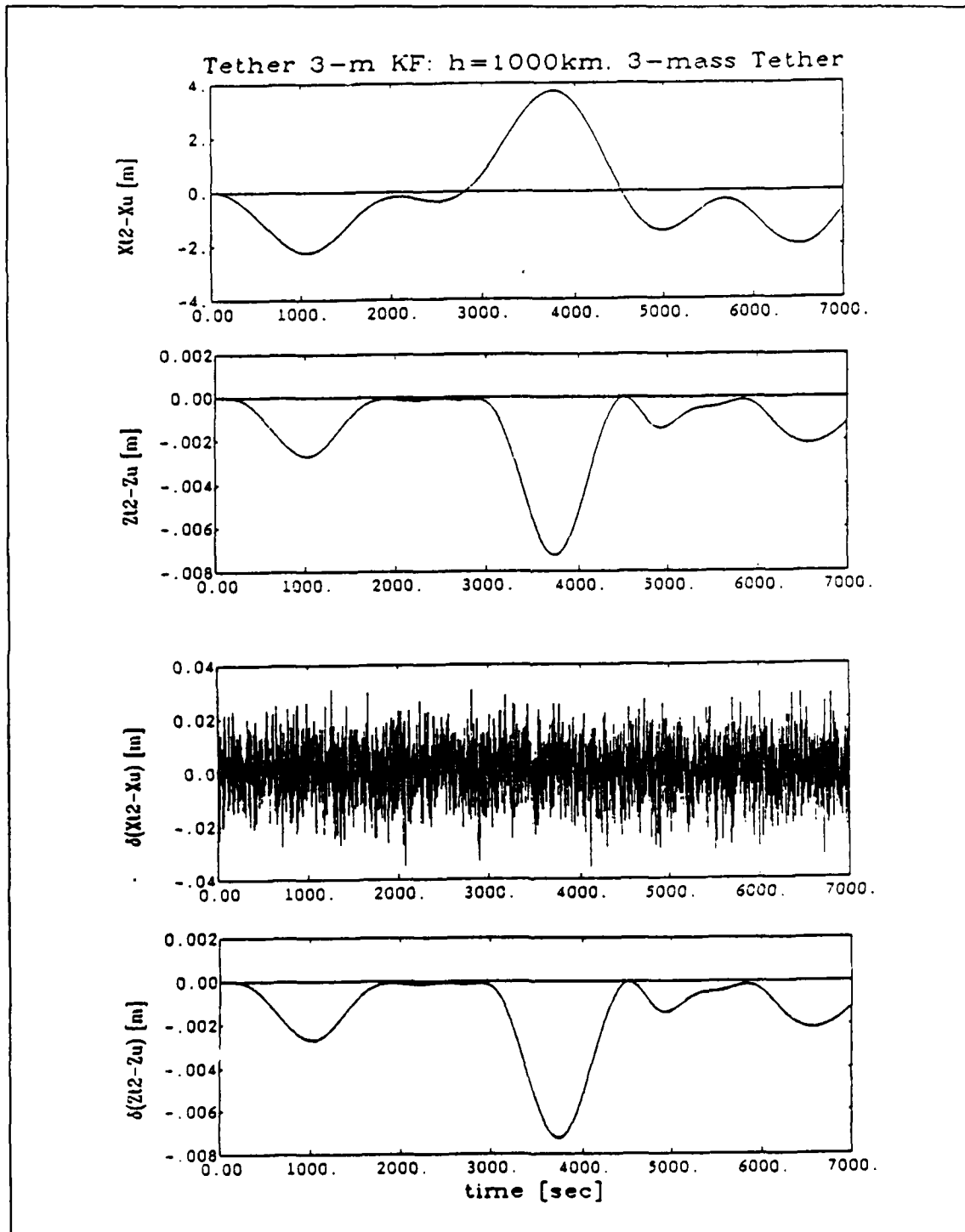


Figure 12: Relative Estimates for Center of Tether.

7. References

- [1] Shayda, P.M., Tomlinson, P.G., Brown, T.C., Chakraborty, D., Kessler, K. M. and Pritchard, J.R., "Large Apertures for Space-Based Radars, A New Concept Using Tether Arrays," Tri-Service Radar Symposium, 20-22 June 1989, West Point, N.Y.
- [2] Bonifazi, Carlo, "Tethered Satellite System (TSS) - Core Science Equipment", AAS 86-214, in Bainum et al. 1986, p. 173-203.
- [3] Beletskii, V.V., *Motion of an Artificial Satellite About its Center of Mass*, Izdatel'stvo Nauka, Glavnaya Redaktsiya, Moskva 1965 (NASA TT F-429).
- [4] *U.S. Standard Atmosphere, 1976*, National Oceanic and Atmospheric Administration report AD/A035 728, Washington, D.C., October 1976.
- [5] Jacchia, L. G., "Revised Static Models of the Thermosphere and Exosphere with Empirical Temperature Profiles," Smithsonian Astrophysical Observatory Special Report No. 332, Cambridge, Massachusetts, May 1971.
- [6] *Ctrl-C[®] User's Manual, Version 4.3*, Systems Control Technology, Inc., Palo Alto, California, 1989.
- [7] *Model-CTM User's Manual, Version 1.2*, Systems Control Technology, Inc., 1989.
- [8] Meehan, Tom, "An Experiment in Attitude, Position, and Velocity Determination with Rogue GPS Receivers," Jet Propulsion Laboratory, Second Symposium on GPS Applications in Space, USAF Geophysics Laboratory, October 1989.
- [9] Axelrad, P., and Parkinson, B. W., "Closed Loop Navigation and Guidance For Gravity Probe B Orbit Insertion," Stanford University, ION GPS 88, September 1988, Colorado Springs, CO.
- [10] Saunders, Penny, "Space Station GPS Implementation Plans and Overview," NASA Johnson Space Center, Second Symposium on GPS Applications in Space, USAF Geophysics Laboratory, October 1989.
- [11] Carson, Lance, and Hailey, Leonard, "Preliminary Experimental Results for the TOPEX GPS Demonstration," Motorola Government Electronics Group, Second Symposium on GPS Applications in Space, USAF Geophysics Laboratory, October 1989.
- [12] Bryson, A. W. Jr. and Ho, Y. C., *Applied Optimal Control*, Ginn and Company, New York, 1969.
- [13] Shayda, P., Tomlinson, P., Brown, T. and Kessler, K., *Interim Report for Space-Based Tethered Array Radar (STAR)*, Decision-Science Applications, Inc. Report 137/1093, December 1989.

SPECIAL PURPOSE INEXPENSIVE SATELLITE (SPINSAT)
GPS RECEIVER

Roger M. Weninger
Richard Sfeir
Satellite & Space Electronics Division
Rockwell International
Anaheim, California

Ronald L. Beard
Naval Research Laboratory
Washington, DC

ABSTRACT

This paper provides a description of the GPS receiver planned for installation on the Office of Naval Research's (ONR) SPINSAT Altimeter (SALT) satellite. The receiver will use an advanced chipset developed under contract to DARPA that enables a 5-watt, 2-pound unit. The receiver functional and hardware description are provided. The navigation solution and intermediate data available to the SALT processor for telemetry are identified. The receiver's environmental and performance requirements are also provided.

INTRODUCTION

In August 1989, the Satellite and Space Electronics Division of Rockwell International initiated work on a GPS receiver for the Office of Naval Research (ONR). The receiver is scheduled for delivery on January 31, 1990, and is planned to be integrated into a Commander Class satellite bus with an intended launch of Spring/Summer 1990. The primary payload of the bus is an altimeter. These efforts are part of ONR's Special Purpose Inexpensive Satellite (SPINSAT) program, and this mission is referred to as the SPINSAT Altimeter (SALT).

PURPOSE

The overall SALT mission is to determine the viability of small inexpensive satellites to perform operational missions of interest to the Navy. It will be specifically used to gather oceanographic data. In order to perform this mission, the position of the satellite must be accurately known for combination with the altimetry measurements. The proven doppler beacon system, used in other oceanographic missions, will provide the primary precision tracking system. It will also provide a comparative measure of the GPS receiver on-orbit performance which is proposed to be utilized in two different modes. The first mode, discussed more fully in this paper, is the real-time navigation mode. This operation is very similar to other applications of GPS for navigating ships and aircraft, and provides accurate three-dimensional information when sufficient GPS satellites are in view of the receiver. The second mode is to determine highly accurate positioning in a post processing mode by differential operation with ground receivers. This mode has the potential of on-orbit positioning to better than a meter in the radial direction. An experiment is being developed to evaluate this second

mode of operation with the SALT GPS receiver.

The SALT satellite will be placed into a circular 800 kilometer orbit at an inclination of 108°. The positioning information calculated by the GPS Receiver and the measured GPS data will be periodically transmitted to the ground for evaluation. The operation of the receiver will be independent of the other onboard systems. The mission life projected for operation of the satellite is three years. The evaluation of using GPS for this mission could lead the way for future scientific and operational missions, and reduce the requirements for ground tracking sites.

FUNCTIONAL DESCRIPTION

The receiver will use a Miniature GPS Receiver (MGR) chipset developed by Rockwell under contract to DARPA(1). The chips are shown in Figure 1 and their physical parameters are summarized in Table 1.

The chipset consists of a GaAs MMIC RF/IF Translator, a Silicon Frequency Synthesizer, a CMOS Signal Processor, a CMOS Multi-Function Interface and an Advanced Architecture Micro-Processor. This chipset is configured with memory and a frequency standard into two modules to make up the SPINSAT GPS receiver described herein.

The receiver has two channels that sequentially track a selected group of GPS satellites. The channels function independently so that data from two satellites can be processed in parallel. During normal tracking, the two channels are allocated a one second processing interval for each satellite, i.e., within one second all of the real-time functions associated with acquisition, tracking and navigation are accomplished. At the end of the one second, the two channels reacquire and track the next two satellites in their respective satellite assignments.

The two channels can operate on either L₁ (1575.42 MHz) or L₂ (1227.60 MHz).

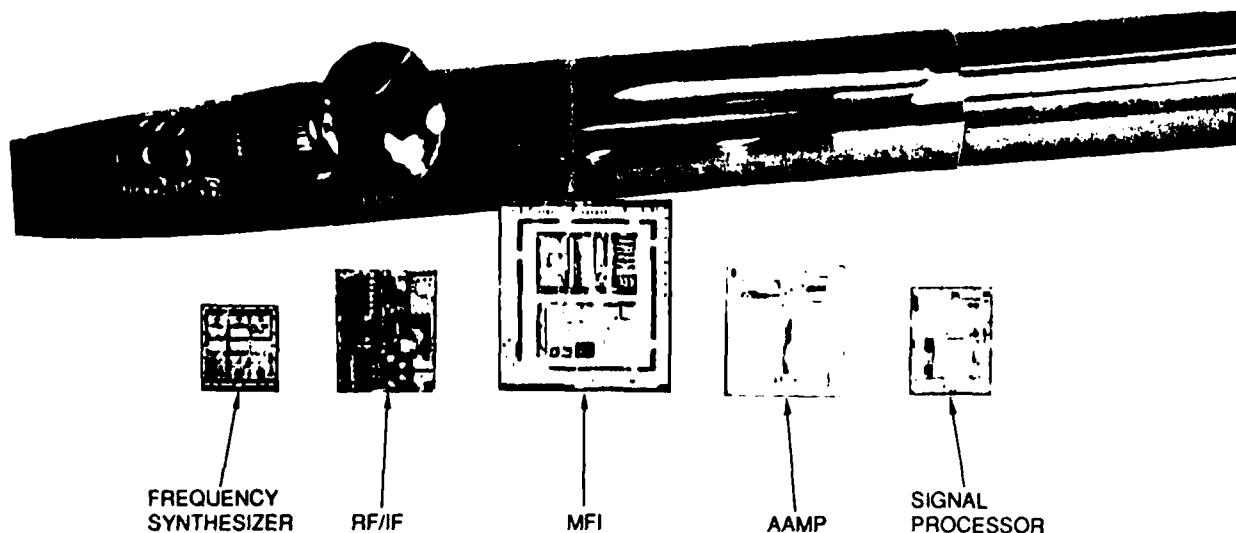


Figure 1. Miniature GPS Receiver (MGR) Chip Set

TABLE 1. MGR CHIP SET SUMMARY

| CHIP TYPE | DEVICE COUNT | DIMENSIONS (inches) | IMPLEMENTATION TECHNOLOGY | POWER (mW) |
|---|--------------|---------------------|---------------------------|------------|
| RF/IF Translator | 420 | 0.340 x 0.350 | Gallium Arsenide | 1500 |
| Signal Processor | 19,800 | 0.185 x 0.220 | 1.25 Micron Bulk CMOS | 90 |
| Multifunction Interface (MFI) | 29,000 | 0.370 x 0.370 | 1.6 Micron Bulk CMOS | 20 |
| Advanced Architecture Microprocessor (AAMP) | 74,000 | 0.250 x 0.261 | 2 Micron Bulk CMOS | 90 |
| Frequency Synthesizer | 350 | 0.165 x 0.165 | Bipolar Silicon | 500 |

Normally L_1 is used for general processing with L_2 being used periodically to obtain a separate set of measurements to aid in correcting for ionospheric errors.

The receiver can acquire and track either or both the Clear Access (C/A) code, or the Precision Code (P-code) depending upon performance requirements. As a general rule when estimated position is not well known C/A code is used for acquisition and then handover occurs to the P-code; however, if the estimated position and time error is within ± 300 P-code chips (± 30000 feet), a satellite can be acquired with P-code.

A functional configuration of the SPINSAT receiver is shown in the flow diagram of Figure 2 which is designed to show the signal/data flow from the antenna input to the data output to the host vehicle. The flow diagram also shows the functional partitioning of receiver elements among RF and digital hardware, and software processing.

HARDWARE DESCRIPTION

The two-channel SPINSAT receiver consists of two modules:

- RF Module

- Digital Module

A block diagram of the receiver is shown in Figure 3. The RF module includes the RF/IF translator, the frequency synthesizer and the frequency standard. The digital module contains the signal processors, Advanced Architecture Microprocessor (AAMP), Multi-Function Interface (MFI), memory and RS232C interface circuitry.

The overall dimensions of the RF module shown in Figure 4 are 7.95 in. x 5.75 in. x 1.25 in. The overall dimensions of the digital module shown in Figure 5 are 7.0 in. x 5.75 in. x 0.6 in. The combined module weight and power requirements of approximately 2 pounds and 5 watts are summarized in Table 2.

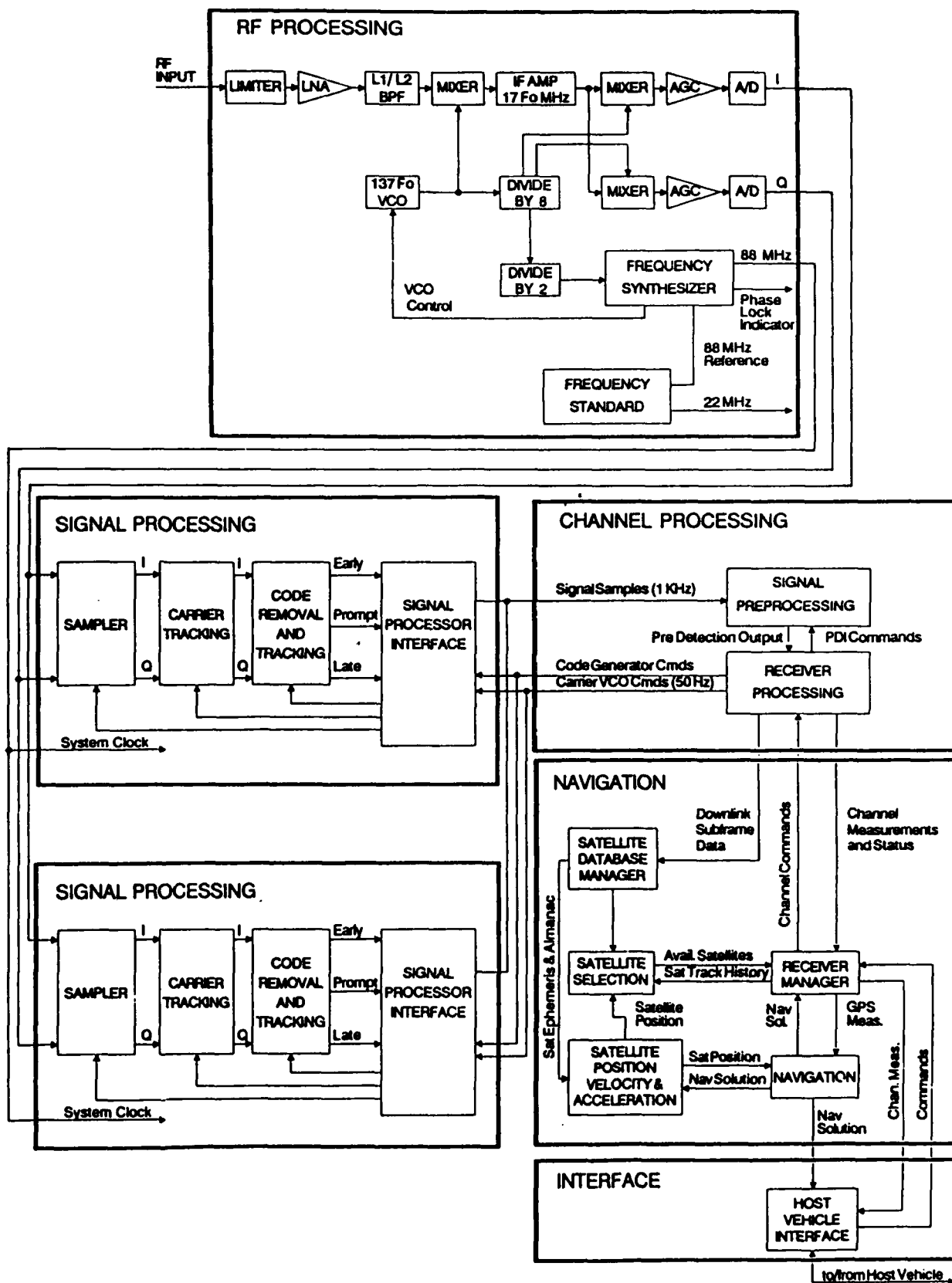


Figure 2. SPINSAT Receiver Functional Flow Diagram

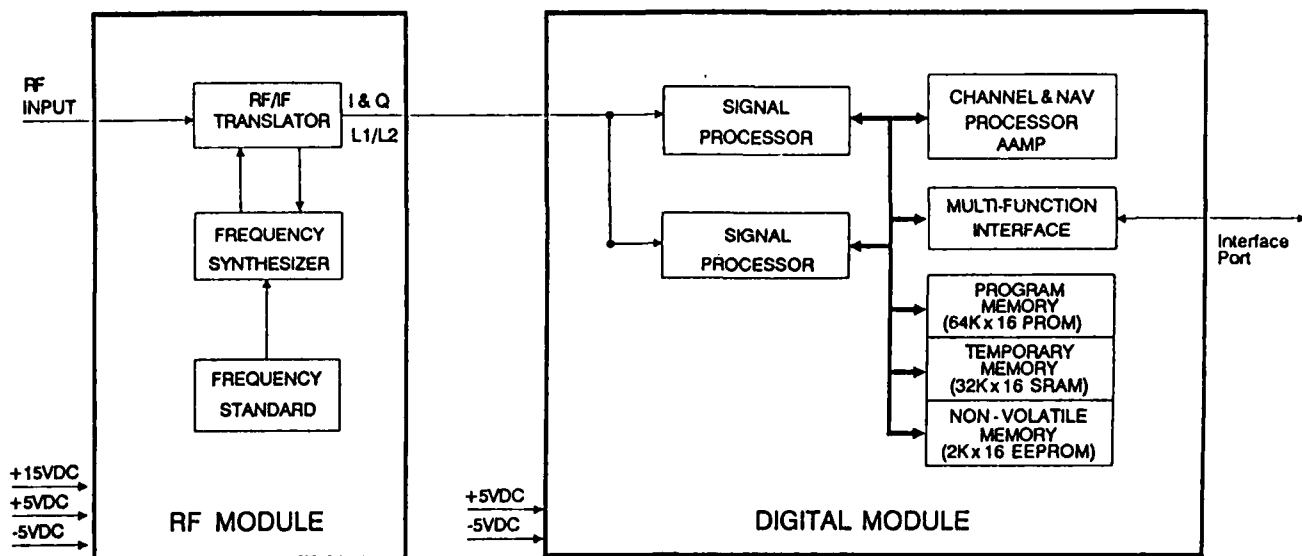


Figure 3. SPINSAT Receiver Block Diagram

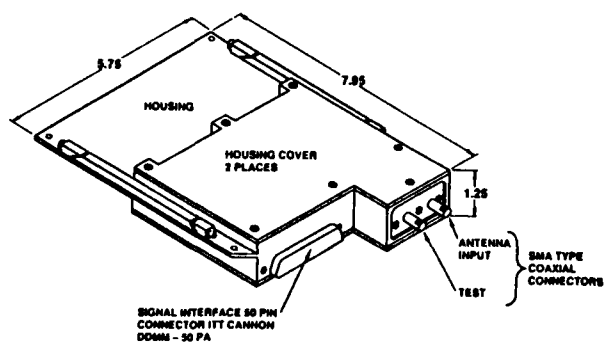


Figure 4. RF Module Assembly

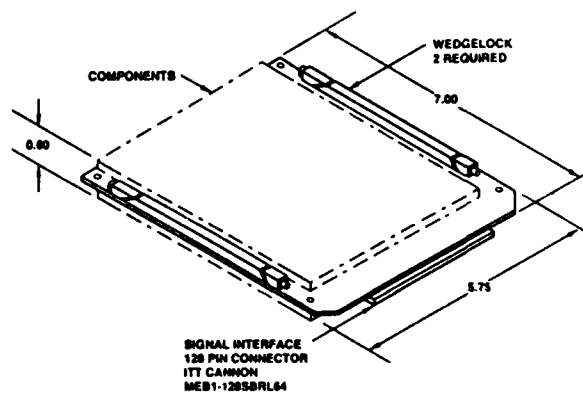


Figure 5. Digital Module

TABLE 2. WEIGHT AND POWER SUMMARY

| MODULE | WEIGHT (LBS) | WATTS | | | TOTAL |
|---------|-----------------|-------|-----|-----|-------|
| | | +15V | +5V | -5V | |
| RF | 1.4 | 0.5 | 1.1 | 0.5 | 2.1 |
| Digital | 0.5 | - | 2.6 | - | 2.6 |
| TOTAL | 1.9 | 0.5 | 3.7 | 0.5 | 4.7 |

OUTPUT DATA

Communications between the receiver and the SALT processor is accomplished through a serial data Interface Port compatible with an RS232C serial port. The receiver provides two messages at a 1 Hz rate. These two messages consist of a Navigation Solution Message (Table 3) and a Pseudo Data Message (Table 4).

TABLE 3. NAVIGATION SOLUTION MESSAGE

| DATA ITEM | NUMBER OF PARAMETERS | DATA TYPE | NUMBER OF WORDS | UNITS |
|--------------------------|-------------------------|-----------|--------------------|--------------------|
| Header | 5 | 1 | 5 | None |
| T20 Count | 1 | D1 | 2 | 20ms |
| GPS Week | 1 | I | 1 | Week |
| GPS Time | 1 | FP | 2 | s |
| UTC | 1 | FP | 2 | s |
| Position | 3 | EPF | 9 | m |
| Velocity | 3 | FP | 6 | m/s |
| Clock Bias | 1 | FP | 2 | m |
| Clock Drift | 1 | FP | 2 | m/s |
| Receiver Mode | 1 | I | 1 | None |
| Figure of Merit | 1 | I | 1 | None |
| Position Error Variances | 3 | EPF | 9 | m ² |
| Velocity Error Variances | 3 | EPF | 9 | (m/s) ² |
| Bias Error Variance | 1 | EPF | 3 | m ² |
| Drift Error Variance | 1 | EPF | 3 | (m/s) ² |
| Checksum | 1 | I | 1 | None |
| TOTAL | | | 58 | |

NOTES:
GPS Week 0 starts 1-6-00 midnight
GPS Time is number of seconds into GPS Week
UTC is number of seconds into calendar year
I : Integer (16 bits)
D1 : Double Integer (32 bits)
FP : Floating Point (8 bits exponent, 24 bits mantissa)
EPF : Extended Floating Point (8 bits exponent, 40 bits mantissa)

TABLE 4. PSEUDO DATA MESSAGE

| DATA ITEM | NUMBER OF PARAMETERS | DATA TYPE | NUMBER OF WORDS | UNITS |
|----------------------------|-------------------------|-----------|--------------------|-------|
| Header | 5 | 1 | 5 | None |
| T20 Count | 1 | D1 | 2 | 20ms |
| Channel 1 Parameters | 1 | I | 1 | None |
| Channel 1 Pseudo Range | 1 | D1 | 2 | m |
| Channel 1 Delta Range Rate | 1 | D1 | 2 | m/s |
| Channel 2 Parameters | 1 | I | 1 | None |
| Channel 2 Pseudo Range | 1 | D1 | 2 | m |
| Channel 2 Delta Range Rate | 1 | D1 | 2 | m/s |
| Primary Constellation SVID | 4 | I | 4 | None |
| Primary Constellation GDOP | 1 | FP | 2 | None |
| Nav Filter Data | 1 | I | 1 | None |
| Checksum | 1 | I | 1 | None |
| TOTAL | | | 25 | |

NOTES:
Channel Parameters include: SVID
Acq/Track State
Carrier Frequency (L1 or L2)
Code Type (C/A or P)
C/N0 Measurement
Nav Filter Data include: Filter Convergence Status
Channel 1 Measurements Used
Channel 2 Measurements Used
I : Integer (16 bits)
D1 : Double Integer (32 bits)
FP : Floating Point (8 bits exponent, 24 bits mantissa)

ENVIRONMENTAL AND
PERFORMANCE REQUIREMENTS

The environmental and performance requirements described in this section relate to testing of the receiver at Rockwell prior to delivery to the spacecraft integrator. The thermal cycle, thermal vacuum and vibration tests are summarized in Table 5. The performance test parameters and their required accuracy are listed in Table 6.

SUMMARY

A GPS receiver planned as an experiment onboard the ONR SPINSAT Altimeter (SALT) satellite scheduled for launch in the Spring of 1990 has been described. This receiver consists of an RF and a digital module having a total weight of 2 pounds and a power requirement of 5 watts. The unit will use an advanced technology chipset developed by Rockwell under contract to DARPA. The data generated by the receiver and available for telemetry

TABLE 5. RECEIVER ENVIRONMENTAL TEST REQUIREMENTS

| TEST | REQUIREMENT |
|--|--|
| Thermal Cycling (Receiver Operating) | 4 cycles - each cycle -15°C Room Temperature +35°C |
| Thermal Vacuum (Receiver Operating) | 2 cycles - each cycle -15°C +35°C |
| Random Vibration (Receiver Not Operating) | 18G - RMS, 1 minute per axis |

was defined. The environmental and performance test requirements of the receiver prior to delivery were provided.

ACKNOWLEDGMENTS

The work described in this paper is being performed under contract from the Office of Naval Research (ONR). The ONR project manager is CDR Robert H. Meurer, Jr.

The chipset to be used in the receiver will be transferred from DARPA contract F29601-85-C-0022.

The authors also acknowledge the support being received from Norbert Hemesath and Juergen Bruckner of Rockwell International's Collins Government Avionics Division.

REFERENCES

1. N. B. Hemesath, J.M.H. Bruckner, "DARPA's Advanced Technology GPS Chipset," Rockwell International Corporation, Collins Government Avionics Division, 1988.

TABLE 6. RECEIVER PERFORMANCE TEST REQUIREMENTS

| PARAMETER | ACCURACY(*) |
|--|---|
| Time-to-First-Fix at $C/N_0 = 36$ dB-Hz (L1 C/A) | Less than 8 min (90% probability) with initial PVT uncertainty of 150 KM in position, 180 M/S in velocity and 1 sec in time |
| Time-to-Achieve-NAV Accuracy | Less than 2 minutes |
| L1 C/A Pseudo-Range Error at $C/N_0 = 36$ dB-Hz | Less than 8 M (1 sigma) |
| L1 P Pseudo-Range Error at $C/N_0 = 33$ dB-Hz | Less than 2 M (1 sigma) |
| L2 P Pseudo-Range Error at $C/N_0 = 30$ dB-Hz | Less than 2.5 M (1 sigma) |
| L1 Delta Range Rate Error at $C/N_0 = 36$ dB-Hz | Less than 0.03 M/S (1 sigma) |
| L2 Delta Range Rate Error at $C/N_0 = 30$ dB-Hz | Less than 0.07 M/S (1 sigma) |
| NAV Position Error | Less than 8 M per axis (1 sigma) |
| NAV Velocity Error | Less than 0.15 M/S per axis (1 sigma) |
| Absolute Time Error | Less than 1 microsecond (1 sigma) |
| *Selective Availability Not Enabled | |

Discussion:

Question: Why is this receiver so much lighter than the one for the OMV?

Answer: This receiver does not have its own case and power supply. There is not as stringent a radiation requirement for SPINSAT and shielding is provided by the spacecraft housing.

Question: Will the GPS receiver be run continuously during the SPINSAT mission?

Answer: That will depend on the GPS constellation available in 1990 and, since it is not the primary payload, on whether it can be accommodated within the data telemetry capacity and other mission objectives.

Question: Will this receiver be operated differentially with some ground tracking station?

Answer: We are looking into that possibility but it was not part of the original plan.

Question: How many satellites will be tracked simultaneously?

Answer: The receiver tracks two simultaneously and switches every one second to maintain track on a set of four primary and a set of other potentially useful satellites. That makes it difficult to operate in the differential mode - again, it was built to provide real-time navigational information.

Question: Do the errors that you quote include satellite segment and control segment errors?

Answer: The pseudo-range and range-rate errors are receiver noise contributions only. The navigation errors include satellite and ground control errors.

THE DEFENSE MAPPING AGENCY'S OPERATIONAL GPS ORBIT PROCESSING SYSTEM

James A. Slater
DEFENSE MAPPING AGENCY SYSTEMS CENTER

The DMA in conjunction with NSWC has been producing global GPS orbits continuously for more than a decade now and will continue to do so as funding provides. DMA provides ephemerides, tracking data, and geodetic positioning to support the development, test, and evaluation of weapons systems. By-products of the orbit determination include estimates of satellite clock states and earth orientation parameters, as well as quality control for Air Force operational broadcast ephemerides.

The GPS tracking network consists of 5 DMA and 5 Air Force monitor stations. These 10 permanent tracking stations provide for global coverage, differential applications, and redundancy. DMA stations are outfitted with TI4100 receivers and a cesium clock; they collect pseudorange, Doppler, navigation message, and weather data for daily transmission to DMA. The receivers are being upgraded to handle anti-spoofing and selective availability. Clock analyses are performed on-site, producing estimates of frequency bias, effects due to aging, and the Allan variance, in order to identify station clock anomalies.

The data flow for GPS ephemeris generation begins with the tracking data from the Air Force and DMA monitor stations which are then merged and fed into DMA's OMNIS orbit determination software which produces an ephemeris and clock offsets. A reference orbit based on various force models is used to correct and edit the observations and is then combined with the edited observations in the multi-satellite filter/smoothen. The data consist of 15-min smoothed ranges from the 10 stations and are processed to produce 8-day fits providing 7-day arcs with half-day overlaps on either end. Estimated parameters include orbital elements, radiation pressure parameters, satellite clock and station clock parameters, polar motion, and rate of change of UT1-UTC. Orbital precisions are typically about 1 m in radial, and 2 - 3 m in along-track and cross-track components. Along-track error increases significantly during eclipse periods. Another check on internal consistency that is being introduced is the repeated computation of absolute positions of each tracking station using the broadcast and precise ephemerides. Typical values in north, east, and up components of position error are 2 - 4 m using the broadcast ephemerides and 0.5 - 1.3 m using the precise ephemerides generated by OMNIS.

Future improvements being planned include tuning the filter for Block II satellites, estimating earth orientation rates, adjusting for station height biases, and possibly accommodating GPS cross-link ranging.

Discussion:

Question: How good are the polar motion and UT1-UTC estimates?

Answer: For polar motion, about 11 cm in x and y; for UT1-UTC, about 0.13 msec/day. These are with respect to the IERS final values.

DMA'S INTEREST IN PRECISE GPS ORBITS

- * HISTORICAL USE OF TRANSIT SATELLITES
FOR GEODETIC POSITIONING WORLDWIDE**
- * CONTINUED NEED FOR GLOBAL POSITIONING**
- * TEST AND EVALUATION SUPPORT OF
WEAPONS SYSTEMS**
- * SUPPORT OF OTHER DMA PRODUCTS
(E.G. MAPS)**

BY-PRODUCTS OF DMA'S ORBIT DETERMINATION

- * PRECISE SATELLITE CLOCK PARAMETER
ESTIMATES**
- * QUALITY CONTROL FOR AIR FORCE
BROADCAST EPHEMERIDES, CLOCKS AND
URE'S (SPS AND PPS)**
- * EARTH ORIENTATION VALUES**

EPHEMERIS GENERATION AT DMA

- * TRACKING STATION NETWORK**
- * DMA MONITOR STATIONS**
- * MONITOR STATION CLOCK ANALYSIS (CHAP)**
- * DATA PREPROCESSING**
- * ORBIT COMPUTATION (OMNIS)**
- * ORBIT QUALITY ASSESSMENT**
- * ORBIT PRODUCTS FOR DISTRIBUTION**

CONTRACTOR

**APPLIED RESEARCH LAB.
UNIVERSITY OF TEXAS**

**NAVAL SURFACE WARFARE
CENTER**

SUPPORT TO DMA

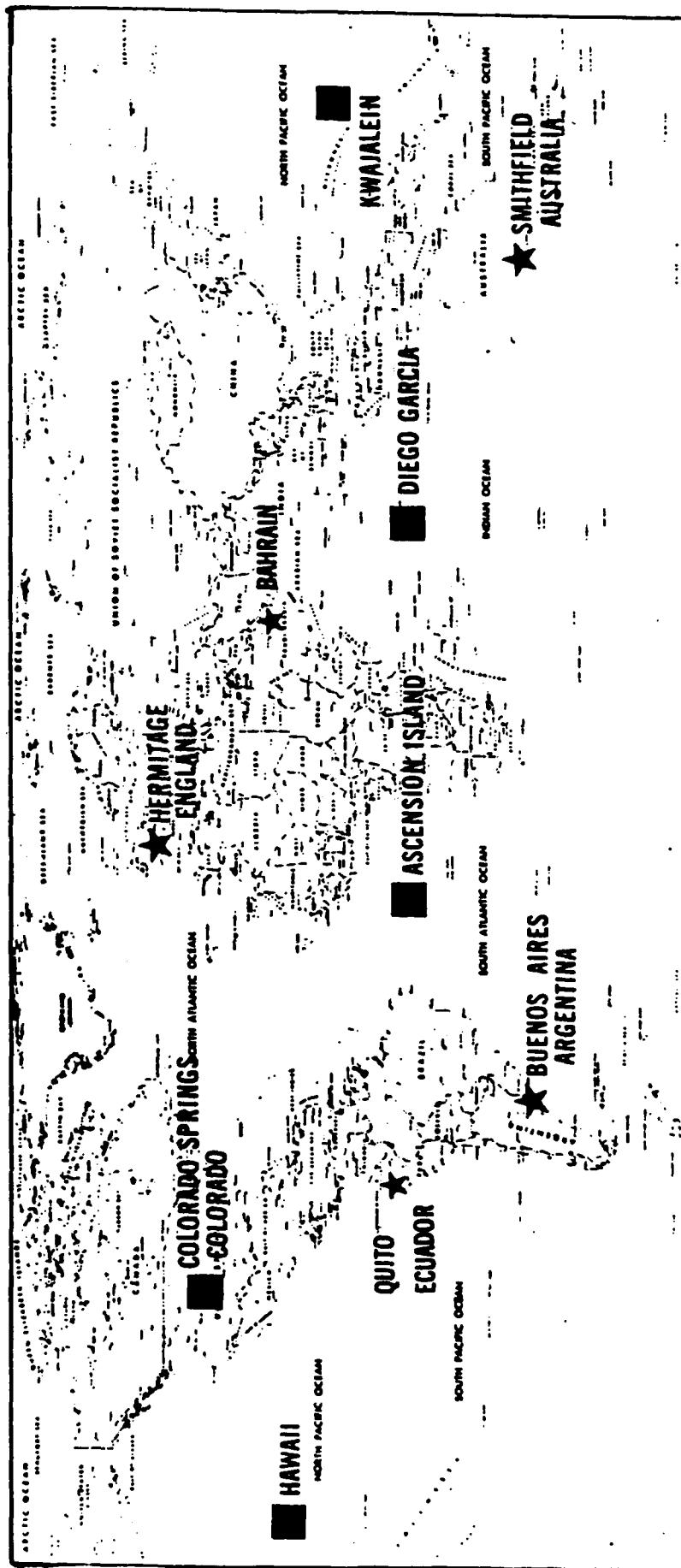
**MONITOR STATION
HARDWARE/SOFTWARE**

ORBIT DETERMINATION

GPS TRACKING NETWORK

(Operational Control Segment)

DMA GPS TRACKING NETWORK



★ DMA GPS TRACKING NETWORK

■ GPS MONITOR STATION (OCS)

DMA STATION LOCATIONS CHOSEN TO --

- 1. ADD HIGHER LATITUDE COVERAGE IN
NORTHERN AND SOUTHERN HEMISPHERES**
- 2. OBTAIN 2 (OR MORE) STATION
TRACKING OF EACH SATELLITE AT ALL
TIMES**
 - * ALLOWS USE OF DIFFERENTIAL
DATA TYPES**
 - * PROVIDES REDUNDANCY IN CASE OF
STATION OUTAGE**
- 3. BE ACCESSIBLE TO U.S. PERSONNEL FOR
OPERATIONS AND MAINTENANCE**

DMA MONITOR STATIONS

INSTALLATION DATES

| | |
|------------------|-----------------|
| ARGENTINA | DEC 1985 |
| ENGLAND | JAN 1986 |
| AUSTRALIA | MAR 1986 |
| ECUADOR | FEB 1987 |
| BAHRAIN | JUN 1987 |

DMA MONITOR STATION FEATURES

- * DATA EQUIVALENT TO AIR FORCE OPERATIONAL CONTROL SEGMENT STATIONS**

- * TI 4100 RECEIVERS WITH**

 - ARL:UT "CORE" SOFTWARE IN RECEIVER**

 - ARL:UT "BEPP" SOFTWARE IN PC**

- * HIGH PRECISION CESIUM CLOCK**

- * COLLECT --**

 - PHASE-SMOOTHED PSEUDORANGE (PPS)**

 - CONTINUOUS COUNT INTERPOLATED DOPPLER DATA**

 - NAVIGATION MESSAGE**

 - SURFACE WEATHER DATA**

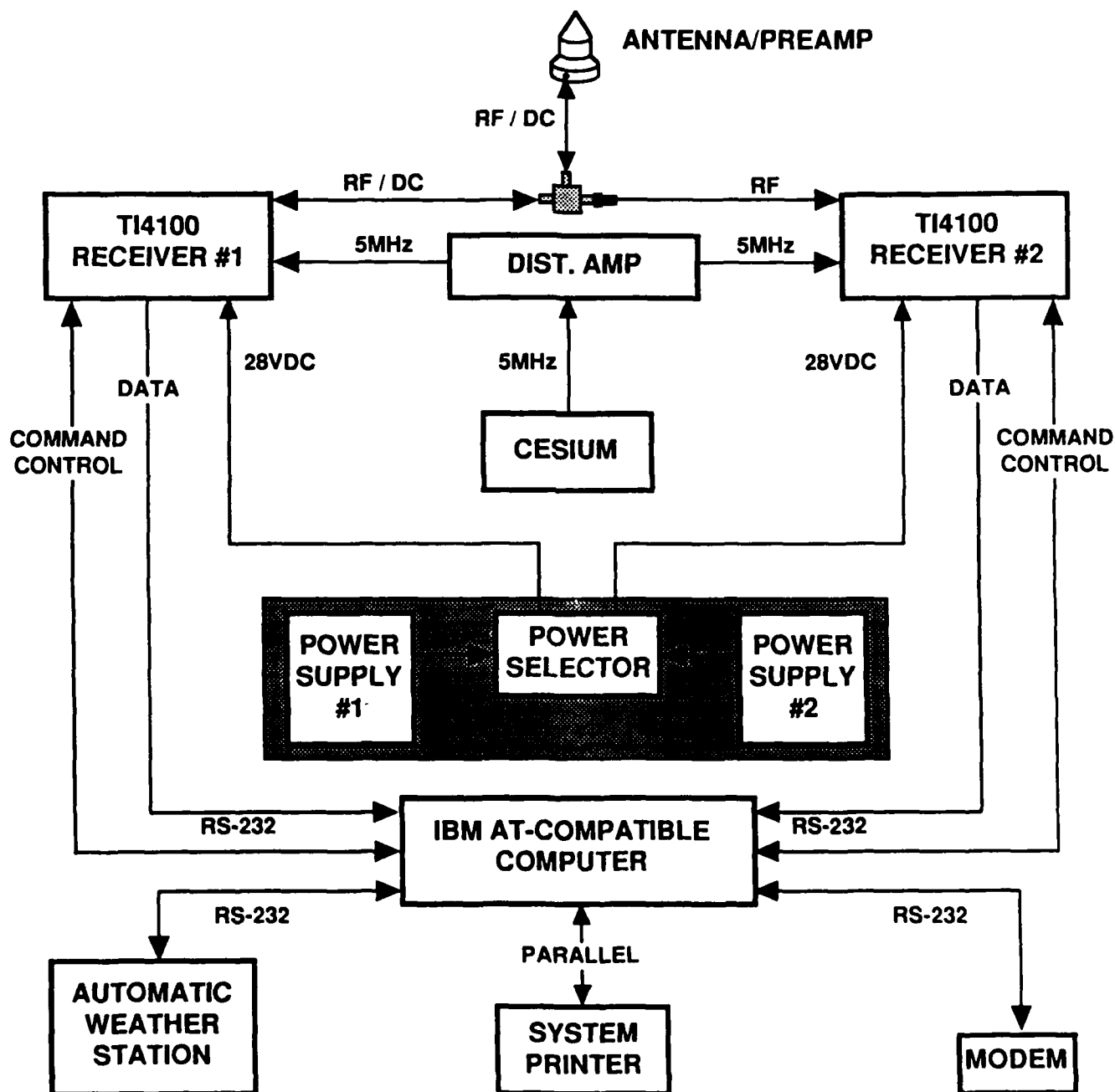
- * ON-SITE QUALITY EVALUATION**

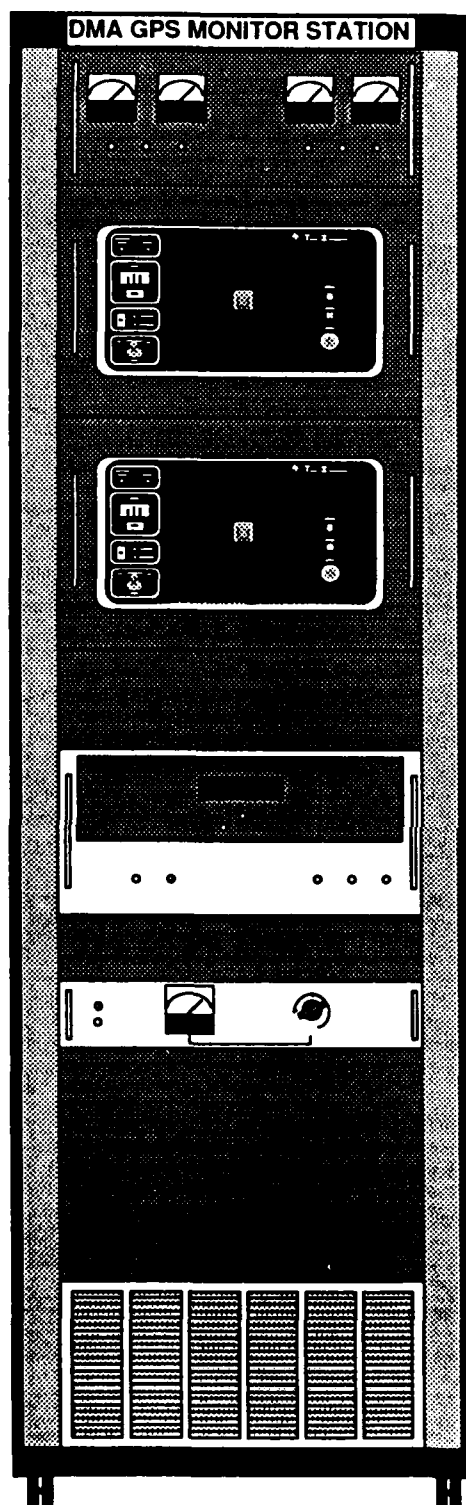
- * DAILY DATA TRANSMISSION TO DMA**

- * ON-SITE DATA ARCHIVING**



HARDWARE BLOCK DIAGRAM





DUAL GPS RECEIVER POWER SUPPLY

TI-4100 GPS RECEIVER #1

TI-4100 GPS RECEIVER #2

BLANK PANEL

HP5061A CESIUM FREQUENCY STANDARD

BLANK PANEL

HP 5087A DISTRIBUTION AMPLIFIER

BLANK PANEL

EQUIPMENT RACK BLOWER

SGD
CB890720-1
CB

EQUIPMENT RACK # 2

SOFTWARE

AUTOMATED DATA COLLECTION LOOP

- SCENARIOS GENERATED FROM TEMPLATE
- DATA STORED ON DISK

DAILY ACTIONS

- OPERATOR INITIATED
- DATA QUEUED IN RECEIVER DURING DAILY ACTIONS
- QUALITY ANALYSIS
- CLOCK ANALYSIS
- FORMAT DATA FOR TRANSMISSION
- MARK DATA FOR ARCHIVING
- TRANSMIT DATA
- ARCHIVE DATA

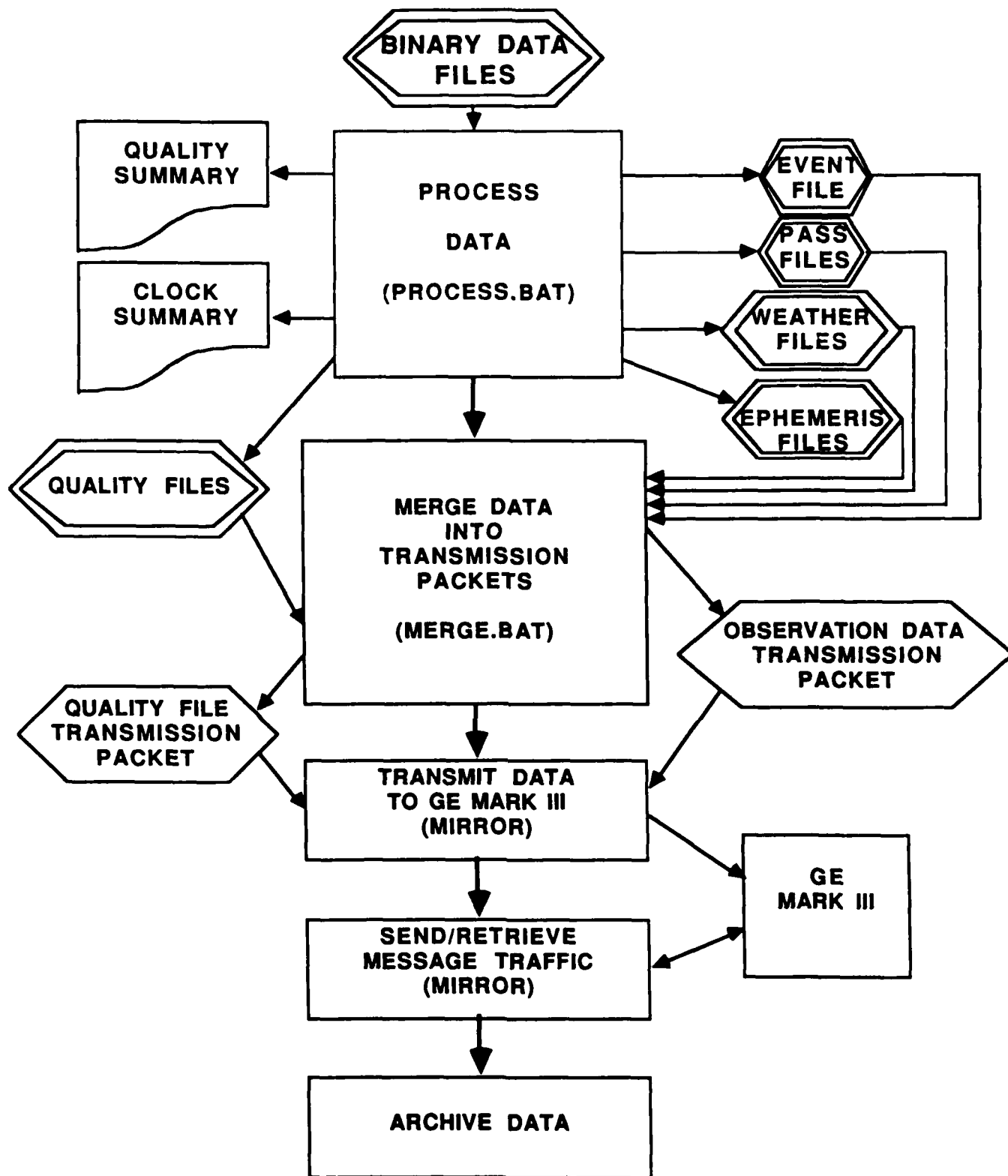


FIGURE 3
DATA PROCESSING AND TRANSMISSION
(OPERATOR CONTROL)

ON SITE ANALYSIS

DATA QUALITY ANALYSIS

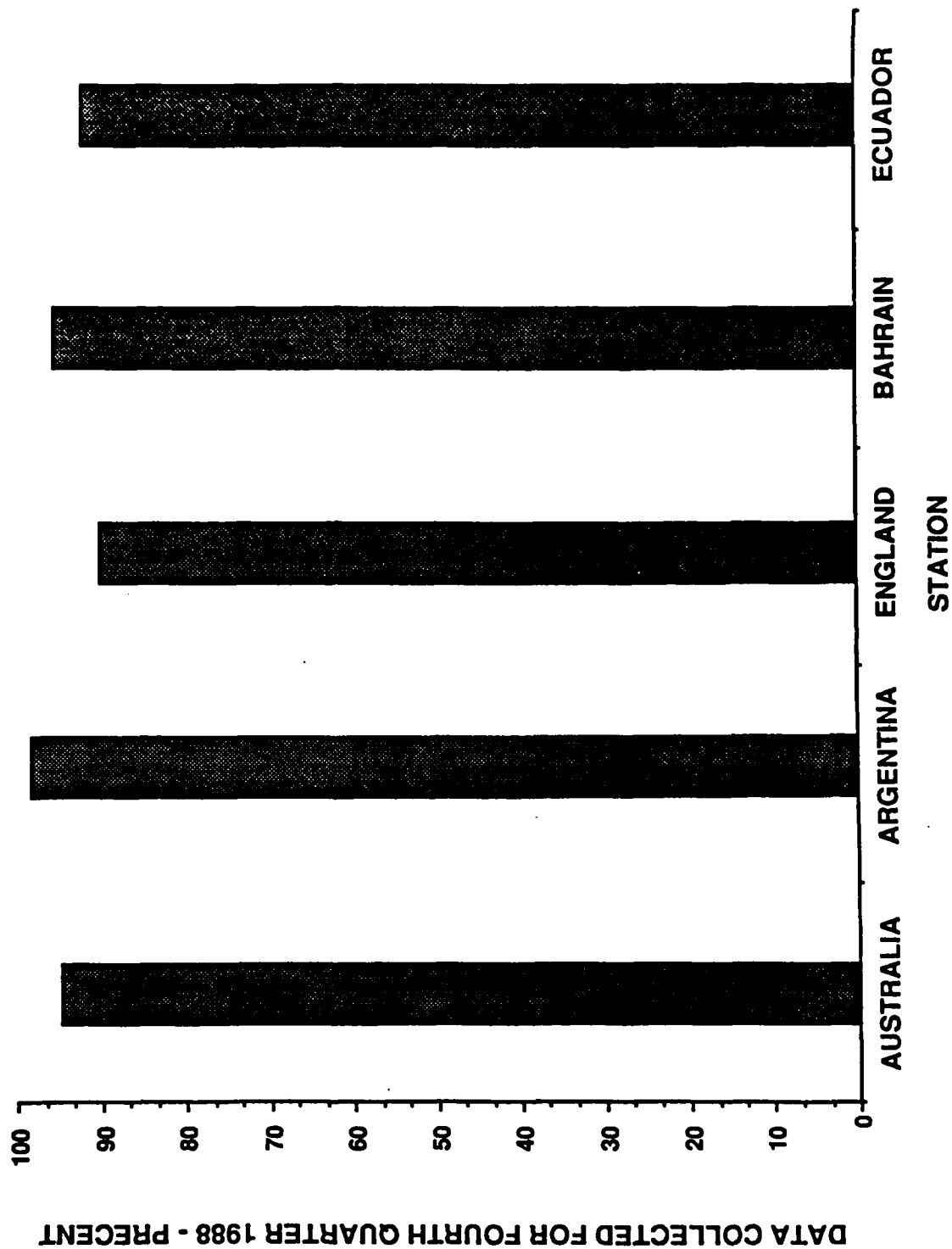
- **SUMMARY BY SATELLITE: TRACKING STATUS**
PERCENTAGE OF GOOD DATA COLLECTED

CLOCK ANALYSIS

- **INPUT DATA:**
15 MINUTE AVERAGED RANGE RESIDUALS
DATA ALIGNED IN SIDEREAL TIME
RESIDUALS BY SATELLITE
- **SAVE SELECTED DATA IN 32 DAY HISTORY FILE**
- **PRODUCE ESTIMATES OF: FREQUENCY BIAS**
AGING
STABILITY (ALLAN VARIANCES)

GPS MONITOR STATION DATA COLLECTION

PERFORMANCE



CLOCK HISTORY ANALYSIS PROGRAM (CHAP)

**OBJECTIVE: IDENTIFY STATION CLOCK
PROBLEMS**

- * COMPUTES AND STORES RECEIVER TIME
BIASES AT EACH RANGE MEASUREMENT TIME**
- * REJECTS BAD DATA**
- * FIXES LARGE JUMPS IN TIME BIAS**
- * ESTIMATES CLOCK PARAMETERS FOR
1 DAY (CURRENT)
2 DAYS (CURRENT AND PREVIOUS)
32 DAYS (HISTORY)**

INCLUDING

**FREQUENCY BIAS
AGING
STABILITY (ALLAN VAR.)**

**CHAP CLOCK ANALYSIS
BASED ON 2 DAYS
ARGENTINA 11 JAN 89**

FREQUENCY BIAS BASED ON 1-DAY DIFFS.

| <u>PRN</u> | <u>NUMBER OF DIFFERENCES</u> | <u>FREQUENCY BIAS (NS/DAY)</u> | |
|------------|----------------------------------|--------------------------------|--------------|
| | | <u>2-SIG. AVG.</u> | <u>SIGMA</u> |
| 6 | 13 | 77.3 | 2.5 |
| 9 | 22 | 90.0 | 4.2 |
| 11 | 2 | 84.2 | 1.4 |
| 12 | 19 | 86.0 | 2.8 |
| 13 | 17 | 86.8 | 4.2 |
| ALL | 73 | 85.7 | 5.4 |

**CHAP CLOCK ANALYSIS
BASED ON 33 DAYS
ARGENTINA 11 JAN 89**

LINEAR REGRESSION ON TIME BIAS TIME SERIES

(UNITS: TIME BIAS = NS, FREQ. BIAS = NS/DAY)

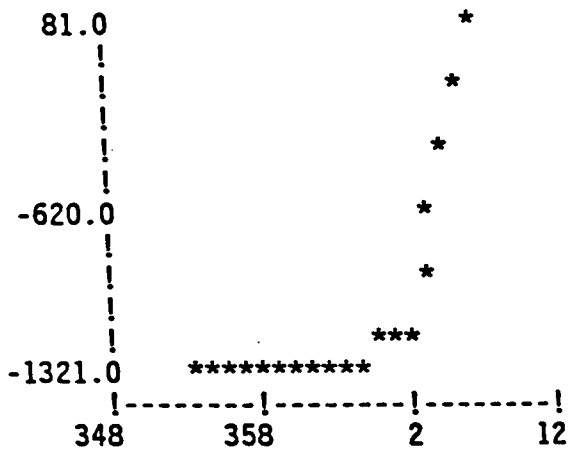
| <u>PRN</u> | <u>TIME BIAS</u> | <u>SIGMA</u> | <u>FREQ. BIAS</u> | <u>SIGMA</u> |
|------------|------------------|--------------|-------------------|--------------|
| 3 | 2835.7 | 22.1 | 87.7 | .7 |
| 6 | 2797.2 | 11.1 | 86.5 | .2 |
| 9 | 2809.9 | 7.8 | 86.7 | .1 |
| 11 | 2747.2 | 7.3 | 86.1 | .2 |
| 12 | 2800.2 | 13.3 | 86.7 | .2 |
| 13 | 2804.2 | 10.6 | 87.0 | .2 |

| <u>TIME</u> <u>(DAYS)</u> | <u>SQRT (ALLAN VARIANCE)</u> <u>(SEC/SEC)</u> |
|------------------------------|--|
| 1 | 2.1E-13 |
| 2 | 6.9E-14 |
| 4 | 2.6E-14 |
| 8 | 1.1E-14 |

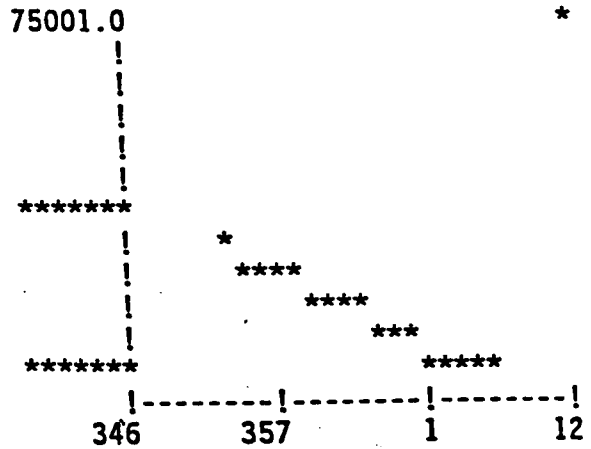
CHAP 33 DAY CLOCK HISTORY

* SV PRN 3 *

3-DAY WALKING FREQUENCY (NS/DAY) (SV-GROUND) VS. DAY OF YEAR

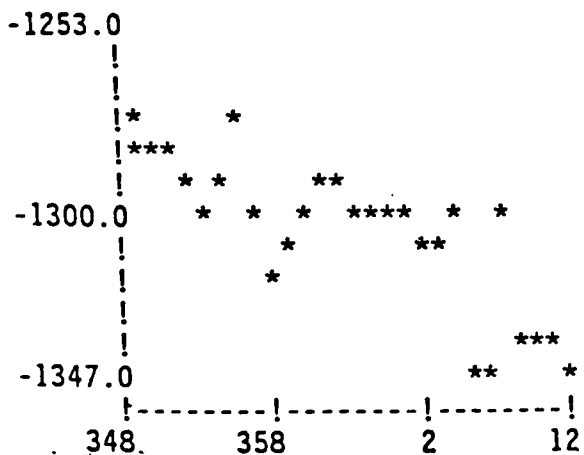


SV-GROUND TIME BIAS (NS)
VS. DAY OF YEAR
478433-NS & -6638 NS/DAY RMVD

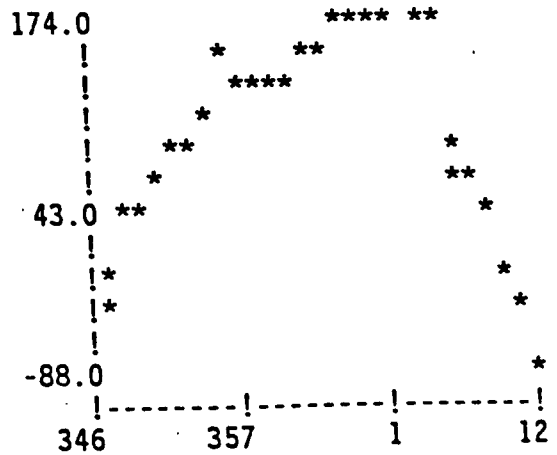


* SV PRN 6 *

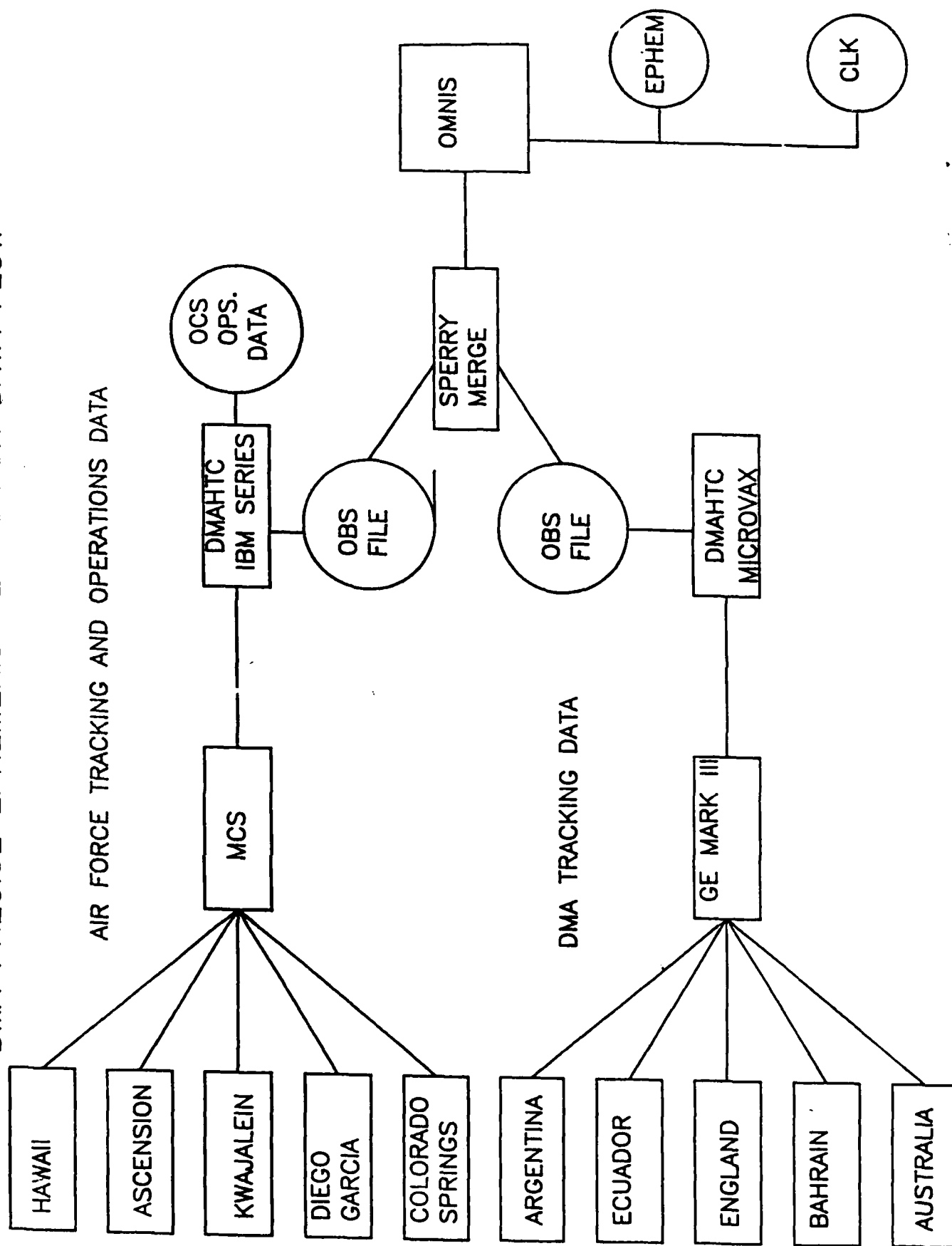
3-DAY WALKING FREQUENCY (NS/DAY) (SV-GROUND) VS. DAY OF YEAR



SV-GROUND TIME BIAS (NS)
VS. DAY OF YEAR
-420000 NS & -1288 NS/DAY RMVD



DMA PRECISE EPHEMERIS GENERATION DATA FLOW



ORBIT DATA PROCESSING

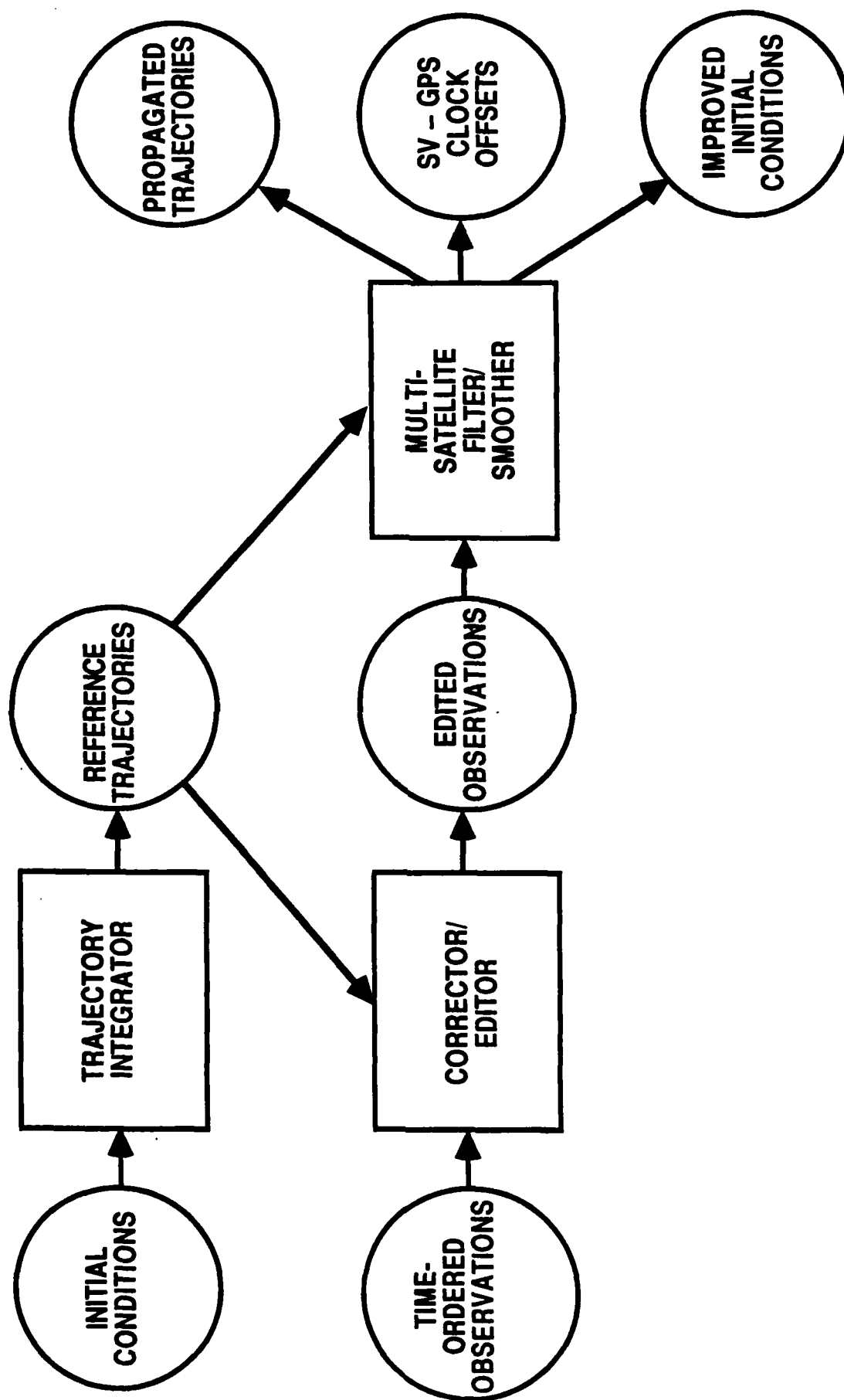
PREPROCESSING:

- * COMBINE AF AND DMA DATA INTO IDENTICAL FORM**
- * MODIFY "NOMINAL CLOCKS AND EVENTS FILE" FOR MASTER CLOCK SWITCHES, MOMENTUM DUMPS AND OTHER CLOCK EVENTS NOT ON FILES TRANSMITTED BY AF OR DMA STATIONS**
- * VALIDATE WEATHER DATA**

OMNIS

- | | |
|---------------------|---------------------|
| * CORRECTOR | * FILTER |
| * EDITOR | * SMOOTHER |
| * INTEGRATOR | * PROPAGATOR |

OMNIS GPS PROCESSING SYSTEM



CORRECTOR/EDITOR

CORRECTIONS APPLIED

TWO-FREQ. IONOSPHERIC REFRACTION ON RAW DATA
VACUUM SIGNAL PROPAGATION TIME

TROPOSPHERIC REFRACTION - HOPFIELD MODEL WITH
MEASURED SURFACE WEATHER DATA

PERIODIC RELATIVITY

SV ANTENNA OFFSET

STATION DISPLACEMENT DUE TO SOLID EARTH TIDE

EDITING PROCEDURES

INTERACTIVE - USING RESIDUALS FROM CORRECTOR

SOLVE FOR POLYNOMIAL CLOCKS AND JUMPS

AUTOMATIC - USING CONSISTENCY OF ADJ. RESIDUALS

TRAJECTORY INTEGRATOR

FORCE MODEL

GRAVITATIONAL FORCES

WGS 84 EGM TRUNCATED TO 8TH DEGREE & ORDER
SUN & MOON - POINT MASSES, DE200 EPHEMERIDES
SOLID EARTH TIDE - 2ND DEGREE LEGENDRE POLYN.

NON-GRAVITATIONAL FORCES

RADIATION PRESSURE - ROCK4 FOR BLOCK I SVS
ROCK42 FOR BLOCK II SVS
Y-AXIS BIAS (ALSO ECLIPSED)
THRUSTS (AS REQUIRED)

TRAJECTORY INTEGRATOR (CONTINUED)

NUMERICAL INTEGRATION

10TH ORDER COWELL
ACCELERATIONS AND PARTIAL DERIVATIVES
FIXED STEP = 5 MIN.

EARTH-FIXED-TO-INERTIAL TRANSFORMATION

J2000 EPOCH
IAU 76 PRECESSION
IAU 80 NUTATION
1982 DEFINITION OF UT1
DMA EARTH ORIENTATION PREDICTIONS

MULTI-SATELLITE FILTER/SMOOTHER (MSF/S) OVERVIEW

WHY A FILTER/SMOOTHER?

UNMODELED ACCELERATIONS ACTING ON THE SATELLITES
ATOMIC CLOCKS EXHIBIT DETERMINISTIC AND RANDOM BEHAVIOR
PROCESSING DONE AFTER THE FACT

WHY MULTI-SATELLITE?

OPTIMAL SEPARATION OF SATELLITE AND STATION CLOCK OFFSETS
ALLOW FOR MULTI-SATELLITE STATION NAVIGATIONS
ACCOMMODATION OF DOUBLY DIFFERENCED DATA TYPES
ACCOMMODATION OF PROPOSED CROSS-LINK RANGING DATA

ORBIT/CLOCK DETERMINATION SPECIFICS

WEEKLY FILTER/SMOOTHER FITS - ACTUALLY 8-DAY FITS WITH
ONE DAY OVERLAP ON EACH END
PROCESS ALL SATELLITES AND STATIONS SIMULTANEOUSLY
10 STATIONS - 5 AIR FORCE AND 5 DMA (CESIUM CLOCKS)
USE WGS-84 GRAVITY AND STATION COORDINATES
USE 15-MIN SMOOTHED PSEUDORANGES (DERIVED FROM
RAW PSEUDORANGE AND PHASE AT 1.5 SEC INTERVALS)
OBSERVATION SIGMA = 75 CM (1988) = 100 CM (1987)
MINI-BATCH INTERVAL = 1 HOUR
ESTIMATE BOTH STOCHASTIC AND CONSTANT PARAMETERS
GENERATE BOTH FITTED TRAJECTORIES AND SV CLOCKS

PARAMETERS ESTIMATED

FOR EACH SATELLITE:

ORBITAL ELEMENTS

RADIATION PRESSURE SCALE WITH STEADY-STATE SIGMA =

.01 AND DECORRELATION TIME = 4 HRS.

Y-AXIS ACCELERATION WITH STEADY-STATE SIGMA = $1.E-12$

KM/SEC**2 AND DECORRELATION TIME = 4 HRS.

TIME OFFSET, FREQ. OFFSET, AND FREQ. DRIFT (STOCHASTIC)

FOR EACH STATION (EXCEPT FOR MASTER):

TIME OFFSET AND FREQUENCY OFFSET (STOCHASTIC)

POLAR MOTION



CONSTANTS

RATE OF CHANGE OF UT1-UTC



DMA GPS ORBIT ACCURACY

WEEK TO WEEK ORBIT CONSISTENCY

ORBIT OVERLAP COMPARISON

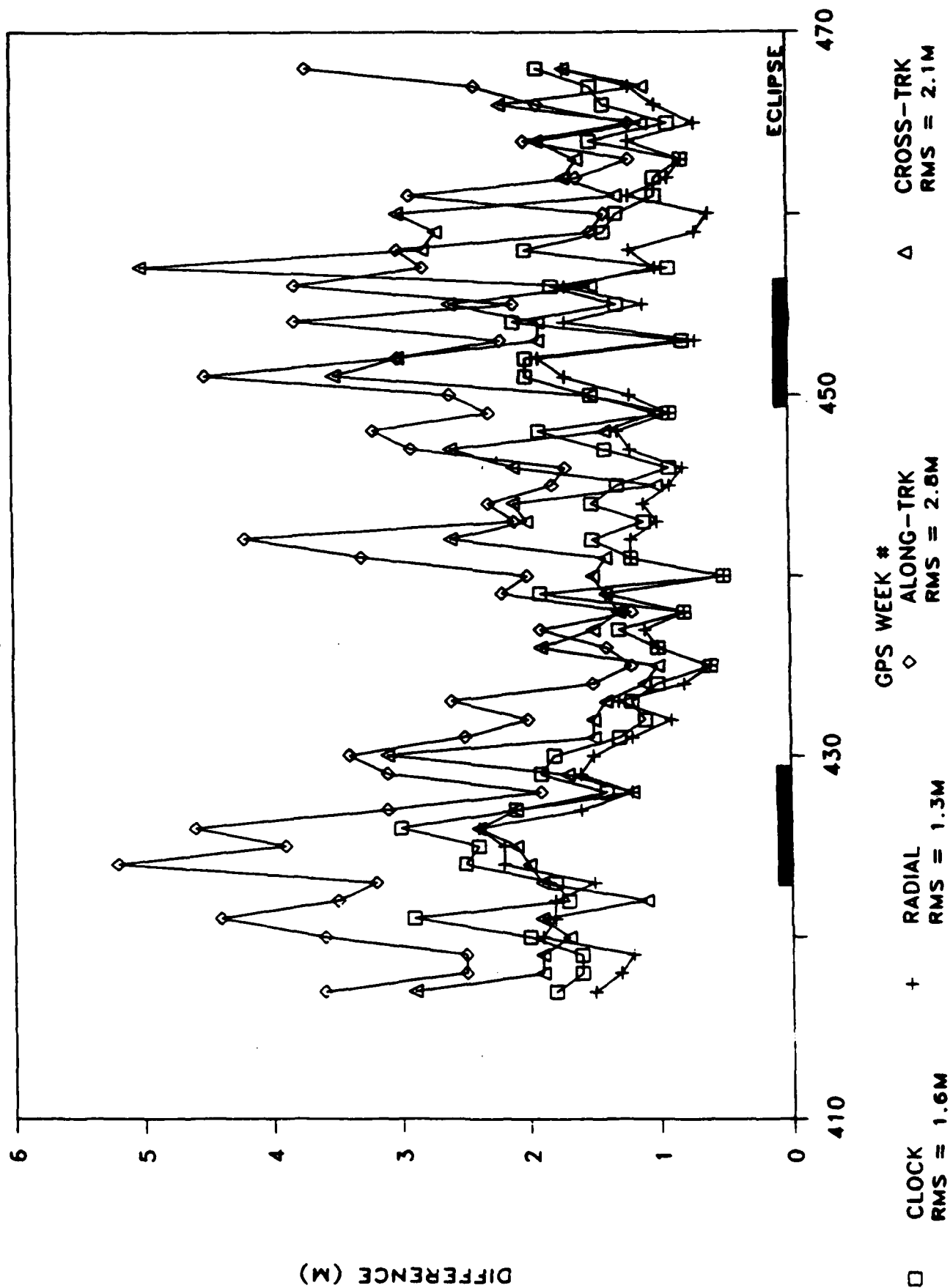
RMS Differences 6 Satellites

1988 (20 Weeks)

| | |
|-------------|-------|
| Radial | 1.2 m |
| Along-Track | 2.6 m |
| Cross-Track | 1.7 m |

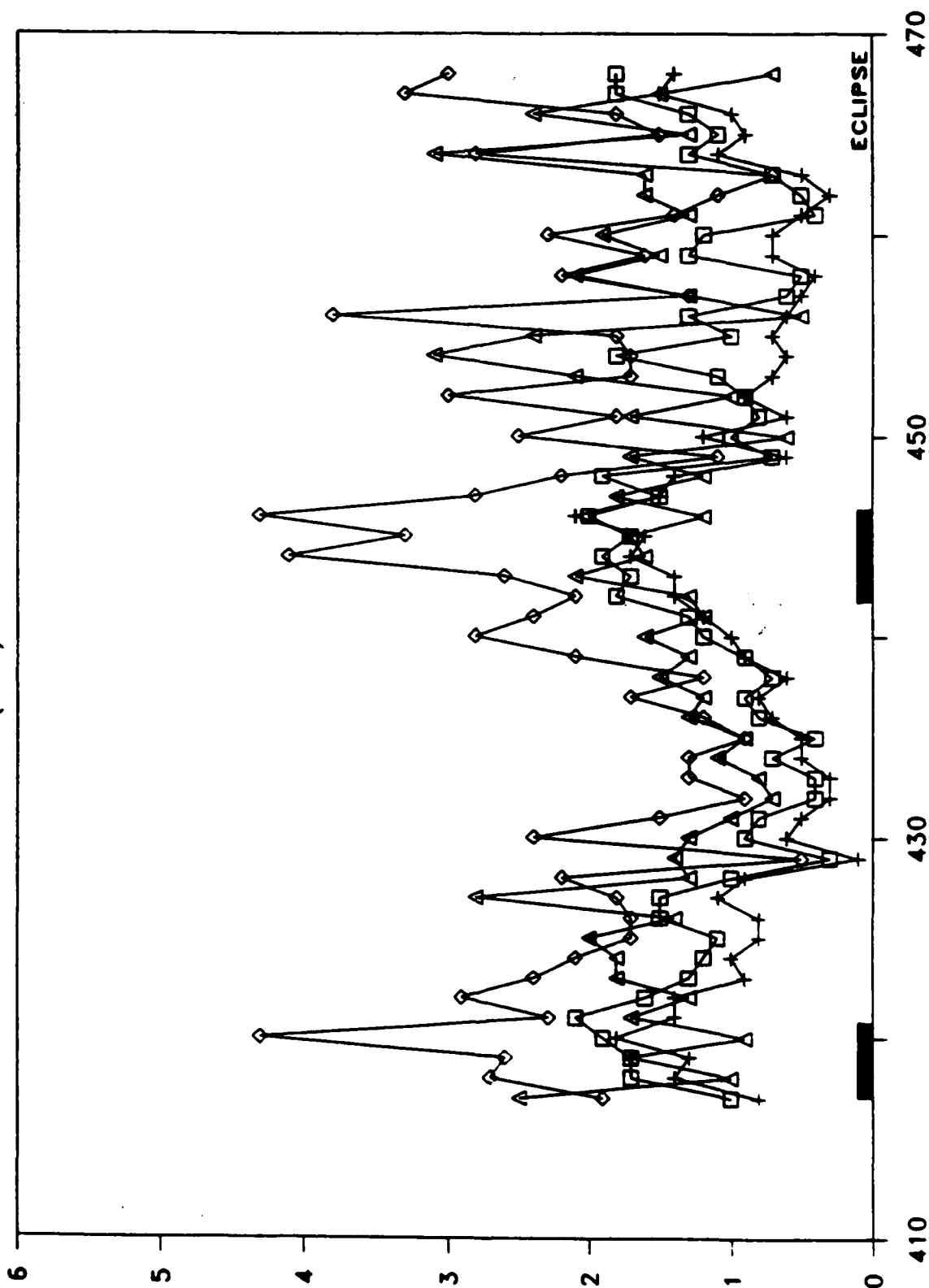
SV06 OVERLAP RMS DIFF. FOR 1988

(in M)



SV13 OVERLAP RMS DIFF. FOR 1988

(in M)



CLOCK
RMS = 1.3M

+

RADIAL
RMS = 1.0M

◇

GPS WEEK #
ALONG-TRK
RMS = 2.3M

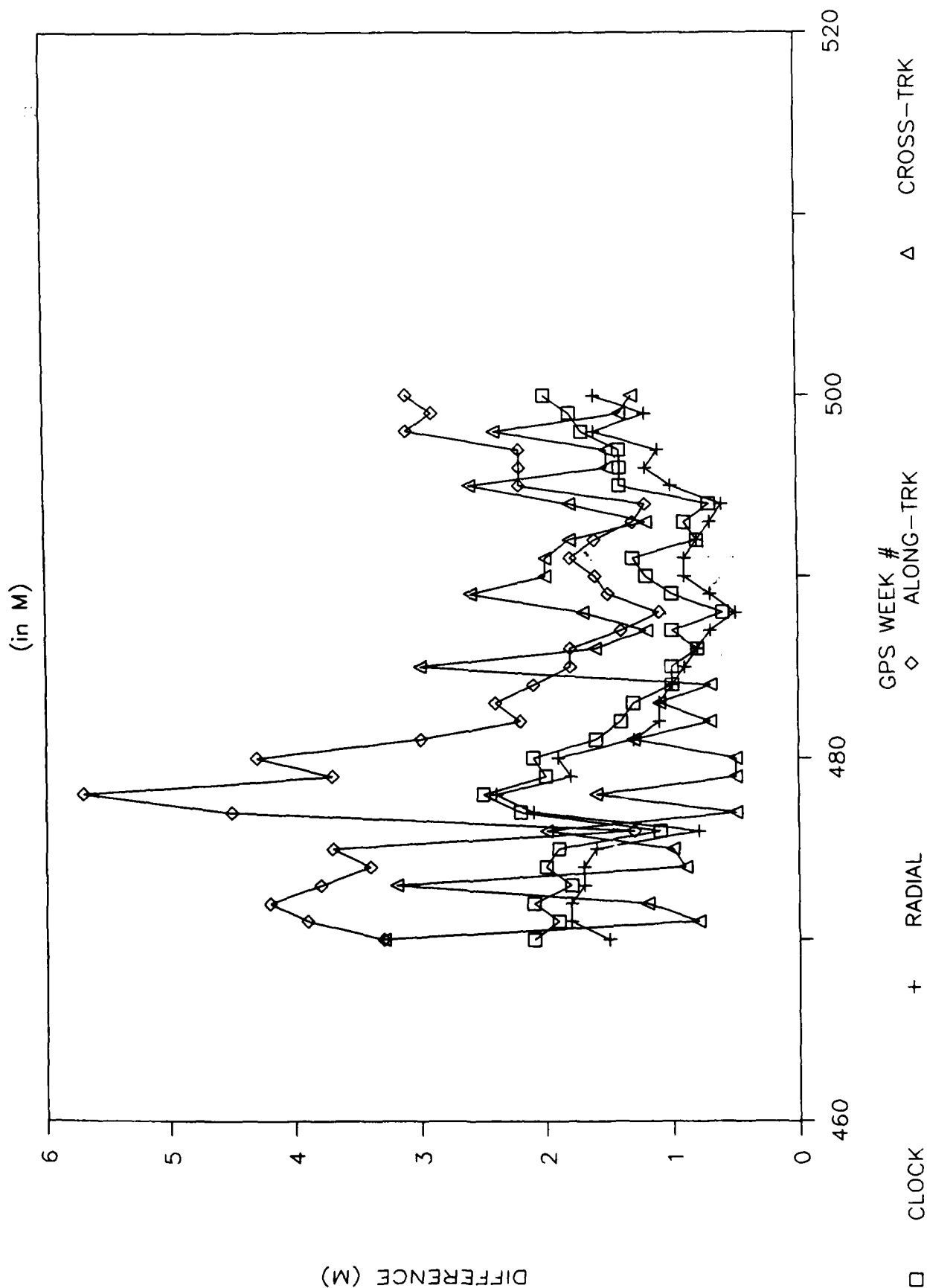
△

CROSS-TRK
RMS = 1.6M

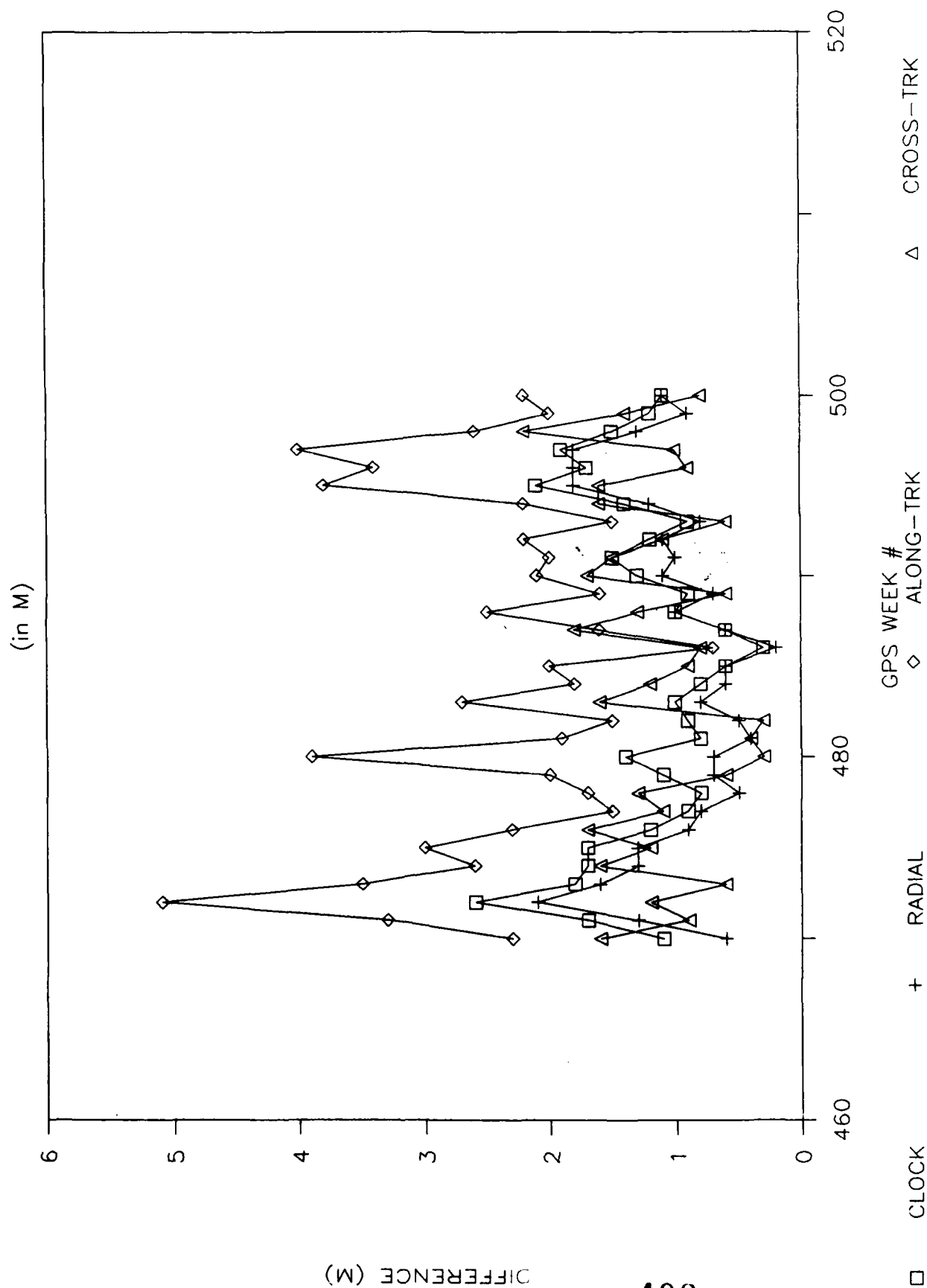
□

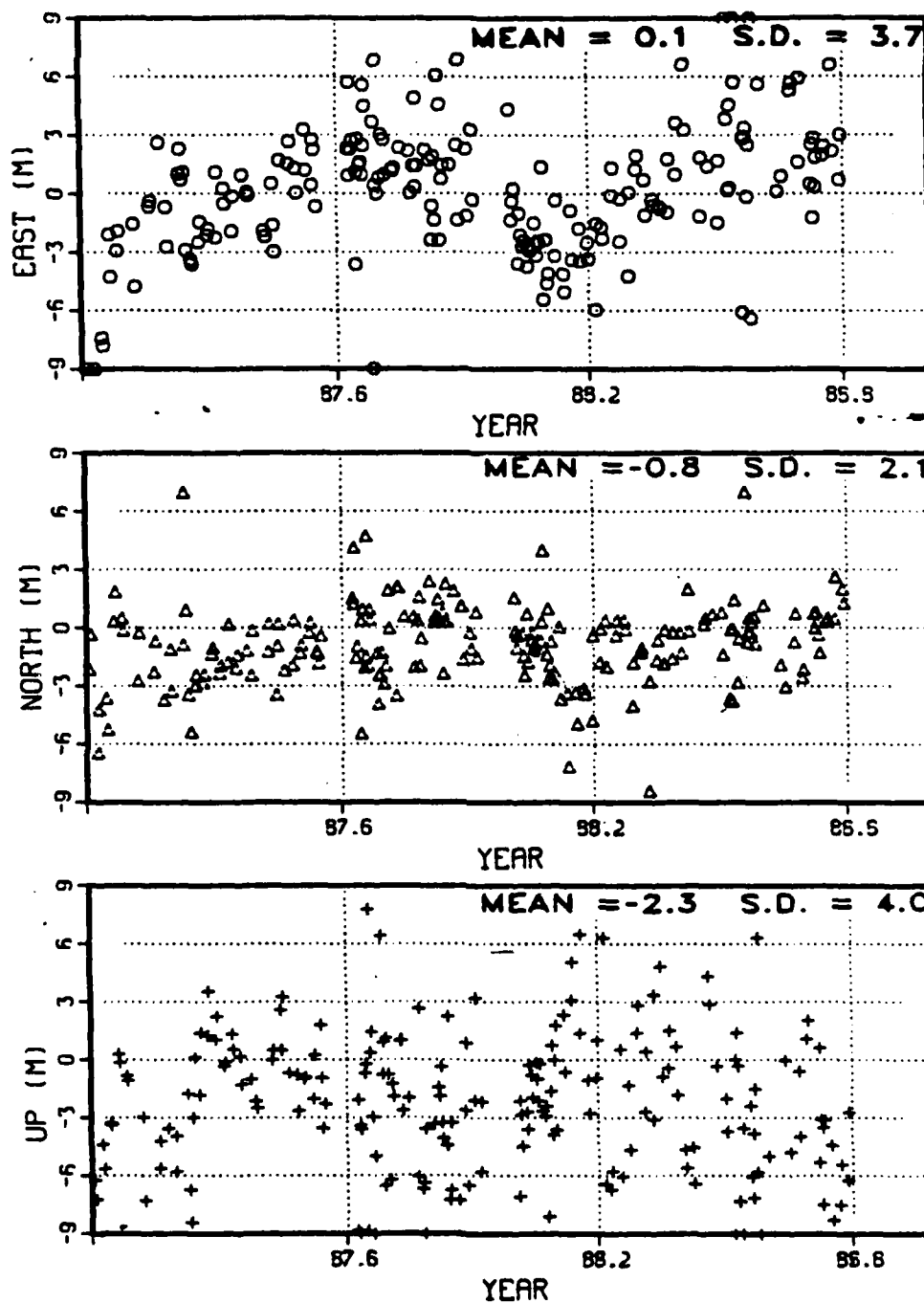
DIFFERENCE (M)

SV06 OVERLAP RMS DIFF. FOR 1989

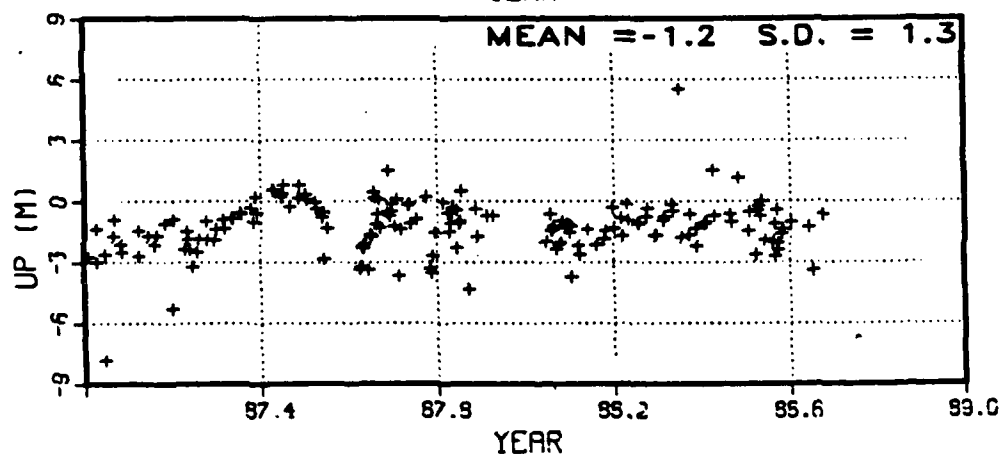
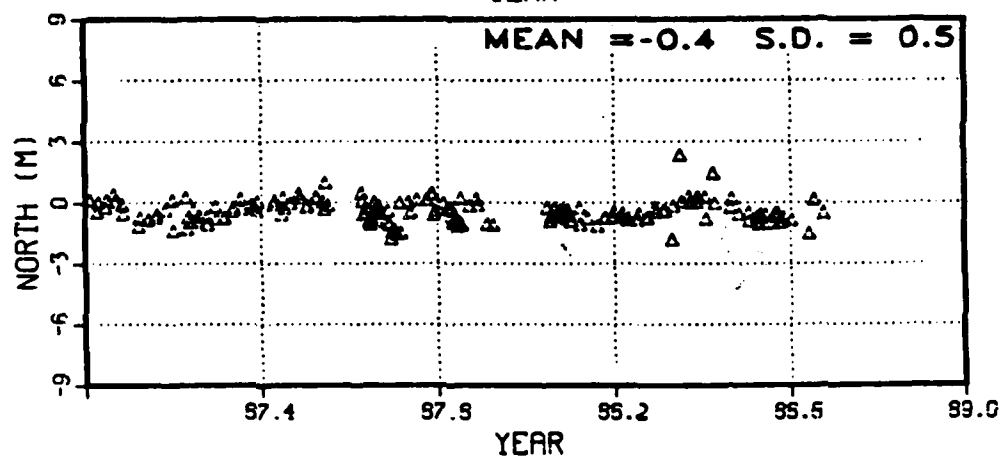
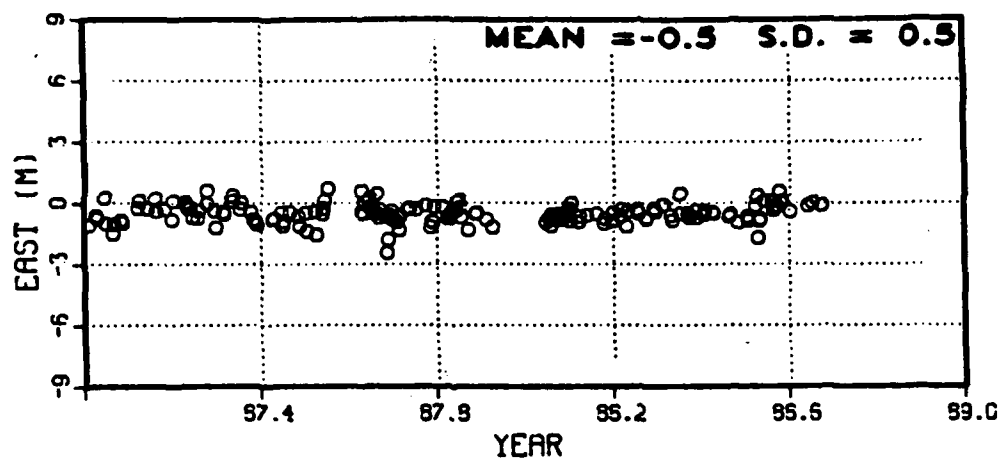


SV13 OVERLAP RMS DIFF. FOR 1989

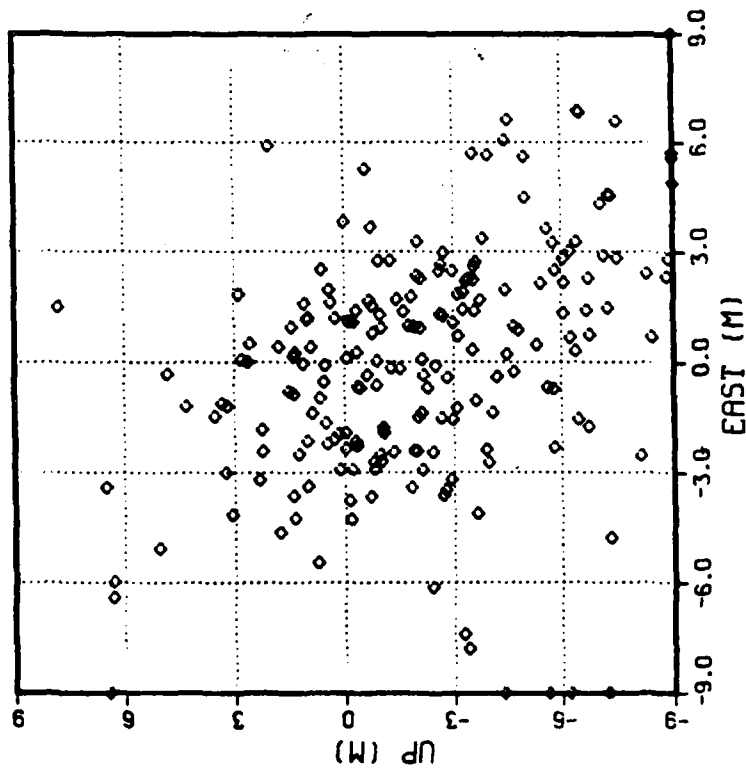
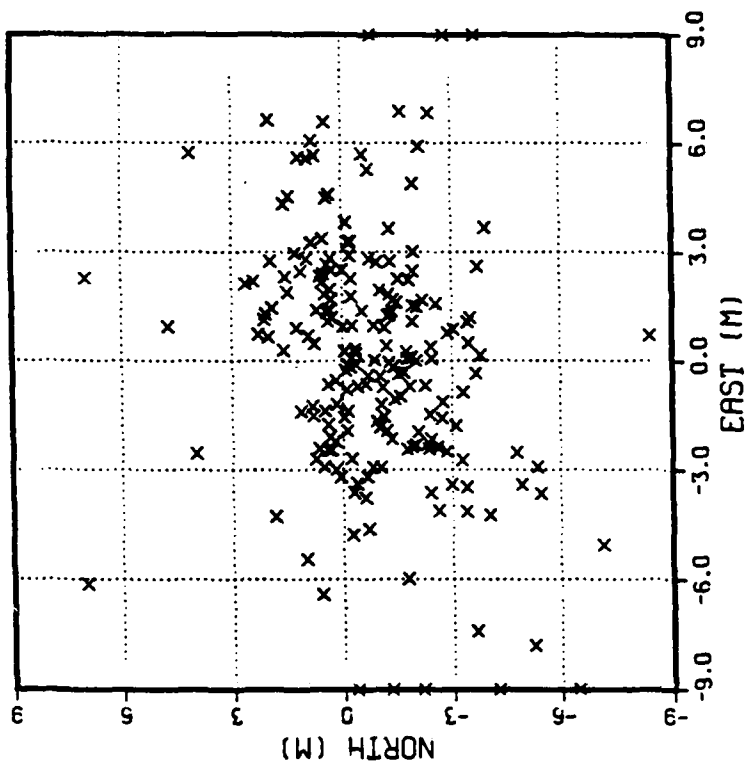




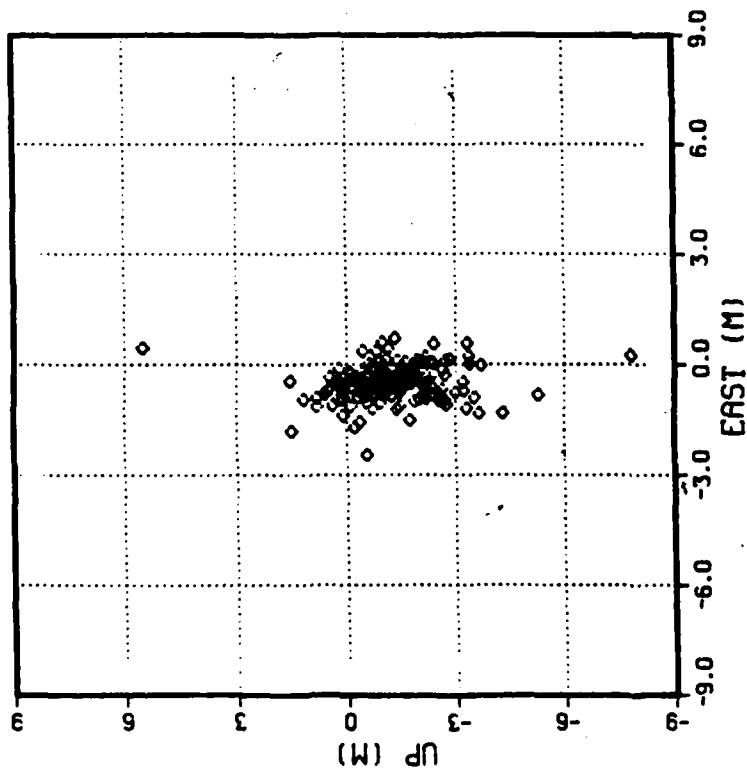
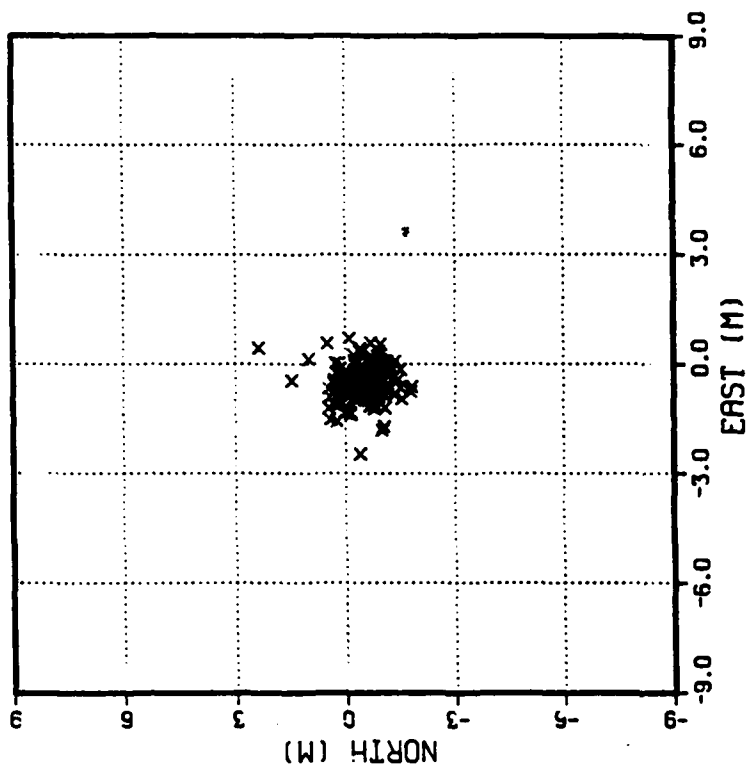
NSWC SOLUTIONS WITH THE BROADCAST EPHEMERIS



NSWC SOLUTIONS WITH THE PRECISE EPHEMERIS



NSWC SOLUTIONS WITH THE BROADCAST EPHEMERIS



NSWC SOLUTIONS WITH THE PRECISE EPHEMERIS

ABSOLUTE POSITIONING

ALBROOK, PANAMA

DMA'S GASP SOFTWARE

NO. OF INDEPENDENT SOLUTIONS = 16

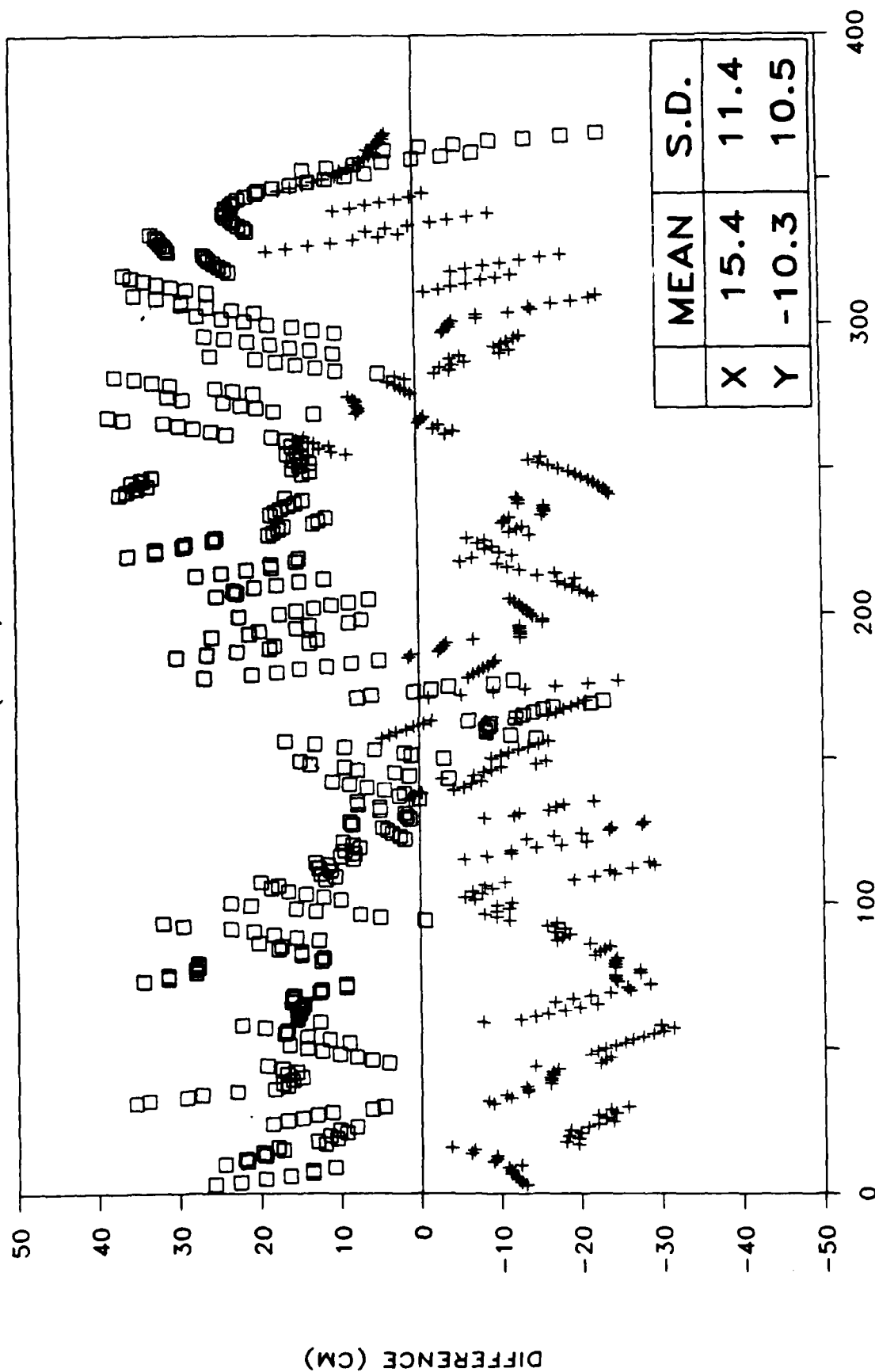
| <u>EPHEM./CLOCK</u> | <u>STD. DEV. OF SOLUTION (M)</u> | | | | | |
|---------------------|----------------------------------|----------|----------|------------|-------------|-----------|
| | <u>X</u> | <u>Y</u> | <u>Z</u> | <u>LAT</u> | <u>LONG</u> | <u>HT</u> |
| BROADCAST | 1.6 | 1.2 | 1.2 | 1.2 | 1.6 | 1.1 |
| PRECISE | 0.7 | 0.7 | 0.6 | 0.6 | 0.8 | 0.7 |

DMA GPS EPHEMERIS PRODUCTS

- * PRECISE EPHEMERIDES
(ECEF, POS., VEL., WGS-84)**
- * PRECISE CLOCK STATE ESTIMATES
(SATELLITE CLOCKS)**
- * EARTH ORIENTATION VALUES**
- * SMOOTHED OBSERVATIONS
(15 MIN CORRECTED RANGES)**

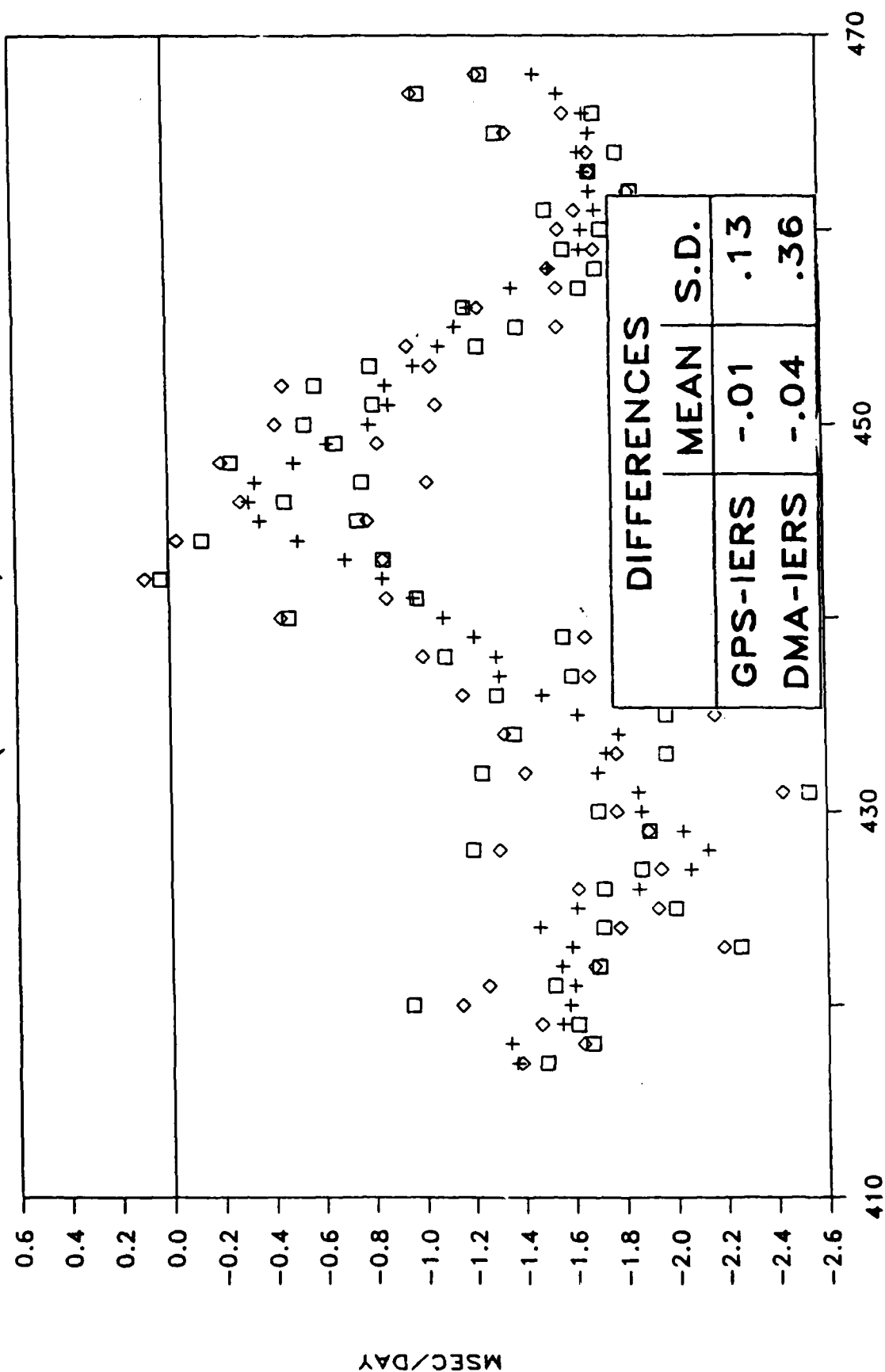
GPS - IERS FINAL X AND Y FOR 1988

(in CM)



UT1-UTC WEEKLY RATES FOR 1988

(in MSEC/DAY)



2500 Kilometer Baseline Limit

Circles represent
equidistant surface distances



DMA Stations-RED
AF Stations-BLUE

FUTURE ORBIT PROCESSING IMPROVEMENTS

- * FILTER TUNING
BLOCK II SATELLITE CLOCKS
ORBIT MODELING (RAD. PRESS.)**
- * PARTITIONING OF FILTER**
- * EARTH ORIENTATION RATES**
- * STATION HEIGHT ADJUSTMENT**
- * CROSS-LINK RANGING**

A SHUTTLE EXPERIMENT TO DEMONSTRATE 6-DEGREE-OF-FREEDOM
NAVIGATION WITH GPS

Duncan B. Cox, Jr. and, Steven Gardner
MAYFLOWER COMMUNICATIONS COMPANY, INC.

and

Neal Carlson
INTEGRITY SYSTEMS, INC.

The objective of this effort is to define an experiment to demonstrate the utility of GPS in determining position and, particularly, attitude in space. The observations used to accomplish this are accumulated phase and pseudorange from multiple antennas. The unique features of a space application include high velocity, greater visibility of GPS satellites, rapidly changing GDOP (many opportunities for good geometry), and special environmental effects (temperature, pressure, vibration due to boost environment). One goal of the experiment is to achieve low cost - use existing equipment and be able to retrieve it for use after the experiment and perform post-mission data analysis. The Shuttle meets many of these requirements for a low cost experiment since it is a vehicle specifically designed to deploy experiments in space.

In order to determine attitude one needs three or more antennas observing at least two satellites, one in the plane defined by the antennas and one over this plane. Although the Shuttle does have antennas, there are no preamplifiers; hence the proposed experiment includes its own deployed array of antennas in the cargo bay. A determination of attitude requires an accurate reference. Errors contributing to the reference include star-tracker errors, inertial navigation system drift, alignment transfers, structural bending between the star-tracker and the experiment package. Based on rotation data from a recent Shuttle OMV-type experiment, the difference between attitudes registered by two independent INS's show a stability of about ± 0.2 mrad over 2000 sec., which is consistent with our goal of a few milliradian accuracy in the experiment.

Ideally, the experiment can be packaged in an existing experiment module, such as the "GAS can" (Hitchhiker program) which is specifically available for space experiments. There are several options for mounting the module in the shuttle bay area and considerable analyses have been done on thermal conditions inside the can for different Shuttle attitudes with respect to the sun.

The experiment is very simple, but various integration procedures would delay actual flight of the experiment to about 3 years.

SIX-DOF GPS NAVIGATION EXPERIMENT

- Autonomy
- Six degrees of freedom
Position and attitude
Filter can estimate other states also
- Position
Standard code pseudoranging
Delta phase, or accumulated phase
- Attitude
Accumulated phase
Multiple antennas and satellites

Mayflower Communications 89100908 *Integrity Systems*

SIX-DOF GPS NAVIGATION EXPERIMENT

- Special navigation conditions in LEO
 - High velocities
 - High rates of change of LOS
 - Many good-geometry opportunities
 - Importance of Doppler
- Other special conditions
 - Environmental effects
 - Temperature, pressure
 - Radiation
 - Boost environment
 - Reliability
 - Safety

Mayflower Communications 89100909 *Integrity Systems*

SIX-DOF GPS NAVIGATION EXPERIMENT

Achieving Low Cost

- Utilize previously developed equipment
 - GPS receiver
 - Antennas
 - Reference systems
 - Attitude, position
 - Recording equipment
 - Test bed and integration procedures
- Utilize post-flight data analysis
 - Characterize the sensor system
 - Illustrate system integration algorithms

Mayflower Communications 89100910 *Integrity Systems*

SIX-DOF GPS NAVIGATION EXPERIMENT

Proposed Approach

- Utilize the STS Orbiter
 - Has needed support systems
 - Data acquisition and storage
 - Electrical & mechanical interfaces
 - Star tracker and IMUs
 - Has manifests set aside for experiments
- Provide an option for ground tracking
 - Corner cube on shuttle

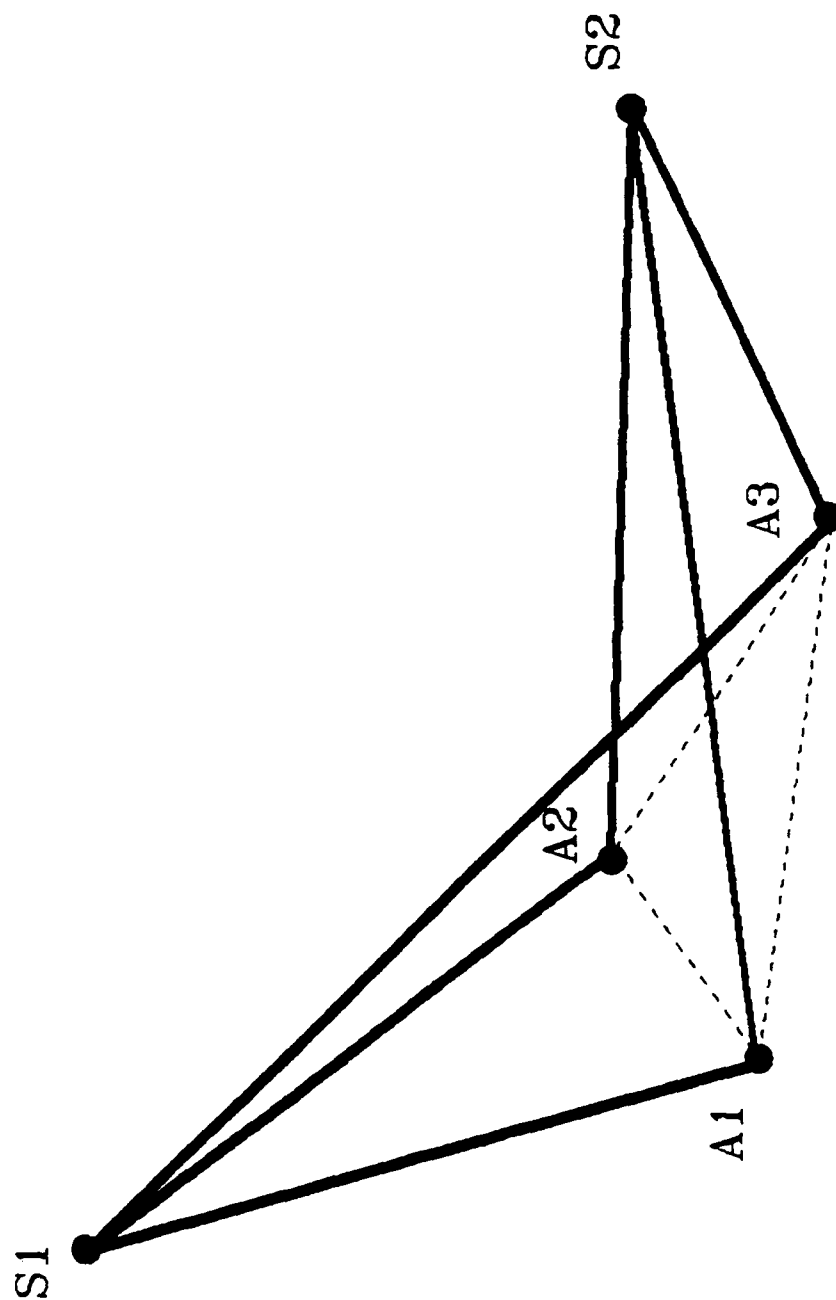
Mayflower Communications

89100911

Integrity Systems

GEOMETRY

FOR ATTITUDE DETERMINATION WITH GPS

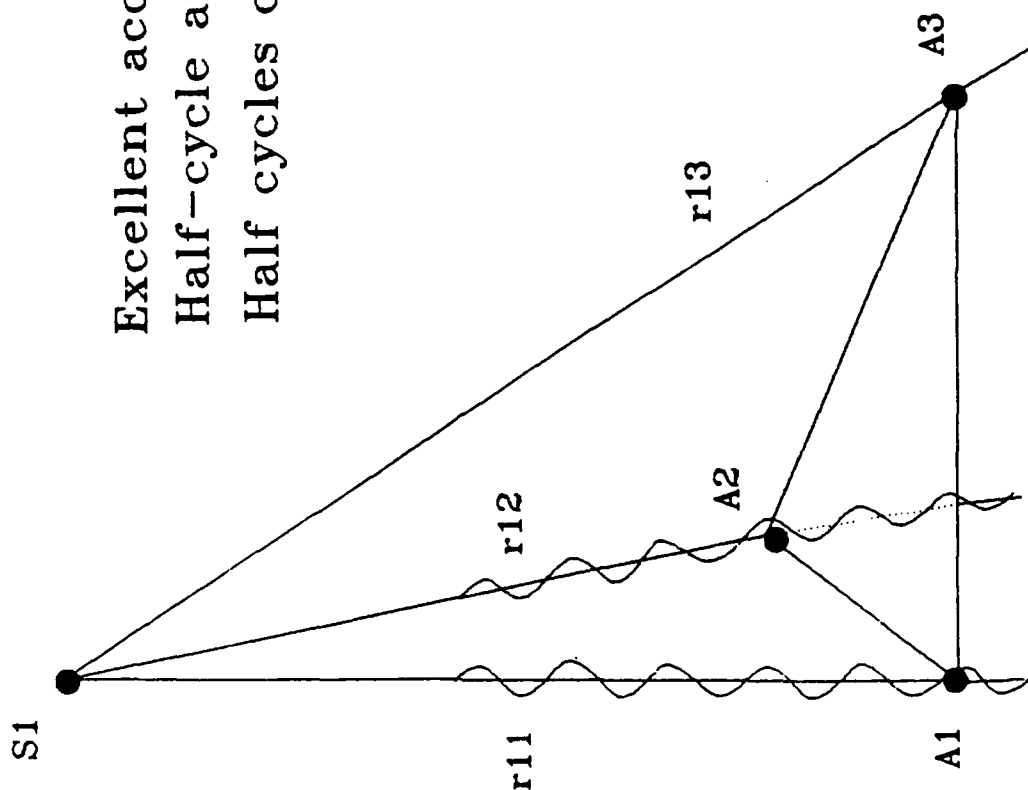


Mayflower Communications

89093003

DIFFERENTIAL PHASE MEASUREMENTS

Excellent accuracy & resolution
Half-cycle ambiguities
Half cycles can be accumulated



Mayflower Communications
89093004.cht

SIX-DOF GPS NAVIGATION EXPERIMENT

Antenna Options

- GPS antennas exist on the Orbiter
Integration cost is significant
- Propose supplying experimental antennas
Small 1-meter array
Accuracies of few milliradians
Corner cube near one antenna

Mayflower Communications

89100914

Integrity Systems

SIX-DOF GPS NAVIGATION EXPERIMENT

Data Transfer/Storage

- SV ID
- Pseudorange
- Accumulated phase
- Differential accumulated phase
- Mission time
- Status

Mayflower Communications 89100915 *Integrity Systems*

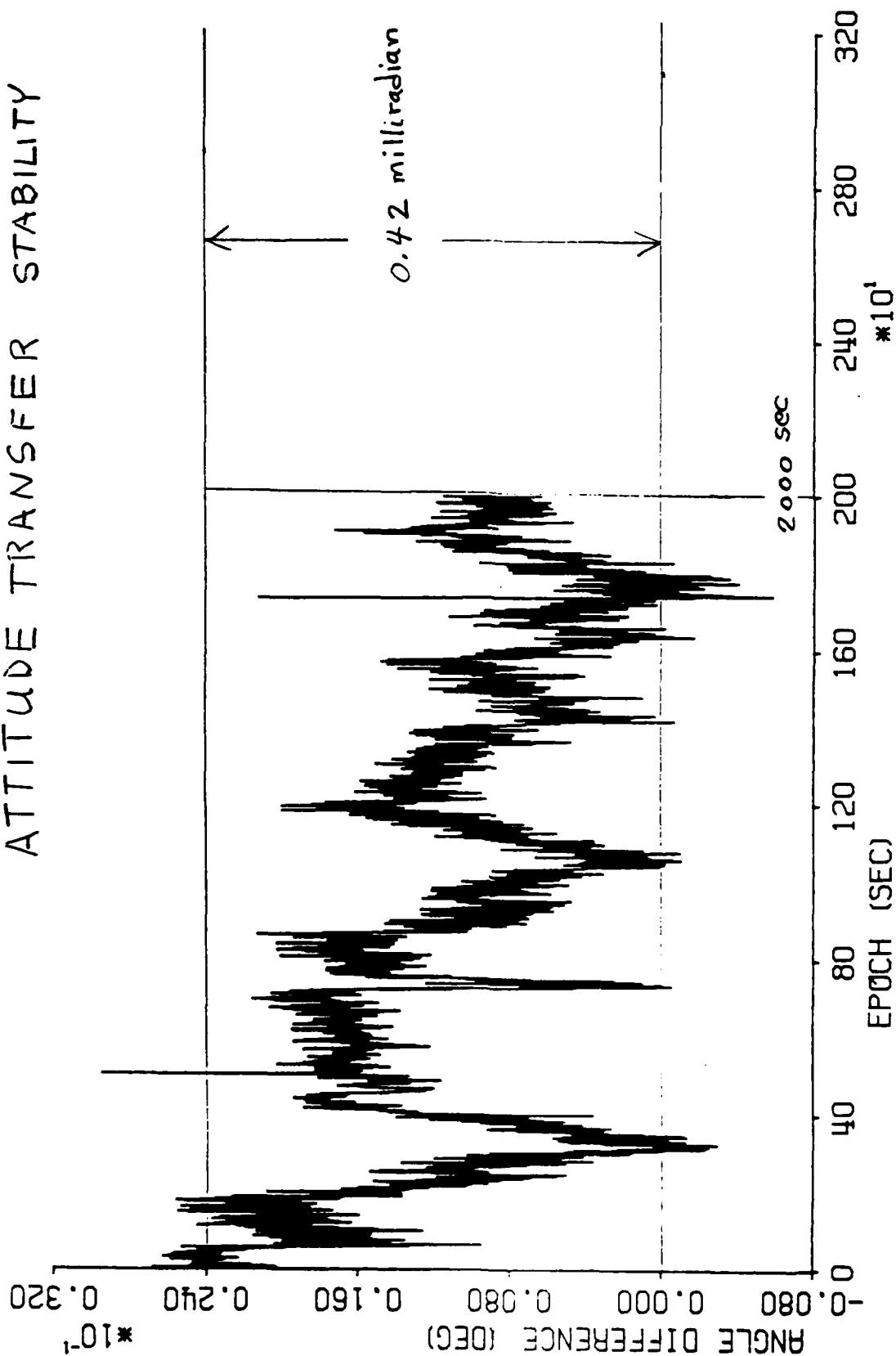
SIX-DOF GPS NAVIGATION EXPERIMENT

Reference Attitude Accuracy

- Error sources
 - Startracker
 - Startracker-to-INS transfer
 - INS drift
 - INS-to-Experiment transfer
- Shuttle bending
 - Forces due to thermal and inertial effects
 - Should minimize distance
 - Should locate on substantial structures
 - Some data available on stability
- Calibration required
 - Post-flight processing

Mayflower Communications 89100913 *Integrity Systems*

ATTITUDE TRANSFER STABILITY



FIRST EULER ANGLE (TOD) DIFFERENCE (S-E) - * OF VALUES PLOTTED = 2001

10/9/89
Mayflower

THE TIME OFFSET OF THE PLOT IS = 23649416 SECONDS (UTC)

SIX-DOF GPS NAVIGATION EXPERIMENT

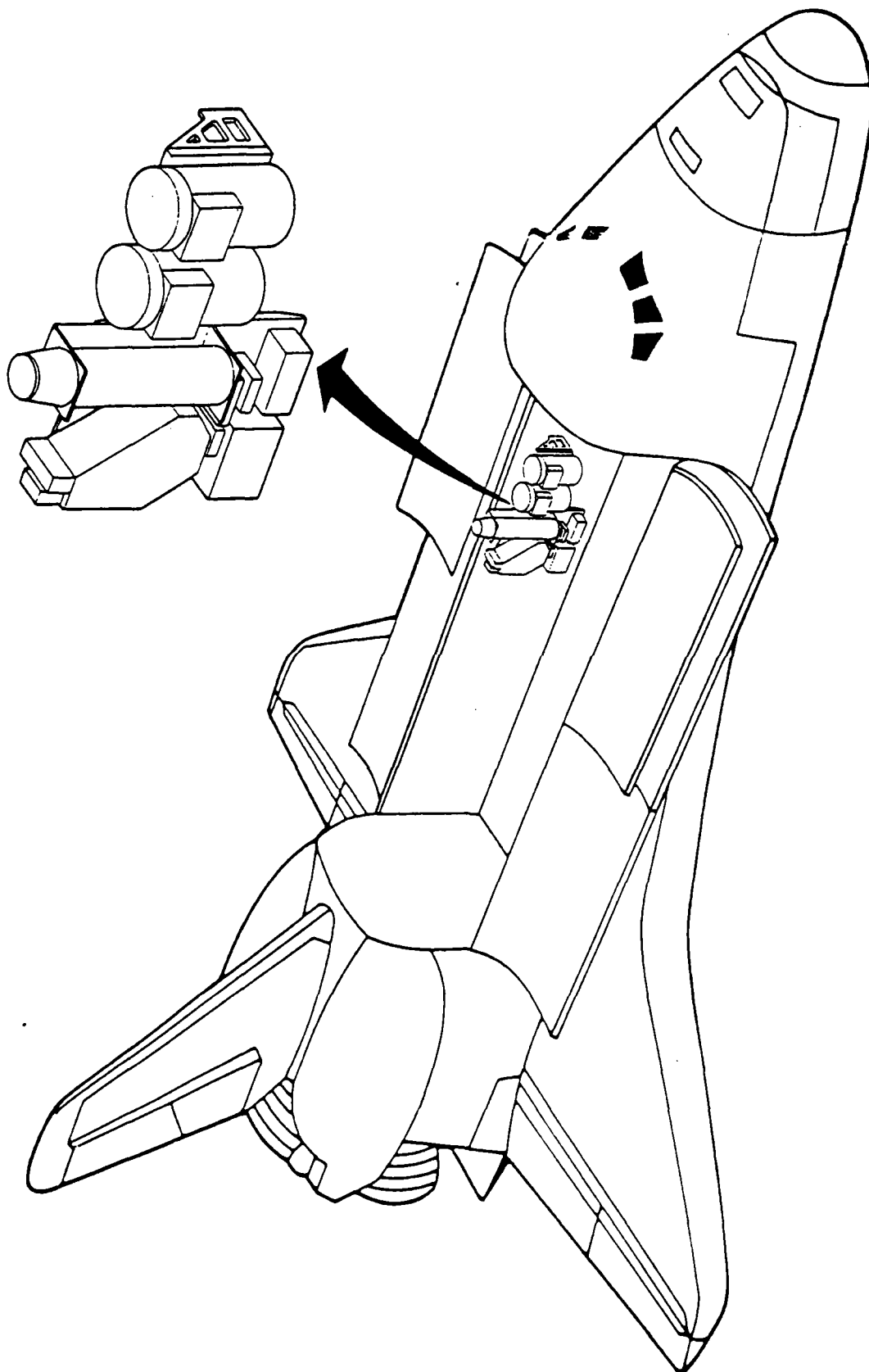
Orbiter Integration

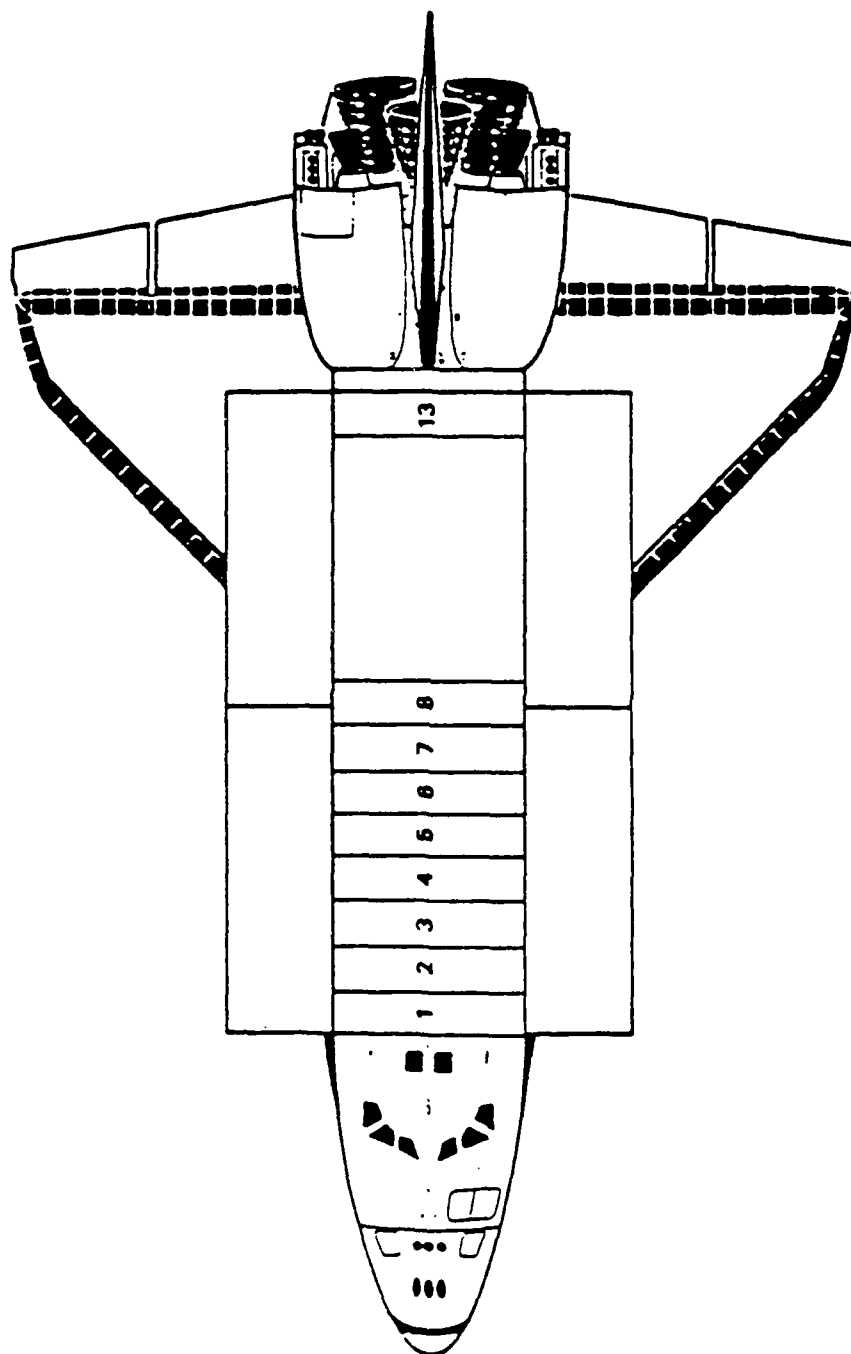
- Utilize Hitchhiker Program
- Utilize "Gas Can" Modules if possible
- Minimal constraints on GPS equipment
Obtain equipment on loan

Mayflower Communications

89100912

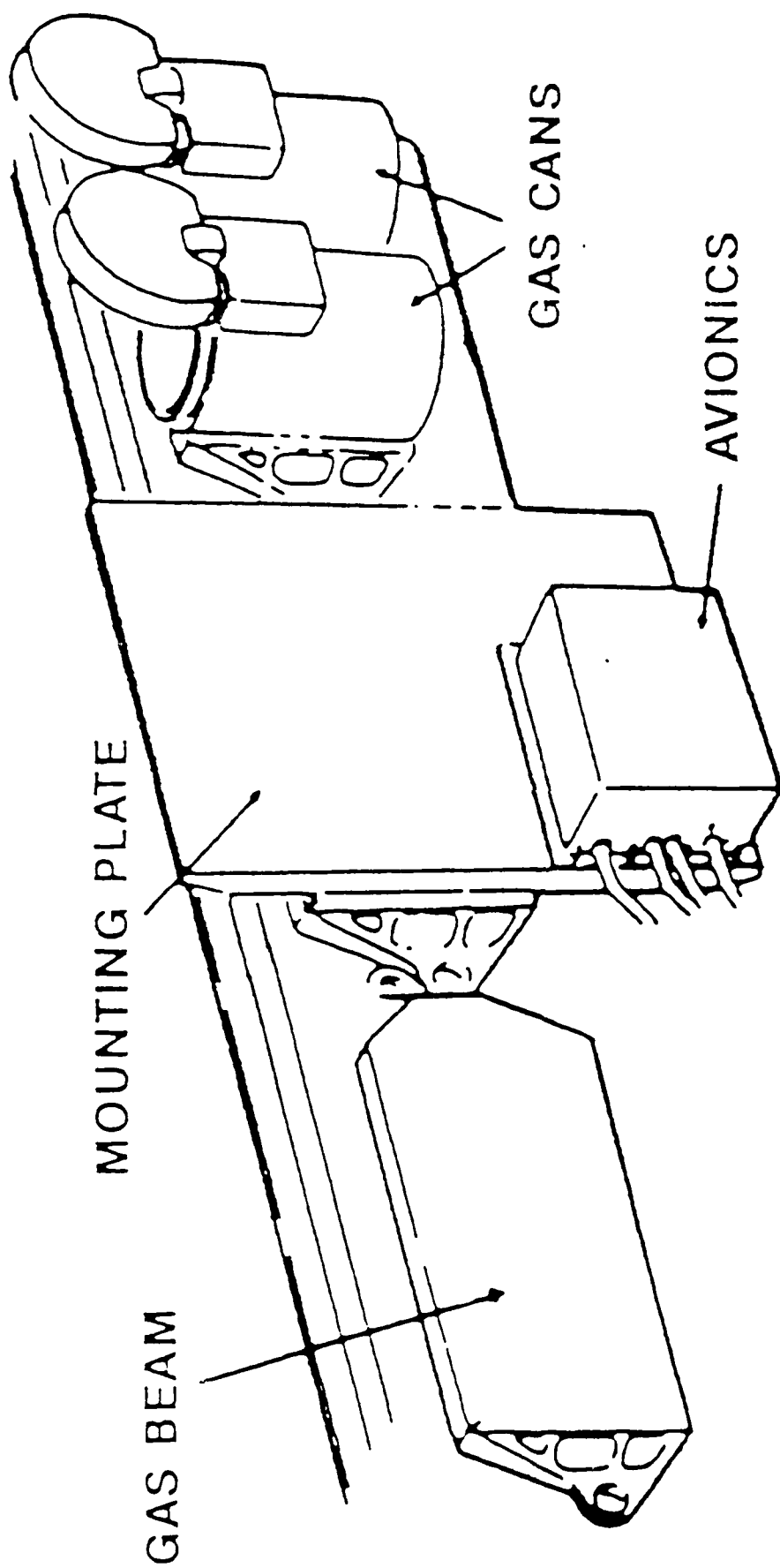
Integrity Systems





ORBITER TOP VIEW AND BAY LOCATIONS

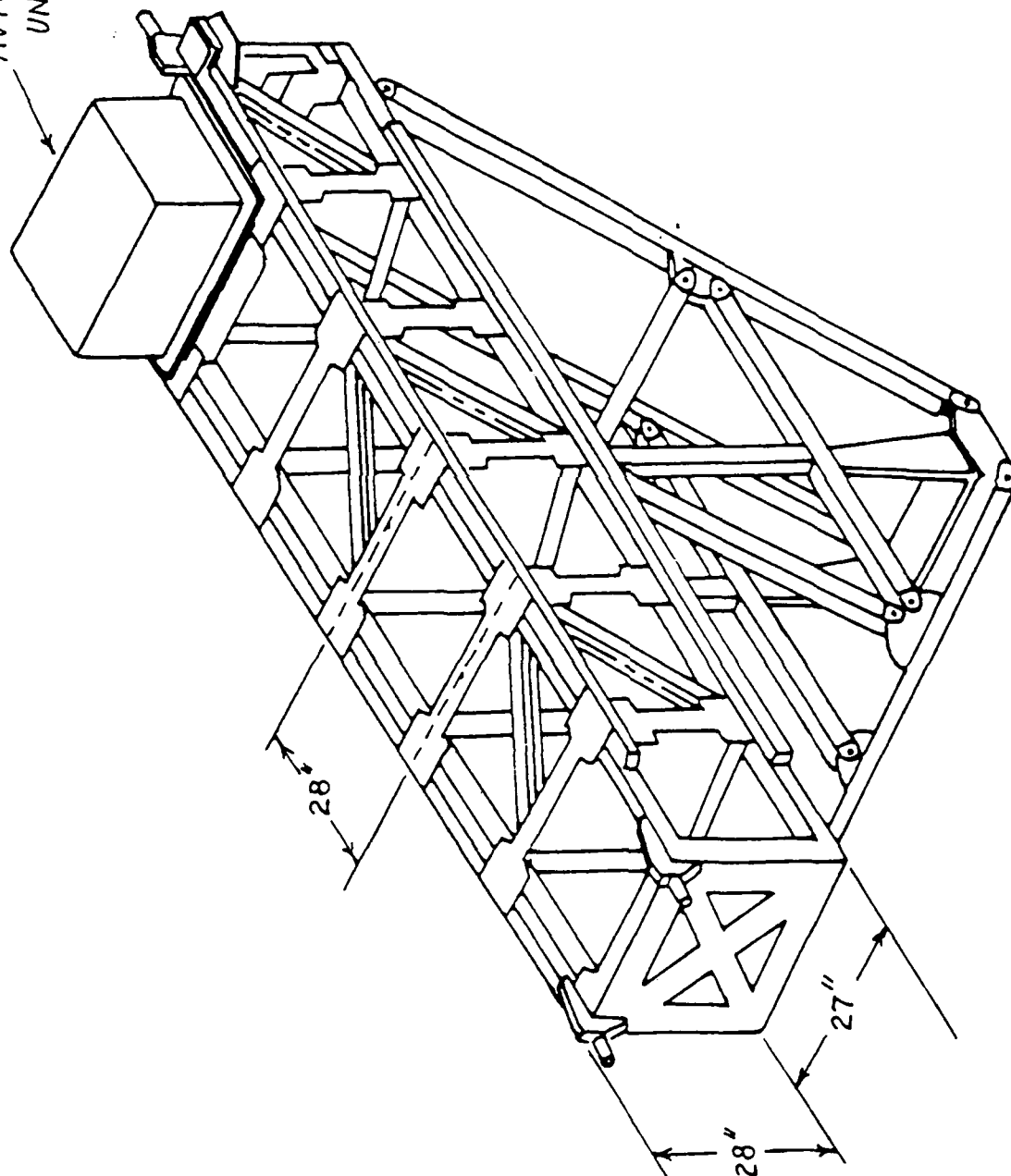
-14-



429

HITCHHIKER-G OFFERS USERS THREE MOUNTING OPTIONS

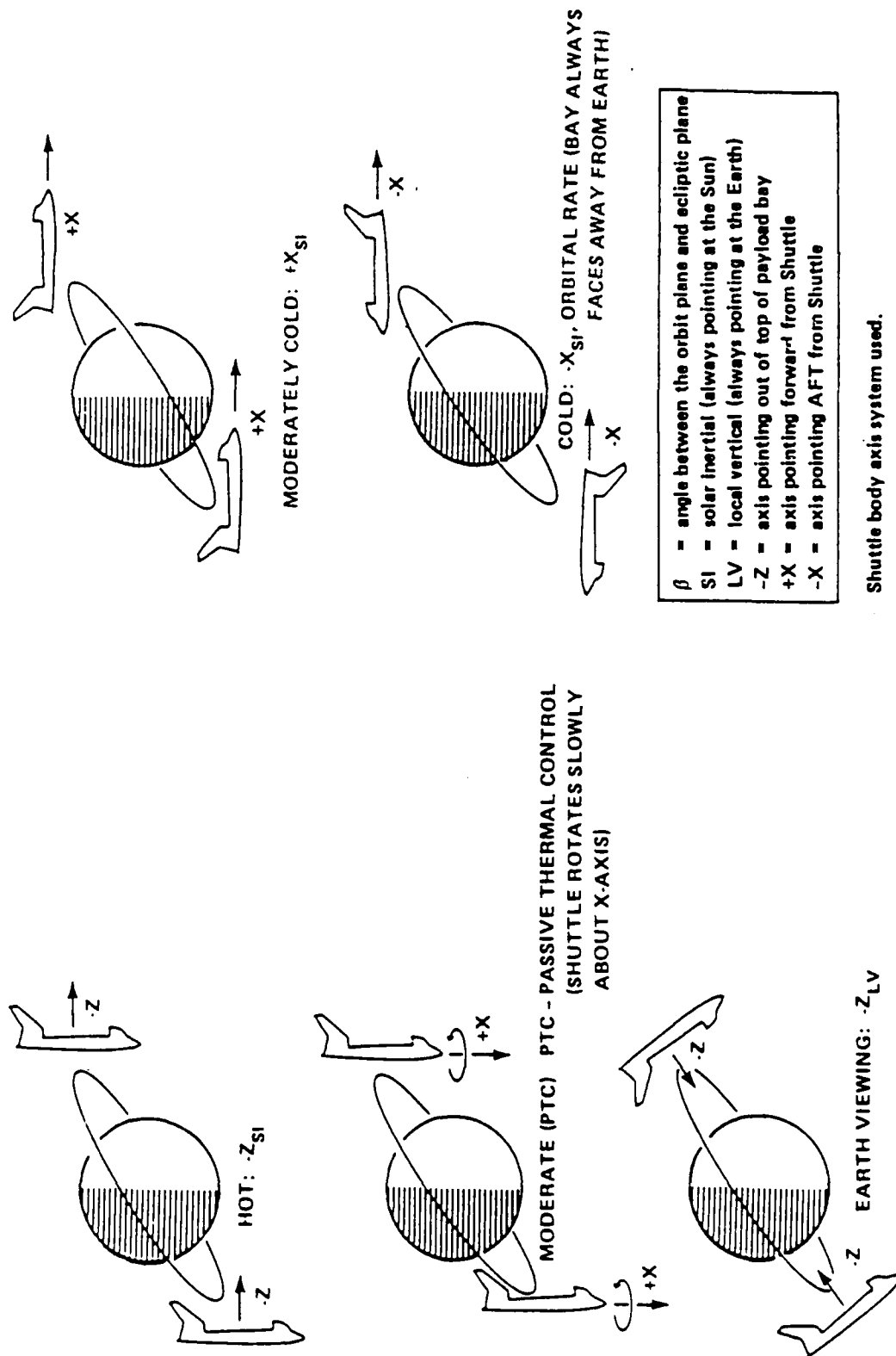
AVIONICS
UNIT



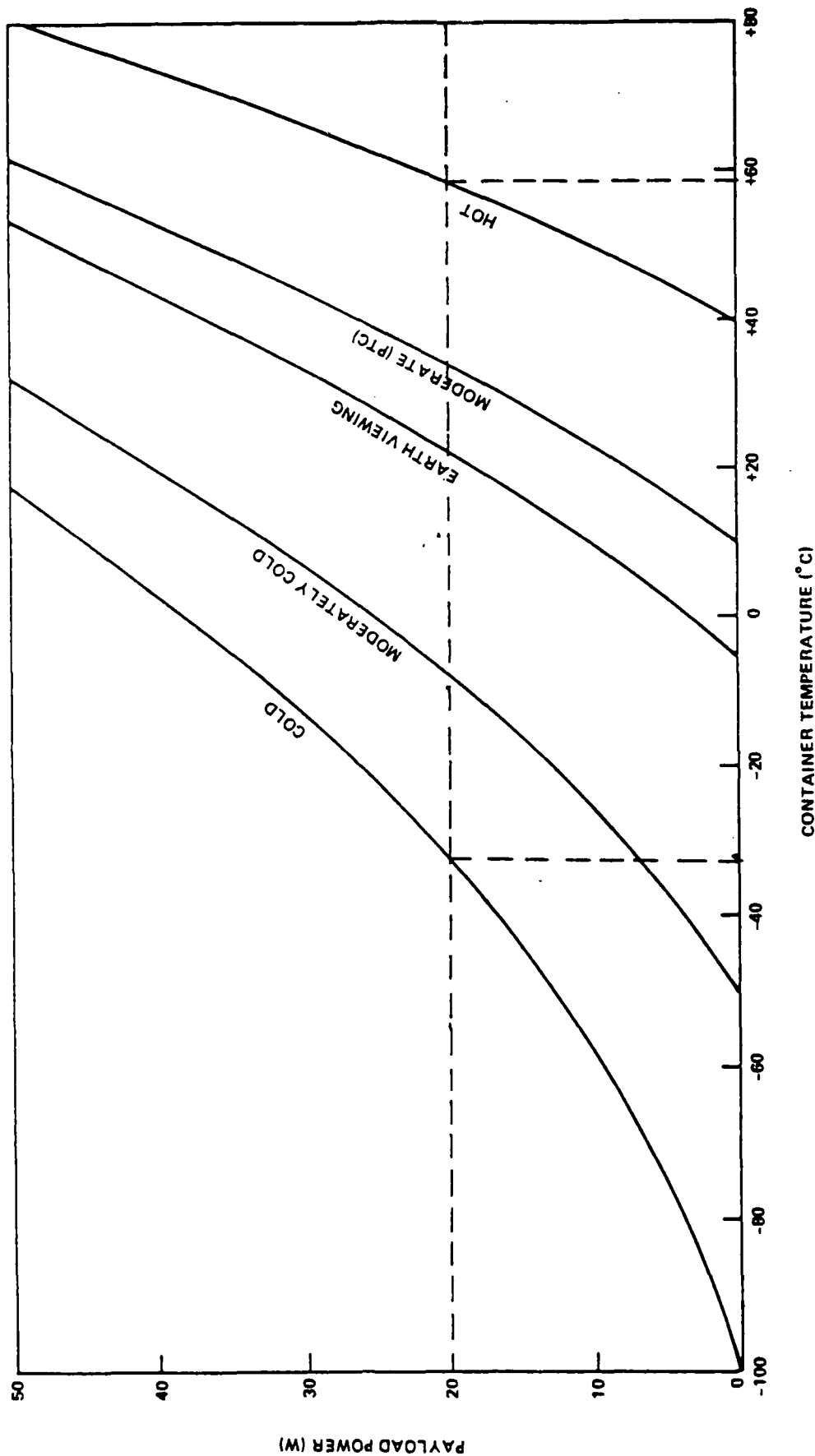
Hitchhiker-M Conceptual Configuration.

GET AWAY SPECIAL SMALL SELF-CONTAINED PAYLOADS TYPICAL ORBITAL THERMAL ATTITUDE

(70% SUN, $\beta = 35^\circ$, AND ALTITUDE = 150 n.mi. (278 km))



GET AWAY SPECIAL SMALL SELF-CONTAINED PAYLOADS 5 FT³ CONTAINER WITH INSULATED END CAP



TOTAL HH-G AND SINGLE CUSTOMER

CUSTOMER PAYLOADS PAYLOAD PORT

(MAX) (MAX)

POWER (28 +/- 4DC) 1300W 500W

ENERGY (KWH) 60 10**

LOW RATE DOWNLINK 6000 b/s 960 b/s*

MEDIUM RATE DOWNLINK 1.4 Mb/s 1.4 Mb/s***

SERIAL COMMAND CHANNELS 6 1

BI-LEVEL COMMANDS 24 4

*NOMINAL INFORMATION RATE OF ONE STANDARD ASYNCHRONOUS CHANNEL

**NOMINAL 1/6 ALLOCATION

***BY MISSION REQUIREMENTS

SUMMARY OF HITCHHIKER-G PAYLOAD CRITERIA

Standard Feature:

- Works as a family of components which can include: a mounting plate, a GAS adapter beam, and a GAS-like container
- Provides access to a substantial portion of the Shuttle avionics and data recording systems

Maximum weight of payloads:

- 750 pounds in containers or on side-mounted plates
- Sealed containers—200 pounds
- Containers with Hitchhiker Motorized Door Assembly—170 pounds
- Large plate—250 pounds, not including avionics
- Small plate—100 pounds

Dimensions:

- 5 cubic-foot container—28.25 inches high with a diameter of 19.75 inches
- Large plate—50 x 60 inches
- Small plate—25 x 39 inches

Center of Gravity (CG):

- No farther than 10" from mounting plate when accommodating 250 pounds

SIX-DOF GPS NAVIGATION EXPERIMENT

CONCLUSIONS

- GPS receivers can supply accurate attitude data for space vehicles
- A demonstration on the Orbiter is practical and cost-effective
- Position and short-arc accuracy can also be demonstrated effectively

Mayflower Communications 89100916 *Integrity Systems*

LARGE SPACE STRUCTURE DISPLACEMENT SENSING USING ADVANCED GPS TECHNOLOGY

Gaylord K. Huth and Sergei Udalov
AXIOMATIX

Aside from space navigation and attitude determination, other space applications of GPS include time transfer and differential tracking control of near co-orbiting spacecraft, and structure control of large spacecraft (flexure control). One motivation for using GPS for any of these other applications is reduced cost compared to competing techniques. This paper addresses the last of the above mentioned application, i.e. structure control.

Consider a beam anchored at one end with GPS antennas at each end. Movement can be monitored by interferometrically observing the phases of the GPS carrier signal at the two antennas. In space the beam is not anchored, and the deflections of the beam are referred to some average position. The number of antennas is proportional to the length of the beam.

A simulation was done with a beam in orbit on the scale of the space station. The receiver model assumed the TOPEX receiver and the multipath contribution was computed on basis of TOPEX receiver antennas situated about 0.3 m above the beam. Multipath was the major error contribution in the simulation. The beam had a 1 Hz vibration with a 5 cm amplitude. The mean error for modeling the vibration using the differential GPS phase measurements was about 0.6 mm, which was due almost entirely to multipath; and the standard deviation was about 5 mm, again influenced mainly by multipath.

It is noted from this simulation that GPS is a viable technique for structure control, but there are other available techniques. With a laser retro-reflective array or with inertial sensors (accelerometers and gyros) one obtains high performance and moderate to low cost. Therefore, if GPS cost can be reduced then it becomes a competitive technique.

Discussion:

Question: How much model error did you introduce into your simulation?

Answer: The vibration was assumed to be perfectly known. We did not try to demonstrate the absolute observability of actual beam vibrations, but merely the capability to observe a given vibration.

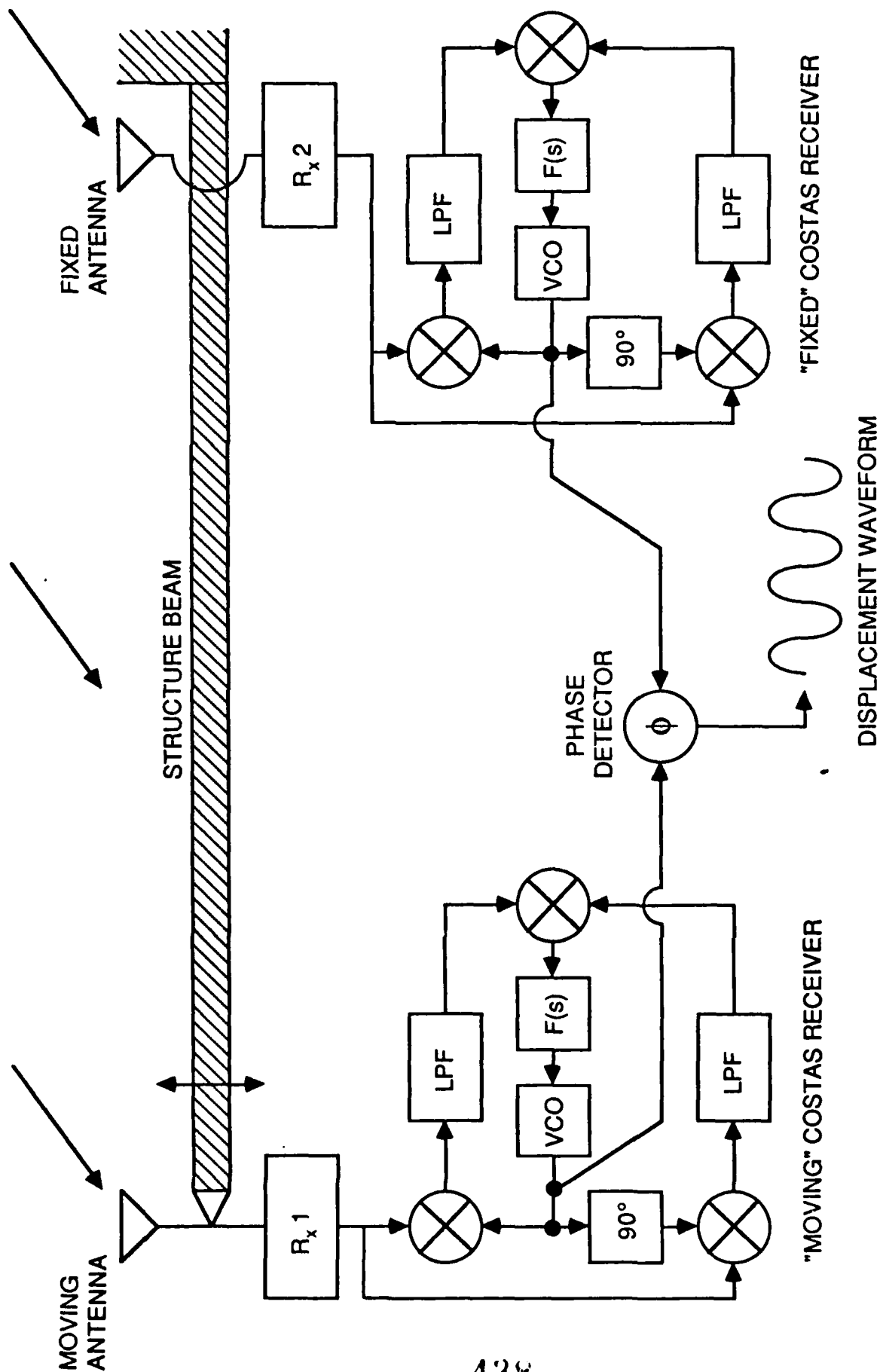
Question: Why is GPS being considered for this application when simple accelerometers and strain gauges will accomplish the same thing?

Answer: We wanted to determine if GPS could do this, in case it becomes cost effective (e.g., if a spacecraft already has a multitude of antennas and receivers on board for other purposes).

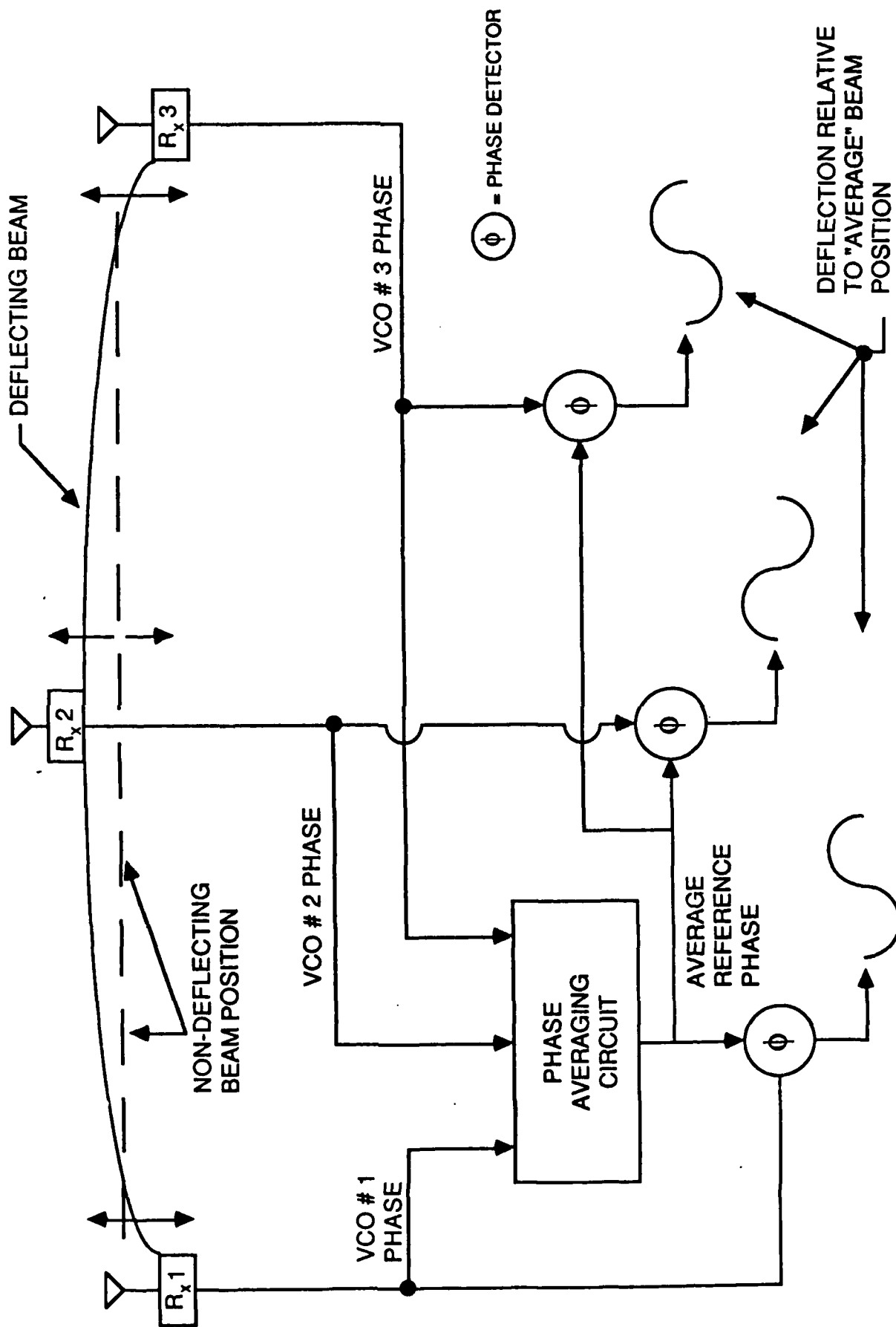
STRUCTURE DISPLACEMENT BASED ON RELATIVE PHASE DIFFERENCE

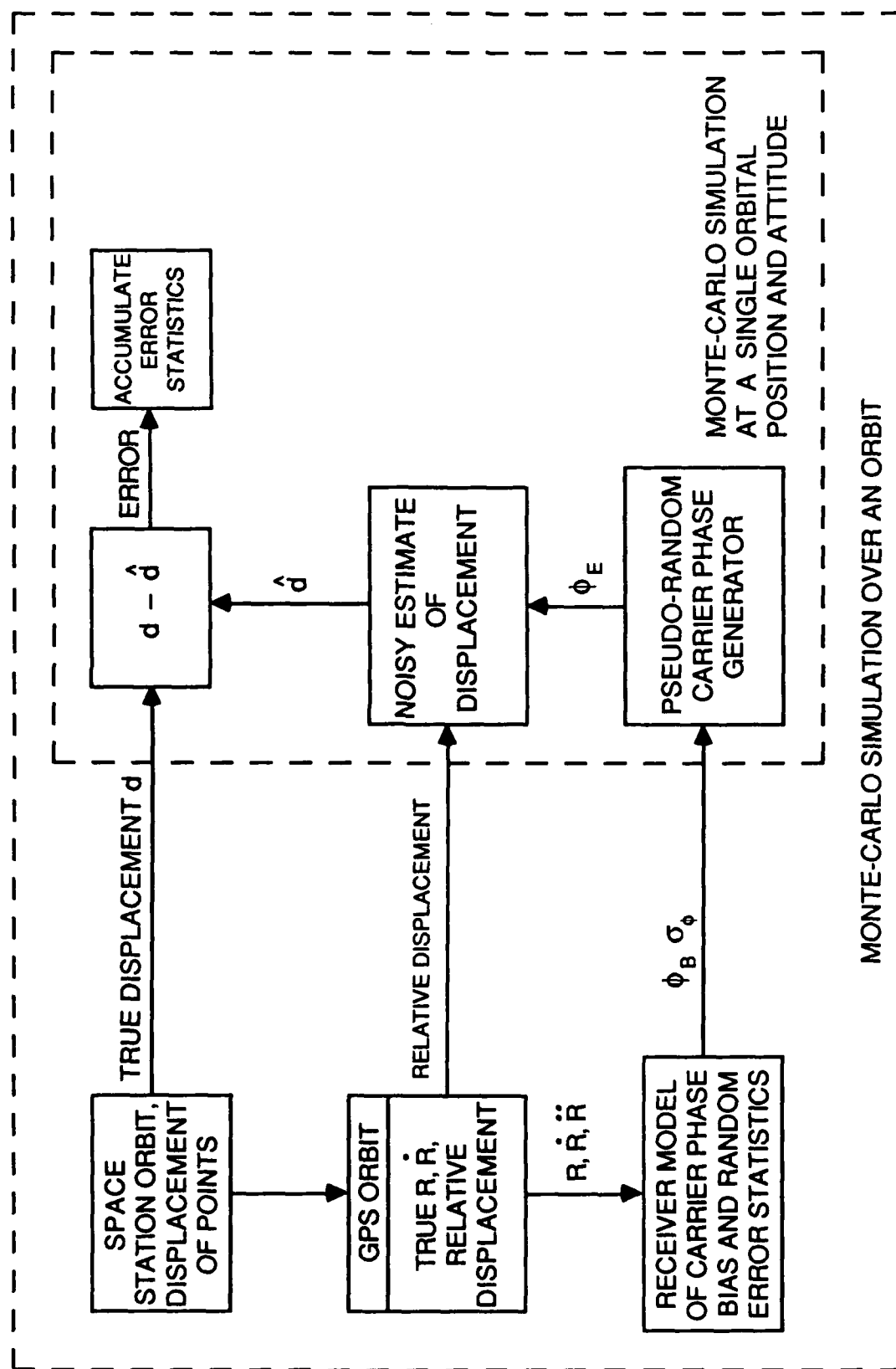


Axiomatix



PHASE MEASUREMENT W/R TO AVERAGE PHASE

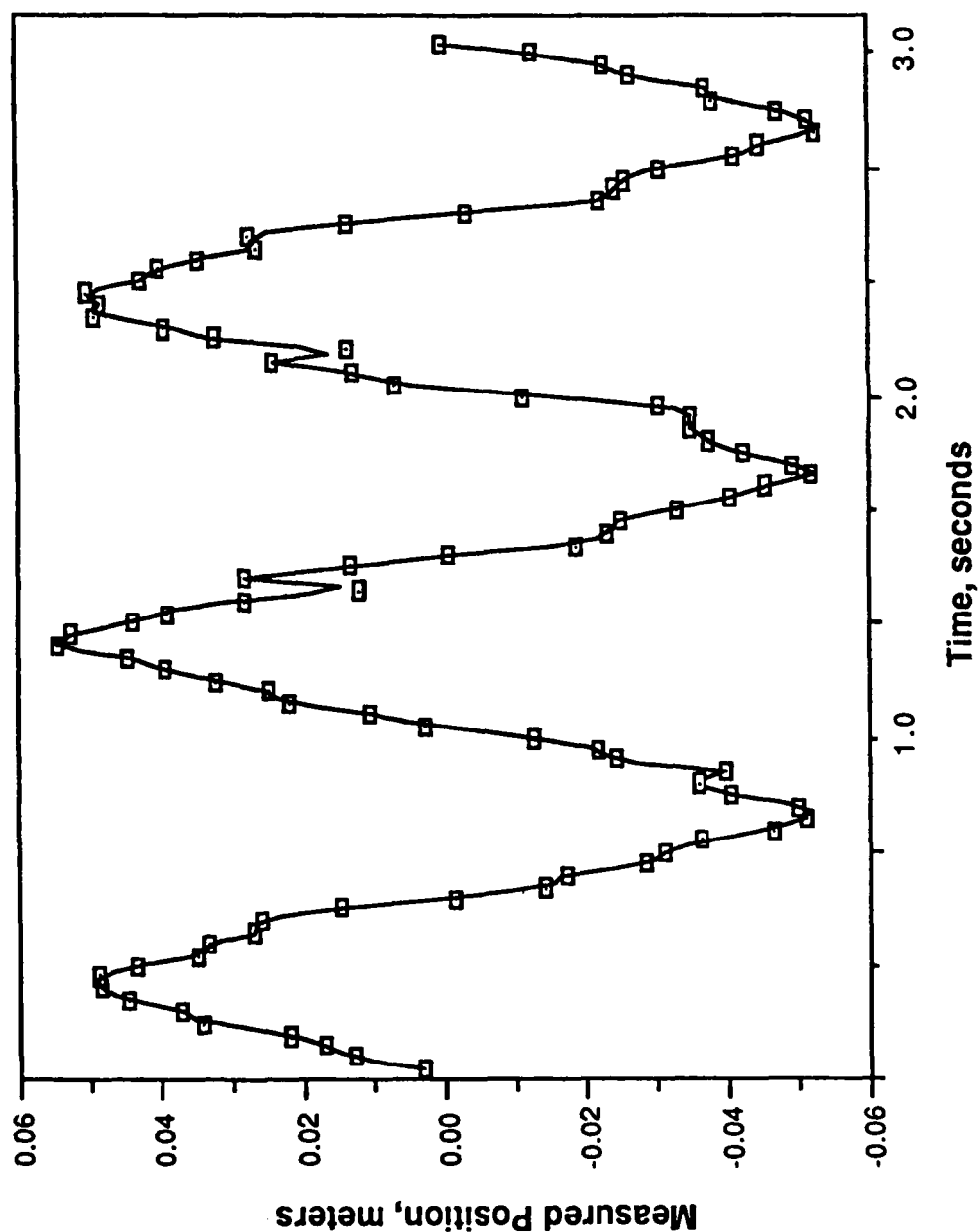




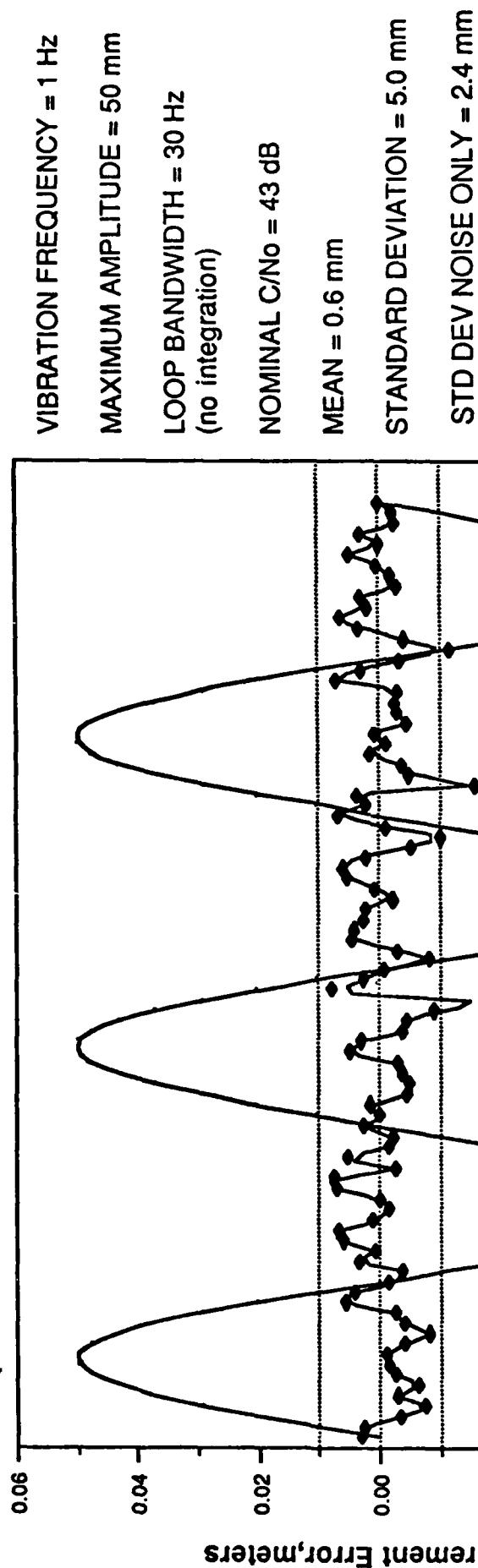
STRUCTURE VIBRATION SENSING
(WITH MULTIPATH)



Axiomatix



VIBRATION FREQUENCY = 1 Hz
MAXIMUM AMPLITUDE = 0.05 m
LOOP BANDWIDTH = 30 Hz
(no integration)
NOMINAL C/No = 43 dB



LARGE SPACE STRUCTURE CONTROL

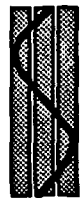


GPS —→ PRECISE RELATIVE PHASE – MULTIPLE ANTENNAS
(SIMILAR TO ATTITUDE CONTROL AND TRACKING)

MINIMUM BANDWIDTH DEPENDENT ON STRUCTURAL
MODE FREQUENCIES

STARTRACKERS —→ OPTICAL OBSERVATIONS OF RELATIVE FLEXURE

INERTIAL SENSORS —→ ACCELEROMETERS/GYRO



| | PERFORMANCE | COST | RELIABILITY | COMPLEXITY |
|---|----------------------------|---------------|-------------|------------|
| GPS | HIGH .001 m RELATIVE | HIGH @\$1M | MED | MED |
| RETRO- REFLECTOR FIELD TRACKER | HIGH | MED | MED | HIGH |
| INERTIAL RATE SENSORS (IFOG) | HIGH | LOW | HIGH | LOW |

ALTERNATIVES TO BECOMING AN "AUTHORIZED USER"

DEALING WITH SELECTIVE AVAILABILITY:

LONG-ARC DYNAMIC SMOOTHING REDUCES SA-INDUCED ERROR
DIFFERENTIAL CORRECTIONS CAN *ELIMINATE* SA EFFECTS

445

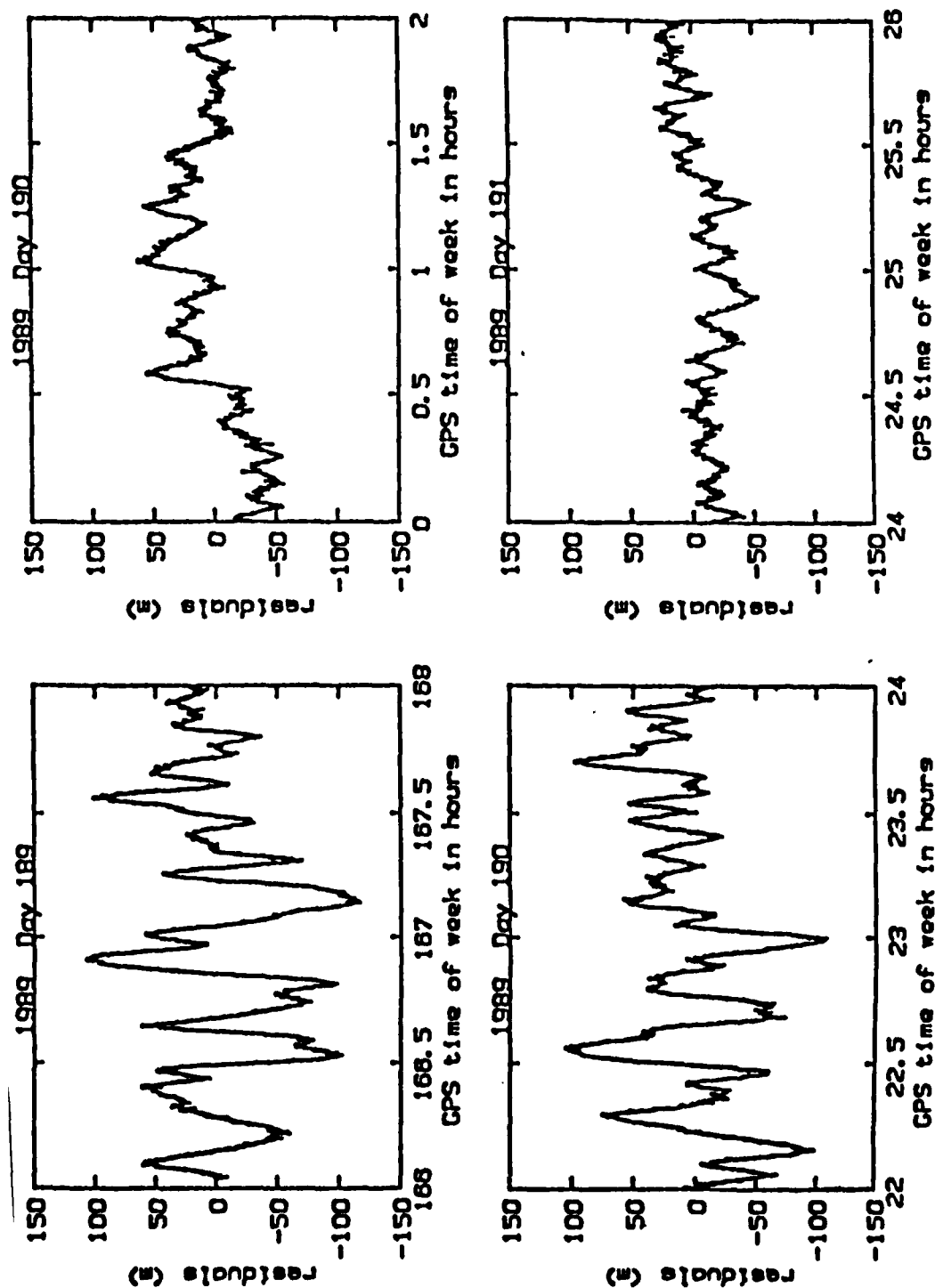
DEALING WITH ANTI-SPOOF:

"CODELESS" RECEIVER TECHNIQUES PROVIDE MORE THAN
ADEQUATE PERFORMANCE FOR ALMOST ANY APPLICATION

THOMAS YUNCK
JET PROPULSION LABORATORY

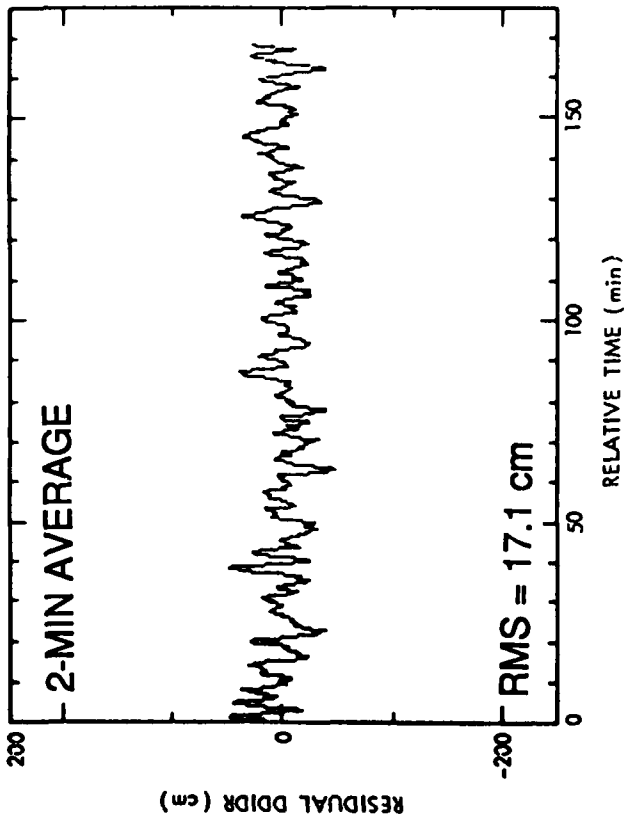
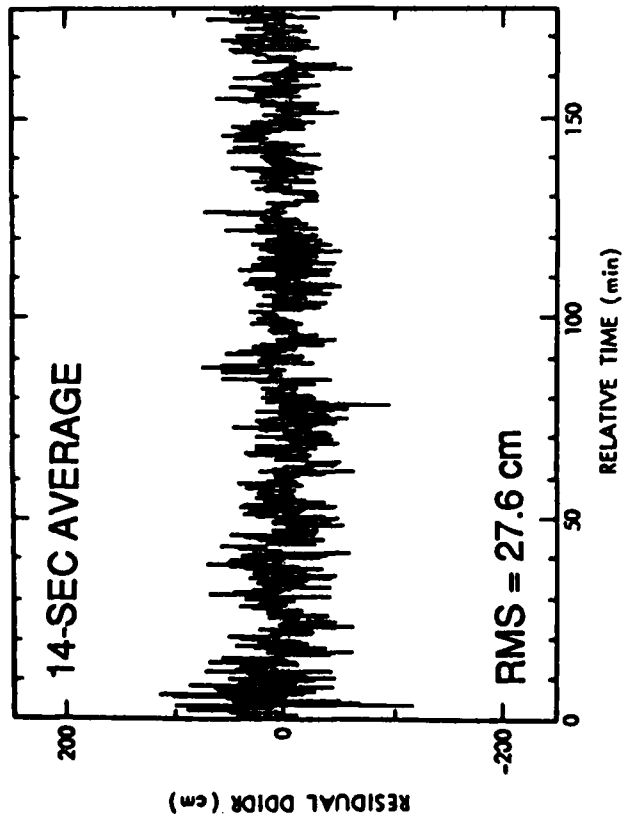
ACTUAL SA EFFECTS OBSERVED IN 1989

— from M. S. Braasch, 1989



Figs. 3 - 6. Pseudorange Residuals

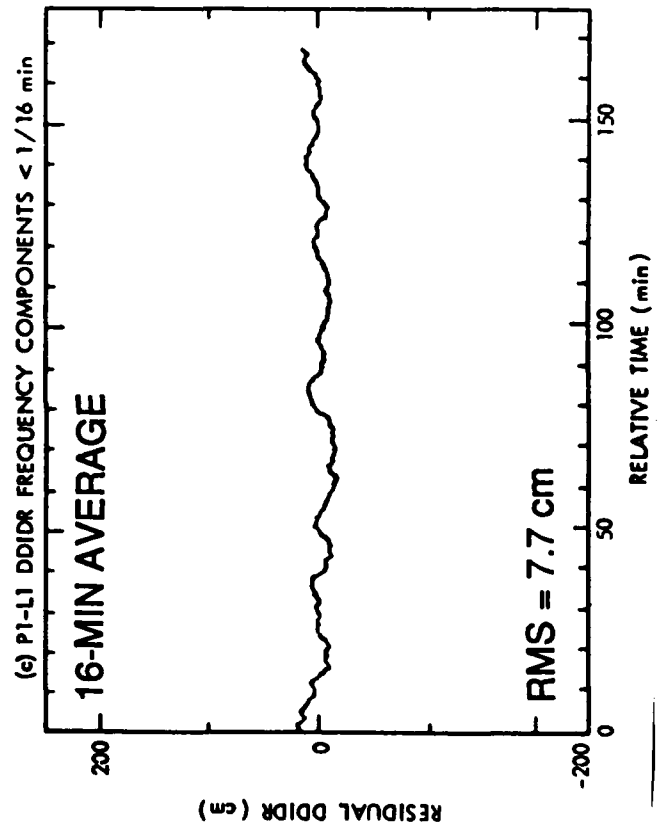
DELAY-MULTIPLY PSEUDORANGE DATA FROM SERIES-X



447

DOUBLY DIFFERENCED

P1 - L1



CODELESS GPS TECHNIQUES

CARRIER RECOVERY BY SQUARING:

$$[P(t) \cos(\omega t)]^2 \Rightarrow \text{D.C.} + \cos(2\omega t)$$

(SERIES-X and others)

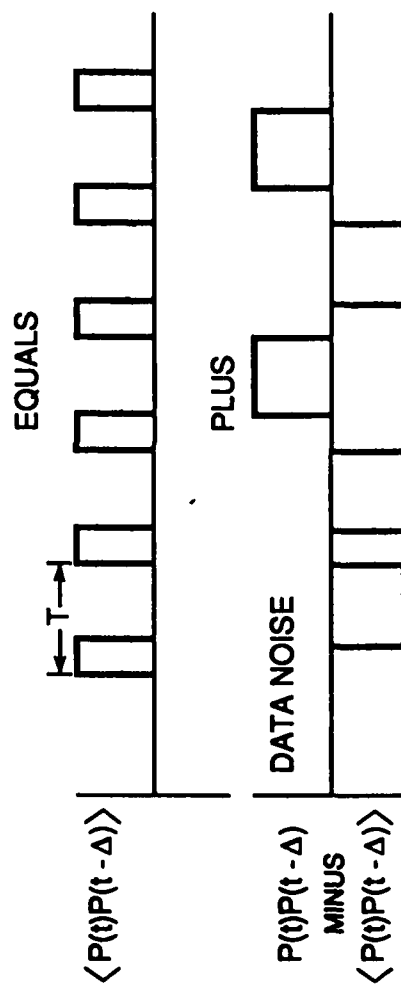
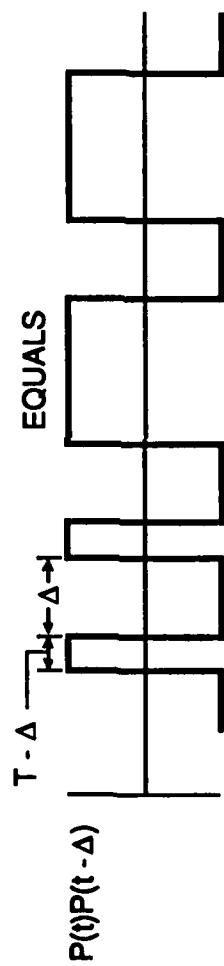
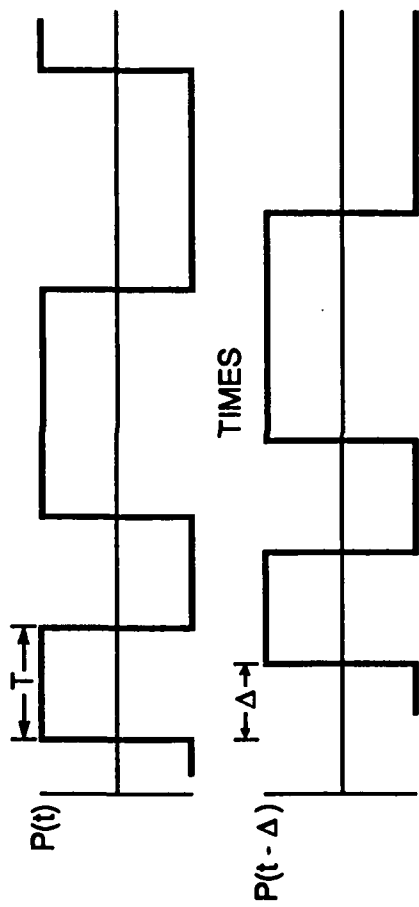
P-CODE GROUP DELAY RECOVERY BY:

DELAY-AND-MULTIPLY (SERIES-X and others)

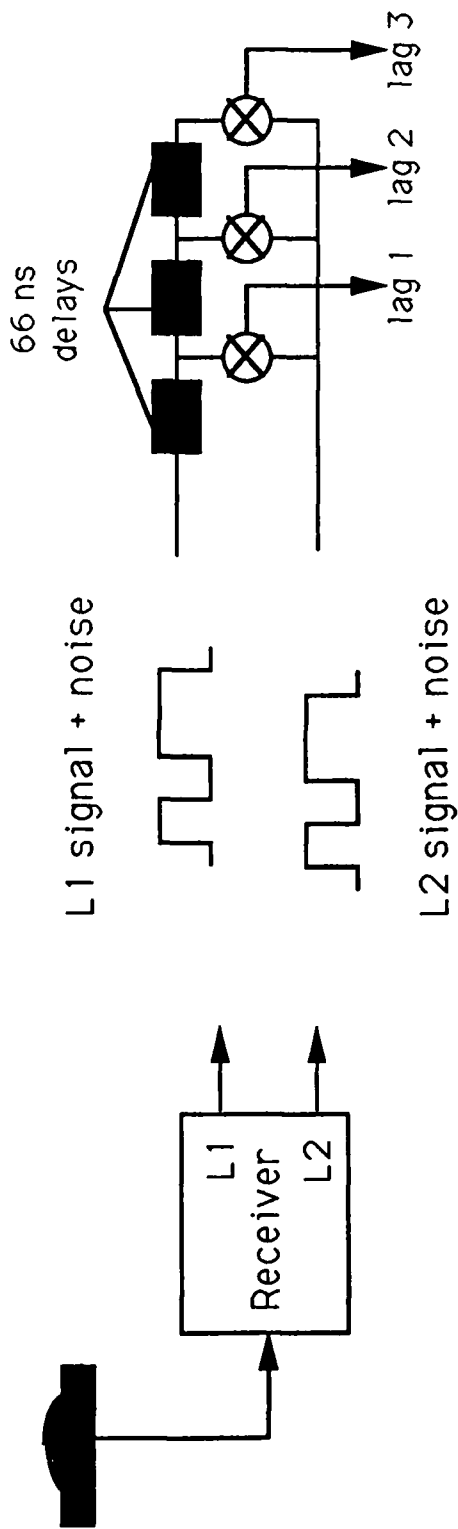
CARRIER & P-CODE IONOSPHERIC CORRECTION BY:

CROSS-CORRELATION OF L1 & L2 (ROGUE)

DELAY-MULTIPLY RECOVERY OF CODE PHASE

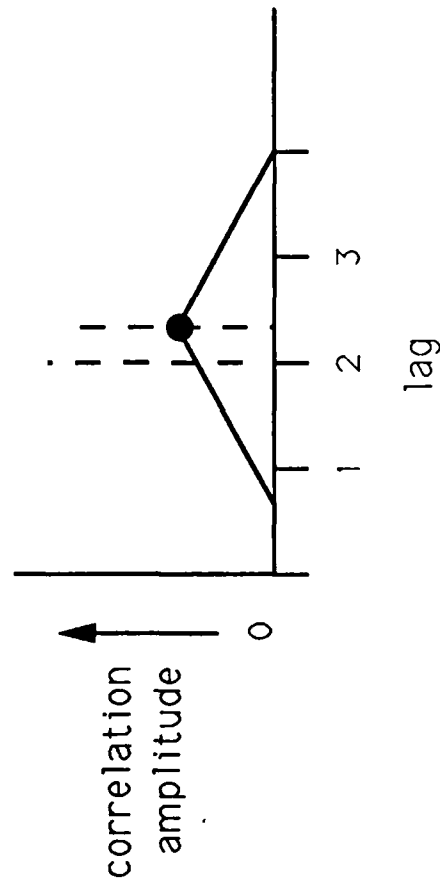


"Codeless" Delay Processing



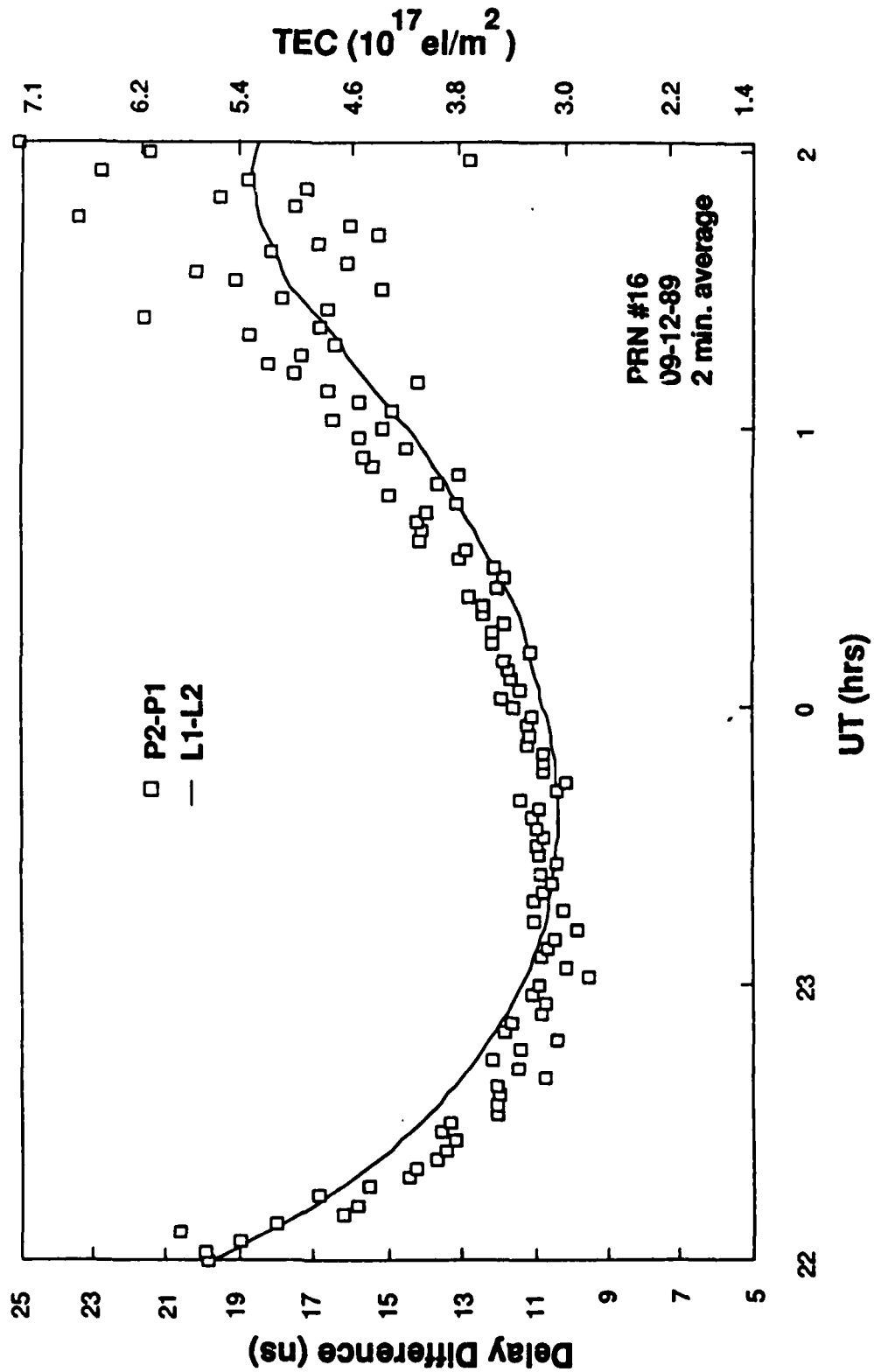
cross correlate L1 signal + noise
with L2 signal + noise

correlation peak offset from
lag 2 is due to ionosphere
(when other errors are
removed)

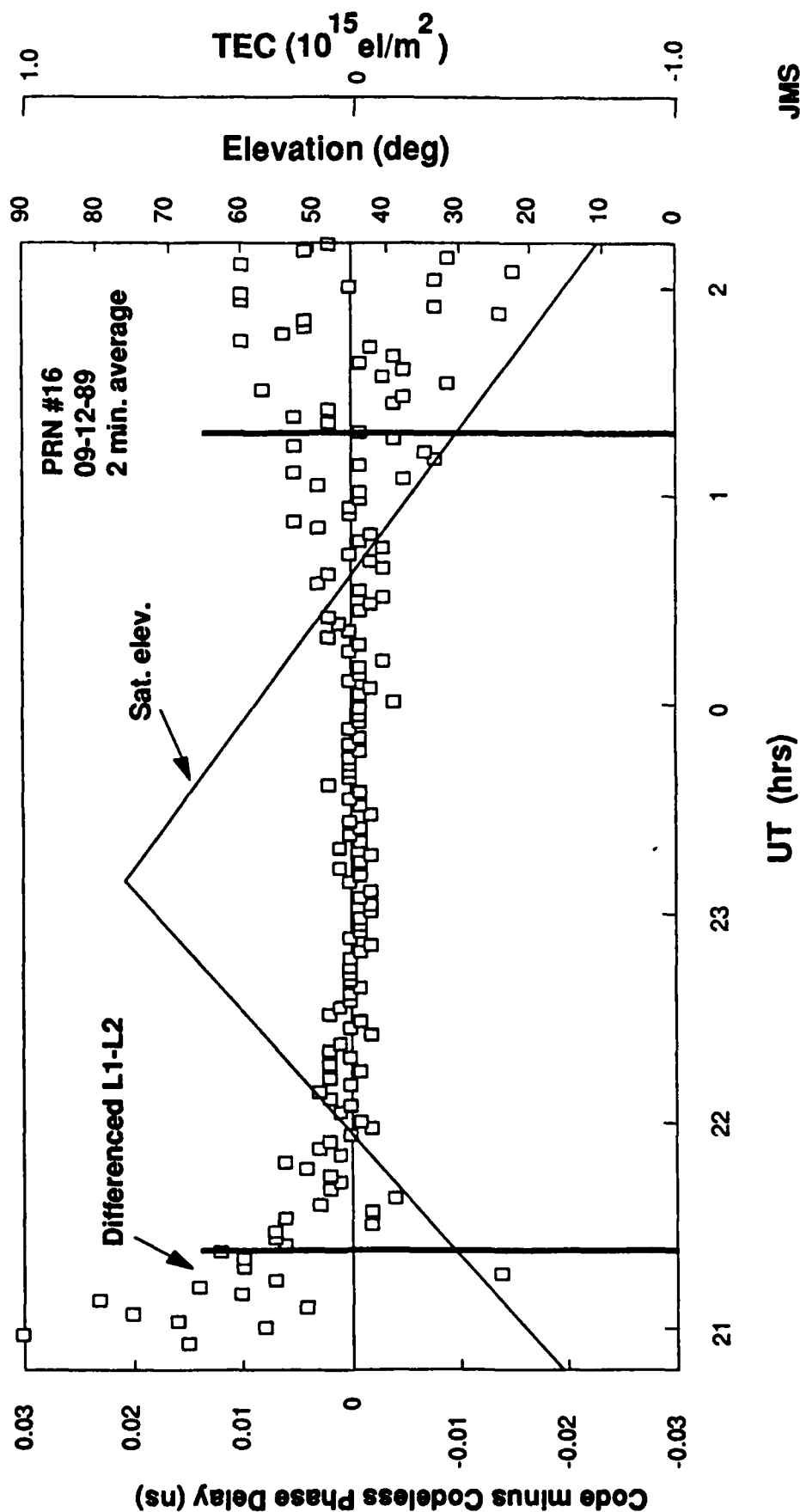




Rogue TEC Results: Group Delay & Phase Delay Comparison, Codeless Tracking



Rogue TEC Results: Phase Delay Comparison, Code minus Codeless



JMS
9/29/89

The Second Symposium on GPS Applications in Space
10-11 October 1989
Attendees

Joseph M. Aein
The RAND Corporation
2100 Street, N.W.
Washington, D.C. 20037

J. David Antonitis
Intermetrics, Inc.
733 Concord Ave.
Cambridge, MA 02138

Penina Axelrad
Stanford University
Hansen Labs (GP-B)
Stanford, CA 94305-4085

Mr. Ronald L. Beard
Code 8320
Naval Research Laboratory
4555 Overlook Ave., S.W.
Washington, DC 20375-5000

Robert Cantwell
Raytheon Company
Box 3203
528 Boston Post Rd.
Sudbury, MA 01776

Neal Carlson
Integrity Systems, Inc.
600 Main St., Suite 4
Winchester, MA 01890

Lance Carson
Motorola/GGG
2501 S. Price Rd.
Chandler, AZ 85248

Greg Charlton
GE-GCSD
Building 13-6-1
Front and Copper Street
Camden, NJ 08102

Oscar Colombo
University of Maryland
Astronomy Program
NASA Goddard SFC, Code 626
Greenbelt, MD 20904

Lewis Cook
NASA MSFC
Huntsville, AL 35812

Charles C. Counselman, III
MIT Room 37-552
Cambridge, MA 02139

Duncan Cox, Jr.
Mayflower Communications Co.
80 Main Str.
Reading, MA 01867

Edgar S. Davis
Jet Propulsion Laboratory
MS 238-540
4800 Oak Grove Dr.
Pasadena, CA 91109

Wayne Deaton
EL23
Marshall Space Flight Center
Huntsville, AL 35812

Dimitri Delikaraoglou
Energy, Mines and Resources
Canada Centre for Surveying/GSD
615 Booth St.
Ottawa, Ontario
CANADA K1A 0E9

David Delphenich
78 Schooner Lane
Shalimar, FL 32579

Newton Durboraw
Motorola, Inc.
Strategic Electronics Division
2501 S. Price Rd.
Chandler, AZ 85248

Donald H. Eckhardt
Geophysics Laboratory/LW
Hanscom AFB, MA 01731

Robert Edge
Proudman Oceanographic Laboratory
Bidston Observatory
Birkenhead
Merseyside L43 7RA
UNITED KINGDOM

Mr. Al Evans
Naval Surface Weapons Center
Dahlgren, VA 22448

Steve Gardner
Mayflower Communications Co.
80 Main St.
Reading, MA 01867

David Gleason
Geophysics Laboratory/LWG
Hanscom AFB, MA 01731

Stephen Goldman
GE-GCSD
Bldg 10-7-1
Front and Copper Street
Camden, NJ 08102

Luke Gournay
HY-Tech Services, Inc.
P.O. Box 1145
Granbury, TX 76048

George Hajj
Jet Propulsion Laboratory/238-640
4800 Oak Grove Dr.
Pasadena, CA 91109

Chris Harrison
Geodynamics Corp.
5520 Ekwil St., Suite A
Santa Barbara, CA 93111

David Hoffman
NASA/JSC
Mail Code FM46
Houston, TX 77062

James Huddle
Litton Guidance & Control Systems
500 Canoga Ave.
MS 67/35
Woodland Hills, CA 91367-6698

Dr. Gaylord Huth
Axiomatics, Inc.
9841 Airport Blvd., Suite 1130
Los Angeles, CA 90045

James Impastato
Rockwell International
Space Transportation Systems Division
12214 Lakewood Blvd.
Downey, CA 90241

Barry Irwin
U.S.G.S.
Quissett Campus
Woods Hole, MA 02543

Christopher Jekeli
Geophysics Laboratory/LWG
Hanscom AFB, MA 01731

J. Edward Jones
HQ AFIA/INTB
Bldg 5681
Bolling AFB, DC 20332-5000

Seymour Kant
NASA/GSFC
Code 701
Greenbelt, MD 20771

Mr. Fred Karkalik
Systems Control Technology
2300 Geng Rd.
P.O. Box 10180
Palo Alto, CA 94303

Leo Keane
The MITRE Corporation
7525 Colshire Drive
Mail Stop Z341
McLean, VA 22102-3481

John Kelley
NASA
Code T-FOB 10
600 Independence Ave., S.W.
Washington, D.C. 20546

Mr. Paul Landis, M.S. 8322
Naval Research Lab
4555 Overlook Avenue, S.W.
Washington, D.C. 20375

Stephen Lichten
Jet Propulsion Laboratory
MS 238-640
4800 Oak Grove Dr.
Pasadena, CA 91109

Dr. John Lundberg
Center for Space Research
Dept. of Aerospace Engineering
The University of Texas at Austin
Austin, TX 78712

Dr. Gerald Mader
Code N/CG114
National Geodetic Survey
11400 Rockville Pike
Rockville, MD 20879

Dr. Andre Mainville
Geodetic Survey of Canada
615 Booth St.
Ottawa, Ontario
CANADA K1A 0E9

Charles Martin
University Research Foundation
6411 Ivy Lane
Greenbelt, MD 20770

James Matthews
Raytheon Company, Box 1K9
528 Boston Post Rd.
Sudbury, MA 01776

Mr. T.K. Meehan
Jet Propulsion Laboratory
4800 Oak Grove Dr., M.S. 238-600
Pasadena, CA 91190

William G. Melbourne
Jet Propulsion Laboratory
MS 238-540
4800 Oak Grove Dr.
Pasadena, CA 91109

Scott Murray
NASA/JSC
Hations Co.
80 Main St.
Reading, MA 01867

Howard Parks
Motorola, Inc.
2501 S. Price Rd.
M/D G-1206
Chandler, AZ 85248-2899

Jeff Patterson
McDonnell Douglas Space Systems Co.
16055 Space Center Blvd.
Houston, TX 77062

Allan Posner
JHU - Applied Physics Lab
Johns Hopkins Rd.
Laurel, MD 20707

George Prioovolos
Mayflower Communications Co.
80 Main St.
Reading, MA 01867

Harley Rhodehamel
Mayflower Communications Co.
80 Main St.
Reading, MA 01867

Mr. William Riley
EG&G Frequency Products, Inc.
35 Congress St.
Salem, MA 01970

Thomas Rooney
Geophysics Laboratory/LWG
Hanscom AFB, MA 01731

Horst Salzwedel
Systems Control Technology, Inc.
2300 Geng Rd.
Palo Alto, CA 94303

Woody Satz
Mayflower Communications Co.
80 Main St.
Reading, MA 01867

Ms. Penny E. Saunders
NASA/JSC
Houston, TX 77058

George Schauer
Motorola, Inc.
2501 S. Price Rd.
Chandler, AZ 85248

Richard Sfeir
Rockwell International
S&SED Space Electronics
3370 Miraloma
Anaheim, CA 92803

Lt Col Gerald Shaw
Geophysics Laboratory/LW
Hanscom AFB, MA 01731

Richard Shi
McDonnell Douglas Space Systems
5301 Bolsa Ave.
Huntington Beach, CA 92647

James Slater
Defense Mapping Agency
Systems Center/SGG
8623 Lee Highway
Fairfax, VA 22031-2138

David Sonnabend
Jet Propulsion Laboratory
MS 301-125J
4800 Oak Grove Dr.
Pasadena, CA 91109

Everett Swift
Naval Surface Warfare Center
Code K-12
Dahlgren, VA 22448

Charles Taylor
Geophysics Laboratory/LWG
Hanscom AFB, MA 01731

Mr. Hal Theiss
Code T
NASA Headquarters
Washington, D.C. 20546

Dr. Catherine L. Thornton
JPL 238-640
4800 Oak Grove Drive
Pasadena, CA 91109

Dan Toomey
Motorola, Inc., CEG
2501 S. Price Rd., MD G-1206
Chandler, AZ 85248-2899

Milton Trageser
9 North Gateway
Winchester, MA 01890

Dr. Triveni N. Upadhyay
Mayflower Communications Co.
80 Main Street
Reading, MA 01867

Jerome Vetter
Applied Physics Laboratory
Johns Hopkins Rd.
Laurel, MD 20707

Mr. Phil Ward
Mail Station 8443
Texas Instruments, Inc.
P.O. Box 869305
Plano, TX 75086

Mr. Roger M. Weninger, Mail Code DB04
Rockwell Space Electronics Systems Div.
P.O. Box 3170
3370 Miraloma Avenue
Anaheim, CA 92803

Leonard Wilk
C.S. Draper Laboratory
555 Technology Square, MS-6E
Cambridge, MA 02139

Sien-Chong Wu
Jet Propulsion Laboratory
MS238-624
4800 Oak Grove Dr.
Pasadena, CA 91109

Dr. Thomas P. Yuncck
JPL 238-640
4800 Oak Grove Drive
Pasadena, CA 91109